NNT : 0000AIXM0000

THÈSE DE DOCTORAT

Soutenue à Aix-Marseille Université
le 3 juillet 2024 par

Barbara FORNO

Une démarche de conception à contre-courant pour un réacteur nucléaire simplifié

Discipline
Physique & Sciences de la Matière

Spécialité
Énergie, Rayonnement, Plasma

École doctorale
ED352 - Physique et sciences de la matière

Laboratoire/Partenaire de recherche
CEA Cadarache

Composition du jury

Pierre-Etienne LABEAU Professeur, Ecole Polytechnique de Bruxelles	Rapporteur Président du jury
Eugene SHWAGERAUS Professeur, University of Cambridge	Rapporteur
Claire VAGLIO-GAUDARD Directrice de recherche, CEA	Examinatrice
Jiri KREPEL Senior scientist, Paul Scherrer Institut	Examinateur
Laurent BUIRON Directeur de recherche, CEA	Directeur de thèse
Pierre SCIORA Ingénieur chercheur, CEA	Invité
Timothée KOOYMAN Cadre scientifique, Naarea	Invité

Affidavit

Je soussignée Barbara Forno déclare par la présente que le travail présenté dans ce manuscrit est mon propre travail, réalisé sous la direction scientifique de Laurent Buiron dans le respect des principes d'honnêteté, d'intégrité et de responsabilité inhérents à la mission de recherche. Les travaux de recherche et la rédaction de ce manuscrit ont été réalisés dans le respect à la fois de la charte nationale de déontologie des métiers de la recherche et de la charte d'Aix-Marseille Université relative à la lutte contre le plagiat.

Ce travail n'a pas été précédemment soumis en France ou à l'étranger dans une version identique ou similaire à un organisme examinateur.

Fait à Aix-En-Provence, le 06 mai 2024.

Barbara Forno

Liste de publications et participation aux conférences

Liste des publications réalisées dans le cadre du projet de thèse :

- B. Forno, P. Sciora, J.B. Droin, C. Boudot, K. Tirel, D. Haubensack, T. Kooyman, L. Buiron. "Potential contribution of the Energy Conversion System to the core reactivity balance". En cours de publication. Soumis à Nuclear Engineering and Design, 2024.

Participation aux conférences et écoles d'été au cours de la période de thèse :

- B. Forno, P. Sciora, T. Kooyman, K. Tirel, L. Buiron. "A coupled neutronic-thermal model for the evaluation of heat pipe reactors transients". ICAPP 2023, International Congress on Advances in Nuclear Power Plants, 23-27 April 2023, Korea.
- 2022 Frédéric Joliot/Otto Hahn Summer School on Nuclear Reactors: "Nuclear Power in the Energy Transition". Held in Aix-en-Provence, France, from August 24th to September 2nd, 2022.

Résumé

Historiquement, le principal objectif de la conception des réacteurs nucléaires était l'optimisation et la maximisation de l'énergie fournie au réseau électrique. En général, les centrales nucléaires sont utilisées pour un fonctionnement en base tandis que d'autres sources (gaz, hydroélectricité, charbon) sont utilisées pour absorber les fluctuations de la demande du réseau. Cependant, le mix énergétique actuel intègre de plus en plus d'énergies renouvelables non pilotables. Par conséquent, les centrales nucléaires pourraient être amenées à adapter leur production à des fluctuations du réseau encore plus importantes. Ce besoin entraîne une complexification de la conception du cœur du réacteur avec la nécessité de plusieurs systèmes actifs pour assurer un contrôle optimisé de la puissance au fil du temps.

Cette thèse propose une approche originale à contre-courant dont l'objectif n'est plus l'optimisation de la production électrique, mais la simplification du cœur du réacteur. La motivation est d'évaluer les performances d'un système qui, une fois démarré, fonctionne de manière autonome avec le moins de contrôles actifs possible. La puissance fournie par un tel réacteur n'est pas contrôlée activement mais est déterminée par le comportement autonome du cœur. Cependant, l'évolution de la production d'électricité au cours du temps serait toujours connue, ce qui permettrait d'anticiper plus facilement les besoins du réseau par rapport à des sources d'énergie intermittentes. L'objectif est de concevoir un réacteur capable de produire de l'énergie de manière simple et autonome. Les performances d'un tel réacteur sont définies et des propositions sont faites pour les améliorer.

La méthodologie choisie consiste en une analyse séparée des systèmes du réacteur. L'approche retenue vise à concevoir un système primaire autonome. Tout d'abord, le contrôle du système de conversion d'énergie est analysé, afin d'évaluer sa contribution possible au fonctionnement du cœur. Ensuite, un schéma de calcul simplifié a été mis en œuvre pour étudier l'évolution du cœur autonome en couplant les champs neutronique et thermo-hydraulique dans un modèle quasi-statique. En effet, un tel cœur autonome est défini par les effets de contre-réactions qui contrebalancent la perte de réactivité due à l'épuisement du combustible.

Dans la littérature, plusieurs designs de réacteurs sont proposés pour différents objectifs. Les microréacteurs (MMR) se caractérisent par des designs simplifiés et une puissance thermique limitée. D'autre part, les réacteurs de taille industrielle sont optimisés pour les besoins du réseau, mais ils comprennent des systèmes complexes pour le pilotage des opérations. Quatre concepts ont été sélectionnés pour ce travail : les réacteurs à caloducs (HPR), les réacteurs à haute température (HTR), les réacteurs à eau pressurisée (REP) et les réacteurs à neutrons rapides refroidis au sodium (RNRNa).

Les quatre concepts sont étudiés pour être exploités de manière autonome, ce qui signifie que tous les systèmes de contrôle de la réactivité sont supprimés.

L’enrichissement fissile initial est ajusté pour avoir un cœur critique en début de vie, puis le cœur est laissé en évolution autonome. Des performances ont été spécifiquement définies pour ces réacteurs, notamment la durée de vie du cœur, le burn-up du combustible en fin de vie et la puissance moyenne en fonctionnement.

Les réacteurs étudiés présentent des performances faibles lorsqu'ils sont exploités de manière autonome t, ce qui était prévisible puisqu'ils ont été conçus pour être exploités activement. Par conséquent, des modifications du design sont proposées afin d'améliorer leurs performances. En particulier, des efforts sont menés pour réduire la perte de réactivité due à l'épuisement du combustible en insérant dans le cœur des actinides ou des poisons consommables. Les designs améliorés sont finalement comparés aux concepts initiaux et des augmentations significatives de performances sont mises en évidence.

Mots clés : Réacteur nucléaire ; Conception de réacteur ; Simplification de conception ; Absence de pilotage actif ; Cœur à pilotage autonome

Abstract

Historically, the main motivation for nuclear reactors design optimisation was the maximisation of energy they can provide to the electrical grid. Generally, in countries with large nuclear power plant fleet, nuclear power plants are used to answer to the base load demand, while other sources (gas, hydropower, coal) are used to absorb fluctuations. However, today's energy mix is increasingly integrating renewable energy sources that are unable to adjust their power output in response to grid demand. Consequently, it could be expected from nuclear power plants to be able to adapt their output to the fluctuations of production caused by renewable sources. This design approach results in the complexification of core design with the need of several active systems to ensure an optimised control of power over time.

This work proposes an original counter current approach which focus is no longer the amount of electricity produced, but the simplification of the reactor core. The motivation is to assess the performance of a system that once started-up operates autonomously with as little active control as possible. The output power of such a reactor is not actively controlled, rather it is determined by the autonomous operation of the core. However, the evolution of power over time would still be known, making it easier to anticipate the grid needs in comparison with unpredictable energy producers. The objective is to conceive a reactor as a component of the grid, capable of generating energy in a simple and autonomous way. The performance of such a reactor is defined and propositions will be made in order to improve it.

The chosen methodology consists in a separate analysis of the reactor systems. The choice is to focus on the design of an autonomous primary system. First, the control of the Energy Conversion System is analysed, to assess its possible contribution to the core operation. Then, a simplified computational scheme has been implemented to study the autonomous core evolution coupling the neutronic and thermal-hydraulic fields in a quasi-static model. Indeed, such an autonomous core is defined by the reactivity feedback effects that counterbalance the reactivity loss due to fuel depletion. This coupling is necessary to compute the power evolution.

In the literature, several reactor designs are proposed for different objectives. The Micro Modular Reactors (MMR) are characterised by simplified designs and enhanced autonomous characteristics, but limited thermal power. On the other hand, the industrial-scale reactors are optimised for large power production adapted to the grid necessities, but they include complex systems for the operation control. This work is based on the analysis of the existing designs. Among these reactors, four concepts were selected for the scope of this work: the Heat Pipe Reactor (HPR), the High Temperature Reactor (HTR), the Pressurized Water Reactor (PWR) and the Sodium-cooled Fast Reactor (SFR).

The four designs are studied to be autonomously operated, which means that all reactivity control systems are removed. The initial fissile enrichment is set to have a null

reactivity at the beginning of life, then the core is left to evolve autonomously. Performance have been specifically defined for such reactors, including core lifetime, fuel burn-up at the end of life and mean power in operation.

The studied reactors firstly show poor performance when autonomously operated, which was expected as they were designed to be actively operated. Therefore, modifications to the designs are proposed to increase their performance. Particular attempt is done to reduce the reactivity loss due to fuel depletion, made by the insertion in the core of actinides or burnable poisons. The improved designs are finally compared to the initial ones and significant performance increases are highlighted in terms of higher energy produced, longer core lifetimes and higher burn-ups at the end of life.

Keywords: Nuclear reactor; Reactor design; Design simplification; Absence of active power control; Autonomous core operation

Remerciements

Tout d'abord, je tiens à remercier le professeur Pierre-Etienne LABEAU et le professeur Eugene SHWAGERAUS d'avoir accepté d'être les rapporteurs de cette thèse et pour leur travail de relecture important. Mes remerciements vont également au docteur Claire VAGLIO-GAUDARD et au docteur Jiri KREPEL pour l'intérêt qu'ils ont porté à mon travail en tant que membres du jury.

Mes plus vifs remerciements vont à Edwige RICHEBOIS, Maxime GUYOT, Jean-Christophe BOSQ, Philippe DARDE et Guillaume MARTIN, du service SPRC et du laboratoire LE2C, où ces travaux de thèse ont été réalisés. Je tiens également à remercier Gérard MIGNOT, Lionel CACHON et Sébastien VINCENT, du service SESI et du laboratoire LCOS, pour m'avoir accueillie et pour avoir permis l'achèvement de ce travail.

Je tiens à remercier mon directeur de thèse Laurent BUIRON pour son implication et son attention tout au long de mon travail de thèse. Je le remercie pour sa confiance et son soutien. J'exprime ma profonde gratitude aux encadrants de cette thèse : Pierre SCIORA et Kévin TIREL tout particulièrement pour leur disponibilité, leurs conseils avisés, leur aide précieuse et leur soutien sans faille.

Merci également à Timothée KOOYMAN pour m'avoir accompagnée en participant à l'encadrement au début de cette thèse. Une profonde reconnaissance à Jean-Baptiste DROIN, Charly BOUDOT et Johann MARTINET pour leur soutien technique et le partage de leur expertise.

Un grand merci également à tous les collègues du 230 qui m'ont permis de travailler pendant ces trois années dans un environnement agréable et stimulant. Merci pour les bons moments partagés et le soutien apporté dans les moments plus délicats, qui a été pour moi si important pour la réussite de ce travail. Un grand merci également à mes nouveaux collègues du SESI pour leur accueil chaleureux et leur sympathie. Enfin un grand encouragement aux doctorants qui poursuivent l'aventure de leur thèse.

Un manuscrit entier ne suffirait pas à remercier chaque personne qui a fait partie de ce parcours. Ceux qui sont dans la région, ceux qui sont partis pour Paris, Nantes… mes amis à Turin et je m'excuse de ne pas pouvoir tous vous citer un par un comme vous le méritez, mais la rédaction était déjà longue, je suis sûre que vous comprendrez…

Enfin, mes remerciements les plus sincères vont à ma famille, qui est mon point de référence et ma force dans ma vie. Toute ma gratitude à mon père, à Mariangela et à mon frère qui, même si je me suis éloignée physiquement, sont toujours à mes côtés.

Résumé étendu

Table des matières

0.1. Introduction 10

0.2. Objectif et démarche de la thèse 10

0.2.1. Objectif de la thèse 10

0.2.2. Démarche du travail 11

0.2.3. Les microréacteurs 12

0.2.3.1. Réacteurs à caloducs 13

0.2.3.2. Réacteurs à haute température 13

0.3. Méthodologie 13

0.4. Comparaison des réacteurs autonomes 14

0.5. Amélioration des performances des réacteurs autonomes 15

0.6. Conclusions et perspectives 17

0.6.1. Conclusions 17

0.6.2. Perspectives 19

0.1. Introduction

Au cours des dernières décennies, l'attention portée à la question du changement climatique s'est accrue, jusqu'à la reconnaissance de la nécessité urgente de modifier l'approche de la consommation et de la production énergétique. Un nombre croissant de pays s'est engagé à atteindre l'objectif de neutralité carbone d'ici 2050 [1]. Une des approches proposées pour atteindre cet objectif comprend la réduction et idéalement l'élimination des combustibles fossiles pour la production d'énergie et leur remplacement par des énergies renouvelables et nucléaires [2].

Dans ce contexte, le rôle du nucléaire, en tant que fournisseur d'énergie au réseau électrique, a changé au fil du temps, constat particulièrement vrai dans le contexte français. Initialement, les variations des demandes des réseaux électriques étaient moins importantes et principalement absorbées par les centrales à combustibles fossiles. Les centrales nucléaires ont été insérées dans les réseaux afin de produire une puissance électrique constante. Avec l'introduction des énergies renouvelables dans le réseau et la tendance à l'élimination des sources carbonées, la nécessité de compenser les fluctuations de puissance a été redirigée vers les centrales nucléaires [3].

L'introduction de l'objectif de suivi de charge a entraîné la nécessité de complexifier le système de contrôle et de pilotage afin d'assurer la possibilité de faire varier la puissance suffisamment rapidement, jusqu'à 5% de la puissance nominale par minute dans la plage de puissance de 50 à 100% de la puissance nominale (centrales nucléaires françaises) [4].

La variation de la demande de puissance du réseau entraîne une variation au niveau du rotor du générateur. L'augmentation de la demande de puissance, par exemple, entraîne une diminution de la rotation du générateur et de l'arbre de la turbine. En conséquence, la vanne d'entrée de la turbine est ouverte. Le débit de vapeur à l'entrée de la turbine est augmenté afin d'accroître le travail produit jusqu'à la valeur demandée par le réseau. La pression et la température de la vapeur diminuent également. Dans le circuit primaire, la température moyenne diminue et les effets de contre-réactions font augmenter la puissance du cœur. Cette séquence d'événements permet de maintenir un équilibre de puissance entre les systèmes primaire et secondaire. De cette manière, la température n'est cependant pas directement contrôlée et peut varier dans une grand intervalle. La réactivité est donc activement contrôlée afin de piloter la température et de la maintenir à sa valeur de consigne [5] [6]. Ce système est basé sur l'insertion ou l'extraction des barres de contrôle et sur la dilution du bore soluble dans l'eau (dans les réacteurs type REP) [7].

Le système décrit ci-dessus est complexe et caractérisé par plusieurs sous-systèmes pilotés de manière active. La complexité est liée à la nécessité d'optimisation du système pour assurer le meilleur suivi de charge possible. De plus, cet ajout de systèmes entraîne potentiellement une augmentation des coûts de la centrale ainsi qu'une augmentation du risque d'erreur humaine et de défaillance des systèmes, et donc la nécessité de prévoir des systèmes redondants pour respecter les exigences de sureté.

0.2. Objectif et démarche de la thèse

0.2.1. Objectif de la thèse

L'approche actuelle de la conception des réacteurs est axée sur le suivi de la charge pour compenser les déséquilibres du réseau causés par l'introduction de sources d'énergie renouvelables. Cependant, il existe également des approches innovantes qui prennent en compte d'autres objectifs, tels que la

production de chaleur ou la réduction de la taille et des coûts d'investissement (comme les Small Modular Reactors par exemple).

Il peut être intéressant d'envisager une approche de conception très différente. Dans ce travail, un objectif différent de la production flexible d'électricité pour le réseau est exploré. On pourrait imaginer l'objectif de concevoir un réacteur aussi autonome que possible, c'est-à-dire que l'on démarre et que l'on laisse ensuite évoluer de manière autonome. L'idée est similaire à l'approche utilisée pour les microréacteurs destinés à produire de l'électricité ou de la chaleur pour les micro-réseaux ou l'industrie. Dans ce travail, l'idée est étendue à la production d'électricité ou de chaleur pour tout type de réseau. On peut imaginer un réacteur comme une source d'énergie, comparable par exemple à une source d'énergie renouvelable, qui est connectée au réseau, mise en marche et produit de l'énergie de manière autonome. L'avantage par rapport à une source d'énergie renouvelable est que la production exacte d'énergie est prévisible et connue pendant toute la durée de vie du réacteur, et n'est donc pas soumise à des facteurs externes (comme la météo pour l'énergie solaire).

La problématique qui motive ce travail de thèse est la possibilité de concevoir un système aussi autonome que possible, tout en maintenant un point de fonctionnement acceptable. Un tel réacteur autonome ne serait pas exploité pour suivre les demandes du réseau, mais sa production d'énergie serait établie par les opérations autonomes du cœur elles-mêmes, donc par la physique du réacteur.

0.2.2. Démarche du travail

Dans la bibliographie, plusieurs concepts de réacteurs sont proposés pour différents objectifs. Les microréacteurs, d'une part, sont des designs définis avec une faible puissance thermique. Ils se caractérisent par des designs simplifiés et des caractéristiques autonomes augmentées, avec l'objectif de produire une énergie constante sans exigences spécifiques de suivi de charge. D'autre part, les réacteurs de puissance sont optimisés pour la production d'une grande quantité d'énergie en fonction des besoins du réseau électrique et se caractérisent par des systèmes complexes de contrôle pour le pilotage.

L'étude des réacteurs autonomes est basée sur l'analyse des conceptions existantes mais adaptées afin d'être pilotées de manière autonome. Parmi ces réacteurs, quatre concepts ont été retenus dans le cadre de ce travail : deux concepts de microréacteurs, que sont les réacteurs à caloducs (Heat Pipe Reactors) et les réacteurs à haute température (High Temperature Reactors), et deux concepts de réacteurs de puissance que sont les réacteurs à eau pressurisée (Pressurized Water Reactors) et les réacteurs à neutrons rapides refroidis au sodium (Sodium-cooled Fast Reactors).

L'approche de ce travail se résume en trois phases :

- Dans la première phase, la physique du réacteur exploité de manière autonome est abordée. Le problème concerne l'ensemble du système du réacteur : le cœur, le système de refroidissement primaire et le système de conversion d'énergie (ECS). Deux approches sont possibles :
    - la modélisation de l'ensemble des systèmes du réacteur et l'analyse de tous les systèmes couplés en même temps ;
    - l'analyse de systèmes séparés, avec le choix de l'hypothèse à fixer aux limites.

  La première approche est la plus complète mais peut prendre beaucoup de temps. Dans ce travail, la deuxième approche a été choisie. Dans un premier temps, le ECS (Energy Conversion System) est analysé et la contribution possible de ce système sur un cœur autonome est calculée. Le reste du travail se concentre donc sur l'évolution et la conception du cœur seulement en

considérant l'hypothèses de température entrée cœur constante. Dans ce résumé, cette analyse du ECS n'est pas détaillée, mais elle est présente dans le Chapitre 3 du manuscrit.

- Les concepts de cœur existants sont modélisés pour un fonctionnement autonome et leur performance associée est évaluée.
- Les réacteurs conçus à l'origine pour un fonctionnement actif présentent des performances dégradées lorsqu'ils sont convertis à un fonctionnement autonome. La troisième phase consiste donc à proposer des modifications de la conception afin d'augmenter les performances des réacteurs exploités de manière autonome. En particulier, l'insertion d'actinides et de poisons consommables dans le cœur est proposé pour répondre à cet objectif.

Dans ce résumé étendu, tout d'abord, une description des microréacteurs est présentée dans le paragraphe 0.2.3. Ensuite, la méthode physique pour l'analyse de la problématique est décrite dans le paragraphe 0.3. Puis, l'analyse des réacteurs existants, en fonctionnement autonome, est proposé dans le paragraphe 0.4 et les paramètres choisis pour définir les caractéristiques et performances d'un réacteur autonome sont présentés. Enfin, dans le paragraphe 0.5, des configurations de cœurs autonomes sont proposées pour augmenter les performances. A la fin de ce résumé, les conclusions et les perspectives du travail sont mises en évidence.

0.2.3. Les microréacteurs

La catégorie des Small Modular Reactors (SMR) suscite de l'intérêt en raison de certaines performances attendues : coût d'investissement réduit, conception modulaire plus simple et caractéristiques de sécurité renforcées [8]. Dans cette catégorie, les concepts de microréacteurs se caractérisent par une taille réduite et sont généralement définis comme des réacteurs produisant jusqu'à 20 MWe [9]. Ils ont d'abord été conçus pour un usage non commercial, par exemple pour fournir de l'énergie à des bases militaires isolées, pour des missions spatiales ou pour la propulsion navale. Ces dernières années, ce concept a commencé à être appliqué également à des fins civiles [10]. Ils peuvent être connectés à des réseaux ou à des micro-réseaux, pour fournir de l'énergie à des communautés isolées ou de petite taille, ou peuvent constituer une source locale d'énergie pour les industries. De nos jours, les générateurs diesel sont le plus souvent utilisés à ces fins. Cette technologie entraîne des coûts élevés, une dépendance à l'égard des combustibles fossiles et la production de CO_2. Une substitution par des ressources nucléaires serait bénéfique pour des raisons économiques et écologiques. Les concepts de microréacteurs se caractérisent par :

- un fonctionnement autonome du réacteur pendant toute la durée de vie, réduisant autant que possible le nombre d'opérateurs sur le site et la complexité de la conception;
- une conception simplifiée et une taille de réacteur plus petite pour inclure la possibilité de construire en usine et de transporter ensuite la quasi-totalité du réacteur sur le site;
- un cœur à longue durée de vie pour éviter l'opération de rechargement en combustible;
- différentes possibilités de production d'énergie (électricité, chaleur ou production combinée);
- la modularité de la puissance de l'installation (c'est-à-dire la possibilité d'ajouter des modules);
- une réduction des coûts d'investissement [11].

Parmi les concepts de microréacteurs, deux designs ont été choisis pour ces études car représentatifs de nombreux concepts présents dans la littérature. Une description succincte de ces réacteurs est faite dans les sections suivantes.

0.2.3.1. Réacteurs à caloducs

Les réacteurs à caloducs constituent aujourd'hui une technologie prometteuse pour les microréacteurs. Ils se caractérisent par un cœur monolithique composé d'une matrice solide avec des canaux pour les crayons combustibles et les caloducs. Ils sont considérés comme ayant un "cœur solide" en raison de la quasi-absence de pièces mobiles telles que des vannes, des barres de contrôle ou des pompes pour la circulation du caloporteur (seuls les tambours de contrôle sont mobiles, comme décrit dans la suite). Les caloducs sont des tubes étanches remplis d'un fluide à changement de phase capable de transporter la chaleur de manière complètement autonome, du cœur au système de conversion [12].

Dans ce type de réacteurs, le contrôle de la réactivité est généralement assuré par un système de tambours. Ceux-ci sont des cylindres rotatifs composés d'un matériel réflecteur (généralement du BeO ou du Be) et sur la moitié de leur circonférence d'un matériau absorbant (généralement du B_4C). Ils sont insérés dans la couche de réflecteur à l'intérieur du réacteur et sont mis en rotation pour insérer ou extraire la réactivité. Ils sont généralement utilisés pour la compensation de l'excès de la réactivité initiale [13].

0.2.3.2. Réacteurs à haute température

La catégorie des réacteurs à haute température comprend tous les réacteurs qui utilisent le combustible TRISO (TRistrictural ISOtropic fuel) pour fournir des températures élevées à la sortie du cœur. Le cœur du réacteur est caractérisé par des particules de combustible dispersées dans une matrice de graphite qui assurent de faibles gradients de température et une température relativement basse du combustible malgré la température élevée du caloporteur. Le caloporteur est généralement du gaz qui peut être chauffé jusqu'à 750 °C pour les générateurs de vapeur ou jusqu'à 950 °C pour les applications nécessitant une chaleur industrielle à haute température [14]. Dans ce type de réacteur, le contrôle de la réactivité est assuré par des barres de contrôle et des poisons consommables pour compenser l'excès de réactivité initial.

Après la description des réacteurs considérés, la méthodologie mise en place pour les étudier et les comparer est présentée.

0.3. Méthodologie

Dans toute la suite du résumé, le terme "cœur autonome" est utilisé pour définir une conception de cœur qui ne nécessite aucune intervention(s) active(s) pour maintenir un "niveau de puissance suffisant" pendant les opérations. Dans un tel système libre, à partir d'un état critique avec une puissance réduite, différents phénomènes physiques déterminent l'évolution temporelle de la puissance :

- l'épuisement du combustible entraîne une perte ou un gain de réactivité (en fonction de la configuration surgénérateur ou brûleur du cœur) ;
- les coefficients de contre-réactions insèrent de la réactivité ou de l'anti-réactivité en cas de variation de température et ou de puissance ;
- les systèmes autonomes consacrés au contrôle de la réactivité peuvent apporter de la réactivité ou de l'anti-réactivité lors de la modification de certains paramètres physiques via un système dédié.

La réactivité totale du cœur, exploité de manière autonome, peut être représentée par la somme des différents termes présentés ci-dessus. Dans l'équation suivante, la variation de la réactivité est représentée par la somme des contributions entre un instant t et l'instant suivant t+1 :

$$\delta\rho_{coeur} = \delta C_{combustible} + \delta C_{contre-réactions} + \delta C_{contrôle\ passif}\ ; \qquad (0.1)$$

où : $\delta\rho_{coeur}$ est la variation de la réactivité totale du cœur entre deux instants; $\delta C_{combustible}$ est la contribution à la variation de réactivité due à la consommation du combustible; $\delta C_{contre-réactions}$ est la contribution à la variation de réactivité due à la variation de température du cœur et $\delta C_{contrôle\ passif}$ est la contribution à la variation de réactivité insérée par les éléments de contrôle passifs dans le cœur.

Pour analyser l'impact des effets de contre-réactions sur l'évolution de la puissance, il est nécessaire de disposer d'un modèle qui tienne compte de l'aspect neutronique et thermique du cœur.

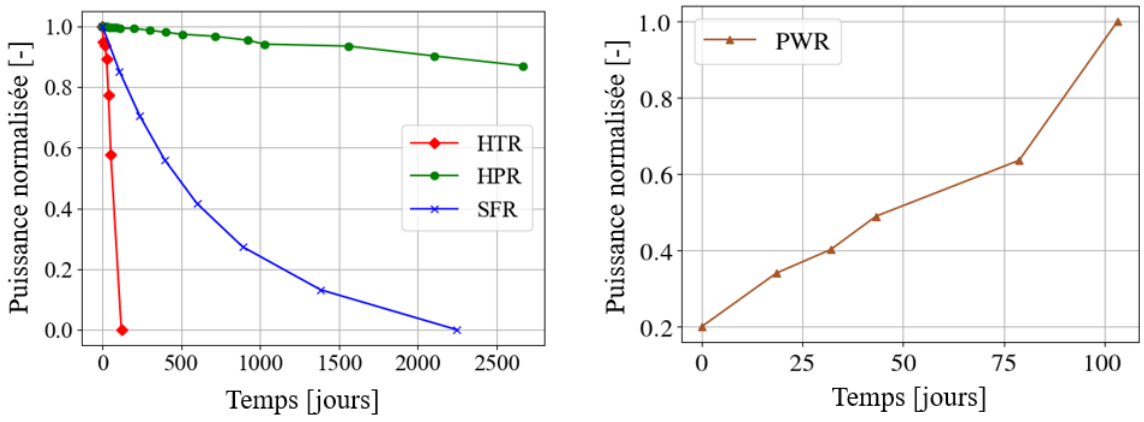
La méthode de couplage adiabatique utilisée dans ce travail est appelée KGH [15]. Cette méthode est basée sur l'hypothèse d'un équilibre statique du cœur à chaque pas de temps, ainsi la réactivité totale du cœur et la variation entre deux pas de temps est imposée à zéro à tout instant comme suit :

$$\Delta\rho_{coeur} = H\ \Delta P_{coeur} + G\ \Delta(\Delta T_{coeur}) + K\ \Delta T_{entrée} + \Delta\rho_{combustible} = 0; \qquad (0.2)$$

où : ΔP_{coeur} est la variation de la puissance du cœur [W] ; $\Delta(\Delta T_{coeur})$ est la variation de la différence de température du cœur entre la sortie et l'entrée [K] ; $\Delta T_{entrée}$ est la variation de la température du cœur à l'entrée [K] ; $\Delta\rho_{combustible}$ est la variation de la réactivité due à l'épuisement du combustible (ou éventuellement la variation due aux poisons consommables ou à d'autres méthodes de contrôle passifs) [pcm]. Enfin, les termes H, G et K sont des coefficients spécifiques qui tiennent compte des effets de contre-réactions. H prend en compte la variation de la réactivité liée à la variation de la puissance de fission ; G représente la variation de la différence de la température du cœur et K considère la variation de la température d'entrée cœur.

0.4. Comparaison des réacteurs autonomes

Tout d'abord, cette section présente l'évolution des caractéristiques des réacteurs existants opérés de manière autonome. En particulier, dans la Figure 0.1, l'évolution de la puissance est présentée.



(a) *(b)*

Figure 0.1 – Comparaison de l'évolution de la puissance des HPR, HTR et SFR (a) et PWR (b) pilotés de manière autonome.

Les réacteurs opérés de manière autonome se caractérisent par des performances très faibles par rapport aux réacteurs industriels actuels. Les performances moyennes des PWR existants (par exemple dans le parc français) consistent en une densité de puissance d'environ 100 W/cm3, un cycle du combustible de 12 à 18 mois et un taux de combustion du combustible au déchargement d'environ 50 GWj/t [90]. Le PWR exploité de manière autonome se caractérise par une durée de vie de quelques mois et un taux de combustion très faible de l'ordre de 0,3 GWj/t. Dans ce cas, la puissance est croissante et donc le réacteur est démarré à une puissance définie comme minimale pour les opérations autonomes (20% de la puissance nominale). Dans le cas du HTR et du SFR, pour les opérations autonomes, la durée de vie est de l'ordre de quelques mois ou années, mais le taux de combustion en fin de vie est très faible, de l'ordre de 2 GWd/t. Ces performances globales ne sont pas compétitives.

Une analyse plus détaillée des réacteurs à caloduc est consignée dans le Chapitre 4 du manuscrit. Ces réacteurs présentent des caractéristiques intéressantes lorsqu'ils fonctionnent de manière autonome, mais ils sont très limités en termes de densité de puissance (en raison du fonctionnement des caloducs). En raison de ses limitations intrinsèques en termes de densité de puissance, les réacteurs à caloducs sont exclus des possibilités de concept des réacteurs exploités de manière autonomes.

L'objectif de la prochaine partie du travail est d'explorer différentes manières d'augmenter les performances (via l'insertion des actinides et poisons consommables dans le cœur) de ces concepts autonomes retenus et de les comparer à celles des réacteurs industriels. Pour comparer les réacteurs obtenus, certains paramètres ont été choisis :

- La concentration d'actinides (ou des poisons consommables) [%] est la teneur en actinide (ou des poisons consommables) insérée dans le cœur;
- U-235 [%] est l'enrichissement en U-235 pour atteindre la criticité en début de vie ;
- RF [pcm/%P] est l'intégrale de contre-réactions entre 20% et 100% de la puissance nominale. Ce paramètre quantifie l'impact des coefficients de contre-réaction. Pour faciliter la lecture, il est exprimé en pcm par pourcentage de la puissance nominale (en considérant une variation linéaire) ;
- $\Delta\rho$ [pcm/EFPD] est la plage maximale de variation de la réactivité pendant la durée de vie du cœur (avec une limite de 20 % de la puissance nominale ou 60 GWd/t) ;
- BU [GWd/t] est le taux de combustion moyen atteint en fin de vie ;
- $\bar{P}$ [%Pmax] est évaluée comme la puissance moyenne de fonctionnement pendant la durée de vie considérée, 100 % correspond au cas idéal ;
- $\Delta\rho_{ECS}$ [%] est le maximum de la contribution possible de l'ECS (Energy Conversion System), caractéristique des différents types de réacteurs. Cette valeur (en pcm) est normalisée par la perte de réactivité due au burn-up pendant la durée de vie, ce qui donne un pourcentage de la contribution possible de l'ECS pour maintenir une réactivité totale critique à puissance constante du cœur. Si la valeur est égale ou supérieure à 100 %, le réacteur peut être contrôlé pendant toute sa durée de vie par la contribution du ECS. En revanche, une valeur comprise entre 0 % et 100 % indique la fraction de pcm qui peut être compensée par le contrôle du ECS.

0.5. Amélioration des performances des réacteurs autonomes

Pour améliorer les performances des réacteurs l'attention a été concentrée sur l'insertion des actinides et poisons consommables dans le cœur, avec l'objectif de réduire la perte de réactivité due à l'évolution du combustible. Pour cet objectif, l'insertion des actinides (américium, neptunium, plutonium et

thorium) a été considérée, ainsi que l'insertion des poisons consommables (bore et dysprosium). Chaque isotope a été inséré dans les cœurs PWR, HTR et SFR avec des concentrations variables. Les étapes de l'étude de chaque configuration sont :

1. calcul d'enrichissement d'U-235 afin d'avoir un réacteur critique en début de vie ;
2. calcul d'évolution de la réactivité par effet d'épuisement du combustible ;
3. calcul des contre-réactions du cœur ;
4. application de la méthode KGH pour évaluer l'effet simultané de la perte de réactivité et des contre-réaction sur l'évolution de la puissance du réacteur opéré de manière autonome.

Dans le manuscrit, une analyse détaillée est présentée et les performances de chaque configuration sont décrites. Ici, une comparaison de tous les cœurs les plus prometteurs est reportée en particulier : les HTR et PWR avec du combustible $UAmO_2$ et le SFR avec du combustible $UPuO_2$. La Figure 0.2 montre l'évolution de la puissance dans les trois cœurs exploités de manière autonome.

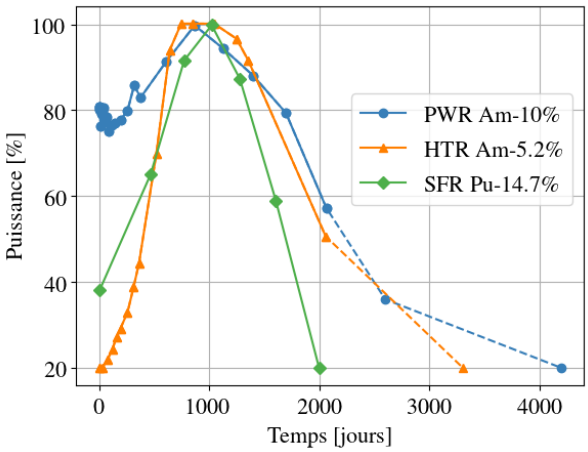


Figure 0.2 – Evolution de la puissance des cœurs exploités de manière autonome avec actinides.

Dans la Figure 0.3 les performances des trois configurations sont comparées. Cette comparaison prend en compte les configurations conduisant à une combustion de 60 GWd/t tout en obtenant un enrichissement en U-235 aussi proche que possible de 25 % afin de rester dans la gamme des combustibles HALEU (critère de faisabilité du combustible) [16].

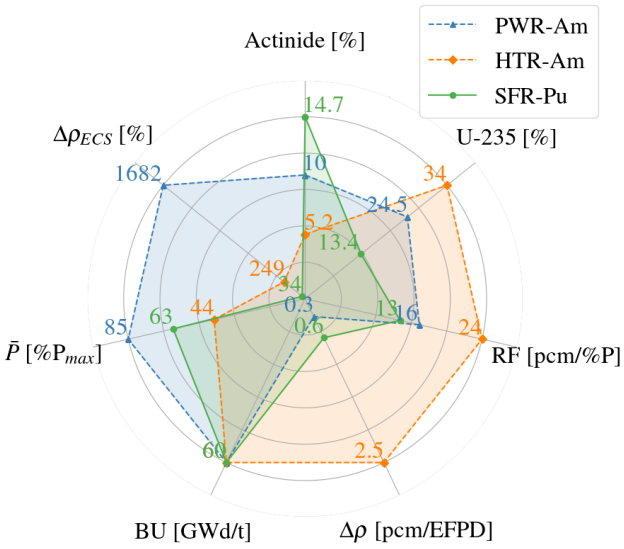


Figure 0.3 – Comparaison des performances des cœurs exploités de manière autonome avec actinides

Tout d'abord, d'un point de vue de l'enrichissement, le HTR a besoin de l'enrichissement le plus élevé (34%). En revanche, le même taux de combustion peut être atteint avec un enrichissement inférieur à la limite de 25 % dans les REP et les SFR. Pour le SFR, l'enrichissement en U-235 est nettement plus faible car le plutonium contient des isotopes fissiles. Les limites de l'enrichissement en U-235 sont choisies pour être inférieures à 25%, comparables à celles du HALEU, en estimant qu'une optimisation peut être faite pour obtenir 20%. C'est pourquoi l'enrichissement du HTR illustré dans ce cas n'est pas autorisé et qu'il convient d'opter pour des configurations à plus faible teneur en Am. Elles conduisent à des performances moindres et, pour cette raison, le HTR est considéré comme moins prometteur que d'autres réacteurs, lorsqu'il est exploité de manière autonome.

Une comparaison des paramètres physiques est ensuite effectuée, en termes d'effet de contre-réaction (CR) et fluctuation de la réactivité du au burn-up ($\Delta\rho$). L'intégrale des contre-réactions est plus importante dans le spectre thermique. En particulier, le HTR présente l'effet de contre-réactions le plus élevé. D'autre part, la perte de réactivité est plus importante dans le HTR et plus faible dans le PWR et le SFR.

En termes de puissance moyenne $\bar{P}$, globalement, les performances du PWR et du SFR sont supérieures à celles du HTR, car ces cœurs permettent une plus grande réduction de la fluctuation de la réactivité. Le REP permet d'atteindre une puissance moyenne de 85%. Cette valeur est comparable à celle des réacteurs actuels, compte tenu des périodes de maintenance et de rechargement en combustible. En d'autres termes, le REP avec insertion d'américium exploité de manière autonome peut atteindre des performances équivalentes en termes de taux de combustion et de puissance moyenne à celles d'un REP exploité activement.

Enfin, la contribution théorique possible de l'ECS est comparée sur l'axe $\Delta\rho_{ECS}$. Le système secondaire d'un réacteur thermique peut fournir une contribution théorique plus importante que le SFR, en raison du coefficient de contre-réactions plus élevé. En effet, le contrôle de l'ECS d'un PWR-Am pourrait insérer une réactivité dans le cœur qui permettrait de garantir environ 1700% de la durée de vie du cœur. Le HTR-Am pourrait être maintenu à puissance constante par le contrôle du système secondaire pendant 249% de la durée de vie. Enfin, on constate que le SFR pourrait être maintenu à puissance constante pendant environ 34 % de sa durée de vie. Cela indique qu'il pourrait être très intéressant d'exploiter un contrôle du système secondaire dans les réacteurs thermiques, alors que cela entraînerait potentiellement une augmentation moins importante des performances dans les réacteurs rapides

0.6. Conclusions et perspectives

0.6.1. Conclusions

Le mix énergétique actuel tend à l'élimination des combustibles fossiles et à l'introduction croissante des énergies renouvelables. Dans ce contexte, les centrales nucléaires doivent adopter de plus en plus le rôle de répondre aux variations des besoins du réseau, pour remplacer progressivement les centrales à combustibles fossiles. Pour cette raison, la conception et les opérations sont devenues de plus en plus complexes avec l'ajout de systèmes de contrôle actif et d'optimisation du suivi de la charge. Cette thèse se positionne en contre-courant et étudie la possibilité de simplifier la conception du réacteur. L'objectif de suivi de charge est mis de côté et une méthodologie pour parvenir à la conception d'un réacteur « exploité de manière autonome » est proposée. L'objectif est un réacteur en tant que source d'énergie,

qui est connecté au réseau ou à des applications spécifiques, mis en marche et produisant de l'énergie de manière autonome.

Un « réacteur autonome » a été défini comme un réacteur qui est démarré, laissé à sa propre évolution autonome et arrêté en fin de vie. À l'exception du démarrage et de l'arrêt, aucun système de contrôle n'est activé pendant les opérations. En d'autres termes, l'enrichissement initial du combustible est choisi pour avoir une réactivité nulle en début de vie. La physique d'un tel réacteur est caractérisée par un cœur qui produit une puissance pilotée par les effets couplés de l'épuisement du combustible et des rétroactions de réactivité. L'étude se concentre sur la physique du cœur et un modèle physique a donc été mis en œuvre pour étudier la réactivité et l'évolution de la puissance d'un tel réacteur. Il est basé sur une méthode adiabatique qui couple les champs neutronique et thermo hydraulique, appelée KGH.

La contribution potentielle de l'ECS (Energy Conversion System) a été analysée indépendamment. Le gain maximal possible sur la performance a été évalué, en considérant un contrôle théorique sur le système ECS. Ensuite, le problème a été simplifié en considérant une température constante à l'entrée du cœur et l'accent a été mis sur le comportement du cœur. Des actinides et des poisons consommables ont été ajoutés au cœur pour en augmenter les performances.

Dans le cas des réacteurs thermiques, l'insertion d'actinides ou de poisons consommables entraîne un durcissement du spectre. Ce changement de spectre a deux conséquences principales : la diminution de l'effet du xénon et un enrichissement fissile plus élevé nécessaire pour être critique en début de vie. Cette dernière conséquence entraîne une diminution globale de la perte de réactivité due à l'épuisement combustible et une diminution des contre-réactions. On observe que l'effet combiné conduit à une augmentation des performances. En d'autres termes, la diminution de la perte de réactivité prévaut sur la diminution des contre-réactions. Toutefois, pour un durcissement équivalent du spectre, l'effet sur l'évolution de la réactivité dépend toujours de l'isotope inséré. Finalement, l'américium et le dysprosium sont les plus prometteurs pour maximiser les performances du cœur. Le neptunium augmente les performances mais il est moins efficace que l'américium. Le thorium et le plutonium n'augmentent pas significativement les performances.

Dans le cas des réacteurs rapides, seul le cas de l'insertion d'actinides a été étudié. En effet, le poison consommable n'est pas efficace en spectre rapide lorsqu'il est inséré sans une optimisation spécifique. Une étude de la littérature dans laquelle une telle optimisation a été effectuée est prise comme référence pour évaluer les performances attendues pour l'insertion de poison consommable. En ce qui concerne l'insertion d'actinides, l'enrichissement initial nécessaire pour obtenir un cœur critique en début de vie est plus élevé en raison de l'augmentation des captures de neutrons. L'effet global est une diminution de la perte de réactivité due à une compensation entre l'épuisement fissile et la consommation d'actinides, et une diminution de la contribution des contre-réactions (sauf pour l'insertion de plutonium). Là encore, les performances sont accrues, ce qui signifie que l'effet de l'épuisement du combustible prévaut. Finalement, l'insertion de plutonium est le plus prometteur pour maximiser les performances du cœur. Le SFR a également été analysé dans une configuration spéciale conçue pour augmenter les effets de contre-réactions. Le fonctionnement autonome d'une telle configuration ne montre pas de performances accrues, ce qui confirme que la réduction des pertes de réactivité est plus déterminante pour le comportement autonome que l'augmentation des contre-réactions.

Le REP et le SFR ont des performances comparables en termes d'ordre de grandeur. Ils sont considérés comme des candidats possibles pour la conception de cœurs autonomes, lorsqu'ils sont chargés avec de l'Am (pour le PWR) et du Pu pour le SFR. D'autres recherches pourraient également être intéressantes en chargeant le REP avec du Dy, qui semble donner des performances intéressantes,

et en faisant varier le vecteur Pu dans le SFR pour optimiser la configuration (une étude préliminaire de ce cas est présentée dans les annexes de cette thèse).

0.6.2. Perspectives

Cette thèse présente une définition d'un réacteur autonome, qui a été développé en faisant une série d'hypothèses et en fixant certaines contraintes. En particulier, le cadre du travail est décrit comme suit :

- Un réacteur autonome est défini comme un réacteur avec un cœur autonome et un système de refroidissement primaire. Il peut également inclure un contrôle actif sur le système de refroidissement du cœur.
- Le cœur n'est pas rechargé pendant sa durée de vie, il est chargé avec du combustible neuf et déchargé à l'arrêt du réacteur. Cette approche est cohérente avec l'objectif de concevoir un cœur aussi autonome et simple que possible.
- La perte de réactivité initiale, due à l'effet xénon lorsqu'il est présent, est considérée comme compensée par un contrôle initial actif. Ce système de contrôle pourrait être le même que celui conçu pour le démarrage et l'arrêt du réacteur.

Le réexamen de ces hypothèses peut entraîner une modification de l'analyse. La liste précédente est reconsidérée en termes de perspectives :

- Le réacteur autonome pourrait être étudié en examinant d'abord un ECS autonome et en concevant ensuite le cœur pour qu'il adapte son comportement, avec un contrôle actif de la réactivité si nécessaire. Cette approche nécessiterait de se concentrer sur le système ECS, de calculer la puissance produite, lors d'opérations autonomes, et de concevoir ensuite le cœur pour produire cette puissance requise.
- Le rechargement du combustible pourrait être introduit dans le cadre du problème. Cela augmenterait le degré de complexité du cœur et réduirait son fonctionnement autonome. Cependant, cela pourrait permettre d'augmenter les performances globales. En effet, la durée de vie du cœur serait augmentée et un meilleur cycle du combustible pourrait être réalisé.
- Ce travail quantifie la perte de réactivité initiale due à l'effet xénon et suppose qu'elle est compensée par un contrôle actif initial. Cependant, ce contrôle n'est pas conçu ici. Une analyse plus approfondie pourrait être effectuée sur les systèmes de démarrage et d'arrêt du réacteur et leurs marges de réactivité. La conception spécifique pourrait déterminer s'il est pertinent de chercher à compenser l'effet du Xe ou si seuls les concepts ayant un effet faible ou nul devraient être sélectionnés.

Summary

Affidavit **2**

Liste de publications et participation aux conférences **3**

Résumé **4**

Abstract **6**

Remerciements **8**

Résumé étendu **9**

0. Résumé étendu **9**

Table des matières 9

0.1. Introduction 10

0.2. Objectif et démarche de la thèse 10

0.2.1. Objectif de la thèse 10

0.2.2. Démarche du travail 11

0.2.3. Les microréacteurs 12

0.3. Méthodologie 13

0.4. Comparaison des réacteurs autonomes 14

0.5. Amélioration des performances des réacteurs autonomes 15

0.6. Conclusions et perspectives 17

0.6.1. Conclusions 17

0.6.2. Perspectives 19

Summary **20**

Acronyms **24**

List of figures **26**

List of tables **31**

1. Introduction **33**

Summary 33

1.1. Introduction 34
1.1.1. The role of nuclear energy in the decarbonisation transition 34
1.1.2. Nuclear Power Plants connected to the electric grid 34
1.1.3. Nuclear reactors diversification 36
1.2. Nuclear power plant design and operation 37
1.2.1. Nuclear power plant systems 37
1.2.2. Nuclear power plant operation and control 39
1.3. Thesis objective 42
1.3.1. A counter-current approach to the design of nuclear reactor 42
1.3.2. How to approach the problem 43
1.4. Approach followed in the present work 45
1.4.1. Framework of the work 45
1.4.2. Approach of the thesis 46
1.5. Conclusions 47
2. Methodology 48
Summary 48
2.1. Introduction 49
2.2. Physics of an "autonomous core" 49
2.2.1. Recall on the core physics 50
2.2.2. Definition of autonomous core 52
2.2.3. Core neutronic/thermal-hydraulic interaction 54
2.3. Presentation of the chosen designs based on literature 59
2.3.1. Micro-reactors 60
2.3.2. Large-scale reactors 66
2.3.3. Sum-up of the reactors candidates for this work 68
2.4. Neutronic and thermal computational models for candidate cores 69
2.4.1. Neutronic calculation scheme 69
2.4.2. Thermal calculation scheme 70
2.5. Conclusions 75
3. Energy Conversion System contribution 77
Summary 77
3.1. Introduction 78
3.2. CYCLOP 78

3.3. Secondary system designs 79
3.3.1. PWR Rankine cycle 80
3.3.2. SFR Rankine cycle 81
3.3.3. SFR Brayton cycle 82
3.3.4. Conclusions on design of secondary system connected to an autonomous core 83
3.4. Potential contribution of the ECS to the core 83
3.4.1. Maximum theoretical variation of core inlet temperature 83
3.4.2. Control of secondary cycle for the driving of the core inlet temperature 85
3.5. Application of the KGH method with the secondary system contribution 89
3.6. Conclusions 91
4. Autonomous reactors comparison 92
Summary 92
4.1. Introduction 93
4.2. Methodology for comparing different designs 93
4.3. Comparison of reference designs 94
4.3.1. Fuel enrichment 94
4.3.2. Reactivity feedback effects 96
4.3.3. Burn-up reactivity swing 97
4.4. Comparison of equivalent designs 98
4.4.1. Burn-up reactivity swing 100
4.4.2. Power evolution 102
4.5. Criteria of definition of autonomous cores 103
4.5.1. Definition of autonomous core operation 103
4.5.2. Performance evaluation 105
4.6. Conclusions 107
5. Thermal spectrum autonomous reactors 108
Summary 108
5.1. Introduction 109
5.2. Actinides and burnable poisons 109
5.2.1. Theoretical description of actinides under irradiation 109
5.2.2. Theoretical description of burnable poisons under irradiation 111
5.3. Autonomous HTR with actinides and burnable poisons 112
5.3.1. Actinides in HTR core 112

5.3.2. Conclusion on actinides insertion in HTR 126
5.3.3. Burnable absorbers in HTR core 127
5.3.4. Conclusion on burnable absorbers insertion in HTR core 132
5.4. Autonomous PWR with actinides and burnable poisons 133
5.4.1. Actinides in PWR core 133
5.4.2. Conclusions on actinides insertion in PWR core 148
5.4.3. Burnable absorbers in PWR core 149
5.4.4. Conclusion on burnable absorbers insertion in PWR core 154
5.5. Conclusions 155
6. Fast spectrum autonomous reactors 161
Summary 161
6.1. Introduction 162
6.2. Autonomous SFR with actinides 162
6.2.1. Actinides in SFR core 163
6.2.2. Parametric study on the americium insertion in SFR fuel 166
6.2.3. Parametric study on the neptunium insertion in SFR fuel 170
6.2.4. Parametric study on the plutonium insertion in SFR fuel 173
6.2.5. Conclusions on actinide insertion in SFR fuel 176
6.3. Autonomous SMSFR with actinides 178
6.3.1. Parametric study on the americium insertion in SMSFR fuel 178
6.3.2. Parametric study on the neptunium insertion in SMSFR fuel 181
6.3.3. Parametric study on the Np and Pu insertion in SMSFR fuel 184
6.3.4. Conclusions on actinides insertion in SMSFR fuel 187
6.4. Discussion on burnable poison in SFR 187
6.5. CADOR core 189
6.6. Conclusions 191
7. Conclusions and perspectives 194
7.1. Conclusions 194
7.2. Future work 199
8. References 202
9. Annexes 210

Acronyms

AMR:	Advanced Modular Reactor
BOL:	Beginning Of Life
BP:	Burnable Poison
BWR:	Boiling Water Reactor
CANDU:	CANada Deuterium Uranium reactor
CFD:	Computational Fluid Dynamics
DPA:	Displacement Per Atom
EFPD:	Equivalent Full Power Day
EOL:	End Of Life
HALEU:	High-Assay Low Enriched Uranium
HP:	High Pressure (turbine)
HPR:	Heat Pipe Reactor
HTR:	High Temperature Reactor
HX:	Heat Exchanger
IAEA:	International Atomic Energy Agency
IPyC	Inner Pyrolitic Carbon
LFR:	Lead cooled Fast Reactor
LP:	Low Pressure (turbine)
LWR:	Light Water Reactor
MMR:	Micro Modular Reactor
MOX:	Mixed OXide (fuel)
MSR:	Molten Salt Reactor
NPP:	Nuclear Power Plant
OPyC	Outer Pyrolitic Carbon
PWR:	Pressurized Water Reactor
RBMK:	Reaktor Bolshoy Moshchnosty Kanalny
RF:	Reactivity Feedbacks
SiC	Silicon Carbide
SMR:	Small Modular Reactor

SFR:	Sodium cooled Fast Reactor
SG:	Steam Generator
SMSFR:	Small Modular Sodium-cooled Fast Reactor
SPX:	Superphénix reactor
TRISO:	TRi-structural ISOtropic fuel
WT:	Wrapper Tube

List of figures

Figure 0.1 – Comparaison de l'évolution de la puissance des HPR, HTR et SFR (a) et PWR (b) pilotés de manière autonome..... 14
Figure 0.2 – Evolution de la puissance des cœurs exploités de manière autonome avec actinides..... 16
Figure 0.3 – Comparaison des performances des cœurs exploités de manière autonome avec actinides 16
Figure 1.1 – Typical electricity demand in a day in Great Britain (from [21]). 35
Figure 1.2 – Example of energy demand fulfilment via different power sources (from [21]). 36
Figure 1.3 – Energy production and transformations in a generic nuclear power plant. 37
Figure 1.4 – NPP system scheme (based on PWR design). 38
Figure 1.5 – Overview of a reactor control system. 41
Figure 2.1 – Theoretical power evolution of a SFR core (b) with reactivity loss due to fuel consumption (a). 54
Figure 2.2 – Neutronic/thermal-hydraulic coupling principle. 55
Figure 2.3 - Neutronic/thermal-hydraulic coupling parameters. 55
Figure 2.4 – Heat Pipe Reactor scheme (a), control drums functioning scheme (b). 61
Figure 2.5 – Lithium Expansion Module scheme. 62
Figure 2.6 – Heat pipe functioning principle. 63
Figure 2.7 – Heat pipe functioning limits. 64
Figure 2.8 – Hexagonal and pebble bed HTR design. 65
Figure 2.9 – TRISO particle description. 66
Figure 2.10 – PWR plant scheme. 67
Figure 2.11 – SFR plant scheme. 67
Figure 2.12 – Loop (left) and integrated (right) structure of pool type SFR. 68
Figure 2.13 – PWR and SFR thermal calculation mean geometry cell. 72
Figure 2.14 – HPR and HTR thermal calculation scheme – mean symmetrical equivalent cell (a), ... 73
Figure 2.15 – Heat pipe thermal equivalent network model. 75
Figure 3.1 – Simplified scheme of Rankine cycle. 80
Figure 3.2 – Variation of the SG inlet temperature (a) with control over the LP re-heater flow rate (b). 81
Figure 3.3 – Variation of the SG inlet temperature and relative cycle efficiency. 81
Figure 3.4 - Variation of the SG inlet temperature and relative cycle efficiency of a Rankine-SFR. ... 82
Figure 3.5 - Variation of the HX inlet temperature without active control. 82
Figure 3.6 – Simplified scheme of Rankine (a) and Brayton (b) thermodynamic cycles. 84
Figure 3.7– Efficiency associated to the variation of SG inlet and outlet temperature of a Rankine-PWR. 86
Figure 3.8 - Control of the HP re-heater pressure (a) and control of the flow rate of the super-heater and re-heaters (b) for the control of the SG inlet temperature. 87
Figure 3.9 - Variation of cycle efficiency for the optimised case (reference) compared to the case with over dimensioned HP turbine steam extraction. 87

Figure 3.10 - Efficiency associated to the variation of SG inlet temperature of a Rankine-SFR. 88
Figure 3.11 - Control of the HP re-heater pressure (a) and control of the flow rate of the super-heater and re-heaters (b) of a Rankine-SFR. 88
Figure 3.12 – Efficiency (a) and needed control over he flow rate (b) for variable HX inlet temperatures in Brayton cycle..... 89
Figure 3.13 – Power evolution of the core with active control on the secondary system – PWR. 90
Figure 3.14 – Comparison of the power at the alternator of the PWR and SFR connected to Rankine and Brayton cycles. 90
Figure 4.1 – Reference reactors spectrum comparison. 95
Figure 4.2 – Reactivity evolution for autonomous reference reactors. 98
Figure 4.3 - Heat Pipe Reactor nominal and maximum operational power. 99
Figure 4.4 – Reactivity loss comparison for the same power density – HPR (a), HTR (b), SFR (c), PWR (d). 101
Figure 4.5 - Power evolution comparison between HPR, HTR and SFR (a) and PWR (b). 102
Figure 4.6 - HTR power evolution in completely autonomous operation 104
Figure 4.7 – Criteria for autonomous core operation. 104
Figure 4.8 – Scheme of comparison of different autonomous cores. 106
Figure 5.1 - Actinides irradiation chain. 110
Figure 5.2 - Thorium irradiation chain. 111
Figure 5.3 - Radial description of HTR core. 112
Figure 5.4 - HTR actinides fuel spectrum. 114
Figure 5.5 – Thermal utilisation factor variation as a function of graphite temperature - HTR. 115
Figure 5.6 – Reactivity evolution of HTR core loaded with actinides. 116
Figure 5.7 - Power evolution for different actinides configurations – HTR. 117
Figure 5.8 – Reactivity evolution according to variation of Am content in $UAmO_2$ HTR fuel. 118
Figure 5.9 - Power evolution for different $UAmO_2$ configurations with adapted initial value – HTR. 119
Figure 5.10 - Power evolution for different $UAmO_2$ configurations – HTR. 120
Figure 5.11 – Sum-up of the core performance for different $UAmO_2$ configurations – HTR. 121
Figure 5.12 - Reactivity evolution according to the variation of Np content in $UNpO_2$ HTR fuel. 123
Figure 5.13 - Power evolution for different $UNpO_2$ configurations – HTR. 123
Figure 5.14 - Sum-up of the core performance for different $UNpO_2$ configurations – HTR. 124
Figure 5.15 - Reactivity evolution according to the variation of Pu content in $UPuO_2$ fuel. 125
Figure 5.16 - Power evolution for different $UPuO_2$ configurations – HTR. 126
Figure 5.17 – Comparison of core performance loaded with $UamO_2$ and $UNpO_2$ – HTR. 127
Figure 5.18 – HTR reactivity evolution with boron in fuel with various contents of B-10 (a) – zoom on the first 1000 EFPD (b). 128
Figure 5.19 – Atomic content evolution relative to the initial value of B-10 (a) 129
Figure 5.20 - Reactivity evolution according to the variation of Dy content in UO_2 fuel - HTR. 130
Figure 5.21 - Power evolution for different Dy in UO_2 configurations – HTR. 131
Figure 5.22 - Comparison of core performance loaded with Dy in UO_2 – HTR. 131
Figure 5.23 – Neutron spectrum in different $UAmO_2$ configurations - PWR. 134
Figure 5.24 – Four factors formula for different UAmO2 configurations – HTR (a); PWR (b). 134
Figure 5.25 - Moderator coefficient for different Am contents depending on temperature – PWR. 135
Figure 5.26 - Moderator coefficient for different Am contents at 320°C – PWR. 136
Figure 5.27 – Burn-up reactivity swing for different $UAmO_2$ configurations - PWR. 136

Figure 5.28 – Power evolution for different $UAmO_2$ configurations - PWR. 137
Figure 5.29 - Sum-up of the core performance for different $UAmO_2$ configurations – PWR. 138
Figure 5.30 - Neutron spectrum in different $UNpO_2$ configurations - PWR. 139
Figure 5.31 - Moderator coefficient for different Np contents depending on temperature – PWR..... 140
Figure 5.32 - Burn-up reactivity swing for different $UNpO_2$ configurations - PWR. 141
Figure 5.33 - Power evolution for different UNpO2 configurations - PWR. 141
Figure 5.34 - Sum-up of the core performance for different $UNpO_2$ configurations – PWR. 142
Figure 5.35 - Neutron spectrum in different $UPuO_2$ configurations - PWR. 143
Figure 5.36 - Burn-up reactivity swing for different $UPuO_2$ configurations - PWR. 144
Figure 5.37 - Power evolution for different $UPuO_2$ configurations - PWR. 145
Figure 5.38 - Neutron spectrum in different $UThO_2$ configurations - PWR. 146
Figure 5.39 - Reactivity evolution for $UThO_2$ configuration - PWR. 147
Figure 5.40 - Power evolution for different $UThO_2$ configurations - PWR. 147
Figure 5.41 - Comparison of core performance loaded with $UamO_2$ and $UNpO_2$ – PWR..... 148
Figure 5.42 - Neutron spectrum in different UO_2 with B configurations - PWR. 149
Figure 5.43 - Burn-up reactivity swing for different UO_2 with B configurations - PWR. 150
Figure 5.44 - Power evolution for different UO_2 with B configurations – PWR. 151
Figure 5.45 - Neutron spectrum in different UO_2 with Dy configurations - PWR. 152
Figure 5.46 - Burn-up reactivity swing for different UO_2 with Dy configurations - PWR. 153
Figure 5.47 – Power evolution for different UO_2 with Dy configurations - PWR. 153
Figure 5.48 - Sum-up of the core performance for different Dy configurations – PWR. 154
Figure 5.49 - Comparison between $UAmO_2$ and Dy configurations in PWR. 155
Figure 5.50 – Comparison between $UAmO_2$ HTR and PWR. 156
Figure 5.51 - Comparison between $UNpO_2$ HTR and PWR. 157
Figure 5.52 - Comparison between Dy in UO_2 in HTR and PWR. 158
Figure 5.53 - Comparison of PWR and HTR $UAmO_2$ performance with the theoretical contribution of the ECS. 160
Figure 6.1 – Radial description of SFR core. 163
Figure 6.2 - SFR actinides fuel spectrum. 164
Figure 6.3 – Reactivity evolution of SFR core loaded with actinides. 165
Figure 6.4 - Power evolution of SFR core loaded with actinides. 166
Figure 6.5 - Reactivity evolution according to the variation of Am content in $UAmO_2$ SFR fuel. 168
Figure 6.6 – Macroscopic cross sections of the main isotopes in the UAmO2 configurations 168
Figure 6.7 - Power evolution of SFR core loaded with $UAmO_2$. 169
Figure 6.8 - Sum-up of the core performance for different $UAmO_2$ configurations – SFR. 169
Figure 6.9 - Reactivity evolution according to the variation of Np content in $UNpO_2$ SFR fuel. 171
Figure 6.10 - Macroscopic cross sections of the main isotopes in the UNpO2 configurations 172
Figure 6.11 - Power evolution of SFR core loaded with $UNpO_2$. 172
Figure 6.12 - Sum-up of the core performance for different $UNpO_2$ configurations – SFR. 173
Figure 6.13 - Reactivity evolution according to the variation of Pu content in $UPuO_2$ SFR fuel. 175
Figure 6.14 - Power evolution of SFR core loaded with $UPuO_2$. 175
Figure 6.15 - Sum-up of the core performance for different $UPuO_2$ configurations – SFR. 176
Figure 6.16 - Comparison of core performance loaded with Am, Np and Pu – SFR. 177
Figure 6.17 - Radial description of SMSFR core. 178
Figure 6.18 - Reactivity evolution according to the variation of Am content in $UAmO_2$ SMSFR fuel. 180

Figure 6.19 - Power evolution of SMSFR core loaded with $UAmO_2$. 180
Figure 6.20 - Sum-up of the core performance for different $UAmO_2$ configurations – SMSFR. 181
Figure 6.21 - Reactivity evolution according to the variation of Np content in $UNpO_2$ SMSFR fuel. 183
Figure 6.22 - Power evolution of SMSFR core loaded with $UNpO_2$. 183
Figure 6.23 - Sum-up of the core performance for different $UNpO_2$ configurations – SMSFR. 184
Figure 6.24 – Reactivity evolution according to the Np and Pu insertion in SMSFR fuel. 186
Figure 6.25 - Power evolution of SMSFR core loaded with $UNpPuO_2$. 186
Figure 6.26 - Comparison of core performance loaded with Am and Np – SMSFR. 187
Figure 6.27 - Comparison of core performance loaded with optimised configuration of BP from literature – SFR. 188
Figure 6.28 - Power evolution comparison between CADOR and V2B cores. 190
Figure 6.29 - Comparison of CADOR and V2B core performance. 191
Figure 6.30 – Comparison of SFR $UPuO_2$ performance with the possible contribution of the ECS. . 192
Figure 6.31 - Comparison of SFR and SMSFR core performance loaded with Np. 193
Figure 7.1 – Comparison of HTR-Am, PWR-Am and SFR-Pu autonomous cores. 197
Figure 9.1 – Temperature distribution in one averaged heat pipe. 214
Figure 9.2 – Temperature distribution in a thermal cell of HTR. 214
Figure 9.3 - Temperature distribution in a thermal cell of PWR. 215
Figure 9.4 - Temperature distribution in a thermal cell of SFR. 215
Figure 9.5 – Sensitivity analysis on the criterion chosen for the criticality state at BOL. 216
Figure 9.6 - Xe-135 and Sm-149 capture cross section [data from JANIS NEA, JEFF-3.1.1 [116]]. 217
Figure 9.7 – Xe-135 and Sm-149 content (a) and absorption rate (b) evolution. 218
Figure 9.8 – Xe-135 content (a) and absorption rate (b) evolution 218
Figure 9.9 – PWR reactivity evolution according to different U-235 enrichments. 219
Figure 9.10 - Comparison of absorption (a) and fission (b) macroscopic cross sections. 220
Figure 9.11 – Fission macroscopic cross section of the major fissile isotopes in PWR loaded with UO_2. 220
Figure 9.12 – Sum of U-235 and Pu-239 fission macroscopic cross sections. 221
Figure 9.13 – PWR index of spectrum evolution with burn-up, for different U-235 enrichments 222
Figure 9.14 – Xe effect according to different core powers in HTR. 223
Figure 9.15 – Reactivity loss due to Xe-effect in function of core power. 224
Figure 9.16 – Power evolution of HTR, comparison with the curve with the Xe contribution. 224
Figure 9.17 – Capture cross section of Am, Np and Th actinides compared to the U [data from JANIS NEA, JEFF-3.1.1 [116]]. 225
Figure 9.18 - Capture cross section of major Pu isotopes in MOX vector compared to the U sections[data from JANIS NEA, JEFF-3.1.1 [116]]. 226
Figure 9.19 – Evolution of the macroscopic cross sections of $UAmO_2$ (a) and $UNpO_2$ (b) 227
Figure 9.20 - Evolution of the index of spectrum of $UAmO_2$ and $UNpO_2$ configurations. 228
Figure 9.21 – Evolution of the content of Am and Np in $UAmO_2$ and $UNpO_2$ configurations (a) and evolution of the Pu-239 content in $UAmO_2$ and $UNpO_2$ configurations (b). 228
Figure 9.22 - Reactivity evolution according to variation of Am content in $UAmO_2$ HTR fuel – analysis on low Am contents. 229
Figure 9.23 – Neutron spectrum comparison between t0=0 EFPD and t1=200 EFPD (a) and evolution of the index of spectrum (b), for different Am contents. 230
Figure 9.24 – Absorption and generation mean macroscopic cross section comparison in $UAmO_2$ configuration, with 0.05% (a) and 10% (b) Am contents. 230

Figure 9.25 – HTR $UAmO_2$ evolution of fission macroscopic cross sections for different Am contents – 0.05% (a) and 10% (b). 231
Figure 9.26 - HTR $UAmO_2$ evolution of capture macroscopic cross sections for different Am contents – 0.05% (a) and 10% (b). 231
Figure 9.27 - Neutron spectrum comparison between t0=0 EFPD and t1=1000 EFPD (a) and evolution of the index of spectrum (b), for different Np contents. 232
Figure 9.28 – Reactivity evolution according to the variation of the Pu vector in MOX fuel in HTR. 235
Figure 9.29 – Reactivity evolution according to specific configuration of Pu vector in MOX fuel in HTR. 236
Figure 9.30 – TRISO particle with an additional burnable poison (BP) thickness. 239
Figure 9.31 – Neutron spectrum of HTR with burnable poison (BP). 240
Figure 9.32 – HTR reactivity evolution with burnable poisons in different configurations. 241
Figure 9.33 – HTR power evolution with burnable poisons in different configurations..... 241
Figure 9.34 – Variation of the moderator coefficient depending on the U enrichment (a) and the Am content (b). 242
Figure 9.35 – Four factor formula in UO_2 PWR with variation of U enrichment. 243
Figure 9.36 - Four factor formula in $UAmO_2$ PWR with variation of Am content, with U enrichment of 1.05% (a) and 8% (b). 243
Figure 9.37 - Four factor variation in $UAmO_2$ PWR with variation of Am content, with U enrichment of 1.05% (a) and 8% (b). 244
Figure 9.38 – Macroscopic cross sections evolutions of the SFR loaded with minor actinides –..... 246
Figure 9.39 - Variation of the Pu vector in MOX fuel in HTR. 249
Figure 9.40 – Reactivity loss variation sensitivity to the reactor volume – HTR (a), SFR (b). 251
Figure 9.41 - Radial cross sections of SFR core. 253
Figure 9.42 - Radial cross sections of SMSFR core. 253
Figure 9.43 – Radial cross sections of SFR and SMSFR fuel assemblies – fuel (red), sodium (yellow). 254
Figure 9.44 – Axial coordinate of the SFR and SMSFR fuel assemblies (LP and UP: respectively Lower and Upper Plenum, SH: Shielding, GAS: gas plenum). 254

List of tables

Table 2.1 – Reference reactors characteristics. 69
Table 3.1– Rankine cycle coupled to PWR and SFR. 79
Table 3.2 – Theoretical PWR and SFR active control over the secondary system. 85
Table 4.1 - Reference reactor designs characteristics. 94
Table 4.2 - Reference reactors enrichment. 94
Table 4.3 - Reference reactors spectrum index. 95
Table 4.4 - Reactivity feedback coefficients of the reference reactors. 96
Table 4.5 - Reference and comparison power density of different reactors. 100
Table 4.6 – Comparison of equivalent reactor designs. 103
Table 5.1 – Sum-up of the HTR core characteristics. 112
Table 5.2 - MOX reference isotopic vector. 113
Table 5.3 - HTR actinides insertion configuration. 113
Table 5.4 – HTR actinides “spectrum index”. 114
Table 5.5 – Reactivity feedbacks for different actinides configurations - HTR. 115
Table 5.6 – Variation of the content of americium in $UAmO_2$ HTR fuel. 117
Table 5.7 - Reactivity feedbacks for different $UAmO_2$ configurations - HTR. 118
Table 5.8 – Comparative parameter of autonomous UO_2 core – HTR. 120
Table 5.9 - Variation of the content of neptunium in $UNpO_2$ HTR fuel. 122
Table 5.10 - Reactivity feedbacks for different $UNpO_2$ configurations - HTR. 122
Table 5.11 - Variation of the uranium enrichment in $UPuO_2$ HTR fuel. 125
Table 5.12 - Reactivity feedbacks for different $UPuO_2$ configurations - HTR. 125
Table 5.13 – Mean absorption cross section of major burnable poisons [101]. 127
Table 5.14 – Variation of the content of B-10 merged inside UO_2 fuel and relative U-235 enrichment. 128
Table 5.15 - Variation of the content of Dy merged in UO_2 fuel - HTR. 130
Table 5.16 - Reactivity feedbacks for different Dy in UO_2 configurations - HTR. 130
Table 5.17 - Variation of the content of americium in PWR fuel. 133
Table 5.18 – Doppler coefficient for different UAmO2 configurations - PWR. 135
Table 5.19 - Comparative parameter of autonomous UO_2 core – PWR. 138
Table 5.20 - Variation of the content of neptunium in PWR fuel. 139
Table 5.21 - Doppler coefficient for different $UNpO_2$ configurations - PWR. 140
Table 5.22 - Variation of the content of plutonium in PWR fuel. 143
Table 5.23 - Doppler coefficient for different $UPuO_2$ configurations - PWR. 143
Table 5.24 - Moderator coefficient for different $UPuO_2$ configurations at 320°C - PWR. 144
Table 5.25 - Variation of the content of thorium in PWR fuel. 145
Table 5.26 - Doppler coefficient for different $UThO_2$ configurations - PWR. 146
Table 5.27 - Moderator coefficient for different $UThO_2$ configurations at 320°C - PWR. 146
Table 5.28 - Variation of the content of boron in PWR fuel. 149
Table 5.29 - Doppler coefficient for different UO_2 with B configurations – PWR. 149
Table 5.30 - Moderator coefficient for different UO_2 with B configurations at 320°C - PWR. 150

Table 5.31 - Variation of the content of dysprosium in PWR fuel. 151
Table 5.32 - Doppler coefficient for different UO_2 with Dy configurations – PWR. 152
Table 5.33 - Moderator coefficient for different UO_2 with Dy configurations at 320°C - PWR. 152
Table 6.1 – Sum-up of the SFR core characteristics. 162
Table 6.2 – SFR actinides insertion configuration. 163
Table 6.3 – Doppler constant of SFR core with actinides. 164
Table 6.4 – Reactivity feedback coefficients of SFR core with actinides. 164
Table 6.5 - Variation of the content of americium in $UAmO_2$ SFR fuel. 166
Table 6.6 - Doppler constant of SFR core with $UAmO_2$. 167
Table 6.7 – Reactivity feedback coefficients of SFR core with $UAmO_2$. 167
Table 6.8 - Variation of the content of neptunium in $UNpO_2$ SFR fuel. 170
Table 6.9 - Doppler constant of SFR core with $UNpO_2$. 170
Table 6.10 – Reactivity feedback coefficients of SFR core with $UNpO_2$. 171
Table 6.11 - Variation of the content of plutonium in $UPuO_2$ SFR fuel. 174
Table 6.12 - Doppler constant of SFR core with $UPuO_2$. 174
Table 6.13 - Reactivity feedback coefficients of SFR core with $UPuO_2$ 174
Table 6.14 – Sum-up of the SMSFR core characteristics. 178
Table 6.15 – SMSFR americium insertion configurations. 179
Table 6.16 - Doppler constant of SMSFR core with $UAmO_2$. 179
Table 6.17 – Reactivity feedback coefficients of SMSFR core with $UAmO_2$. 179
Table 6.18 - SMSFR neptunium insertion configurations. 182
Table 6.19 - Doppler constant of SMSFR core with $UNpO_2$. 182
Table 6.20 – Reactivity feedback coefficients of SMSFR core with $UNpO_2$ 182
Table 6.21 - SMSFR neptunium and plutonium insertion configurations. 185
Table 6.22 – Doppler constant of SMSFR core with neptunium and plutonium. 185
Table 6.23 - Reactivity feedback coefficients of SMSFR core with neptunium and plutonium. 185
Table 6.24 – CADOR and SFR-V2B comparison of UO_2 configurations. 189
Table 6.25 - Reactivity feedback coefficients of CADOR core. 190
Table 6.26 – Reactivity loss comparison between CADOR and V2B cores. 190
Table 9.1 - Characteristics of the reference MSR core 211
Table 9.2 – Geometrical dimensions of the reference MSR core. 212
Table 9.3 - Sensitivity of the HTR fuel enrichment on the reactivity at BOL. 217
Table 9.4 – Xe effect on the initial reactivity loss according to different core powers in HTR. 223
Table 9.5 – Variation of Pu isotopes inside the Pu vector 234
Table 9.6 – Configurations of the sensitivity analysis on the Pu isotopes contents. 236
Table 9.7 - Sensitivity analysis on the Pu isotopes and associated Pu content for criticality at BOL. 236
Table 9.8 – U-235 enrichment for different configurations of burnable poison insertion in HTR. 240
Table 9.9 - Reactivity feedbacks for different burnable poisons configurations - HTR. 240
Table 9.10 – Variation of Pu isotopes inside the Pu vector 247
Table 9.11 – Pu equivalence coefficients relatives to the variation of the Pu vector. 248
Table 9.12 – HTR and SFR reduced volumes cores comparison. 251
Table 9.13 – SFR and SMSFR power and volumes comparison. 252
Table 9.14 - SFR and SMSFR geometry characteristics comparison. 252

Chapter 1

Introduction

Summary

1.1. Introduction 34

1.1.1. The role of nuclear energy in the decarbonisation transition 34

1.1.2. Nuclear Power Plants connected to the electric grid 34

1.1.3. Nuclear reactors diversification 36

1.2. Nuclear power plant design and operation 37

1.2.1. Nuclear power plant systems 37

1.2.2. Nuclear power plant operation and control 39

1.2.2.1. Reactor operation 39

1.2.2.2. Reactor control 40

1.3. Thesis objective 42

1.3.1. A counter-current approach to the design of nuclear reactor 42

1.3.2. How to approach the problem 43

1.4. Approach followed in the present work 45

1.4.1. Framework of the work 45

1.4.2. Approach of the thesis 46

1.5. Conclusions 47

1.1. Introduction

In the last decades, the attention on the climate change issue has grown, up to the acknowledgement of the urgent need to change the approach to energy consumption and production. A growing number of countries has shown commitment to the goal of carbon neutrality by 2050. This goal refers to the decarbonisation of energy production and CO_2 capture, to achieve net zero carbon emissions. This objective is believed to be mandatory in order to contain the global warming to 1.5 °C temperature increase (with respect to the pre-industrial level) [1]. The main pathway for this objective includes the reduction, and ideally elimination, of all fossil fuels for energy production and their replacement with renewable and nuclear power. Furthermore, the CO_2 capture and removal is foreseen, together with the reduction of energy consumption and the increase of efficiency in energy production and use [2].

1.1.1. The role of nuclear energy in the decarbonisation transition

Nuclear energy appears to play an important role in this context of energy transition. It contributes to the carbon production only in the fuel production and plant construction phase. The estimation of the CO_2 produced by nuclear energy over its entire lifetime is about 1.18% with respect to the coal power plant emissions. It is comparable to the wind-based power plant and inferior to the contribution of solar energy [17].

Nowadays, the final energy consumption is divided between 44% for electricity and heat supply, 26% for transportation needs, and the remaining share concerns the industry needs, buildings and other applications. On the other hand, the energy production has also multiple sources. The world electricity production, for example, is supplied mainly by coal and gas fuels (together about 60% of the world electricity production suppliers), followed by hydroelectric (16%) and nuclear (10%) [18]. Nuclear energy appears to be a potential mean to eliminate the contribution of fossil fuels. The French supply repartition is an example of distribution of the sources already based on nuclear power. For an historical need of energetic independence and security of fuel supply, the French electric production is based on 75% on nuclear power [19]. The role of nuclear supply in the electrical system will be investigated in the next paragraph.

1.1.2. Nuclear Power Plants connected to the electric grid

Nuclear energy has seen an important growth between 1970 and 1985, when the worldwide number of nuclear reactors has risen from 80 to 360 [20]. After 1986 nuclear development has slowed down due to the increase of oil utilisation and the change of worldwide perception of nuclear power due to Chernobyl accident. Nowadays, 32 countries use nuclear in their energy mix and the concerns over climate change is focusing attention on the possible developments, uses and applications of nuclear energy. Nuclear Power Plants (NPPs) have historically been designed for large-scale electricity production and insertion in the grid.

The electrical grid is a system composed of energy suppliers (as, for example, fossil fuels or nuclear power plants), means of electricity transportations (as high or low voltage power lines) and final energy users (as the industries or domestic energy consumers).

Since its creation, the electrical grid has evolved in terms of size, necessities and supply sources. At the beginning of the energy production, there was no unique and large electrical grid available, energy producers were localised closely to the consumers. With the increase of the energy demand, an extended grid was created, connecting more centralised and larger power producers and distributing the electricity

to remote users. The electrical grid has kept growing and has become more and more complex, being interconnected at international levels and with the introduction of a more liberalised market [4].

The main objective of this complex system is to manage to maintain, at each instant, the equilibrium between energy production and consumption. This task is challenging as both energy production and consumption can vary over time. Energy demand fluctuates on different time scales: there are fluctuations during the day (for example, the energy demand is lower at night, as shown in Figure 1.1), the week (generally lower energy demand during the week-end) and the season of the year (in colder regions for example, the summer energy demand is lower). The variation of the users' needs depends also on the less predictable weather conditions (for example for buildings heating).

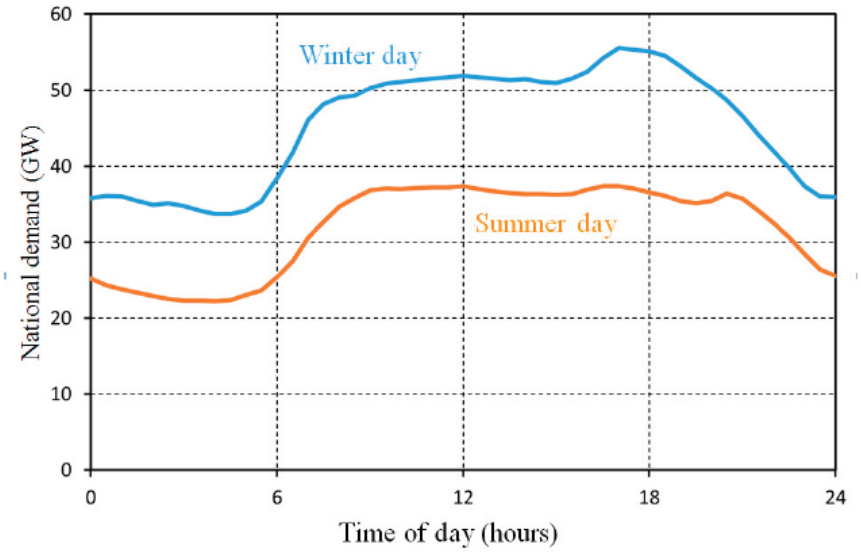


Figure 1.1 – Typical electricity demand in a day in Great Britain (from [21]).

On the other hand, energy suppliers are also characterised by fluctuations. With the growing concern on the climate crisis, renewable energy sources have spread. Their introduction in the electrical grid has led to a higher level of fluctuation of power supply depending on the renewable source conditions (for example the weather conditions in case of solar energy or the wind conditions for the wind-powered plant) [21].

In this context, the role of nuclear energy, as supplier in the electric grid, has changed in time (particular reference is made to the French case in this section). Initially, the grid variations were less large and mainly absorbed by fossil fuel plants. The nuclear power supply was connected to the grid mainly as a constant contribution to the energy production. Indeed, the NPPs were operated in base-load mode, thus producing a constant nominal electric power. With the introduction of renewable sources in the grid and the propensity to shift towards the elimination of carbonised sources, the necessity of power fluctuations accommodation has been readdressed to nuclear power plants [3]. In Figure 1.2, an example of total energy demand is shown. The contribution of the renewable is highlighted and the residual demand is shown. In the past, the nuclear constituted a base load, providing a constant contribution to the remaining demand and the fossil fuel plants accommodate the remaining fluctuation. The prevailing trend suggests that nuclear power will become increasingly utilized to meet the growing demand for electricity, particularly during periods of fluctuating demand.

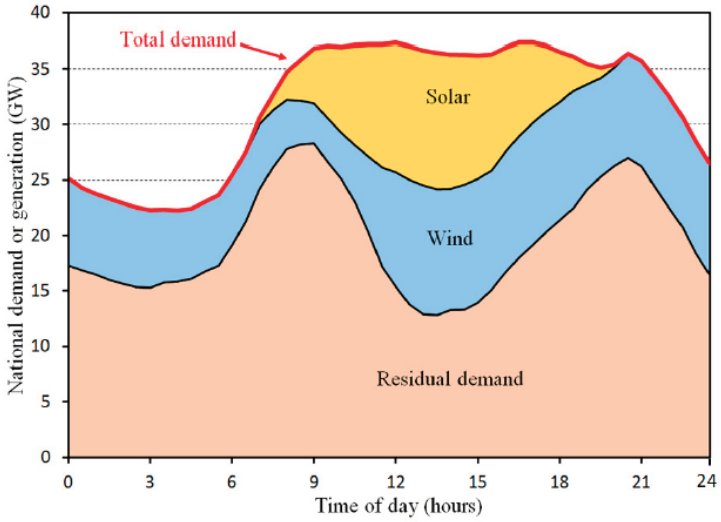


Figure 1.2 – Example of energy demand fulfilment via different power sources (from [21]).

1.1.3. Nuclear reactors diversification

NPPs have historically been thought to produce a high amount of energy in order to benefit from the scale effect. However, other possible applications have started to emerge recently. Energy needs are actually diverse, and nuclear energy could be used in order to provide more than just electricity. The nuclear energy can be employed for the heat production, uniquely or combined to electric production (in cogeneration plant). The possibility to use nuclear source for hydrogen generation is also foreseen, together with the possible use for desalinisation or specific industries that need high temperatures heat (e.g. in cement or steel factories).

In the last decades, innovative nuclear reactors have been under study. In particular, reactors for energy production are classified into four generations depending on the design characteristics, the level of safety and the economic aspects. The currently employed reactors for energy production are the ones belonging to generation II such as Light Water Reactors (LWR). The generation III and III+ includes water reactor with enhanced safety features, while the generation IV is focusing on the improvement of the economical characteristics, sustainability, reliability, safety issues, waste minimization and proliferation prevention. In this category, new designs are proposed such as Liquid Metal cooled Reactors, High Temperatures Reactors and Molten Salt Reactors [22].

Furthermore, due to the diversification of the possible reactors uses, smaller designs are currently investigated, the SMR (Small Modular Reactors). They are designed to contribute to the energy production in different fields and allow the modularity of nuclear plant, decreasing the investment costs. Among this category, the Micro Modular Reactor (MMR) concepts are characterised by a very reduced size, being usually defined as reactors producing up to 20 MW_e [9]. The objective of micro-reactors is to be used to produce electricity and/or heat for an industrial purpose; to be placed in micro-grids in isolated communities or in defence installations. The main performance expected from a micro-reactor is to be able to produce energy as autonomously as possible, reducing the number of operators and simplifying operation as far as possible.

In conclusion, the NPPs have historically been used to produce large scale base-load energy supply to the electric grids. The paradigm is changing in the present as the nuclear plants are more and more adapted to operate in load-following mode to accommodate the energy variation demands. In addition,

innovative designs starts to be proposed, diversified in terms of applications and objectives. The next section will focus on the generic description of reactor design, operation and control.

1.2. Nuclear power plant design and operation

As explained in the previous paragraph, the electric production system is changing its approach. The change in needs, insertion of renewables in the grid, localised energy production have increased fluctuations of the grid and have pointed out the necessity to manage this evolving system. The NPPs, in particular, have to adapt its operation to these changing grid necessities. The base-load energy production has more and more set aside toward a load-following nuclear system. In this section this adaptation is described in more detail.

At first, the description of the design of a traditional "electricity supplier" Nuclear Power Plant is given. An outline of the NPP systems and their major component is show. A brief description of the different kind of plant is also provided. Secondly, the operation of the reactor is described. The different phases, as start-up, energy production or shutdown are described and the control and driving systems needed for the reactor operation are presented.

1.2.1. Nuclear power plant systems

The nuclear power plant is a system that converts the thermal energy of the neutron fission into electric energy to be connected to the grid. This energy production is possible through multiple sub-systems and various energy transformations. First, in the core of the reactor, the fissile nuclei are split due to a neutron collision and heavy nuclei fission process, and a large thermal energy is released. This fission thermal energy is removed from the core via a primary cooling system that transports energy from the core to the secondary system (if the secondary system is included in the plant design, as explained hereinafter). The heat in the secondary system is transformed into mechanical work via the use of turbines. Finally, in the generators, the mechanical work at the turbine shaft is converted into electrical energy and adapted to be connected to the electrical grid. A simplified overview of the system is summed up in Figure 1.3.

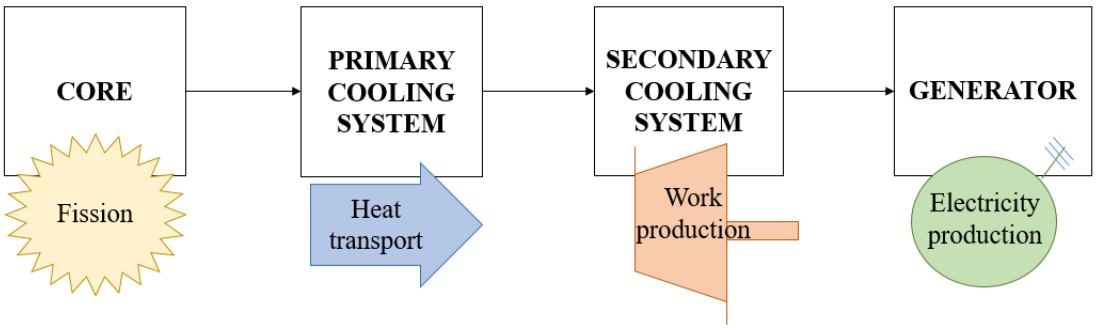


Figure 1.3 – Energy production and transformations in a generic nuclear power plant.

Each system changes according to the Nuclear Power Plant type. In this first description, the outline of the NPP will be provided for a Pressurised Water Reactor (PWR) type. In the following of this chapter, the other reactor types will be introduced and the differences in the design will be highlighted in comparison to the PWR.

The core of the reactor is composed of multiple components and materials, such as fuel, coolant, moderator (if any), structural materials, shielding system and control system for the reactivity management. The fuel part of the core contains fissile isotopes in order to enable a sustainable chain reaction. The most common element used as a fuel is the uranium that generally has to be enriched in U-235 to provide sufficient fissionable nuclei. The coolant flows in the core to remove the fission heat and to transport it in the primary system. The moderator (if present in the reactor design, as explained hereinafter) has the role of slowing down neutrons in order to work in an energy range where cross-sections are higher. Neutron moderation is a way to reduce the initial fuel enrichment. Structural materials are necessary to guarantee the integrity and the mechanical stability of the core. The shielding system is present in the core periphery and has the role to absorb radiation and to prevent their release into the environment, during normal operation and in case of accident. Finally, the reactivity control system is generally constituted by control rods (and boron dissolved in the coolant for Pressurized Water Reactor designs, as explained in the following). The control rods are composed of a material that has large neutron absorption cross section. They are inserted or withdrawn from the core according to the necessity to decrease or increase the neutrons population and consequently the fission power produced.

The primary cooling system is constituted by a coolant that flows into the core and transfers the heat to the secondary system through pipes and components as heat exchanger and pumps. The primary coolant is heated up in the core, mainly by convection due to the fluid flowing in the core. It is transported through a pipe to a heat exchanger, where the coolant transfers the heat to the secondary system. Then the primary coolant is sent again to the core via primary pump that ensures the fluid circulation. In the specific case of PWR, the primary system is also characterised by a pressurizer, which aims to keep the correct operational pressure in the circuit.

The Energy Conversion System (ECS) system (or secondary system) is composed of the heat exchanger, the turbine, the condenser and the secondary pump. The secondary coolant is heated up to evaporation in the heat exchanger, the steam is sent to the turbine, where it is used to produce mechanical energy at the turbine shaft. At the turbine outlet, the steam moves to a condenser that turns it into liquid. Finally, the coolant is sent to the heat exchanger inlet via a secondary pump that ensures secondary fluid circulation. The electric generator converts the rotational energy of the turbine shaft into electrical energy. This energy is adapted in terms of phase and tension to be connected to the grid and then distributed to the users via the electrical lines.

The simplified representation of the above mentioned systems is made in Figure 1.4.

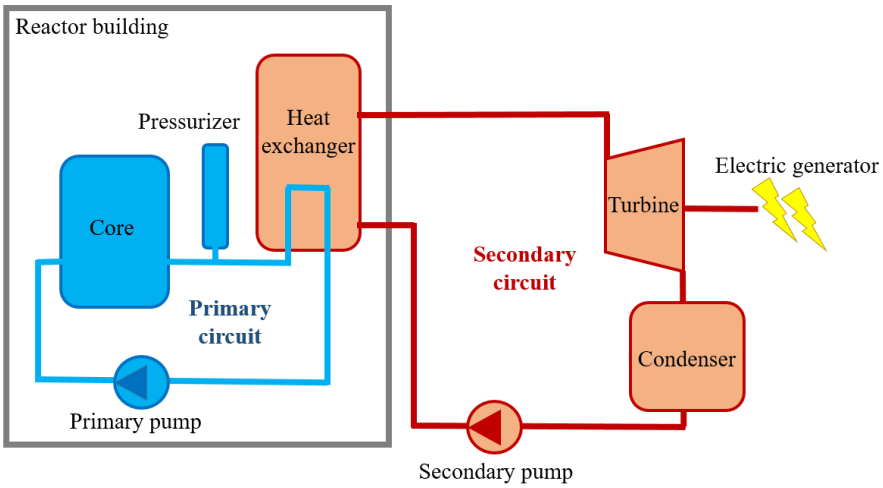


Figure 1.4 – NPP system scheme (based on PWR design).

The representation given up to now, is made based on the specific design of PWR that is one of the most common plant design. Other reactor designs exist and differ from the previous one by their system characteristics and cooling fluids. In general, the cooling fluids implied can be water, liquid metals, gas or molten salt. The water cooled reactors are distinguished in PWR, Boiling Water Reactor (BWR) and heavy water reactors. The BWR has similar characteristics of PWR but the primary water changing phase in the core and is directly sent to the turbine without secondary system. The heavy water reactors, called CANDU (CANadian Deuterium Uranium) are characterised by D_2O cooling and natural uranium fuel. In these above-mentioned reactors, water in the core has the dual function of coolant and moderator. In other reactor types, the moderator can be solid, like in High Temperature Gas Reactors (HTR) or the RBMK for water cooled reactor. In the HTR, the primary cooling fluid is gas and the neutron moderation is ensured by a solid graphite matrix. Other reactors types are characterised by the absence of a neutron moderator, such as Sodium or Lead cooled Fast Reactors (SFR or LFR). They are concepts characterised by fast neutrons spectrum and cooled by liquid metals. Finally also molten salt are foreseen to cool the reactor core, including innovative design where the fuel is merged and circulating in the coolant [23].

1.2.2. Nuclear power plant operation and control

In this section, an overview of the operation of a NPP is given. The operation needed to exploit a reactor are presented and the control systems are described.

1.2.2.1. Reactor operation

The main operation required during the reactor life can be summed up as: start-up of the plant, energy production phase, maintenance, refuelling period, scheduled shutdown or emergency and incidental shutdown.

The start-up is characterised by multiple phases. First, the reactor primary and secondary systems are heated up from “cold” (low temperature and pressure) to “hot” conditions. Successively, the core power level is increased from zero to a low power state. Finally, the core is led to the operational necessary power. The shutdown of the reactor follows the inverse process. When the fission power of the core is brought back to zero, the thermal power produced in the core is still to be evacuated and the cooling system has to be kept in operation for the decay heat removal even after reactor shutdown [24].

The refuelling phase is necessary when the fuel loaded in the core is depleted and the excess reactivity is exhausted. In PWR, for example, after a 12-months fuel cycle (18 or 24 for the modern PWRs) the reactor is shut down for a couple of weeks for the refuel. Generally, it consists of the removal and substitution of 1/3 of the core assemblies. Indeed, in the PWR design, the fuel management is organised in batch. The initial core is loaded with different assemblies with different enrichments and during the refuelling the 1/3 of the depleted assembly is removed while the others are rearranged. The objective is to guarantee a flat flux distribution and to optimize the fuel exploitation. During the same outages periods (scheduled or unforeseen), the maintenance is made on the reactor systems to guarantee the safety level necessary for operation [25].

The main phase among the reactor operation is the energy production. Different operational modes are possible, according to the needed energy supply to the grid. If the power produced from the NPP is constant, the reactor is operated in base-load mode. On the other hand, the power introduced to the grid can be variable, according to a scheduled program or arbitrarily varied according to the current grid necessity. The first, constant-load, operational mode consists of inserting the reactor in the grid as a pile, with constant power supply to the grid. This method was largely used in the past. Nowadays, with larger

energy needs and larger grids, more power suppliers are connected and provide energy at different rates. For example, with the introduction of renewable energy sources, the power supply has become variable and not always predictable. Consequently, the fluctuations in the grid depend on both the varying needs of the users and the availability of the power supply. For example during winter season, more energy is needed to provide buildings heating, while in spring this need is lowered. On the other hand, the energy supply, especially from renewable, depends on the source availability. For example the presence of the sun or the wind respectively in zones with solar and wind-powered plants [26]. The NPP could increasingly be expected to accommodate their power and be used in load-following mode. This kind of operational mode is distinguished in scheduled or arbitrarily load-following. The first foresees the reactor operating at partial power for scheduled period of time, when the need of the grid is reduced. On the other hand, the arbitrary load-follow allows the reactor to accommodate the variation of the grid necessities including relatively fast transients, up to 5% of power per minute in the power range of 20-100% of the nominal power (example according to the limitation set for the French NPPs) [4].

The constant or load-following operational modes have both advantages and drawbacks. In the first case, the total electricity generation cost over reactor lifetime is lower as the reactor operates always at its nominal power. Furthermore, the reactor materials are submitted to lower mechanical stresses. Indeed, in the load-following mode, the frequent load variation requires more expensive components and more reactor maintenance due to the thermal cycles. Also instrumentations and controls are more extended and expensive. On the other hand, load-following mode allows to accommodate the grid necessities with quick loading variation capabilities and shorter start-stop periods. Otherwise, the grid variations have to be accommodated by other non-nuclear energies suppliers that are generally carbonised sources [27].

In conclusion, regarding the operation mode, the NPPs can be exploited according to two different approaches, the base-load or the load-following reactor mode. In the next section, the control method of the NPP, for both the load-following or constant-load modes, is presented.

1.2.2.2. Reactor control

Two control methods are possible during the reactor lifetime, referred in particularly to a generic NPP operating in France. The first is the “core-driven” mode, used when the reactor is not connected to the grid, as in the start-up phase. In this mode, the core reactivity is driven and the produced power is not influenced by any other constraints from the secondary system, which follows the core operation. On the other hand, the “secondary-driven” mode designs a reactor with a power load imposed by the grid at the turbine and the core system controlled to follow the turbine. This second method is the one used during the power production phase and load-following.

In Figure 1.5, a simplified scheme of a reactor control system for reactor operation is presented. The main core, primary and secondary systems, described above, are represented with the main information exchanged through the components and the controllers. The system is complex and many parameters govern the control strategies over the core power, primary and secondary systems operation. In load-following mode, the system operation is imposed from the lower part of the graph to the top. In PWR, the increase in the power demand, for example, causes a decrease of the generator rotation and of the turbine shaft. To adapt the NPP power production, a control on the turbine inlet valve is made. The steam flow rate at the turbine inlet is increased and so the produced work up to the grid demanded value. The steam quantity at the steam generator decreases and consequently the associated pressure and temperature decrease too. In the primary circuit, the mean temperature decreases and the reactivity

feedback effects make the core power increase. This sequence of events makes it possible to maintain a balance of power between the primary and secondary systems. In this way, however, the core temperature is not directly controlled and can vary over a wide range. So, the reactivity is actively controlled in order to drive the temperature and to keep it to its design value [5] [6].

The reactivity control system is acting both on control rods and chemical shim. The control rods are made of neutrons absorber materials and are withdrawn or inserted in the core according to the power level needed to be produced in the reactor. The chemical shim, only present in PWR, is an additional system that foresees the dissolution of an absorber material within the coolant and controls its concentration in order to increase or decrease the core reactivity and power and to keep the core components temperatures within the design limits. This adjustment is made accordingly to the signal received by the core control system [7]. In addition to load following, the core control system is used in the reactor to compensate the reactivity loss due to fuel depletion. Indeed, as detailed in next chapter, the fuel consumption introduces variations of the produced power that have to be compensated during the reactor lifetime.

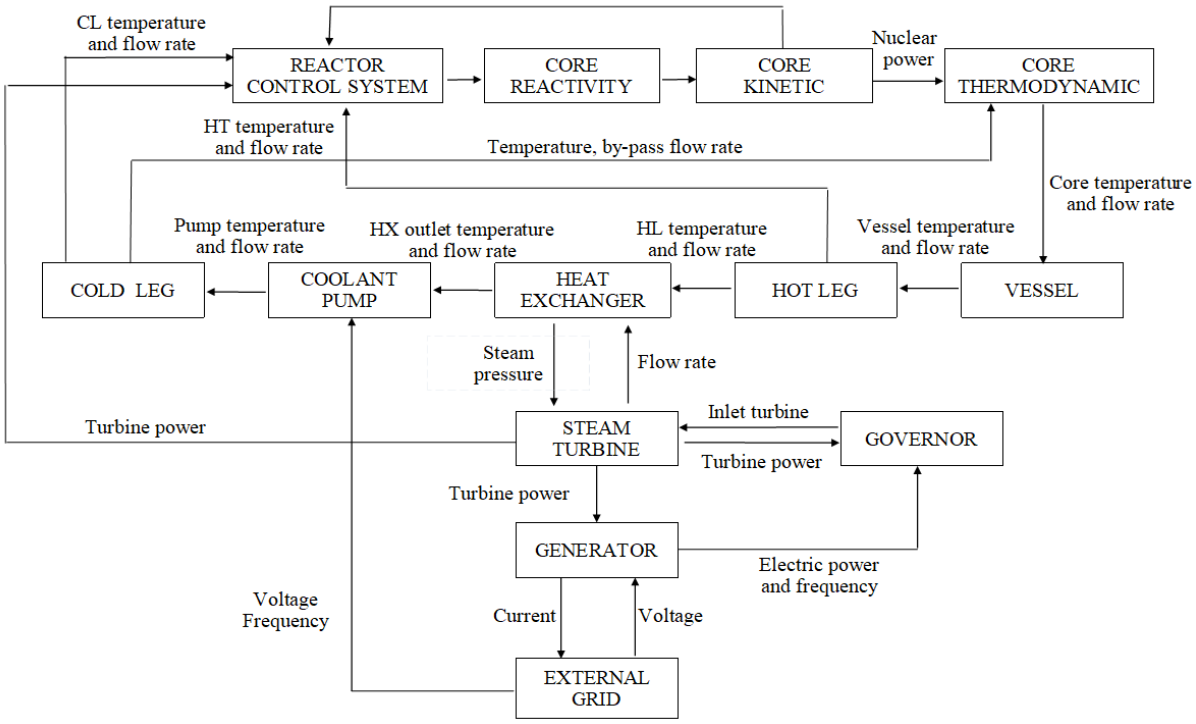


Figure 1.5 – Overview of a reactor control system.

A fine control of these operation is exploited with dedicated systems that regulate the dynamics of the operation described above. A primary control is made on the turbines via the regulation of the speed. It imposes a linear relationships between the turbine frequency and the power produced in the core. A secondary control is made additionally to absorb the residual gap between the demanded shaft frequency and the primary regulation. A third level of regulation is manually activated to find optimum of the power production economics. The control over the turbine entails a control over the power produced in the core. Different regulation modes are available, based on different combinations in the use of control rods and chemical shim. The mode proposed in the nowadays French reactors (called X mode) is based on different groups of control rods. The objective is the simultaneous control of the axial power imbalance and the mean moderator temperature [28].

All these described control systems and components are actively operated, meaning that a signal is necessary to initiate their intervention. For example, control rods movement is activated by a controller that is inside the core control system and that sends a signal to the control rod mechanisms when precise parameters reach predefined values. In other words, the core power continuous control is driven by a demand, that is transmitted by a set of signals (in both base mode and load following). These signals are then interpreted as the activation of several systems that modify the core reactivity.

In the current reactors, during load-following, if the core control system was not actively executed, the reactor would still be able to adapt its operating point to the grid demand change. Indeed, the variation of the demand would induce a variation on the secondary system pressure and consequently a variation on the mean primary coolant temperature. Following a variation of the primary temperature, the core reacts with an opposite variation of the power due to the reactivity feedback effects. Therefore, the reactor would adapt "naturally" its operation to restore a new equilibrium point. However, in this case, the steam pressure and temperature vary and the Energy Conversion System (ECS) efficiency varies accordingly to the power variation. Furthermore, the primary temperature could be characterised by large variations and so the primary system should be provided by a large pressuriser to accommodate them. Finally, if the primary temperature increases too much, the margin-to-boiling limit could be reached. More generally, this evolution would include operating points that are not the optimum in terms of economical plant performance and would lead to components and sub-system operation points potentially not optimised from a safety point of view [6].

The objective of load-following and the associated reactor control are discussed in the next section, highlighting the new design approach proposed in this work.

1.3. Thesis objective

1.3.1. A counter-current approach to the design of nuclear reactor

In the new context of mix-grid power generation including a large share of renewables energies, NPP could be expected to be able to adapt their production on demand. Reactor design strategies could then focus more on load-following management to compensate grid imbalances caused by the introduction of intermittent energy sources. From this perspective, the flexibility of NPP production is enhanced, although this is accompanied by an increase in design complexity and the potential for stress on NPP systems.

Other design approaches are currently emerging and consider different kind of objectives. For instance, some reactors are being conceived as a means of producing high temperatures in order to address specific industry needs. Concepts such as SMR are focused more on capital cost reduction by designing the reactor as a modular system, with each module constructed in a dedicated factory. The size reduction also enables to provide energy to isolated grid or systems. These examples highlight the fact that nuclear design is no longer solely guided by the scale effect (the larger the core the better) and the integration into large grids.

In such a context, it may be interesting to propose a very different design approach. One could imagine reactor design that operates as autonomous as possible, i.e. that is started-up and then left to autonomously evolve. The idea is similar to the approach used for micro-reactors designed for electricity or heat production for micro-grids or industry. This relies on the idea of reactor as "an energy source", comparable for renewable energy source, which can be connected to the grid, switched on and then

produces energy autonomously. In this case, the reactor does not adapt its operation for the load following, but its autonomous operation determines the power produced. In the absence of control, it is not evident that the power produced would be constant. Nevertheless, the advantage of a non-renewable energy source is that its energy production is predictable throughout the reactor's lifetime and therefore not subject to external factors (such as the weather for solar energy).

Is it possible to design a simplified reactor characterised by autonomous operation?

The consequent questions are about the feasibility and viability of such a design. Is it possible to conceive a reactor that operates without any intervention? What is the effective definition of autonomous reactor? Would it concern some systems or the entire design? And would it concern the entire reactor lifetime or just certain phases?

Furthermore, the performance of autonomous cores should be assessed and compared to actively controlled ones. There are several ways to evaluate core performance: among them power delivered, amount of energy produced, cycle length, needs for advanced technological developments, etc. Considering a defined set of performance parameters, what would be the effect of autonomous operation? Would it be possible for an autonomous core to exhibit performance comparable to the ones of an actively controlled reactor? Would such a reactor be suitable to provide electricity to the grid?

The following paragraph will provide a more detailed discussion of these questions.

1.3.2. How to approach the problem

The question of autonomous reactors may be approached from several different perspectives, as the definition of autonomously operated reactor can be given in different ways. In literature, the main use of passive components/systems has been considered as a promising way to increase the safety of NPPs [29]. Other studies proposes the addition of an autonomous control system into the core based on the passive insertion of neutron poison in the core [30] [31].

Specifically referred to the safety systems, the IAEA (International Atomic Energy Agency) has defined and classified the active and passive systems according to the degree of passive operation [29]. It consists in defining a passive system according to different levels, starting from the higher degree of passivity:

- absence of moving parts or fluids and no need for an active initiator signal nor for external energy;
- absence of moving parts but employment of operating fluids but no need for an active initiator signal nor for external energy;
- use of moving parts without the necessity of external power for the activation and the operation;
- use of moving parts requiring external power for the start-up but not for the operation and without manual intervention.

In this work, the focus is neither on the insertion of additional systems nor on the design of a safety system. This work investigates the operation of a core not driven by any active reactivity control system.

To do this, firstly, one should identify what phases of the reactor lifetime are “autonomously operated” (start-up/shutdown, energy production, refuelling). Secondly, the degree of passivity should be identified which means identifying the active systems that are eliminated or made autonomous. Thirdly, the performance of such a reactor should be defined and evaluated.

The first question is about the phases that could be made autonomous during the reactor lifetime. For reasons related to the generic field of "safety", a system to actively initiate a shutdown should be present in case of accidental situation and need for the core scram. The shutdown system could thus operate actively for incidental or end of life shutdown. An actively operated system would be also necessary at the beginning of life to start-up the reactor and drive it from the offline to the nominal conditions. Concerning the reactor refuelling phase, in the perspective of design simplification, this phase could be in a first approach set aside. The reactor could operate up to the fuel consumption that would define the end of life of the core. It can be, for example, completely changed at the end of its cycle (once through way). This would simplify the fuel handling system necessary for the fuel reloading during the core lifetime, between each core cycle.

Following the previous principles, an autonomous reactor could be defined as autonomously operated during the power production phase. It is started-up actively and then left to its autonomous evolution, with no need of any intervention up to the consumption of the fuel and then the shutdown. The "power operation mode" control system is eliminated and the reactor power production and its inherent performance are imposed by design.

The second question concerns the degree of "passivity" of the reactor. The definition of an "autonomously operated" reactor could foresee the elimination of active systems or could consider the active system to be autonomously operated. Furthermore, the autonomous systems and components can be defined according to multiple degrees of passivity. They can be characterised, for example, by the complete absence of moving mechanical parts or fluids or defined by the absence of an active initiator signal. Finally, an autonomous reactor could include the autonomous operation among all of its systems or just in some of them while the others should adapt actively its operation to the firsts.

Finally, the third question is about the expected performance. To design such a system, the objective of operation driven by the grid is, at first approach, to be reconsidered. The proposed NPP *a priori* does not include the load-following possibility. Indeed, the power production is imposed by the autonomous operation of the core and thus defined by design. Due to the change of the final objective of the reactor, the concept of performance is to be redefined in this framework. The definition of "performance" can be set in various way. It can be on the grounds of economic considerations. For example for the industrial reactors, the economic is evaluated on the efficiency of the electricity production for the grid. On the other hand, this kind of reactor could have different fields of applications, such as heat production or energy production for particular industries. The definition of "performance" would, thus, be different, including, for example, the temperature of the produced heat as major important aspect. Furthermore, the performance of the reactor could be evaluated in terms of "safety". A reactor characterised by larger degree of passive safety is considered intrinsically safer. Finally, it could be evaluated in terms of fuel cycle. A reactor that produced less waste could be considered more efficient, or different final uses could be foreseen for such a reactor, as being a waste burner or a fissile generator. For an autonomous reactor a specific definition has to be pointed out and evaluated.

In conclusion, in this section, multiple questions on the autonomous reactor definition have been risen. They concern the phase of autonomous operation during a reactor lifetime, the specific definition of autonomous degree of the NPP and the performance related to this kind of reactors. In the next section, a proposition of autonomous reactor definition is presented, the scope of this thesis is defined and the approach of the work is shown.

1.4. Approach followed in the present work

1.4.1. Framework of the work

The objective of this work is to obtain a reactor that is started-up actively, evolves autonomously and shutdown when the reactivity loss due to depletion can no longer be compensated by variation in the core operating conditions.

The autonomous evolution defines a power production that is thus established by design. The core is not refuelled during its life, but only loaded once at the Beginning Of Life (BOL) and discharged at the End of Life (EOL).

The analysis of this problem starts from the examination of the existing reactor designs, operational or at design stage. Multiple types of reactor concepts exist in the literature, as introduced in Section 1.2.1. The first step of this work is the investigation of the possibility to autonomously operate some of the existing reactor designs. Some concepts are selected from the literature as reference designs to be analysed. This choice is detailed in Chapter 2. The constraints and limitations of the adaptation to autonomous operation will be investigated.

Furthermore, each of the active reactor designs has specific objectives and is designed with the highest possible performance in terms of economics, adaptation to the grid safety or fuel cycle. For example, reactor designs can be classified by technology. The PWR are designed to be connected to the electric grid maximising the economic efficiency. On the other hand, the fast reactors are conceived to contributes to the fuel cycle closure, thus providing a promising solution for actinides management or enabling the fuel supply sustainability [32]. The High Temperature Reactors have been designed to produce heat at high temperatures while ensuring a high level of safety in the related operation [33].

The reactor size is another way to build a reactor classification. While large reactors have been favoured to benefit from the economy of scale effect, new interrogations have emerged as new needs have been identified. Micro-reactors is a family of designs which objective is to supply energy to an isolated infrastructure or system while being easily transported [34]. Small Modular Reactors (SMR) have been thought to have a reduced investment cost by benefiting from the series effect and a modular design. Additionally, their small power should help increasing the core safety while being more appropriate than larger cores for specified applications such as providing electricity to a small grid or helping decarbonize an industrial area [35].

In conclusion, each reactor type is designed with a particular objective and is optimised for certain scopes. All the existing designs include an active control for the optimisation of the operation. In this work, when adapting the design to be autonomously operated, the new performance will have to be defined and assessed. Depending on the performance obtained while converting a core to be autonomously operated, the reactor could be connected to the grid to supply only power or it could be used to produce heat for certain applications (such as industrial factories heat supply) or even be connected to micro-grids for the power supply of small users.

Several technologies are studied in this work in order to test a wide range of reactors. As the selected concepts differ from one another, it will be necessary to define the differences in terms of design characteristics. A methodology will be proposed to find a zone of comparison between them. It includes the standardisation of some design aspects in order to compare the possible applications and performance of autonomous designs originally conceived for very different objectives.

Once a comparison is made and the performance of each is assessed, proposals of design modifications for performance improvement will be made.

1.4.2. Approach of the thesis

The approach of this work is summed up in three phases:

- in the first phase, the basic physics phenomena of the autonomous reactor are discussed. The problem includes the whole reactor system: the core, the primary cooling system and the Energy Conversion System (ECS). Two approaches are possible:
    - the modelling of the whole reactor systems and the analysis of all the systems coupled at the same time;
    - the analysis of separate systems, with the choice of hypothesis to be settled at boundaries.

  The first approach is the most exhaustive one but can be very time consuming. In this work, the second approach has been chosen. First, the ECS is analysed and the possible contribution of this system to the autonomous core is evaluated. The remainder of the work focuses on the design of an autonomous core.
- the existing core designs are modelled for autonomous operation and their associated performance are quantified;
- the reactors originally designed for active operation, show degraded performance when converted to autonomous operation. Therefore, the third phase consists of proposing design modifications in order to improve their performance.

This approach is developed according to the following chapters organisation:

- Chapter 2:

  in this chapter, the methodology used in this the work is presented. The physics of an autonomous reactor is described. Then, computational models implemented for the study will be put forward. Finally, different reactor designs in the literature are analysed and presented.
- Chapter 3:

  the possibility of controlling the Energy Conversion System (ECS) is explored, in order to evaluate its possible contribution to the core autonomous behaviour and to set hypothesis on the core temperatures for the following of the work, which is uniquely focused on the core analysis.
- Chapter 4:

  Among the designs found in the literature, four have been selected. In this chapter, they have been analysed when autonomously operated. A methodology is chosen to define the characteristics of autonomous reactors and to compare them. A number of parameters have been selected in order to characterise their performance in terms of feasibility, physical parameters, core performance and the potential contribution of the ECS.

- Chapter 5:

  A way to increase the autonomous performance is proposed. It focuses on core power evolution and on the compensation of the fuel depletion reactivity loss. Thermal cores are analysed in this chapter.

- Chapter 6:

  This chapter is dedicated to the analysis of fast cores, using the same method as in the previous chapter.

In the conclusions, in this work, comparison of autonomous cores behaviour will be presented. Possibilities to increase their performance will be proposed and possible design modifications will be compared. The most promising ways will be highlighted and some of the initially proposed solutions will be excluded.

1.5. Conclusions

The global climate change concern has turned the attention on nuclear energy as one of the possible energy sources to reduce the worldwide carbon emissions. In this context, the research on innovative and safer reactor designs has increased. Furthermore, the fields of possible application of nuclear energy supplies are diversified and include, beyond the electricity production, the heat generation, the hydrogen production or the application to a specific industries energy necessity.

The nowadays industrial scale reactors are characterised by a specific operational mode that includes an active control and the possibility to adapt the NPP power production to the necessity of the electrical grid. In particular, the operation is driven by the energy extracted at the secondary system turbines and an active control is put in place to adapt the core operation. The control system, is complex due to the large number of instrumentation, actuators and sub-system needed to account for the several parameters necessary to drive the reactor operation.

This thesis proposes to rethink the reactor design approach according to new different objectives. It explores the possibility of designing a simplified reactor with the aim of producing power autonomously, reducing active control as much as possible. The proposed design is an autonomous reactor that is started-up, evolves autonomously according to the design characteristics and is shut down at its end of life. It is based on the autonomous operation of the core. The power produced by this kind of reactor is established by design and *a priori* it does not vary according to the grid necessities.

The approach to this work will be to decouple the reactor systems (core, primary cooling system and ECS). A first analysis on the ECS is made and then attention is focused on the core. First, it will be verified if it is possible to operate autonomously existing reactor designs, chosen in the literature. Second, a comparison between these autonomously operated designs will be made, to compare their performance when actively or autonomously operated. Finally, ways to increase the performance will be proposed, in order to verify if this kind of reactor concept is feasible and possibly applicable in the energy production scenarios. In the next chapter, the methodology is described in detail.

Chapter 2

Methodology

Summary

2.1. Introduction 49

2.2. Physics of an “autonomous core” 49

2.2.1. Recall on the core physics 50

2.2.2. Definition of autonomous core 52

2.2.3. Core neutronic/thermal-hydraulic interaction 54

2.2.3.1. The coupling model 56

2.2.3.2. The KGH method 57

2.2.3.3. KGH method on a core with positive reactivity feedbacks 58

2.3. Presentation of the chosen designs based on literature 59

2.3.1. Micro-reactors 60

2.3.1.1. Heat Pipe Reactors 61

2.3.1.1.A. Heat pipes operation 63

2.3.1.2. High Temperature Reactors 65

2.3.2. Large-scale reactors 66

2.3.2.1. Pressurised Water Reactors 66

2.3.2.2. Sodium-cooled Fast Reactors 67

2.3.3. Sum-up of the reactors candidates for this work 68

2.4. Neutronic and thermal computational models for candidate cores 69

2.4.1. Neutronic calculation scheme 69

2.4.2. Thermal calculation scheme 70

2.4.2.1. Heat pipe thermal modelling insight 74

2.5. Conclusions 75

2.1. Introduction

In this chapter, the methodology used in this work is presented. The main objective is to define and analyse the inherent "performance" of an "autonomous reactor" that could be able to evolve under irradiation without any active control during core operation (except for the start-up and shutdown phases).

To study such a reactor, two approaches are possible: the modelling of the whole reactor systems coupled at the same time or the analysis of separated systems. This second approach has been chosen in this work. The ECS is analysed (in Chapter 3) and the possible contribution of this system to the autonomous core is evaluated. The remainder of the work focuses on the core behaviour and the core design. For this reason, in this chapter, the core physics and computational model have been described.

First, the description of such a reactor is given. Hereafter, an "autonomous core" label is used to define a core design that does not need any (or a few) active intervention to maintain a "sufficient power level" (i.e. within a range to be defined in the following sections) during nominal operation. Inside such a "free" system, starting from critical state with a defined power, different physical phenomena drive the time evolution of the power:

- fuel depletion leads to reactivity loss or gain (depending on the breeder or burner configuration of the core at a given time);
- various feedback coefficients act to counterbalance the previous behaviour to some extent;
- autonomous systems (triggered by temperature or pressure thresholds) devoted to reactivity control can bring additional feedback effects.

The approach of this work focuses at first on the phenomena in play in core power evolution that are at least characterised by neutronic and thermal effects. The need for a neutronic/thermal coupled calculation scheme is highlighted to accurately model and study such a core behaviour. In this chapter, a computational model is proposed to account for the interdependency of the two fields. The main assumptions are presented, including the hypotheses bounded to the time-scale of the problem that justify the choice of a quasi-static coupling method. This method, based on the KGH [15] approach, is described in details in the first part of this chapter.

The second part of this chapter is dedicated to the introduction and description of four selected reactor designs to be studied as "autonomously operated". They belong to the micro-reactors and industrial-scale reactors categories. The former are characterised by small size (in terms of produced power) and by enhanced autonomous features in the designs. Among this category, the Heat Pipe Reactors (HPR) and High Temperature Reactors (HTR) have been considered in this work. They are compared to large size reactors such as Pressurized Water Reactors (PWR) and Sodium-cooled Fast Reactors (SFR). The specific neutronic and thermal models implemented to study each reactor type are described. The neutronic models are based on Monte-Carlo calculations with the code Serpent 2 [36] for thermal reactors and deterministic calculations with the ERANOS code [37] for fast reactors. For thermal calculations at core scale, simplified conduction-convection models are used.

2.2. Physics of an "autonomous core"

Compared to traditional power reactor design, in "autonomous" cores the objective of an imposed maximum achievable thermal power, with constant rate, is left aside. In our cases, at the very first stage,

the main foreseen objective is not devoted to large power production nor optimisation of electricity production to be connected to the grid.

In an autonomous reactor, the power level is not actively controlled, and its natural evolution is only imposed by autonomous reactor operation. Nevertheless, the components of the reactor must be sized for a nominal power level, which should not be exceeded during the rector lifetime.

In this section, the definition of autonomous core is analysed in terms "physics" estimators. A quick reminder of the main physical parameters is made, in the next paragraph. Then, the neutronic and thermal parameters contributing to the definition are highlighted. Successively, the need for a computational model to study the core design is pointed out. The hypotheses of this specific problem are set, among them and the implemented calculation scheme is presented.

2.2.1. Recall on the core physics

In this paragraph, a recall on the core physics is made. This discussion is intended to provide the minimal basic notions useful for the reading of this work. The objective, of this recap is to summarize the main parameters that give indication regarding core time evolution. In particular the concept of neutron flux level and core reactivity are summed-up.

The life of a neutron in a nuclear reactor is characterised by collisions with atoms. The neutrons that reach an atom can be captured, scattered or absorbed in a fission events. Following a fission, two or more neutrons are produced and the targeted atom is split into two lighter isotopes.

The description of this process is thus based on the analysis of the population of neutrons (that will be indicated in this work as$n$) and the target isotopes content (referred in this work as N_i, content of the i-isotope).

The angular neutron flux ϕ [cm^{-2} s^{-1}] is defined as follows:

$$\phi(\vec{r},\vec{\Omega},E,t) = v(\vec{r},\vec{\Omega},E,t) \cdot n(\vec{r},\vec{\Omega},E,t)\,; \qquad (2.1)$$

where: v is the neutrons velocity [cm s^{-1}] and n is the neutrons concentration [cm^{-3}]. These parameters are dependent on: $\vec{r}$, the space position of the neutron, $\vec{\Omega}$ the angular direction of neutron trajectory, E the neutron energy and t the time.

To introduce the concept of reactivity, first, the notion of cross section is presented. The i-isotope microscopic cross section σ_{i_x} [barn = 10^{-24} cm^2] represents the probability for a mean neutron to interact with the isotope i for the specific interaction x (capture, scattering or fission). This parameter $\sigma(E)$ depends uniquely on the neutron energy (or more specifically on the relative neutron energy between the neutron and the target atom).

The macroscopic cross section Σ_{i_x} [cm^{-1}] of an i-isotope represents the probability for a neutron in a specific position and with a specific energy to interact with a nucleus on his trajectory. It is described as:

$$\Sigma_{i_x}(\vec{r},E,t) = \sigma_{i_x}(E) \cdot N_i(\vec{r},t)\,; \qquad (2.2)$$

where: N_i is the i-isotope content dependent on the space coordinate and the time evolution of the material.

The multiplication factor describes the equilibrium of the neutronic population. It is defined as the ratio between the neutrons produced in a generation and the ones produced in the previous generation. The definition is the following:

$$k_{inf} = \frac{neutrons\ produced\ at\ the\ i\ generation}{neutrons\ produced\ at\ the\ i-1\ generation} \tag{2.3}$$

In particular, it is mathematically defined as:

$$k_{inf} = \frac{\sum_i \int \tau_{gen_i}\, d\vec{r}\, dE\, d\vec{\Omega}}{\sum_i \int \tau_{abs_i}\, d\vec{r}\, dE\, d\vec{\Omega}} = \frac{\sum_i \int (\nu_i\, \Sigma_{fiss_i}\, \phi)\, d\vec{r}\, dE\, d\vec{\Omega}}{\sum_i \int (\Sigma_{abs_i}\, \phi)\, d\vec{r}\, dE\, d\vec{\Omega}}; \tag{2.4}$$

where: $\sum_i$ represents the sum over all the isotopes; ν is the mean number of neutrons emitted per fission event; $\int d\vec{r}\, dE\, d\vec{\Omega}$ represents the triple integral over space, neutrons energies and directions; τ_{gen} and τ_{abs} are the generation rate and the absorption rate, thus the number of neutron-isotope interactions per unit of volume and unit of time [cm^{-3} s^{-1}]; Σ_{fiss} and Σ_{abs} are the macroscopic cross sections of fission and absorption [cm^{-1}] and ϕ is the neutron flux [cm^{-2} s^{-1}].

This definition is given for the infinite multiplication factor, which does not account for the loss of neutrons on the boundaries of the domain. The effective multiplication factor accounts for the losses impact and is thus defined as follows:

$$k_{eff} = k_{inf}\ P_{NL}; \tag{2.5}$$

where P_{NL} represents the probability of neutron non-leakage from the boundaries of the domain.

The equilibrium state of the core, thus the equilibrium between the neutrons production and the neutrons disappearance, is defined as criticality. A reactor with constant number of neutrons at each generation is defined critical reactor, if the number of neutrons increases, the reactor is defined supercritical and if the neutrons population is decreasing, the reactor is defined subcritical. To define the state of the core in terms of deviation with respect to critical state the reactivity parameter is introduced:

$$\rho = \frac{k_{eff} - 1}{k_{eff}}; \tag{2.6}$$

this parameter ρ mathematically is dimensionless, but is usually expressed in percent mille [pcm]. This unit consider a factor of 10^{-5} in the ρ definition.

The relation between the reactivity and the neutron flux is represented by the point kinetic equation that accounts for the effect of delayed neutrons emission:

$$\begin{cases} \dfrac{dA}{dt} = \dfrac{\rho - \beta}{\Lambda}\, A(t) + \sum_i \lambda_i c_i(t) \\ \dfrac{dc_i}{dt} = -\lambda_i c_i(t) + \dfrac{\beta_i}{\Lambda}\, A(t) \end{cases}; \tag{2.7}$$

where: $A(t)$ is the total amplitude of the neutron flux; ρ is the reactivity; β is the total delayed fraction [-]; β_i is the *i*-delayed fraction [-]; Λ is the prompt neutron generation time [s]; λ_i is the i-group delayed fraction [s^{-1}]; $c_i(t)$ is *i*-precursor density [38].

In the next paragraph, the behaviour of an autonomous reactor is described via the core reactivity and neutrons flux parameters.

2.2.2. Definition of autonomous core

The operation of an industrial reactor is characterised by different phases: start-up, energy production phase (usually at constant power), power transient in case of load following necessities and, finally, shutdown. Before reactor start-up, control rods are inserted in the core, the neutronic population is low and not multiplying, the reactor is largely sub-critical. During start-up, control rods are gradually withdrawn from the core in order to decrease the neutronics absorption and increase the reactivity. This phase lasts until the neutrons population is stable, thus the core has reached the criticality state at zero power. When the reactor is critical, the control rod extraction leads to increase the power, up to its nominal value. After power stabilization, the core starts its nominal energy production phase. The power produced is constant at the turbine of the secondary system (considering a phase of constant electricity production operation). The core reactivity is kept constant in time to guarantee stability and a constant core power output by adjusting the absorbents to counterbalance the fuel depletion.

The total core reactivity can be represented by the sum of different components. In the following equation, the variation of the reactivity is represented by the sum of the contributions between an instant of time t and the subsequent $t+\Delta t$:

$$\delta\rho_{core} = \delta C_{fuel} + \delta C_{feedbacks} + \delta C_{control}\ ; \qquad (2.8)$$

where: $\delta\rho_{core}$ is the total reactivity of the core variation between t and $t+\Delta t$ instants; δC_{fuel} is the contribution to the reactivity variation due to the fuel depletion; $\delta C_{feedbacks}$ is the contribution to the reactivity variation due to core temperature variation and $\delta C_{control}$ is the contribution to the reactivity variation inserted by control elements in the core.

The total core reactivity is zero when the reactor is stable and produces a constant power. This equilibrium is reached thanks to the compensation of the various reactivity terms.

In particular, the variation of the reactivity due to the fuel is caused by the fuel irradiation in the core. The fuel changes its composition during its irradiation cycle. The fissile material disappears due to fissions, while new fissile isotopes can appear by the absorption of neutrons by fertile materials. After the fission events, the split atoms constitutes the fission products. Some of these isotopes are characterised by a large capture cross sections, thus influencing the reactivity. For example, xenon and samarium isotopes that appear in the first days of a reactor operation are characterised by large absorption cross sections in a thermal reactor, thus they contribute to a large reactivity decrease in the first days of a reactor cycle. The reactivity variation of the fuel composition can be a positive or negative contribution, depending on the quantity and ratio of fissile and fertile materials in the core.

The second parameter that impact the core reactivity is the contribution of the reactivity feedback effects. This contribution comes from temperature variations in the core, as further described in Section 2.2.3.1. In case of constant fission power produced, core temperatures are constant, thus the associated contribution does not provide any variation in core reactivity. Anyway, various temperature effects can be used to control the reactor in case of transients. For example, driving actively the primary pump, the primary coolant mass flow rate may vary and temperatures do change, introducing a reactivity contribution.

Finally, active reactivity control is the last parameter in the equation shown above. Indeed, to guarantee a constant net zero reactivity (or to drive reactivity variation in case reactor transients), one or more means of reactivity control have to be inserted into the core. They can be actively actuated or autonomously operated. Among active control means, beside dissolved boron in coolant, control rods are widely used. They are movable rods constituted by absorber material (usually boron) that can be inserted or withdrawn from the core to increase or decrease the neutrons absorptions, thus leading to positive or negative contribution on reactivity. Other possible control means are designed in the innovative reactors, such as rotating drums or sliding walls insertion in the reflector on the core boundaries [39].

On the other hand, "passive" strategies can be adopted to contribute to the reactivity control in the core. For example, the insertion of burnable poisons. These materials are characterised by a large absorption cross section and leading to non-fissile isotopes with low capture cross section. Their contribution to reactivity is negative at the beginning of cycle and then, when gradually consumed, associated residual absorption reduce until the complete burnable poison consumption [40].

With this distinction, the equation (2.8) is rewritten as:

$$\delta\rho_{core} = \delta C_{fuel} + \delta C_{feedbacks} + \delta C_{control_{ACTIVE}} + \delta C_{control_{PASSIVE}} . \qquad (2.9)$$

Definition of "autonomous" core, that has been given earlier and that is the objective of this work, can be now rephrased as "***the elimination of the active control term in the equation***" of core reactivity balance. An autonomous reactor, in this work, is then described by the following equation:

$$\delta\rho_{core} = \delta C_{fuel} + \delta C_{feedbacks} + \delta C_{control_{PASSIVE}} . \qquad (2.10)$$

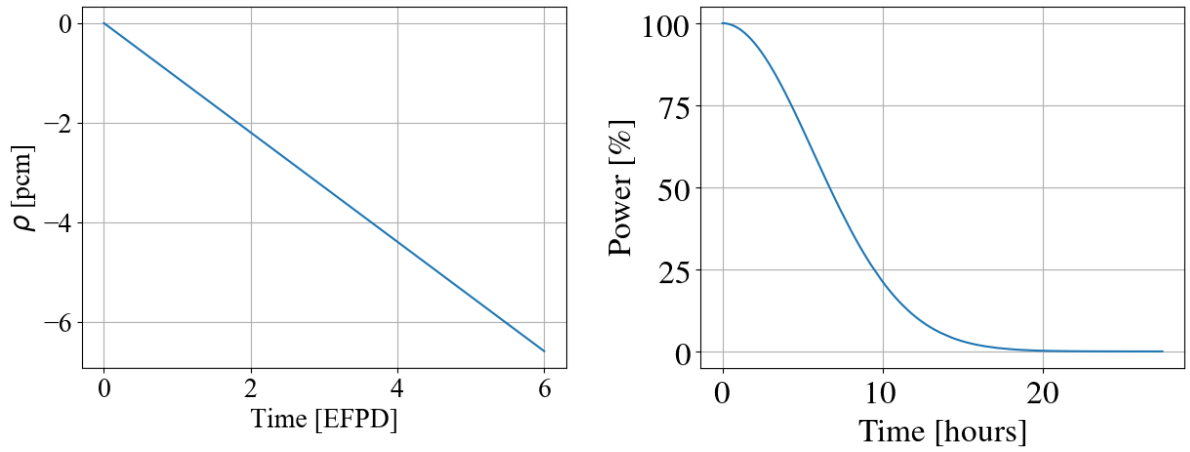
In a first approach, no control means are considered, even the autonomous ones. Considering the previous formulation describing the evolution of autonomous core without insertion of autonomous drivers, equation (2.10) becomes:

$$\delta\rho_{core} = \delta C_{fuel} + \delta C_{feedbacks} . \qquad (2.11)$$

If the reactivity term due to fuel consumption was only one acting, it would not be possible to keep the reactor stable (with a total core reactivity equal to zero during the core evolution). Indeed, for a large range of nuclear reactor designs, fuel consumption implies a negative contribution to the reactivity (due to the consumption of the fissile isotopes, for burner reactors). Thus, total core reactivity would be decreasing and the associated power as well. For illustration, Figure 2.1 displays the reactivity (a) loss of a large industrial SFR core [6] and the power decrease (b) for six day of operation without control rod compensation using previous equations. The example refers to the purely theoretical case of reactivity evolution only driven by the fuel depletion effect as in the formulations:

$$\delta\rho_{core} = \delta C_{fuel} \neq 0. \qquad (2.12)$$

In this equation the concentration of neutron precursors is considered at equilibrium at beginning of the simulation, as the core has been started with active systems.



(a) *(b)*

Figure 2.1 – Theoretical power evolution of a SFR core (b) with reactivity loss due to fuel consumption (a).

The mean reactivity loss is -1.1 pcm/EFPD (Equivalent Full Power Day) taken as example for the SFR-V2B 3600MWth [41]. Figure 2.1 has been computed via the inversion of the point kinetic equation [38].

In this "theoretical" case, where reactivity evolution follows uniquely the fuel consumption as shown in Figure 2.1(a), the reactor is not critical during the whole lifetime and the associated power evolution is decreasing rapidly. As shown in Figure 2.1(b), the power of a 3600 MW_{th} SFR would drop to zero in some hours. The considered reactor (SFR-V2B) is characterised by low reactivity loss (main design purpose), other SFR featured larger reactivity losses (-16 pcm/EFPD for the PHENIX reactor and -7.0 pcm/EFPD for SUPERPHENIX reactor [41]) and thus their lifetime in this analysis would be even shorter.

In real cores, the term associated to the reactivity feedbacks contributes to the total reactivity. To be in a stationary state (thus avoiding divergences or shutdown), a reactor requires to have critical core (zero total reactivity) during its lifetime. Thus, the design of an autonomous core would need to rely on an adapted set of reactivity feedbacks that should be able to compensate for effect of fuel consumption.

To analyse the impact of the reactivity feedback effects on the power evolution, a model that accounts for coupled neutronic/thermal aspect is necessary. In the next sections, the neutronic/thermal-hydraulic interaction are described as well as the possible computational models to study this multi-physical problems.

2.2.3. Core neutronic/thermal-hydraulic interaction

The neutronics and thermal-hydraulics are strictly dependent in core physics. In this section, interactions between these two fields are presented.

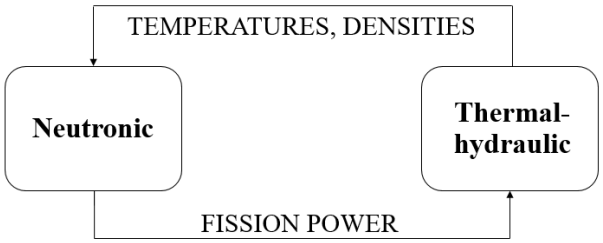


Figure 2.2 – Neutronic/thermal-hydraulic coupling principle.

Figure 2.2 represents schematically the interdependency between both physics.

The neutronics describes the core in terms of fission power produced. This parameter is computed as follows:

$$P_{fiss}(t) = \sum_i \int E_{fiss_i}\, \tau_{fiss_i} \;\; d\vec{r}\, dE\, d\vec{\Omega} \;\; = \sum_i \int E_{fiss_i}\, \Sigma_{fiss_i}\, \phi \;\; d\vec{r}\;\, dE\, d\vec{\Omega}\,; \qquad (2.13)$$

where E_{fiss_i} is the energy produced by each fission of the *i*-isotope and the integral in the formulation is the integration over space, neutrons energies and directions of their trajectories. The power produced by fission is the energy released per fission, multiplied by the fission rate ($\Sigma_{fiss_i}\, \phi$).

The determination of fission power is based on the cross sections as input parameters. Cross sections depend directly on the temperature and density of the materials. The thermal-hydraulics defines the temperature and density fields in the reactor core depending on the produced fission power, output of the neutronic calculations.

The previous Figure 2.2 can be represented with physical parameters characterising the coupling as follows in Figure 2.3.

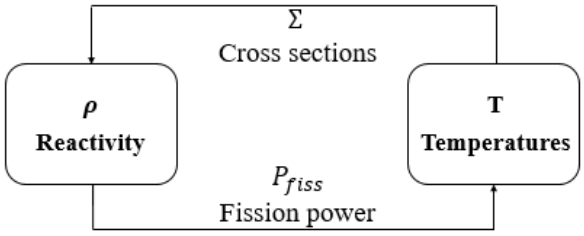


Figure 2.3 - Neutronic/thermal-hydraulic coupling parameters.

The macroscopic coefficients that gather the effect of the variation of temperature or (associated density) of different materials on neutronic are the reactivity feedbacks coefficients:

$$d\rho = \alpha\, dT; \qquad (2.14)$$

where α is the generic reactivity feedbacks coefficient [pcm/K].

The reactivity feedbacks concern various core materials. The Doppler effect denotes the impact of fuel temperature variation on reactivity. In particular, the phenomenon is related to the resonances of microscopic cross sections (mainly of U-238). Indeed, when the fuel temperature increases, the peaks of absorption that characterise the U-238 resonance energies decrease while their width are enlarged. Therefore, increasing the fuel temperature leads to increase U-238 absorptions and the reactivity

decreases. The Doppler coefficient is thus negative, providing an opposite effect between the temperature and the reactivity variations.

The fuel temperature increase also determines a density decrease. Thus, the fuel isotopes content in volume decreases. This effect can be characterised by a positive or negative reactivity insertion depending on the fuel composition (according to the presence or not of fertile materials).

In addition, moderator, coolant and the structures material may change in temperature and density during nominal and transient configurations. The moderator conditions variation determines a change in the moderating capability and thus in the neutron spectrum acting on the reactivity depending on the core characteristics. The coolant variation determines a change in the moderation (if the coolant acts as moderator for thermal reactors) or a smaller variation in the scattering and absorption rate in the core (as in the case of fast reactors). Finally, the structure temperature and density variation affects the absorption ratio ($\Sigma_{abs}\ \phi$) of the core. The specific coefficients, for different reactors, are computed and discussed in Section 4.3.2.

In the next paragraph, methodologies and models to account for the coupled effect of neutronic and thermal-hydraulic fields are presented.

2.2.3.1. The coupling model

For the analysis of the autonomous reactor design the chosen computational model is described in the next lines. The behaviour of such a reactor core is based on fuel burn-up and the coupled thermal feedbacks on the reactivity evolution. For this reason, a coupled neutronic/thermal computational scheme is necessary for the analysis of the problem.

One of the difficulties of the nuclear power plants physical analysis is the multi-scale characteristic of the problem in terms of space and time. For examples, the reactor vessel has dimensions of the order of meters, the fuel pins and the mean free path of a neutron is of the order of centimetres (for LWR [42]), up to the microscopic cross sections measured in barn (10^{-28} m^2). On the other hand, a reactor lifetime is of the order of magnitude of decades, the Xenon effect in thermal reactors is of the order of one day, the mean delayed emission of delayed neutrons is of about 10 seconds and the neutron lifetime is 10^{-5} – 10^{-9} seconds (according to the neutron energy) [43]. Consequently, the computational simulations differ between the ones at macroscopic scales, capable of representing an entire system, up to the micro scale simulations, focused on a specific phenomenology that requires accurate description.

As the physics is complex and involves two major fields, this coupling has to be accounted via some specific models that ensure the description of this correlation. Coupling could be done at several stages:

- monolithic coupling, in which all neutronics and thermal-hydraulic equations are solved at the same time;
- strong coupling, in which equations are solved separately but iteratively with close interactions in time so-that convergence could be reached to have quite the same level of accuracy as the previous hone (to some extent);
- weak coupling, which proceed like strong one but with larger time step and averaging of main coupled parameters. This model is often used for large time scale with quasi-static approach for design purpose.

Here, a weak coupling model, based on total reactivity feedback coefficients is used. The problem to be solved is described thereafter in order to justify this choice.

The core power is computed via the macroscopic cross sections and the neutron flux. The time evolution of the fuel properties, through the burn-up, affects the isotopes contents and thus the macroscopic cross sections. On the other hand, fuel temperatures affect both the macroscopic cross sections (because they influence the neutron spectrum and thus the microscopic cross section) and the flux evolution. The dynamic of the problem is based on the evolution of the fuel composition that affects the core reactivity and the fission power. Consequently, core temperatures change and reactivity feedback effects contribute to the reactivity variation.

The time-scale and space scale of the problem have been analysed in order to make some hypotheses on the coupling strategy.

The time-scale of the core is very large considering the different phenomena accounted in the problem. Between the power variation and the temperature change, the thermal inertia introduces a delay into the system equilibrium restoration. Similarly, between a temperature variation and the reactivity new equilibrium attainment, the neutron kinetic inertia introduces a delay. These two inertial phenomena are characterised by a time-scale of seconds, tenths of seconds and microseconds respectively for the thermal, the kinetic and prompt kinetic delay. In this problem, the fuel evolution due to the burn-up, introduces a much larger time-scale of the order of hours (for example in the first day of a thermal reactor with the xenon effect), days and years. The burn-up time-scale magnitude is much larger with respect to the time-scale of the inertial thermal and kinetic phenomena. With these premises, one major assumption can be made on the coupling methodology. If the problem is analysed with sufficiently large time step, it can be considered that the kinetic and thermal equilibrium is reached very quickly at each step and thus considering the coupling as a static problem and neglecting any neutronic and thermal inertia. Among the available approaches, the one employed in this work is the quasi-static one, where the thermal and kinetic equilibrium is assumed at each time step.

The neutronic analyses have been made on the 3D core geometry because the fuel consumption is largely affected by the geometrical core definition. On the other hand, the thermal problem has been studied with 1D-radial model, considering that the major contribution of heat exchange in the core happens on the radial direction [44]. The coupling is thus made considering the total mean power of the core as input parameter for the thermal calculations and the mean core temperature in each parameter as the input of neutronic calculation. At the same time, the evolution of the fuel is made considering the 3D entire core.

Once described the methodology used in this work, with the major time and space hypotheses, in the next sections, the specific equations used in the coupling method are presented.

2.2.3.2. The KGH method

The static coupling method used in this work is called KGH [15]. It is analogous to the method ABC developed at ANL [45]. They differ in the formulation of the equation, but the same conclusions on the results can be obtained [15]. It is based on the assumption of steady equilibrium of the core at each time step. The base hypotheses is the criticality at each time step, thus the total core reactivity is assumed to be zero at each step as follows:

$$\Delta\rho_{core} = 0\,. \qquad (2.15)$$

The formulation is based on the sum all elementary contributions to the reactivity, accounting for the reactivity variation induced by reactivity feedbacks and the reactivity variations due to the neutronic evolution of the core. Indeed, the total reactivity is written as follows:

$$\Delta\rho_{core} = H\ \Delta P_{core} + G\ \Delta(\Delta T_{core}) + K\ \Delta T_{in} + \Delta\rho_{fuel} = 0; \quad (2.16)$$

where: ΔP_{core} is the variation of the core power [W]; $\Delta(\Delta T_{core})$ is the variation of the core temperature difference between outlet and inlet [K]; ΔT_{in} is the variation of the inlet core temperature [K]; $\Delta\rho_{fuel}$ is the variation of the reactivity due to the fuel depletion (or potentially the variation due to burnable poisons or other passive control methods, as explained later) [pcm]. Finally, the H, G, K terms are specific coefficients that account for the reactivity feedback effects a global scale.

In particular, the first term $H\ \Delta P_{core}$ accounts for the effect of core power variation on reactivity. The H coefficient is defined as follows:

$$H = \alpha_{fuel}\ \Delta T_{H\ fuel} + \alpha_i\ \Delta T_{H\ i} \dots \left[\frac{pcm}{\%P_n}\right]; \quad (2.17)$$

where: α_i is the reactivity feedback coefficient related to the *i* reactivity feedback [pcm/K]; $\Delta T_{H\ i}$ is the *i*-material temperature difference between the core at the nominal power P_n and the core at $P_n + 1\%\ P_n$.

On the other hand, the term $G\ \Delta(\Delta T_{core})$ represents the variation of the reactivity following a variation of the difference of the core temperatures between outlet and inlet. The G parameter is defined as follows:

$$G = \alpha_{fuel}\ \Delta T_{G\ fuel} + \alpha_{mod}\Delta T_{G\ mod} + \alpha_i\ \Delta T_{H\ i} \dots \left[\frac{pcm}{K}\right]; \quad (2.18)$$

where: ΔT_G is the variation of material temperatures, corresponding to a variation of 1K of the core outlet coolant temperature, keeping the core power and coolant inlet temperature constant.

$$K = \alpha_{fuel}\ \Delta T_{K\ fuel} + \alpha_{mod}\Delta T_{K\ mod} + \alpha_i\ \Delta T_{H\ i} \dots \left[\frac{pcm}{K}\right]; \quad (2.19)$$

where: ΔT_K is the variation of each material temperatures, corresponding to a variation of 1K of the core inlet coolant temperature, keeping the core power and the core temperature difference (between outlet and inlet) constant.

This formulation provides a way to estimate the core power for each timestep considering the reactivity evolution and the associated reactivity feedback effects. It provides a coupling methodology between neutronics and thermal-hydraulics. Each "physics" is solved independently and then coupled in the KGH scheme. In Section 2.4, the specific model for the neutronic and thermal calculations are described.

In the next section, a discussion on the existence of the solution with KGH is made.

2.2.3.3. KGH method on a core with positive reactivity feedbacks

This paragraph discuss the existence of the solution of the KGH equation, when the reactivity feedback coefficients show positive values. The KGH formulation is rewritten taking into account the core temperature difference and the inlet temperature in function of the power. To illustrate, we consider an inlet temperature that is linearly dependent on the power.

$$\delta\Delta T_{core} = \frac{\delta P_{core}}{\dot{m}\ c_p}; \quad (2.20)$$

$$\delta T_{in} = a\ \delta P_{core}. \quad (2.21)$$

The KGH equation (2.16) can be rewritten as follows:

$$(H)\ \delta P_{core} + \left(\frac{G}{\dot{m}\ c_p}\right)\ \delta P_{core} + (K\ a)\ \delta P_{core} + \delta\rho_{fuel} = 0; \tag{2.22}$$

We are interested in assessing the stability of the function. So a global coefficient A is defined as

$$A = H + \left(\frac{G}{\dot{m}\ c_p}\right) + Ka. \tag{2.23}$$

And the KGH equation can be written as:

$$A\ \delta P_{core} + \delta\rho_{fuel} = \delta\rho_{core}. \tag{2.24}$$

Let us consider the neighbourhood of each equilibrium state. The initial condition on the core reactivity is $\rho_{core} = 0$ and the condition in the core power is $P_{core} = P_0$ at each state. In the small range of time considered, the parameter $\delta\rho_{fuel}$ can be neglected and the solution of this equation is in the form of:

$$\rho = A(P - P_0). \tag{2.25}$$

On the other hand, we consider the point kinetic equation [38], with the hypothesis of equilibrium of the precursors:

$$\frac{dP}{dt} = \frac{\rho}{\Lambda}P; \tag{2.26}$$

The equations (2.25) and (2.26) are rewritten as:

$$\frac{dP}{dt} = \frac{A}{\Lambda}\ (P - P_0)\ P; \tag{2.27}$$

If the power is observed to decrease ($0 < P < P_0$), the function $\frac{dP}{dt}$ will diverge towards the asymptotic value of $P = 0$ in the case of A>0 and converges to $P = P_0$ in the case of A<0. If the power is observed to increase ($P > P_0$), the function diverges to infinite if A>0 and converges to $P = P_0$ if A<0.

In conclusion of this very simplified analysis, having a positive A coefficient leads to a stationnary state non compatible with an operating objective of the reactor. In this case, the initiator of the transient is the reactivity loss due to the fuel depletion, and thus $\delta\rho_{fuel} < 0$. To obtain a physical acceptable, non-divergent results, the global coefficient of reactivity feedbacks must be negative. In the rest of the work, all the cases of study have been verified and some cases with a positive coefficient A will be found and considered as not acceptable.

2.3. Presentation of the chosen designs based on literature

The first step proposed in this work includes the analysis of reactor designs coming from open literature. Designs are about to be analysed in terms of systems components and operation. In particular a focus is made on reactivity control methods and its influence of core “performance” and objectives. Here, the analysis of two categories is proposed: the industrial-scale reactors, where the primary objective is the optimisation of the energy production and the micro-reactors, which objective is the increase of autonomous operation degree and increase of “safety” aspects.

A specification is made here on the Molten Salt Reactors (MSR). They are reactor conceived with continuously recirculating fuel. They show increased intrinsic safety characteristics (bounded to the

already molten fuel and the non-pressurized system), advantages over the removal of fission products (thanks to the recirculating fuel) and flexibility of operation concerning the adaptation to the grid demand (the use of control rods during operation is very limited thanks to the large reactivity feedback effects) [46]. The circulating fuel allows a constant refuelling (in the majority of the literature designs) of the reactor during operation. Although allowing flexible operation, it adds several degrees of complexity to the design (recirculation of radioactive fuel and dispersion issues, corrosion of the materials, etc.) that represents technological challenges to tackle in the future. Even if these reactors are characterised by interesting features in term of large reactivity feedbacks and flexibility, the molten fuel design would not be easily comparable with a solid fuel designs. For this reason they are not analysed into details in this work.

Nevertheless, even if not treated here, a preliminary analysis on an autonomous system based on MSR design has been done. The overview of the possible application of the present method to MSR is given in Annex II.1 and concludes that a first application of the method described in this work is not sufficient to assess the possibility of designing an "autonomous" MSR core. A more detailed analysis should be carried out, taking into account the entire reactor system. For these reasons, MSRs are in principle not considered in this work, but are seen as a promising prospect to be investigated further as part of a specific exercise.

In the next sections, a more detailed description of the chosen reactor designs is given. The micro-reactors category is described with their main features and the Heat Pipe Reactors (HPR) and High Temperature Reactors (HTR) are also presented in details. Furthermore, a description of the industrial-scale reactors chosen in this work, Pressurised Water Reactors (PWR) and Sodium-cooled Fast Reactors (SFR), is given. Both HPR and HTR have been selected among the micro-reactor designs as most common design.

2.3.1. Micro-reactors

The large-scale nuclear reactor plants designed and operated nowadays are characterised by a wide experienced systems and designs, but also come across high capital investment risks and long building time. Therefore, the need for diversification, costs lowering and intrinsic safety enhancement has led to the exploration of new approaches for nuclear energy production leading to the next generation of nuclear power reactors [47] (Gen IV).

On such basis, the Small Modular Reactors category has raised interest for the reduced investment cost, the simpler modular design and the enhanced safety features [8]. Among this category, the micro-reactors concepts are characterised by a reduced size, being usually defined as reactors producing up to 20 MW_e [9]. They have initially been designed for non-commercial use such as providing energy to remote locations, for space missions or as naval propulsion; while in the last years that concept started to be applied also for civil purposes [10]. The main desired features of this category are:

- a desirably autonomous operation of the reactor during the lifetime, reducing as much as possible the number of operators on site and the design complexity;
- a simplified design and a smaller reactor size to include the possibility of building in-factory and then transporting almost the whole reactor on site;
- a long-live core to avoid the refuelling operation;
- different possibilities of production (electricity, heat or combined production);

- modularity of the installation power (i.e. the possibility of appending modules);
- a reduction of the investment costs [11].

The most important challenges for micro-reactors up to now are bounded to the fuel enrichment need, the licensing current process and the costs. The request for a small size core implies high negative reactivity contribution due to neutron leakage. Different strategies are possible to compensate for this effect: the neutron flux can be increased, low absorption cross section materials can be employed as well as neutrons multipliers and a higher enrichment of uranium-235 can be taken into account. An optimisation between these parameters is necessary for the design of micro-reactors. In the current projects, the requested enrichment is up to 20% in the so-called HALEU (High-Assay Low-Enriched Uranium [16]) while in industrial size reactors the maximum fuel enrichment is around 5%. This aspect is a constraint in terms of higher costs for the enrichment process and proliferation issues. Furthermore, up to now licensing process does not contemplate all the micro-reactors proposed features, such as the possibility of operating without any worker on-site or the possibility to transport a fuelled core. In the end, the high costs per MW nowadays constitute an issue for the micro-reactors commercialisation. Nevertheless it has been demonstrated that, compared to other technologies applied in micro-grids such as renewable sources and diesel generators, micro-reactors might exhibit competitive costs [48]. Several micro-reactor concepts have been proposed worldwide. Among them, Heat Pipe Reactors and High Temperature Reactors. They have been chosen as reference for this work.

2.3.1.1. Heat Pipe Reactors

Heat pipe reactors are characterized by a monolithic core composed of a solid matrix with channels for fuel pins and heat pipes. It is named “solid core” because of the nearly absence of moving parts such as valves, control rods or pumps (only control drums are movable as described afterwards) [12]. The schematic design of a heat pipe reactor is shown in Figure 2.4(a).

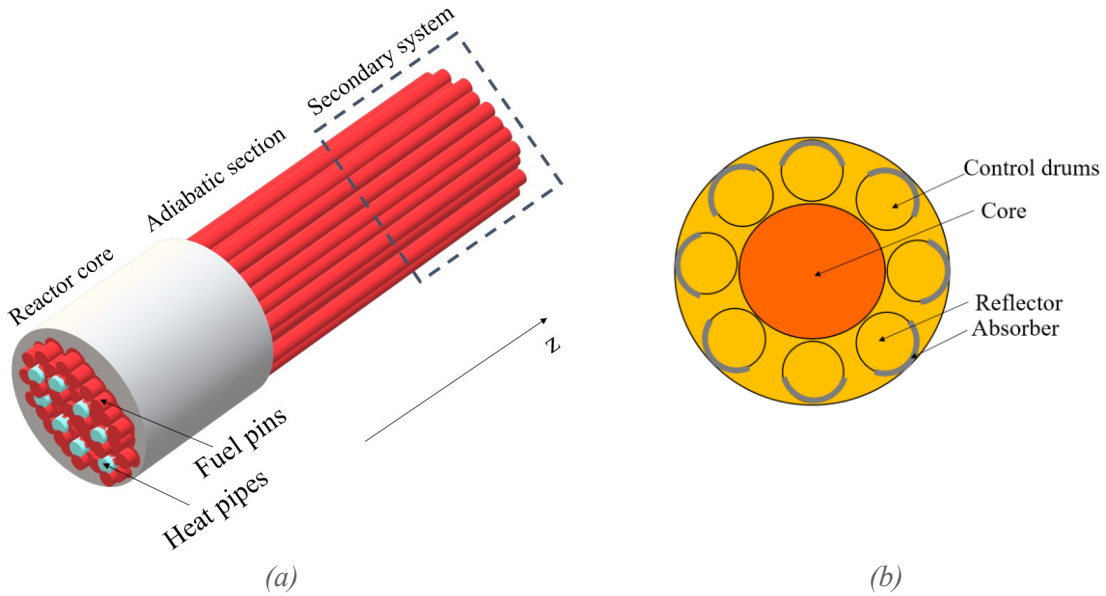


Figure 2.4 – Heat Pipe Reactor scheme (a), control drums functioning scheme (b).

In this design, reactivity control is ensured usually by the control drums system. These drums are rotating cylinders of reflector material (usually BeO or Be) surrounded for half of the circumference by an absorber material (usually B_4C). They are inserted in the reflector layer inside the reactor and rotated

to insert or extract reactivity as shown in Figure 2.4(b). Other possibilities for the reactivity control are proposed in the literature. One of them, which works in a completely passive way, is the Lithium Expansion Module (LEM) [49]. It consists of one or more reservoirs of lithium-6 located above the core and connected to pipes that axially traverse the core. The lithium is kept suspended over the core thanks to the presence of argon in the pipes. When the temperature increases, the lithium expands compressing the gas and entering the core. Therefore, during normal operation, the reactivity is not influenced by this component as the argon is an inert and transparent to neutrons gas. On the other hand, during a temperature ramp the insertion of the lithium allows a completely passive decreasing of reactivity. An image of the system is represented in Figure 2.5. Despite these excellent characteristic of intrinsic safety, this system has some disadvantages. The large Li-6 reservoir over the core makes the fuel handling operation harder and it is influenced by the neutrons leakage on the top of the core, requiring an adequate shielding system. However, the main issue of this system occurs in case of break of the liquid/gas interface, when the gas bubbles flows upside causing a positive reactivity insertion and the uncertainties bounded to this phenomenon must be more deeply studied [49].

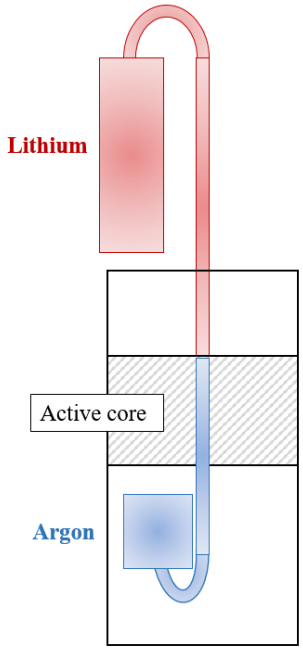


Figure 2.5 – Lithium Expansion Module scheme.

Other systems are proposed in the literature: the control shutter (or sliding reflector) concept and the slat reflector or the petal reflector concepts. An improvement of the traditional rotating drums is also available that is the accident tolerant control drum [39]. Control shutters consist of a segmentation of the reflector system into shutters that are extracted or inserted axially from or inside the core, changing the neutron leakage amount. This system is lighter than control drums but, on the other side, shutters need additional space within the area covered by shadow shield, increasing the mass of the reactor. A variation on the design of the shutters are the control slats, they involve the use of boron carbide slats that are inserted or withdrawn in face of the internal radius of the reflector zone in the core. They do not typically increase the mass of the whole system, because they do not need to be withdrawn completely outside of the shadow cone. The control petals consists of slices of reflectors that are rotated away from the core. They do not involve the use of an absorbing material (as the control shutter) thus increasing the neutrons economy, but they always increase the space needed for the operation. Finally, the accident tolerant control drums differs from the traditional one for the composition. Indeed, they have a side of reflector material, while the other contains a portion of the fuel zone. This configuration entails a larger

control drums worth and allows the reactor to reach a subcritical state even in the "worst-case accidental scenarios" without control rods. More details can be found in [13].

2.3.1.1.A. HEAT PIPES OPERATION

An insight on the heat pipe functioning is given in this section. Heat pipes are sealed tubes filled with a phase changing fluid capable of transporting heat in a completely passive way, from the core to the conversion system. The tube is divided in three sections: the evaporator (inserted into the core); the condenser (placed in the secondary heat exchanger) and the adiabatic section between the two previous. On the tube wall, a porous mean is inserted to provide capillary force to the liquid as explained right after. The working principle of heat pipe is the following: the fluid evaporates in the evaporator and moves to the condenser thanks to pressure force, then it condenses and returns to the core through capillarity and gravity (if the evaporator is placed below the condenser) forces on the heat pipe surfaces. The working principle of this mechanism is shown in Figure 2.6.

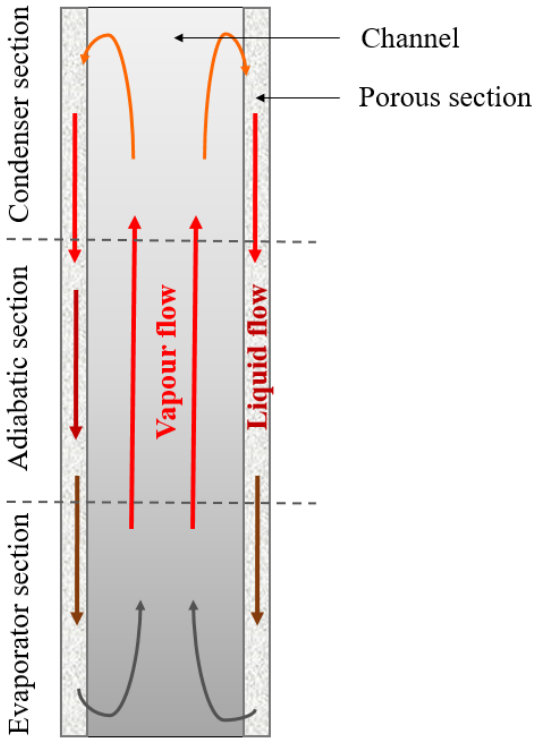


Figure 2.6 – Heat pipe functioning principle.

The main benefits of the use of heat pipes for the core cooling are:

- a completely passive heat extraction system;
- the much higher thermal conductance compared to any other heat transfer method of the same dimensions;
- the capacity of transporting heat with significantly low temperature gradients;
- the independence of operation of each heat pipes, that ensure a sufficient core cooling in case of failure of one of them;
- the possibility of adapting the pipe geometry to the core configuration [50].

As the heat pipe operation is based on the fluid phase change and the capillarity force, it is limited by various physical phenomena. According to the working temperature of the pipe, the maximum possible transferred power is limited [51]. The main phenomena involved are:

- viscous limit: the pressure difference between the evaporator and the condenser allows the displacement of the vapour. When this mechanism is cancelled by the opposed viscous force, this limit is reached;
- sonic limit: it is related to the vapour achievement of sonic velocity at the evaporator exit. In this condition, the chocked flow effect is met. Subsequently, the mass flow rate cannot overcome a maximum value, thus limiting the heat transfer capability;
- entrainment limit: it corresponds to the condition in which the interface shear forces become greater than liquid tension forces and liquid droplets enter in the vapour flow. The flow of liquid droplets to condenser causes the liquid content decrease in the evaporator, possibly resulting in wick dry-out;
- capillarity limit: related to the pressure difference between evaporator and condenser that has to be higher that the pressure losses. If the capillarity pressure is not sufficient to allow the displacement of liquid from the condenser to the evaporator, the wick in the evaporator section will undergo a dry-out and the passive pumping power will be insufficient for the correct operation;
- boiling limit: if nucleate boiling occurs, the vapour can remain trapped in the porous wick enabling the dry-out of the wick itself.

All these constraints limit the functioning zone in which the heat pipe can operate, as shown in Figure 2.7. This region depends on material and geometry choices as well as on the operating conditions. For these reasons, the calculation of the limits have to be taken into account for the design decisions and for the verification of operability of the system.

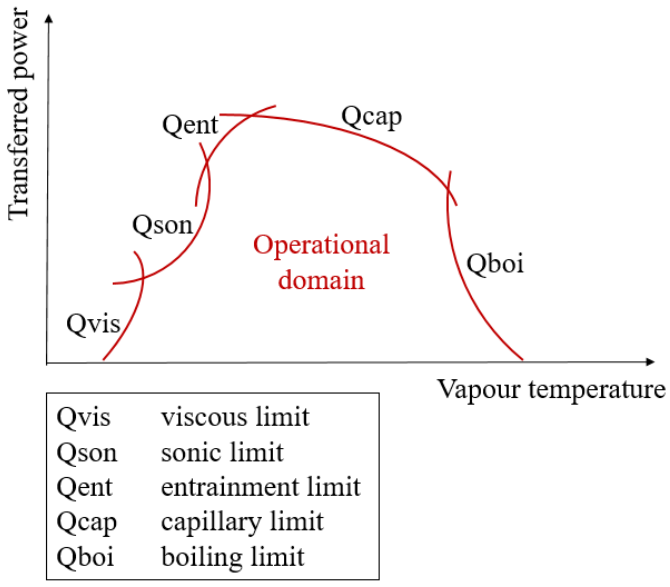


Figure 2.7 – Heat pipe functioning limits.

In conclusion, the main advantage of such a reactor concept relies in the completely natural circulation of the primary coolant in the heat pipes. This guarantees a higher level of passivity in the design that is one of the features of the micro-reactors concepts.

2.3.1.2. High Temperature Reactors

The category of the High Temperature Reactors includes all the reactors that employ the TRISO (TRistrictural ISOtropic fuel) fuel to provide high coolant temperatures at core outlet. The core is characterized by fuel particles dispersed into a matrix (usually graphite) that ensures low temperature gradients and relatively low fuel temperature despite the high coolant temperature. The coolant is heated up to 750 °C for steam generators or up to 950 °C for applications requiring high temperature process heat [14]. Graphite matrix ensures a good mechanical stability, a large thermal inertia and a good fission product retention. In addition, graphite can ensure a negative reactivity coefficient that contributes to high safety level in case of power excursion transients [52].

Two typologies of design are used: prismatic and pebble bed (as shown in Figure 2.8) that are cooled by either gas or molten salts. The prismatic geometry involves a number of fuel assemblies (with TRISO fuel particles dispersed inside) and coolant channels, inserted in a graphite matrix. The pebble bed design, on the contrary, includes the fuel particles dispersed in a matrix of spherical shaped and the continuous re-circulation of the fuel spheres inside the core, crossed by the cooling gas. In this work, as the passivity and simplicity of the design is desired, the pebble bed design is not analysed in detail. Indeed, this design needs an active control for the pebble bed recirculation and an additional system for the pebble debris.

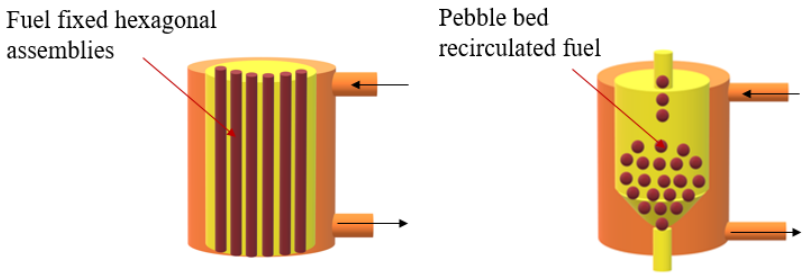


Figure 2.8 – Hexagonal and pebble bed HTR design.

The TRISO is a particular nuclear fuel of spherical shape consisting of a central kernel of fuel surrounded by multiple layers as shown in Figure 2.9. Starting from the centre, beyond fuel radius two carbon buffers (Buffer and inner pyrolytic carbon -IPyC) act as fission gas barrier during nominal operation. Externally, a silicon carbide layer (SiC) has the multiple purposes such as barrier for the metallic products, reservoir for the gas pressure and the structural function. In the external zone, another layer of pyrolytic carbon (OPyC) is raised for the protection of the SiC coating. This particular structure of fuel allows the system to reach high temperatures compared to reactors with standard fuel assemblies such as water reactors.

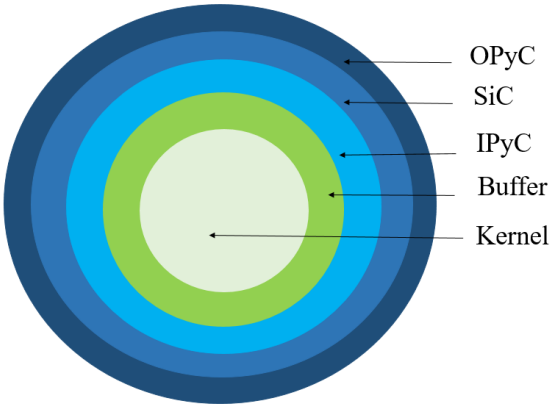


Figure 2.9 – TRISO particle description.

The interest of HTR designs resides in the very high temperature achievable and the highly thermal neutron spectrum due to the graphite matrix that provides a large reactivity feedback effect.

Reactivity control in HTR is ensured by two diversified systems: control rods and the burnable poisons. Control rods are used for the reactor start-up, nominal operation or emergency shutdown. Burnable poisons function is to compensate the initial excess reactivity with irradiation. They allow reaching higher fuel enrichments and longer lifetime.

In conclusion, micro-reactors and HTR are interesting in this work as the already show some of simplification features matching our main objective. Their design is taken as reference and will be compared to large scale reactors presented in the next section.

2.3.2. Large-scale reactors

The two considered designs are Pressurised Water Reactors and Sodium-cooled Fast Reactors. In the next paragraph, a generic description of PWR and SFR is given.

2.3.2.1. Pressurised Water Reactors

The PWR are worldwide the most common nuclear reactors for the electricity production. They are characterised by the ordinary water as coolant and a pressurised primary system (155 bar) that allows the water to reach high temperatures (of the order of 300°C at core outlet) without boiling. The core is characterised by fuel pins organised in square assemblies. The water has a double function in the core: coolant and neutron moderator. The design of the PWR nuclear power plant has been shown in Chapter 1 and reported in Figure 2.10. The classical operating point of this kind of reactor is characterised by a core inlet temperature of 290 °C and core outlet temperature of 323°C. The coolant system is pressurised: 155 bar for primary system and 65 bar for secondary system with corresponding temperature around 281°C. The core is composed of assemblies of square geometry. The number of fuel assemblies is variable according to the PWR design, equal to 193 for a LWR-1300MW. Each assembly is composed of fuel pins, tubes for the control rod insertion (boron carbides pins) and one instrument tube. The diameter of the primary vessel is around 4.394 m. These data correspond to the design of LWR-1300MW, taken as example [53] [54].

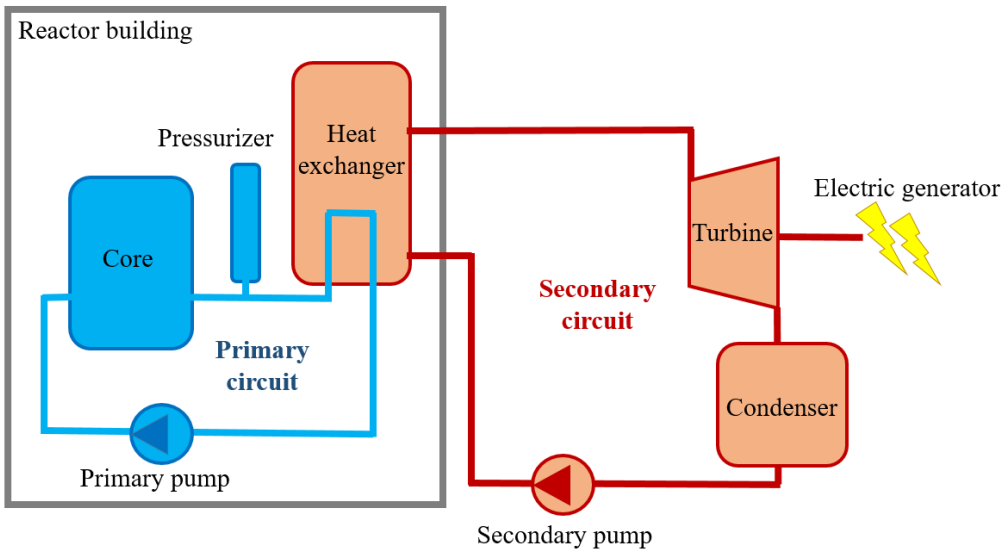


Figure 2.10 – PWR plant scheme.

The means of reactor control for the PWR designs, have already introduced in Chapter 1. It consists of the control of the reactivity made by control rods and boron dilution in coolant. The boron has the primary objective to compensate the reactivity loss due to fuel consumption and the Xe-effect in the first days of the reactor operation. The control rods ensure the power variation following, as well as the start-up and shutdown functions.

2.3.2.2. Sodium-cooled Fast Reactors

Pool type of SFR are characterised by a sodium cooling system and circuit with the turbines feed by water. Between the primary sodium that cools the core and the steam water that feed the turbines, there is an intermediate sodium loop. There are two main reasons: first, it is necessary to impede water and sodium reaction in the primary system that would have serious consequence on the core safety. Secondly, in case where sodium reacts with water or a leakage and possibly a fire happens, no radioactive sodium would be dispersed. The scheme of the reactor plant is dispayed in Figure 2.11.

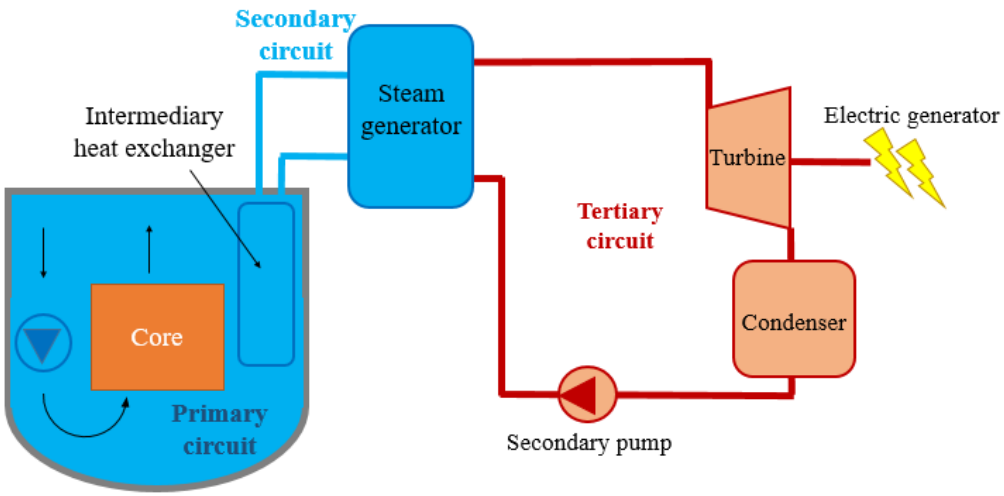


Figure 2.11 – SFR plant scheme.

Another characteristic of the intermediate circuit of the reactor is its position with respect to the vessel. The two main structures under investigation in the Gen IV framework are based on an integrated and a loop concept, they are shown in Figure 2.12. The first one involves the intermediate heat exchanger and the intermediate pump into the vessel structure, while the second concept requires additional pipes and a heat exchanger and intermediary pump outside the vessel.

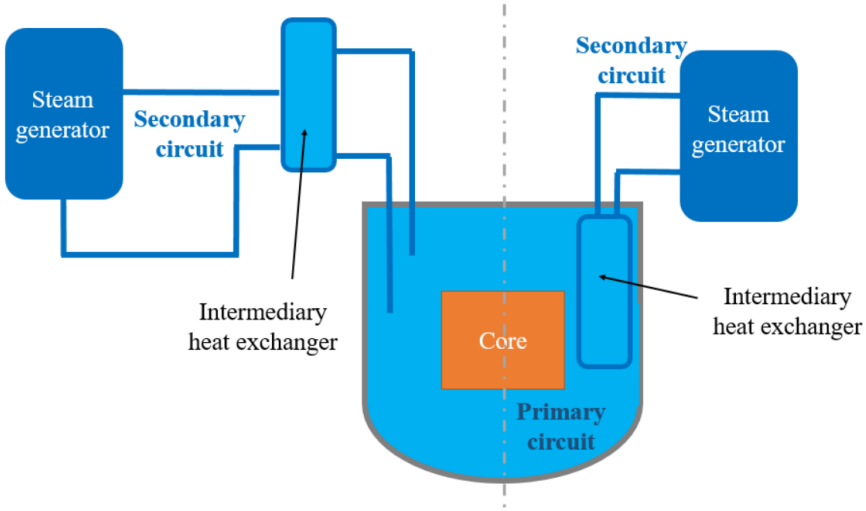


Figure 2.12 – Loop (left) and integrated (right) structure of pool type SFR.

The use of sodium as coolant, with excellent thermal characteristics, allows operating SFR at higher power densities compared to PWR. Furthermore, sodium does not need to be pressurised and the reactor is operated at ambient pressures. The classical operating temperatures for a SFR are around 395°C and 545°C respectively at the core inlet and outlet. The steam temperature, at the steam generator outlet is around 490 °C with a corresponding pressure of 184 bar. These data are particularly referring to SUPERPHENIX (SPX) reactor (1200 MW_e [55]).

The core is composed of hexagonal fuel bundle assemblies (364 in SPX core with 271). Boron carbide control rods use hexagonal structure of the same size of fuel assembly and are inserted in the core in place of some assembly location (24 control assemblies in SPX).

Control rods is the only system that allows the start-up, shutdown, and reactivity loss management as well as power variations. Fast reactors are, in principle, conceived to contribute to the closed fuel cycle and to fissile material breeding. Depending on the desired breeding ratio, fuel consumption effect on the reactivity could vary but is normally lower by far than in thermal reactors [56].

2.3.3. Sum-up of the reactors candidates for this work

In this paragraph, a brief sum-up of the major characteristics of the chosen designs is made. The reference are given for the designs taken into account. In Table 2.1, the main designs characteristics are compared.

Table 2.1 – Reference reactors characteristics.

	HPR	HTR	SFR	PWR
Core power [MW_{th}]	5	200	3600	3817
Core volume [m^3]	~1	35	18	38
Fuel	UO_2	UO_2	$UPuO_2$	UO_2
Cooling system	Heat pipes	2 circuits	3 circuits (loop structure)	2 circuits
Primary coolant	Sodium	Helium	Sodium	Water
Assemblies geometry	Hexagonal in solid matrix	Hexagonal in solid matrix	Hexagonal	Square
Reference	MegaPower [57]	PMR200 [58]	V2B [59]	REP1300 [54]

Up to now, the reference designs chosen have been presented. In the next part of this chapter, the attention is focused on the neutronic and thermal models applied to these specific reactor designs.

2.4. Neutronic and thermal computational models for candidate cores

In this section, neutronic and thermal computational models, specifically implemented for each kind of reactor studied, are presented. These two calculations fields are run separately and used together in the KGH method, as presented in 2.2.3.2, in order to evaluate core behaviour in coupled cases.

2.4.1. Neutronic calculation scheme

Solving the Boltzmann equation can be done in two ways: the stochastic (Monte-Carlo) and the deterministic methods. The former employs stochastic sampling to simulate neutrons behaviour in the reactor core. The latter uses numerical approximation methods to solve the transport equation (Boltzmann equation). In the Monte Carlo approach, a selected number of neutron path and interaction is simulated and the macroscopic cross section is considered as a probability of interaction per unit distance travelled by a neutron. This method can guarantee a high level of precision if sufficient neutrons are simulated, on the contrary, it can be very expensive in terms of computational costs. On the other hand, the deterministic method uses phase-space discretisation (neutrons energy, angular direction, space and time) of the Boltzmann equation. Various numerical methods have been developed, such as the collision Probabilities, the Method of Characteristic, the Spherical Harmonics methods and others. For a complete description of these calculations scheme specific book on reactor physics can be consulted such as [60] and [61].

In this work, two models have been used based on Monte-Carlo and deterministic methods. For the simulation of HPR, HTR and PWR the Serpent 2 [36] Monte-Carlo code package has been used. For SFR cores, the deterministic ERANOS [37] code package has been used, being a code specifically built up for fast reactors.

Serpent is a continuous-energy Monte-Carlo particles calculation code implemented at VTT Technical Research Centre of Finland [62]. Simulation are based on random sampling of phenomena repeated multiple times (cycles) up to a convergence of the result. In this work, Serpent 2 has been used in combination with JEFF-3.1.1 nuclear library.

This code has been used for criticality steady-state calculations and for core depletion calculations. The steady-state calculations are based on the criticality source method. It consists of simulating each neutrons cycle starting from a neutronic source distribution based on the fission rates of the previous cycle [63]. The depletion calculations are made by coupling steady-state solution and Bateman equation at each time step [64] (quasi-static approximation). The predictor-corrector method is used to couple the both calculations [65].

ERANOS is a deterministic code developed in a European framework in the 90's. It is a two-step lattice/core based code. The first stage is based on ECCO module that computes the self-shielded cross sections collapsed to few groups (33 groups energy mesh) for core calculation purpose, used in conjunction to the JEFF-3.1 nuclear data library [66]. The second phase solves the Boltzmann equation in steady state. In this work, the solver used in the 2D RZ core calculation is the transport equation SN method, based on the evaluation of the neutron flux in a number of discrete neutrons direction [61].

2.4.2. Thermal calculation scheme

The reactor cooling system is a complex system, characterised by multiple components. The thermal-hydraulic description of the entire system is characterised by multiple phenomena. In this paragraph, first, a general-purpose description is proposed, then specific assumption are made and applied models associated to each reactor design are presented.

Thermal-hydraulic analysis of the cooling system is a multi-scale problem. Three levels can be distinguished for modelling purpose:

- the "system";
- the components;
- the specific locations.

At "system level", thermal-hydraulics model takes into the entire cooling system (primary, secondary and intermediary loops - if present) as a whole. The system is represented as circuits and components. The system is normally solved in 1D except for some of most important components, such as the core, where a 3D analysis can be used. The thermal-hydraulics of the system account for the mass, momentum and energy conservation equations.

The component (or sub-channel) analysis deals with the more detailed analysis of each component. The core thermal-hydraulic, for example, is analysed at the scale of each sub-channel. Thus, the calculation (in case of PWR taken as example) is made on the fuel, gap, cladding and channel geometry. In this analysis, normally a 3D calculation is used, especially to study the accidental transients and be able to foresee the inhomogeneity in the core. The considered equations describe the thermal-hydraulic phenomena around the fuel channel (conduction and convection equations mainly).

Finally, the specific location scale refers to the study of specific locations in a component that need a high level of precision in the result prediction for specific transient evaluations. It is usually done with the CFD method, that solves the system of the Navier-Stokes equations using different numerical techniques [67].

In this work, a first study at "system level" has been performed in Chapter 3, and will be described in detail in this chapter. Then, in the rest of the work, the analysis is based on global core behaviour, for this reason the sub-channel approach is used. The description of the conduction and convection equations is presented here and then applications to specific reactor designs are highlighted.

Heat transfer in the core is characterise by conduction and convection. The former represents the thermal energy transfer in a static mean, due to the particles agitation. The latter corresponds to the heat transfer with a fluid in motion. In the core, the energy is produced by fissions inside the fuel, it is transferred in the fuel, the gap and the cladding by conduction and then removed by the liquid or gas coolant by convection.

The general heat conduction equation is in the form of:

$$D c_p \frac{\partial T}{\partial t} = \nabla(k \cdot T) + Q''' ; \qquad (2.28)$$

where: D, c_p, k are respectively the density [kg/m^3], the specific heat [J kg^{-1} K^{-1}] and the thermal conductivity [W m^{-1} K^{-1}] of the mean (properties described above) and Q''' is the power density generated inside the material [W m^{-3}].

The equation representing the heat convection between a solid matter and a fluid flowing on its surface is the following:

$$Q'' = h\,(T_{wall} - T_{bulk})\,; \qquad (2.29)$$

where: T_{wall} and T_{bulk} are respectively the temperature of the solid at the interface and the bulk temperature of the fluid flowing on this surface [K]. As explained above, h [W m^{-2} K^{-1}] is the heat transfer coefficient that can be deduced by the Nusselt number of the specific flowing case.

Some non-dimensional numbers are used to characterise the fluid-dynamic:

- Nusselt number Nu:

$$Nu = \frac{h\,L}{k}\ ; \qquad (2.30)$$

where: h is the heat transfer coefficient [W m^{-2} K^{-1}]; L is the characteristic dimension of the geometry (the diameter for example in the case of a fluid flowing in a circular channel[1]) [m]; k is the thermal conductivity [W m^{-1} K^{-1}].

- Reynolds number Re:

$$Re = \frac{D\,v\,L}{\mu}; \qquad (2.31)$$

where D is the fluid density [kg/m^3]; v is the fluid flowing velocity [m/s]; L is the characteristic dimension of the geometry and μ is the dynamic viscosity [kg m^{-1} s^{-1}].

- Prandtl number Pr:

[1] If the case of a fluid flowing in a channel that is not circular an equivalent diameter, called hydraulic diameter is used. It is defined as follows: $D_{hydr} = \frac{4A}{P}$; where A is the channel surface [m^2] and P is the channel perimeter [m].

$$Pr = \frac{\mu\, c_p}{k}; \qquad (2.32)$$

where: μ is the dynamic viscosity [kg m^{-1} s^{-1}]; c_p is the specific heat [J kg^{-1} K^{-1}] and k is the thermal conductivity [W m^{-1} K^{-1}].

Although characterised by different core configuration, HTR, SFR and PWR designs share common heat transfer principle: fuel produced energy is transmitted by conduction to the cladding (through a gap when present), to the moderator matrix (in the case of HTR) and finally to the coolant. The coolant removes heat flowing from the inlet to the outlet of the core by forced convection with the cladding or the solid matrix. On the other hand, the HPR are characterised by a slightly different behaviour. The heat is similarly transferred by conduction in the fuel and solid matrix, but the cooling system is based on the coolant phase changing and the coolant natural flowing between the core and the secondary system. The approach to the model of thermal behaviour is thus slightly different. In the following lines, the description of the thermal model in the HTR, SFR and PWR is made and successively the specific calculation scheme for the HPR is presented.

The calculations have been made on equivalent thermal cells based on the systems symmetry. The SFR and PWR are characterised by assemblies composed of pins inserted in the flowing coolant. The mean geometry cell is thus based on the pin-gap-cladding element surrounded by the flowing coolant. The SFR and PWR base thermal cell is represented in Figure 2.13.

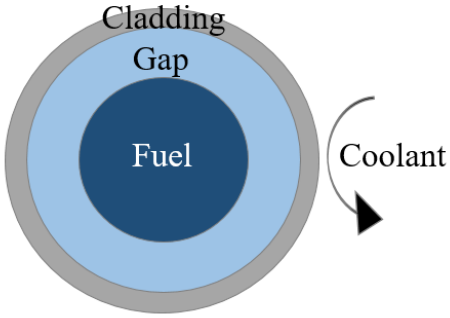
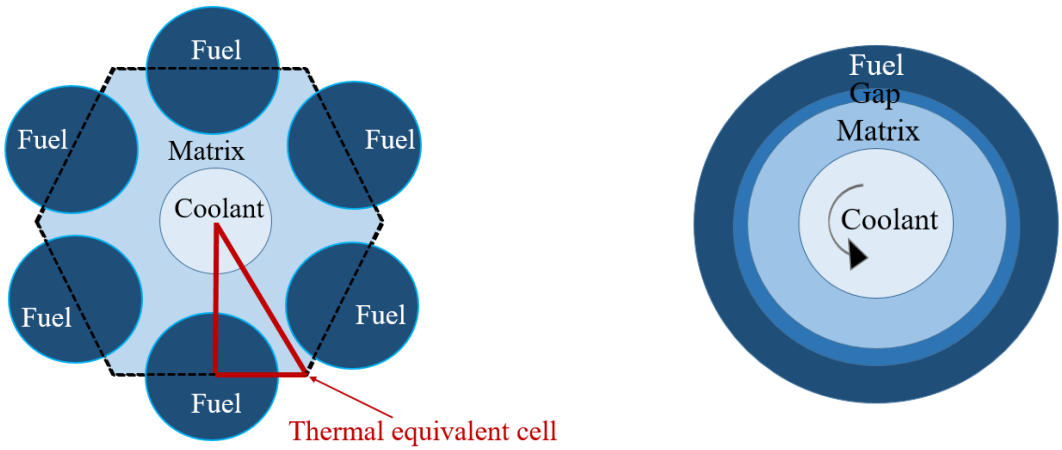


Figure 2.13 – PWR and SFR thermal calculation mean geometry cell.

The HTR and HPR are characterised by slightly different geometry because the fuel pins are inserted into a solid matrix that is also crossed by the cooling channels. Due to the geometry symmetry, a thermal equivalent cell can be identified - as in Figure 2.14(a) - and the equivalent geometry for the thermal calculations can be described - as in Figure 2.14(b). The equivalent geometry has been identified considering volumes conservation.



(a) *(b)*

Figure 2.14 – HPR and HTR thermal calculation scheme – mean symmetrical equivalent cell (a), equivalent geometry for heat transfer calculation scheme (b).

In the HTR case, fuel pins are constituted by a graphite matrix with dispersed TRISO particles. In the equivalent geometry, the graphite and TRISO materials have been considered homogenised and thus their properties have been computed on average with respect to the mass proportions.

With the previously described equivalent geometries, the conduction equation is applied to compute the heat transfer from the fuel to the coolant. The equation (2.28) is thus rewritten in steady-state and radial coordinates and constitute a system of equations for the heat transfer in each material (fuel, cladding, matrix, gap). The gap is filled by a gas that is not circulated in the channel, thus the heat exchange in the gap can be approximated as pure conduction. The system of equations is constituted by the following equation in each material:

$$\frac{1}{r}\frac{\partial}{\partial r}\left(k\, r \frac{\partial T}{\partial r}\right) + Q''' = 0\,; \qquad (2.33)$$

where: r is the radial coordinate [m]; k is the conductivity of each materials [W m^{-1} K^{-1}]; T is the material temperature; Q''' is the power density generated inside the material (term only present in fuel) [W m^{-3}].

This system of equation is constituted by interface conditions between each material that are based on the conservation of heat from one material to the adjacent. Furthermore, two boundary conditions are applied in the system. At the centre of the fuel pin, the adiabatic condition is imposed, due to the symmetrical geometry of the pin. On the other side, the convection with the coolant is imposed as follows:

$$Q = h\, A_{wall}\, (T_{wall} - T_{mean}); \qquad (2.34)$$

where: Q is the heat transferred by convection [W], h is the heat transfer coefficient [W m^{-2} K^{-1}]; A_{wall} is the surface [m^2] of the wall on which the fluid flows and removes heat by the convection (the cladding for PWR and SFR and the channel wall in the case of HTR); T_{wall} and T_{mean} are the temperatures respectively of the wall and of the fluid bulk [K].

The definition of the coolant mean bulk temperature is possible with the equation of the energy conservation in the core. It is written as follows:

$$Q = \dot{m}\, c_p\, (T_{out} - T_{in}); \qquad (2.35)$$

where: Q is the heat removed by the fluid [W]; $\dot{m}$ is the coolant mass flow rate [kg/s]; T_{out} and T_{in} are respectively the core outlet and inlet temperatures [K].

2.4.2.1. Heat pipe thermal modelling insight

The conditions on the convective heat exchange in HPR is slightly different. The mean coolant temperature in a heat pipe needs a specific calculation due to the thermal-hydraulic conditions of the fluid. Indeed, the fluid is characterised by phase changing at the evaporator and condenser sections of the pipe and by the natural convection driven by pressure difference in the pipe and capillarity force on the wall. In the following lines a detailed description of the heat pipe thermal modelling is given.

Several studies have been made in literature on the heat pipe thermal physics and different approaches are possible. As many phenomena occur in the heat pipe, very elaborate models have been developed to accurately predict the temperature evolution. However, such models lead to complex development and require do sophisticated and adapted numerical tools [68]. Here, a choice was made to use existing models that neglect the fluid dynamic feature of the problem. The effective heat conduction model uses corrected thermal properties to simulate heat pipes thermal-hydraulic phenomena with simple conduction formulations [69] [70]. The lumped capacitance thermal scheme divides the volumes into a defined number of sub-volumes and computes heat transfer between them. This method has been validated for slow transients [69], which covers the need of the present purpose. Finally, the thermal network analysis computes each heat exchange defining an equivalent thermal resistance and solves the problem in analogy to an electrical circuit. This model does not account for fluid-dynamic physics, but show a required accuracy on thermal behaviour prediction during transients [71]. In this work, this last model has been chosen for both adequate determination of the pipe temperature field and simplicity of implementation. As the model does not consider the dynamic phenomena, the limits of operation have to be calculated to account for the good heat pipe operation, as presented in Section 2.3.1.1.A.

In the application of the equivalent resistances model, some valid additional assumptions have been made. In particular, some phenomena can be neglected:

- heat exchange in the liquid-vapour interface;
- liquid flow phenomenon, as it contributes marginally to heat transfer;
- vapour flow phenomenon as it as a small thermal resistance with respect to the others [72].

The liquid and vapour flows have anyway an importance on the pipe hydraulics and they have to be accounted in the limits calculations to ensure the proper heat removal by the pipe, as mentioned above.

The boundary condition set at the evaporator is the heat flux produced by the core fission power. On the other side, at the condenser, the condition of convective heat exchange is set with the secondary system.

The description of the equivalent thermal circuit is represented in Figure 2.15. In this scheme, the heat transfer in the pipe wall, wick (structural material and liquid) are modelled in the three heat pipe sections (evaporator, condenser and adiabatic section).

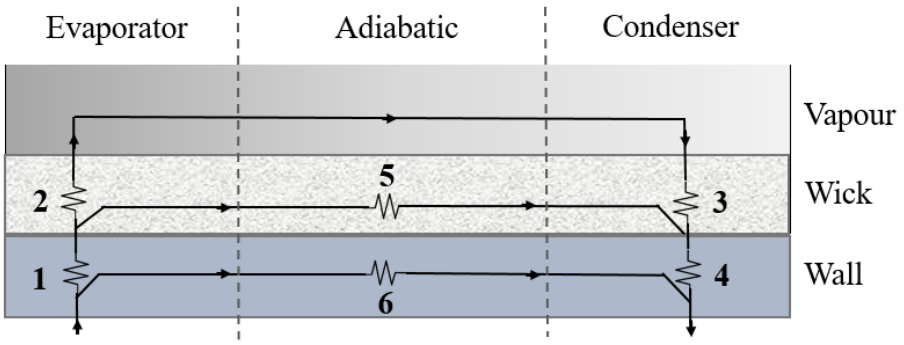


Figure 2.15 – Heat pipe thermal equivalent network model.

The presented resistances network is solved in analogy to an electrical one with a system of equations based on the heat conduction equation in each resistance and the energy conservation at each node of the system.

The heat conduction equation for each resistance in steady-state is the following:

$$2\,\frac{\alpha_i}{\lambda_i^2}\,(T_{i^-} + T_{i^+} - 2\,T_i) = 0; \tag{2.36}$$

where: $\alpha = \frac{k}{\rho c_p}$ is the thermal conductivity [W m^{-1} K^{-1}]; ρ is the material density [kg m^{-3}]; c_p is the specific heat [J kg^{-1} K^{-1}]; λ is the resistance thickness [m]. The subscripts i, i^- and i^+ refers respectively to the i-resistance temperature, the previous and the subsequent node temperatures.

The energy conservation at each node is described by the equation:

$$Q = 2\,\frac{k_i\,A_i}{\lambda_i}\,(T_n - T_i) \tag{2.37}$$

where: A_i is the cross section surface of the resistance [m^2]; T_i is the i-resistance temperature and T_n is the n-node temperature [K].

The thermal calculation scheme validation has been made with respect to the literature references for all the chosen reactors and is shown in Annex II.2.

2.5. Conclusions

In this chapter, the description of the autonomous core in terms of physical phenomena in play is given. The definition is based on the absence of active reactivity control except for start-up and shutdown phases and absence of refuelling phases. Instantaneous criticality criterion is ensured by compensation between terms that all contribute to the reactivity evolution (fuel depletion, feedbacks coefficients and, if needed, dedicated passive systems). As this work focuses on the core behaviour and design, in this chapter, the core physics and computational model have been described.

First, time evolution of reactivity is influenced by the fuel depletion that brings a negative contribution (due to the consumption of the fissile isotopes except in particular kind of fuel of breeder reactors). If this term is the only one to act on the reactivity, an passive core would not be possible to in order to meet the criticality criterion. Reactivity would then decrease and the power would go to zero

very fast. However, other contribution exists, bounded to the variation of the core thermal conditions. The so-called reactivity feedback effects introduces a contribution that, in this work, is defined by design to be able (if so) to compensate the reactivity loss due to fuel consumption during the whole reactor lifetime.

In this chapter, the implemented computational models to study the above-defined problem are presented. In particular, the need for coupling between the neutronic and the thermal hydraulic fields has been highlighted. The coupling method applied in this work has been presented, based on the KGH approach that couples in quasi-static way the neutronic and thermal-hydraulic calculations of the core. Also the neutronics and thermal stand-alone computational schemes are presented.

Finally, the reactor designs accounted in this work have been introduced. They includes the micro-reactor concepts as the Heat Pipes Reactors and High Temperatures Reactors. These designs are compared to industrial-scale reactors as Pressurised Water Reactors and Sodium-cooled Fast Reactors. The reference designs chosen are presented and the computational methods implemented, for the study of their autonomous operation, are introduced.

In this study, it is chosen to study the reactor systems separately. The focus is on the core behaviour, but the Energy Conversion System behaviour is first separately analysed. Chapter 3 describes the possible contribution of the ECS to the autonomous core. Then, in the rest of the work, the attention will be focused on the core behaviour.

Chapter 3

Energy Conversion System contribution

Summary

3.1. Introduction 78

3.2. CYCLOP 78

3.3. Secondary system designs 79

3.3.1. PWR Rankine cycle 80

3.3.2. SFR Rankine cycle 81

3.3.3. SFR Brayton cycle 82

3.3.4. Conclusions on design of secondary system connected to an autonomous core 83

3.4. Potential contribution of the ECS to the core 83

3.4.1. Maximum theoretical variation of core inlet temperature 83

3.4.2. Control of secondary cycle for the driving of the core inlet temperature 85

3.4.2.1. PWR Rankine cycle 86

3.4.2.2. SFR Rankine cycle 88

3.4.2.3 SFR Brayton cycle 89

3.5. Application of the KGH method with the secondary system contribution 89

3.6. Conclusions 91

3.1. Introduction

The complete study of an autonomous reactor should be approached with the modelling of the whole system (core, primary and secondary system). Indeed, the temperatures influencing the reactivity are controlled by the primary and the secondary cooling systems. However, the modelling of the whole system of the different types of reactors could be very time consuming. With the objective to simplify the approach and to separate it into two parts, a specific analysis is conducted in this chapter.

Considering the KGH formulation, given in Chapter 2 equation (2.16), the impact on the power of the core is given by:

- the reactivity feedbacks coefficients, characteristics of the core design;
- the reactivity swing bounded to the fuel depletion, characteristic of the core design;
- the core temperature difference, bounded to the operation of the primary cooling system;
- the core inlet temperature, bounded to the operation of the secondary cooling system.

The control of the inlet temperature is thus supposed to be mainly driven by the secondary circuit[2] (keeping power and primary flow rate constant, which is the objective of an autonomous core). This chapter proposes to evaluate the contribution of the only Energy Conversion System (ECS) on the reactivity of each kind of reactor.

Two ECS designs are analysed, a Rankine and a Brayton cycle, as the one used in the nowadays operating reactors and the other proposed in SFR Astrid French design [73] as a good candidate for future reactors operating at high temperature. The analysis of these systems is made with a CEA tool CYCLOP, considering a steady-state approach. Paragraph 3.2 describes this code. Then, paragraph 3.3 describes in details the two cycles and discuss about their connection to an autonomous core. Successively, in paragraph 3.4, the contribution of the secondary system is studied. A theoretical study is made on the maximum core inlet temperature variation and thus the maximum contribution of each ECS to an autonomous operating core. In a second step, a control over the secondary system is proposed to actively drive this temperature. Finally, the KGH method is applied to an example case of reactor with active contribution of secondary system.

3.2. CYCLOP

This section presents a specific code for the design of thermodynamic cycles. The software tool CYCLOP, developed by CEA, is designed for the modelling of on-design power conversion cycles. [74]. It has been subjected to rigorous testing across a diverse range of research and development initiatives, including the utilisation of the helium Brayton cycle in gas-cooled fast reactors (GFRs) [75] [76] and the sc-CO2 cycle for SFRs [77]. The software has undergone validation with Rankine steam cycles linked to a range of reactors, including the Cruas PWR and the French Sodium Fast Reactor (SFR) SUPERPHENIX. The software is equipped with an exhaustive database of material properties, in accordance with the recommendations of the National Institute of Standards and Technology.

A network of fluid loops represents a cycle within CYCLOP. The energetic components of these loops include a heat source and sink, as well as a turbine, pump, and compressor, among other devices. Hydraulic elements, such as pipes and valves, are also included. Macroscopic parameters such as

[2] In this work, the Energy Conversion System (ECS) will also be addressed as secondary system. It is assumed that in the SFR designs the cooling systems are addressed as primary, intermediary and secondary systems.

isentropic efficiency for turbomachinery are used to characterise the performance characteristics of these components. The software computes the mass and energy balances for all cycle components with minimal input data requirements. It also includes a deterministic algorithm based on the Nelder-Mead algorithm [78], for the optimisation of the thermodynamic cycle.

The part-load performance of components is not simulated by CYCLOP, as in the DEOP-IAEA software. Therefore, the component performance and pressure ratios of turbine groups remain constant and are determined by values that were established from the initial design with a 100% electrical load.

This code is used here to verify the feasibility of designing a secondary system with minimal active components and to assess the potential for an active control system to regulate the HX inlet temperature. The study is conducted with a focus on the smallest possible variations in the operational point, with the underlying assumption that the performance of the components will remain constant. The objective is to demonstrate the potential for variation in the operational point.

3.3. Secondary system designs

In this work, a Rankine and a Brayton cycle are studied. The Rankine is analysed connected to a PWR and a SFR. On the other hand, the Brayton is only connected to a SFR, because the efficiency of a system PWR-Brayton is considered too low to be taken into account.

The data considered for the Rankine cycle are reported in Table 3.1.The systems have been taken as the ones in literature for cores producing thermal power of 2785 MW for the PWR and 400 MW for the SFR. The effect of scale of the core powers provides proportional results (from the secondary point of view) and does not change the conclusions of this chapter, focused on the trend of the system control.

Table 3.1– Rankine cycle coupled to PWR and SFR.

		PWR	SFR
SG	Flow rate [kg/s]	1409	177
	Power [MW]	2785	400
Primary coolant SG outlet	T [K]	543	783
	p [Pa]	55e5	180e5
	Steam	Saturated	Superheated
Primary coolant SG inlet	T [K]	463	513
	p [Pa]	67e5	192e5

The cycle is made up by two turbines (high and low pressure) a super-heater and two re-heaters. A simplified scheme is given in Figure 3.1. The technological constraints imposed on this system are supposed as a minimum temperature pinch of 15 °C for the super-heater and 5°C for the re-heaters. In the case of Rankine connected to SFR, there is no super-heater, as not useful for high temperature operation.

The simplified Brayton cycle considered is made up of one turbine, one compressor and a heat recuperation unit.

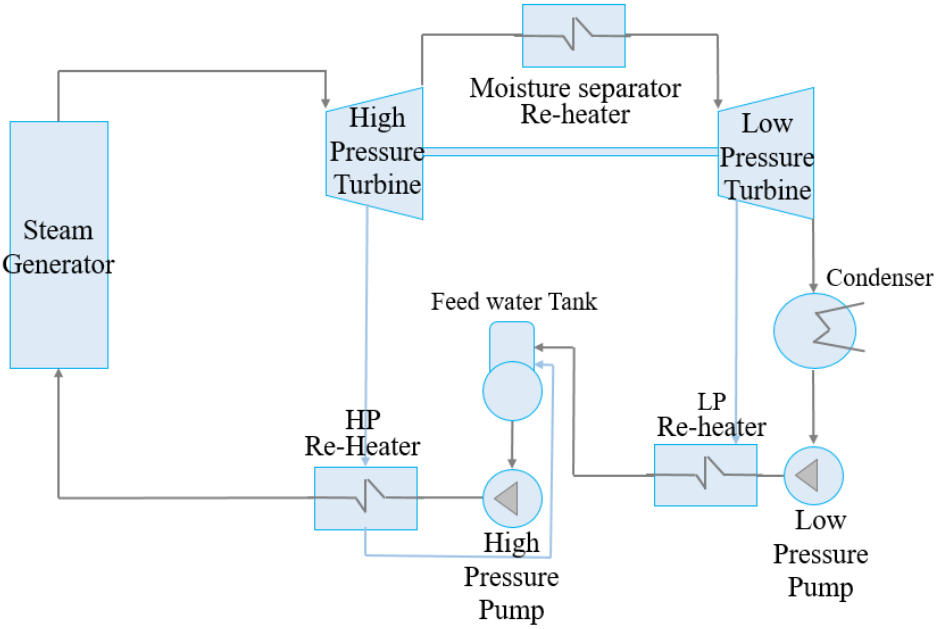


Figure 3.1 – Simplified scheme of Rankine cycle.

The possible connection of ECS to an autonomous core is now analysed for the described systems.

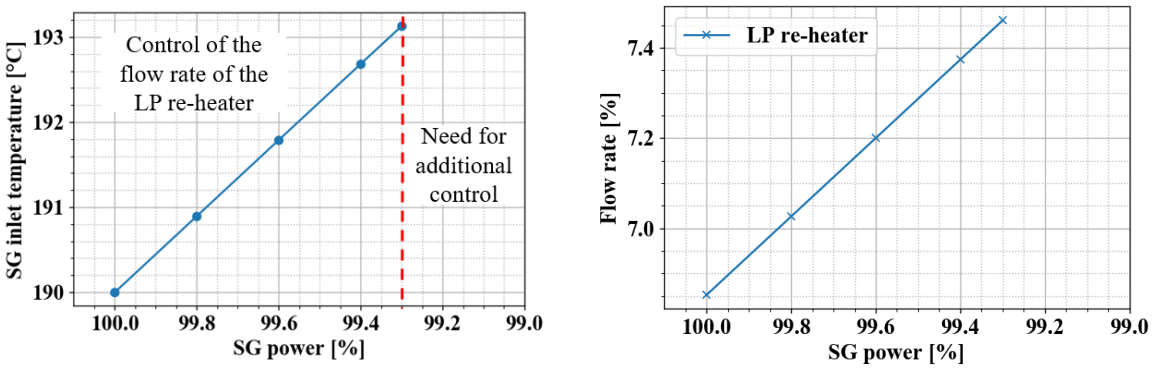
Two assumptions are made:

- The pinch between primary and secondary system hot temperatures is considered constant in an ideal steam generator, as a design limitation.
- On the secondary system, a constant total flow rate and constant conditions (temperature and pressure at the HX outlet) are imposed in a first step. This point will be challenged later in this chapter.

With these assumptions, it can be stated that the core inlet temperature is, at first order, depending on the secondary HX inlet temperature. The objective is thus to have a first overview of what could be the behaviour of the HX inlet temperature.

3.3.1. PWR Rankine cycle

First, a PWR-Rankine system is studied. The control proposed here acts on the flow rate of the re-heaters and super-heaters and on the pressure of the HP re-heater (this control over the pressure will be discussed later). With a first control only on the flow rate of the LP re-heater, it is possible to ensure good operation of the Rankine only for very low variation of the power (up to 0.7%), as shown in Figure 3.2.



(a) *(b)*

Figure 3.2 – Variation of the SG inlet temperature (a) with control over the LP re-heater flow rate (b).

To widen the operating range, for lower power, a control over all the flow rates is necessary and the HP re-heater pressure is necessary. In particular, the decrease of the power corresponds to the need for increasing the HP re-heater flow rate and pressure. This is due to the hypothesis of constant temperature and pressure at the HX outlet. The HP re-heater must therefore transfer more heat at higher temperature to the SG inlet to increase the inlet temperature. The other two flow rates (super-heater and LP re-heater) are slightly reduced. Further details of this operation are given in the next paragraph.

Figure 3.3 represents the variation of the inlet temperature (according to a variation of the power) and the associated efficiency. A variation of 15% of the power is considered. It is assumed that in this range of power, the efficiency of the components can be considered constant and not accounted in the calculations. This range of variation is considered in accordance to the assumption that the performance of the components will remain constant in CYCLOP.

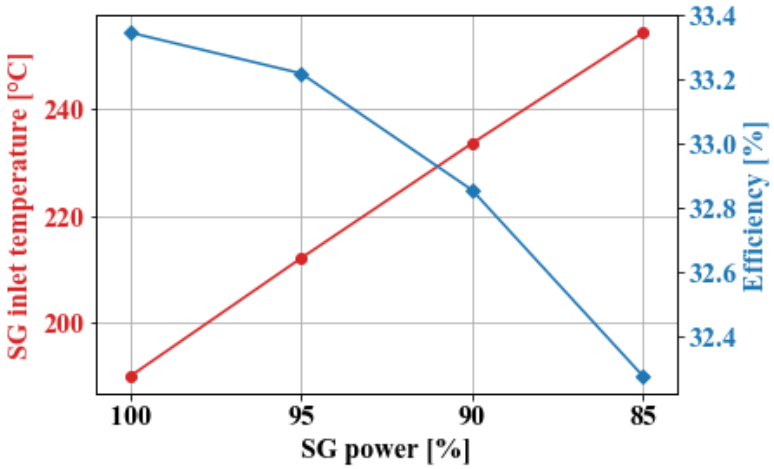


Figure 3.3 – Variation of the SG inlet temperature and relative cycle efficiency.

As the cycle is built and optimised for a SG inlet temperature of 190°C, corresponding to the nominal power, other points of operation are characterised by a lower efficiency. A control over the system is possible to find an existing point of operation, but at the expense of the efficiency.

3.3.2. SFR Rankine cycle

The same study is made on a SFR-Rankine system. The same system as for PWR is considered, with the same control, but without the super-heater, as explained before. In response to a power decrease, in this case, the only control of LP re-heater flow rate is not sufficient, as before. The LP flow rate has to

be slightly decreased and the HP flow rate and pressure have to be increased to accommodate a decrease of power.

The results is an increase of the SG inlet temperature and a decrease of the efficiency, as in the previous case. These parameters are shown in Figure 3.4.

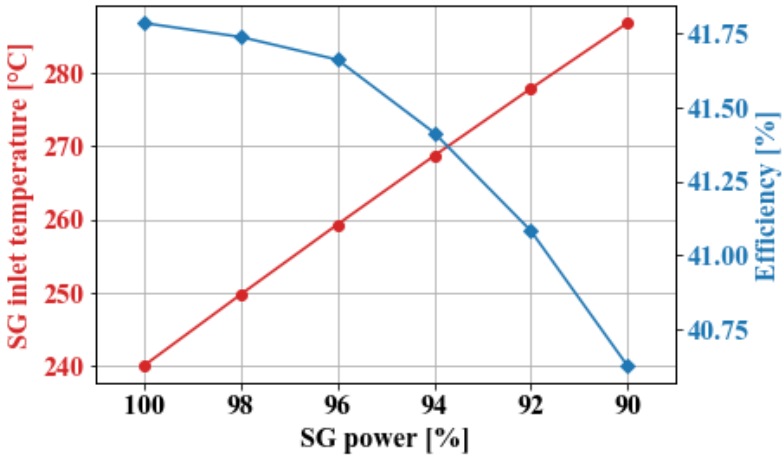


Figure 3.4 - Variation of the SG inlet temperature and relative cycle efficiency of a Rankine-SFR.

The increase of the SG inlet temperature is $-4.17\ °C/\%$ in the SFR and $-3.25\ °C/\%$ in the PWR. The temperature variations are comparable, while the efficiency of the SFR-Rankine is higher due to the higher temperatures of operation.

3.3.3. SFR Brayton cycle

Finally, a SFR-Brayton system is considered. As a reminder, the simplified Brayton cycle considered is made up of one turbine, one compressor and a heat recuperation unit. As a consequence of power decrease, the system can adapt its operation without active control up to a variation of 6% of the power, as shown in Figure 3.5. The adaptation is possible because the system decreases the heat transferred to the cold sink. For larger power variation, the temperature pinch at the heat recuperation unit becomes negative, causing the system not to function properly. The minimum pinch considered for the good operation is of 5°C.

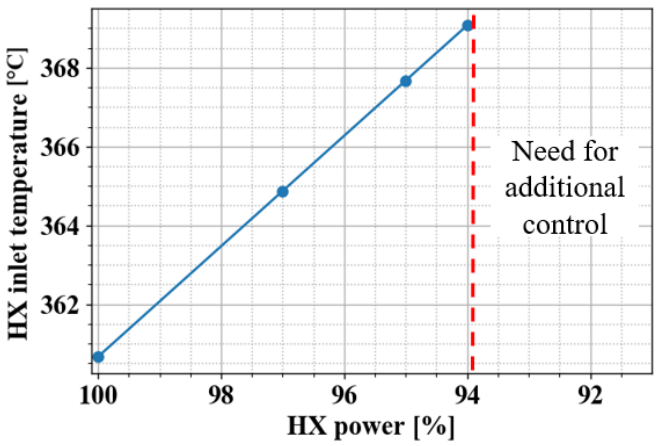


Figure 3.5 - Variation of the HX inlet temperature without active control.

To adapt the system for larger variation of the power, a control over the gas flow rate is proposed here. This is possible with a tank that can introduce a mass of gas in the cycle with variable volume. In

real Brayton cycle, the control is made through by-pass flow rates. This is not considered here because it would open a complexification of the problem and the possible solutions.

Here, the flow rate is linearly decreased with the power decrease. The flow rate variation has an impact on the component efficiencies, but it is not considered in this work. For this reason, the efficiency of the cycle in these conditions is constant. Indeed, the efficiency is defined as

$$\eta = \frac{P_{turbine} - P_{compressor}}{P_{HX}} \; ; \tag{3.1}$$

where P is the power of the turbine, compressor and heat exchanger. The decrease in the flow rate is proportional to the decrease of P_{HX} and the $P_{turbine}$ and $P_{compressor}$ are proportional to the flow rate.

3.3.4. Conclusions on design of secondary system connected to an autonomous core

Up to now, the possibility to connect a secondary system with an autonomous core has been verified in a limited power variation because of the assumption of constant efficiency of each component. However, the extension to a larger power range seems possible with a potentially more important impact on the efficiency. The operation of the ECS needs an active control even for very small variation of the power transferred to the HX. A control based on the flow rate variation is proposed in this work and can guarantee the adaptation of the system to the power produced by the core.

Anyway, in these examples, the decrease of the power corresponds to an increase of the HX inlet temperature. This would introduce a feedback effect in the core that would boost the power decrease. In the next part of this chapter we focus on the control that could allow to actively decrease the HX inlet temperature and improve the performance of the autonomous core.

3.4. Potential contribution of the ECS to the core

To contribute to the autonomous core, the secondary system should drive the core inlet temperature in order to take advantage of the reactivity feedbacks. To counterbalance the decrease of the power due to the fuel burn-up, the reactivity feedbacks should lead to an increase of the power. The feedback coefficients have negative values, so the core inlet temperature should be actively decreased.

In the next section, the maximum theoretical range of variation of the HX inlet temperature is discussed. In the last section, the control of the secondary system to decrease this temperature is studied and the associated cycle efficiency is calculated.

3.4.1. Maximum theoretical variation of core inlet temperature

This section is dedicated to the analysis of the theoretical impact of the secondary system on the reactivity balance. To determine the maximum possible gain in reactivity provided by the secondary system, the equation (2.16) is rewritten as:

$$K\ \delta T_{in} + \delta \rho_{fuel} = 0; \tag{3.2}$$

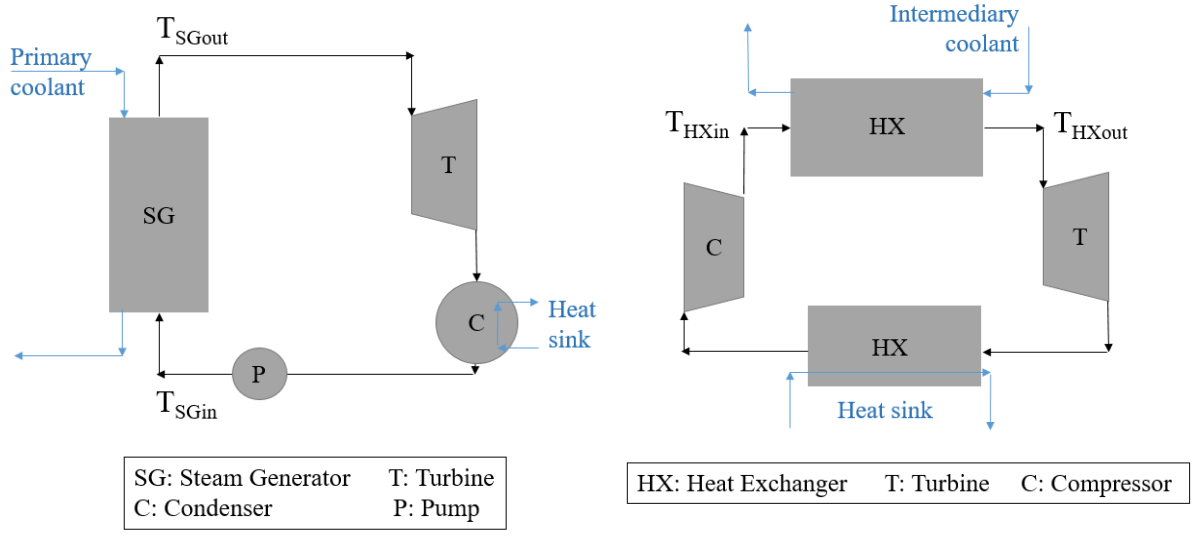
In this formulation, active control over the secondary system allows for complete compensation of the reactivity loss due to fuel depletion. This allows to guarantee a stability of the reactor at constant power. The time interval, during which the secondary system can be controlled to guarantee a stable autonomous core, depends on the maximum $K\ \delta T_{in}$. Integrating the equation (3.2) over time:

$$\int (K\ \delta T_{in})_{max}\ dt + \int \delta\rho_{fuel}\ dt = 0; \qquad (3.3)$$

The first term represents the maximum amount of reactivity that can be provided by the secondary system. The second term is obtained through neutronic calculation. The equation enables the assessment of the compensation in terms of reactivity that can be brought by the secondary system in order to maintain a constant power. The compensation value allows for the determination of the time period during which the secondary system can contributes to maintain a constant power.

The maximum gain in reactivity is reached for the maximum value of δT_{in}. In the following section, a simplified and purely theoretical analysis is performed in order to provide an estimation of the temperature range (δT_{in}) that is theoretically achievable, depending on the core design and on the thermodynamic cycle.

PWR and SFR could operate with either a Rankine or a Brayton cycle. The Rankine cycle is the most common thermodynamic cycle considered for both PWR and SFR reactors. The Brayton cycle is currently under investigation as it may offer some improvements in terms of safety for SFR [73]. Figure 3.6 provides a simplified representation of both cycles.



(a) *(b)*

Figure 3.6 – Simplified scheme of Rankine (a) and Brayton (b) thermodynamic cycles.

The following lines show a complete theoretical scheme that does not take into account the technological constraints of a real cycle architecture, but it is useful to individualise the order of magnitude of the problem. It is a first theoretical discussion that does not take into account the real secondary system architecture.

When disregarding the technological limitations of a real Rankine cycle, the minimum core inlet temperature corresponds to the value of the minimum temperature of the secondary system. This temperature corresponds to the condenser outlet. In this calculation the assumption of an ideal steam generator with ideal heat exchange is taken, together with the neglecting of the heating of the coolant by the pump. The temperature at the condenser outlet is of the order of 46°C [79]. In a Brayton cycle, the lowest achievable value for the core inlet temperature corresponds to the secondary temperature at the compressor outlet. Indeed, in this case, the compressor plays a significant role in increasing the gas temperature, to approximately 60°C [80].

It can be postulated that the primary temperature of the PWR (connected to a Rankine cycle) can ideally be decreased to a value of 46°C. On the other hand, the lower value of the SFR primary temperature is constrained by the sodium melting temperature, which is higher than the Rankine or Brayton minimum. Consequently, for a SFR connected to either of the two cycles, the minimum sodium temperature is 150°C (the temperature considered for SFR maintenance, with margins above the melting point).

In the theoretical case of an infinite primary flow rate, the maximum core inlet temperature may correspond to the maximum core outlet temperature. The PWR is characterised by a primary core outlet temperature of 329°C [81]. The SFR core outlet temperature is of the order of 545°C [80].

It is then possible to compute the maximum theoretical inlet temperature range $\delta T_{in_{MAX}}$: 283°C for the PWR, and 395°C for the SFR. Then, a non-optimised K coefficient is considered: -28.9 pcm/°C for the PWR and -0.64 pcm/°C for the SFR. So, the "gain" in reactivity can be calculated: $K\ \delta T_{in_{MAX}}$. Finally, the time interval, when reactor is operated at constant power level due to the control of the secondary system, can be calculated. The results are shown in Table 3.2.

Table 3.2 – Theoretical PWR and SFR active control over the secondary system.

System	Maximum variation of the core inlet temperature $\delta T_{in_{MAX}}$ [°C]	Maximum reactivity compensation from the secondary system [pcm]	**Maximum time at full power with the control of the secondary system [day]**
PWR	283	8179	**284**
SFR	395	253	**87**

Assuming there is a thermodynamic cycle that accommodates temperature variation as described above, the active control over the secondary system may result in a theoretical increase in the core lifetime of approximately 284 and 87 days, respectively, for PWR and SFR. Considering an industrial reactor type PWR and SFR, the mean fuel irradiation time is about 4 and 5 years respectively [82]. This means that with the secondary system control we could ensure a theoretical contribution of about 20% of the lifetime with respect to an active PWR and a contribution of about 5% with respect to an active SFR.

Nevertheless, these values are purely theoretical. In practical applications, technological limitations preclude the possibility of achieving such a wide range of temperatures. It can be reasonably assumed that the actual time interval is likely to be smaller than the computed one. In the following paragraph, active thermodynamic cycles are designed with CYCLOP to assess the possible operation with the active control of the secondary temperature.

3.4.2. Control of secondary cycle for the driving of the core inlet temperature

In this section, a control on the secondary system is proposed in order to drive the core inlet temperature and keep the power produced by the core constant. Indeed, there are two main possibilities to decrease the inlet temperature keeping the power constant:

- case 'a': fix the secondary HX outlet temperature as constant and decrease the HX inlet temperature;
- case 'b': decrease both the secondary HX inlet and outlet temperature.

In the first case, to ensure a constant power extraction, the primary flow rate has to be actively controlled. In the second case, the flow rate can be kept constant. The first case calls into question the initial hypothesis of constant HX outlet temperature. It will be analysed only in PWR-Rankine case in the following section to assess the difference and then the second case will be analysed on the PWR-Rankine, SFR-Rankine and SFR-Brayton cycles.

3.4.2.1. PWR Rankine cycle

First, the major assumption of constant secondary HX outlet temperature (case 'a') is considered and the inlet temperature is varied. The system has been optimised for 190°C and a variation of ±15°C is considered. It is assumed that in this range of temperatures, the efficiency of the components can be considered constant.

The starting point is considered to be at a SG inlet temperature of 205°C. In Figure 3.7, the red curve (point markers) represents the variation of the cycle efficiency for the case 'a'.

Considering the case 'b', in the same figure other curves (dotted lines) represent the efficiency of the same system linked to different outlet temperatures. The blue line (square markers) represents a potential decrease of the efficiency considering the simultaneous decrease of the HX inlet and outlet temperatures (with an arbitrary regulation of the secondary flow rate). The efficiency is reduced with respect to the case 'a' because the decrease of the outlet temperature leads to a decrease of the turbine inlet steam temperature. The slope of the blue curve can however be adapted depending on the secondary flow rate.

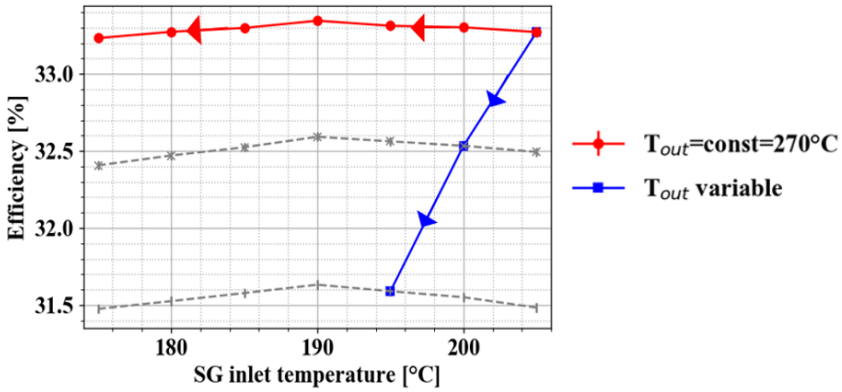
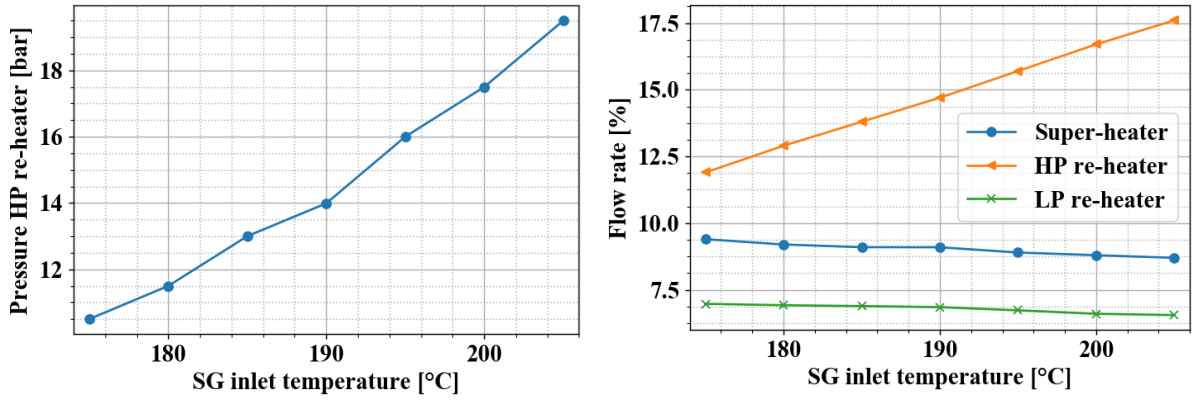


Figure 3.7– Efficiency associated to the variation of SG inlet and outlet temperature of a Rankine-PWR.

In conclusion, the case 'a' is characterised by higher efficiencies, but requires an active control over the primary flow rate. On the other hand, the case 'b' can be put in place with constant primary flow rate but lead to lower cycle efficiencies.

For simplicity, only the case 'a' will be further analysed in this chapter but the same could have been carried out with case 'b', with similar conclusions. The control of the system in the case of constant SG outlet temperature is proposed in Figure 3.8. The decrease of the inlet temperature is possible via the decrease of the flow rate and pressure of the HP re-heater. Consequently, the flow rate of the super-heater and LP re-heater are slightly increased.



(a) *(b)*

Figure 3.8 - Control of the HP re-heater pressure (a) and control of the flow rate of the super-heater and re-heaters (b) for the control of the SG inlet temperature.

The decrease of the pressure and flow rate of the HP re-heater impacts the efficiency with two opposing effects. The decrease of the hot leg temperature decreases the cycle efficiency. On the other hand, less steam and at lower pressure is extracted by the re-heater, thus leaving a larger mass of high pressure steam to expand in the turbine. This contributes positively on the efficiency. In Figure 3.7, the red curve shows that for temperature lower than 190°C, it is the first effect that prevails, while for temperatures decreasing from 205°C to 190°C, it is the second one that prevails.

A discussion is pursued here about the turbine steam extraction at variable pressure. The method to decrease the cold temperature of the circuit are based on the less extraction of heat from the turbine (reduction of the flow rate) or the extraction of heat at lower temperature (reduction of bleeding pressure). In this case, for a system optimised for 190 °C (SG inlet temperature), the two methods have to be used simultaneously. From a technological point of view, the variation of the flow rate is easily feasible with a valve controlled actively. On the other hand, the variation of the pressure depends on the location of the re-heater relative to the turbine that is fixed. The possibility to vary this pressure could be done with multiple turbine channels, controlled by valves to obtain the desired pressure. However, this method is not optimal from a technological point of view. Another option could be to over design the bleeding pressure and to vary only the re-heater flow rate. In this case, the pressure would be preset for the maximum inlet temperature (205 °C in this case) and kept constant during operation. This case is analysed in Figure 3.9.

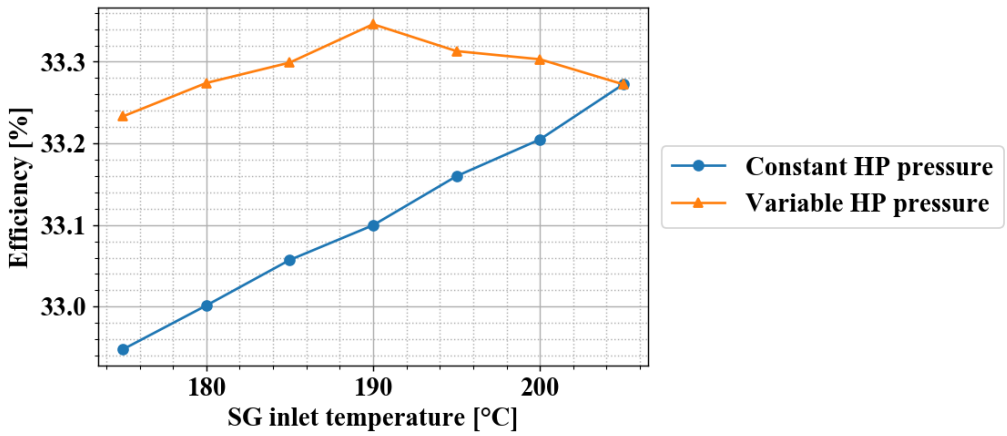


Figure 3.9 - Variation of cycle efficiency for the optimised case (reference) compared to the case with over dimensioned HP turbine steam extraction.

In Figure 3.9, the orange curve (triangular markers) represents a scenario in which both the flow rate and pressure of the HP re-heater are variable. The blue curve (circular markers) represents the case with constant pressure. Being designed to be optimised for 190°C, the efficiency of the system with over pressure is inferior. It decreases for decreasing temperatures. The decreasing HP re-heater flow rate decreases the HX inlet temperature and increases the mass of steam that expands in the turbine. In this case, the decrease of the HX temperature prevails decreasing the efficiency of the cycle.

As a conclusion: keeping the HP steam extraction constant is feasible technologically, but implies lower cycle efficiency.

3.4.2.2. SFR Rankine cycle

The Rankine-SFR system is analysed here. The SG outlet temperature is kept constant and the inlet one is varied around the optimised point (at 240°C). The other points are not optimised and an uncertainty bar is associated with them. The results are shown in Figure 3.10.

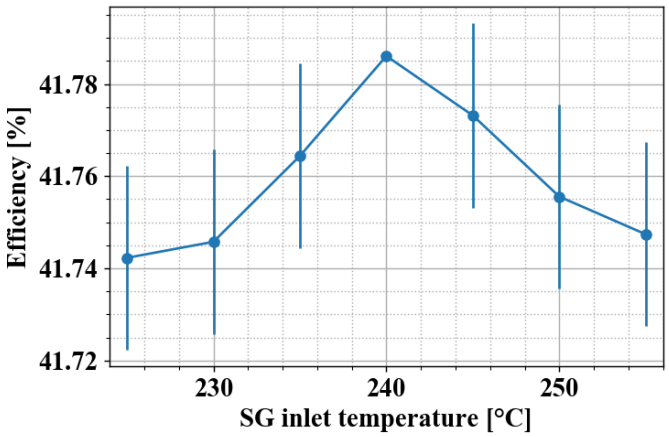
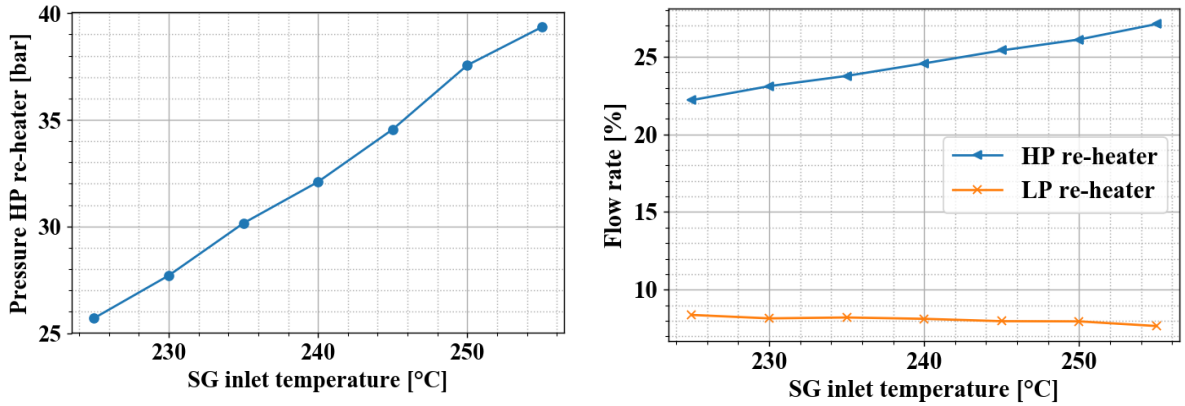


Figure 3.10 - Efficiency associated to the variation of SG inlet temperature of a Rankine-SFR.

The trend of the efficiency is the same as the PWR-Rankine cycle case. Also the control proposed is the same and it is presented in Figure 3.11. Decreasing the HP re-heater flow rate and pressure due to the two competing effects explained before, causes an increase and then a decrease of the efficiency.

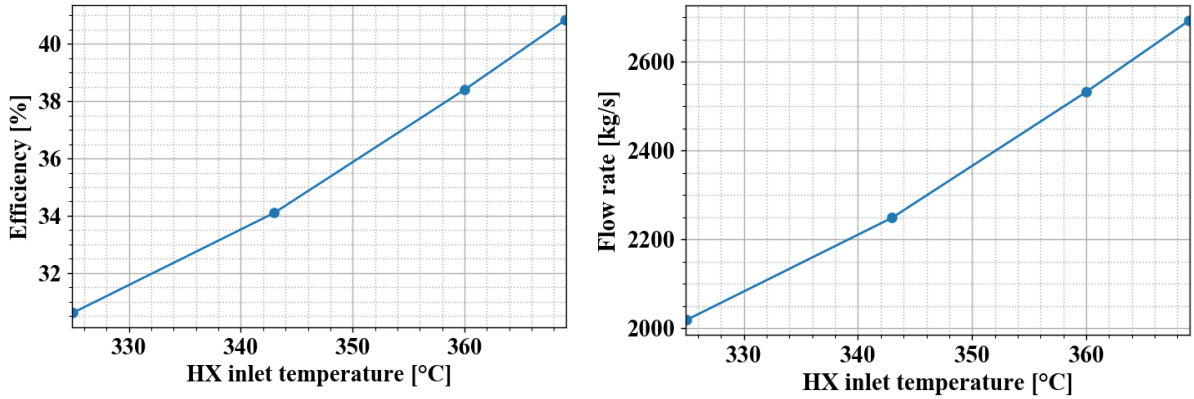


(a) *(b)*

Figure 3.11 - Control of the HP re-heater pressure (a) and control of the flow rate of the super-heater and re-heaters (b) of a Rankine-SFR.

3.4.2.3 SFR Brayton cycle

Also for the SFR-Brayton system the outlet temperature is kept constant and the inlet one can be decreased. The resulting effect on the efficiency are shown in Figure 3.12(a). The inlet temperature is varied around the value of 360°C (reference value for the system). The control is based on the decrease of the gas flow rate, as shown in Figure 3.12(b).



(a) *(b)*

Figure 3.12 – Efficiency (a) and needed control over he flow rate (b) for variable HX inlet temperatures in Brayton cycle.

The decrease of the flow rate determines a decrease of the power produced in the turbine and consequently (as the core power is constant) a decrease of the efficiency of the cycle.

In this case, the inlet temperature cannot go over 375°C due to the system design. Indeed, the increase of the inlet temperature causes a decrease of the temperature pinch in the heat recuperation unit and over 375°C it becomes negative.

In conclusion, this section has analysed the potential for controlling the secondary system and studied a possible temperature range. A limited range of temperature at the core inlet has been considered, with the hypothesis of constant efficiency of the cycle components. In the next section, the secondary system operation considered here will be applied to the KGH method.

3.5. Application of the KGH method with the secondary system contribution

This section provides an overview of the contribution of the secondary system to the evolution of power. The control over the secondary system enables to keep the core power constant, compensating a certain reactivity variation. In Figure 3.13, for example, the behaviour of a PWR core is shown, with the secondary system actively controlled in the temperature range 175<T<205°C. The core power is constant and the produced electric power is slightly varied according to the efficiency calculated before. The behaviour of the core after this period will be analysed in the rest of this work.

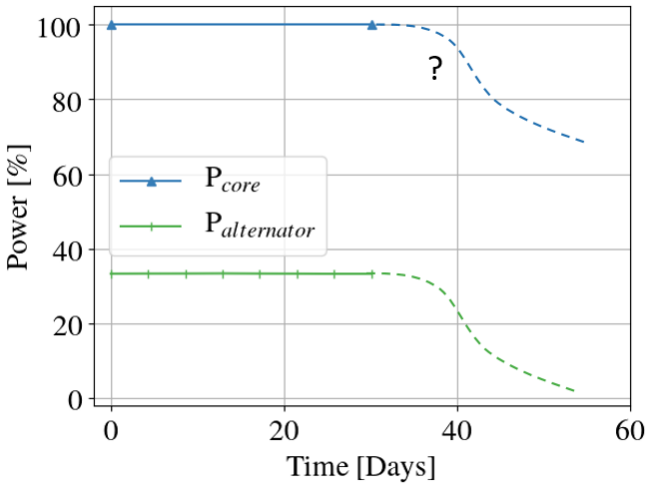


Figure 3.13 – Power evolution of the core with active control on the secondary system – PWR.

Figure 3.14 shows a comparison between the considered systems, in terms of power produced at the alternator.

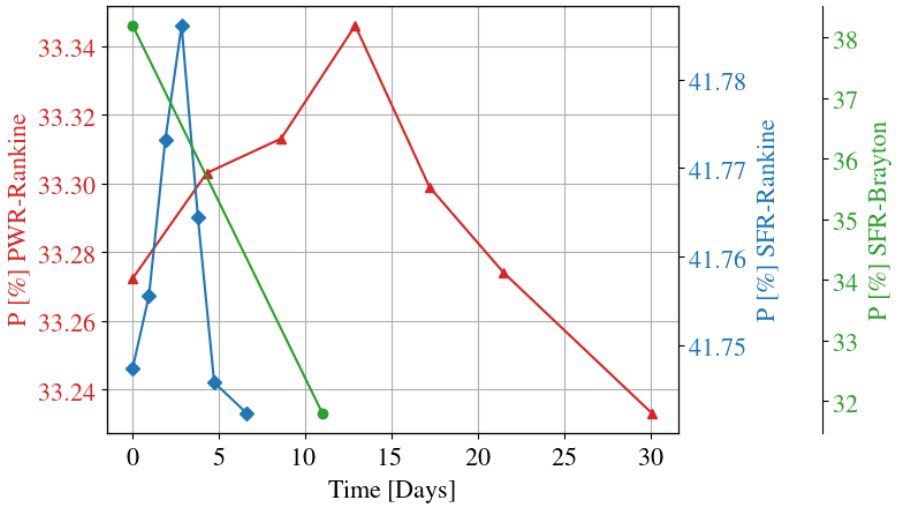


Figure 3.14 – Comparison of the power at the alternator of the PWR and SFR connected to Rankine and Brayton cycles.

The combination of PWR and SFR in a Rankine or Brayton cycle results in varying contributions to the produced power. The Rankine cycle exhibits a non-monotonic efficiency behaviour, which results in a similar trend in electrical power output. The Brayton cycle is distinguished by a monotonic decrease in efficiency (correlated with the decrease in temperature) and a parallel decrease in alternator power.

The study carried out so far is based on a static approach. The contribution of the ECS to the core has been estimated by the reactivity integral, not considering the system dynamic. However, the physics of the systems (core, primary, ECS) is characterised by many dynamic features such as thermal inertia. The possibility of controlling the ECS to keep the core power constant leads to the question whether the dynamic of the cooling system is compatible with the needed control of the core reactivity. This is considered as a future perspective.

3.6. Conclusions

In this chapter, a discussion is made of the possible contribution of the ECS on an autonomous core. From the theoretical calculations it is possible to obtain the maximum contribution of temperature variation in the core induced by a control of the ECS. It is expressed in days when the secondary system is actively controlled in order to keep the core power constant. The PWR are characterised by a contribution of 8179 pcm and 284 days and the SFR of 253 pcm and 87 days. Anyway, these values are maximum theoretical calculations that do not account for technological constraints. Furthermore, any modification of the design could modify the 'K' coefficient and thus this contribution.

The design of real secondary cycles was studied with CYCLOP [74]. Rankine and Brayton cycles were studied in connection with PWR (only Rankine) and SFR. The results conclude by highlighting the need to use active control in order to connect an ECS to an autonomous core. A control method has been proposed for the two cycles. It is based on the control of the flow rate of the re-heaters in the Rankine cycle and the control of the gas flow rate in the Brayton cycle. In the Rankine cycle, a control based also on the pressure variation of the HP re-heater is proposed and the feasibility of this solution is discussed.

Active control of the secondary cycle can be implemented to decrease the inlet temperature to the core. In this way, the power produced by the core could be constant over a certain period of time. However, the efficiency of the secondary cycle varies. This efficiency has been calculated with CYCLOP and allows to calculate the associated electrical power produced.

To study the possible operation of an autonomous reactor, an analysis of the entire system (core, primary and secondary) would be the most comprehensive method. But it is time-consuming and expensive to implement. So in this chapter, the contribution of the secondary system has been assessed, independently of the primary circuit contribution. In the following, the focus will be on the core operation. The primary system is considered with a constant flow rate as the passive reactor is considered to be operating without any control on the primary side. The term of the core temperature difference is thus proportional to the power in the KGH equation. In parallel, the secondary system is considered actively operated not to allow the core inlet temperature to increase. The minimum contribution of the secondary system is applied in the following studies, considering the inlet temperature constant. A global estimation of each reactor performance will be made in the conclusions of each section, considering the system as a whole (primary and secondary). These hypotheses allow to rewrite the KGH equation as:

$$H\ \delta P_{core} + G\ \frac{\delta P_{core}}{\dot{m}\ c_p} + \delta \rho_{fuel} = 0; \tag{3.4}$$

Chapters 4, 5 and 6 are based on this equation.

Chapter 4

Autonomous reactors comparison

Summary

4.1. Introduction 93
4.2. Methodology for comparing different designs 93
4.3. Comparison of reference designs 94
4.3.1. Fuel enrichment 94
4.3.2. Reactivity feedback effects 96
4.3.3. Burn-up reactivity swing 97
4.4. Comparison of equivalent designs 98
4.4.1. Burn-up reactivity swing 100
4.4.2. Power evolution 102
4.5. Criteria of definition of autonomous cores 103
4.5.1. Definition of autonomous core operation 103
4.5.2. Performance evaluation 105
4.6. Conclusions 107

4.1. Introduction

This chapter presents a comparison between the reactor designs selected for potential autonomous operation. These designs, presented in Chapter 2, are the Heat Pipe Reactor, the High Temperature Reactor, the Pressurised Water Reactor and the Sodium-cooled Fast Reactor. The aim of this chapter is to compare the designs in autonomous operation and to define their performance. The first section presents the method used for the comparison. An initial comparison is made with reactor designs from the literature, but autonomously operated and all fuelled with UO_2, for the purposes of the exercise. The comparison is then made between autonomous reactors with a standardized power density. The last part of this chapter is dedicated to the assumptions definition and results presentation used in the rest of the work.

4.2. Methodology for comparing different designs

Industrial-scale reactors are characterised by their high thermal and electrical power. The power density of the core is greater (by far) than the one of micro-reactors. Core and vessel volumes depend on the reactor design; for example, HTRs have very large active core volumes (of the order of 35 m^3), comparable to the volume of a PWR with 18 times the power. The HPR is characterised by a power density comparable to that of the HTR. The size and geometry of the assemblies also differ from one concept to another; they are characterised by a hexagonal or square (in the case of PWR) layout and by the arrangement of fuel inside separate assemblies or a solid matrix (as in the case of the micro-reactors envisaged). Core materials are also different, with each reactor featuring a different moderator (for thermal designs) and coolant. The fuel also varies between UO_2 and MOX fuels (as in the case of SFR, for example). The neutron spectra are different. HTR and PWR reactors are considered thermal reactors, while HPR and SFR reactors as fast reactors. Finally, the primary and secondary cooling systems are very different from one concept to another, with the HPR featuring a totally autonomous primary heat removal system, while the other concepts require active cooling systems. In addition, the coolants are different, as is the secondary heat conversion system.

Comparison between reactors is possible if certain common points are established. Firstly, in accordance with the scope and approach of this work, all the designs in the literature are studied as autonomously operated reactors. The first common feature for comparison is therefore the removal of all means of active control. Then, among the neutronics and thermal characteristics, the fuel material was chosen to be the same between the four concepts and fixed at UO_2, which is the fuel most widely used in current reactors. The choice is based on the possibility of comparing the same fuel in the different neutronics environments of the four concepts in order to study the different effects on its isotopic evolution. The other neutronics and thermal characteristics are those taken from the literature (for example, coolant materials or cooling systems). The enrichments of the concepts taken from the literature are therefore modified in this work in order to transform them into autonomous reactors, meaning that the initial reactivity is zero at BOL. From now on, in this work, the reactors taken from the literature, will be referred to as “literature design”, whereas the autonomous reactors taken from this work will be referred to as the “reference design”. They are called “reference” because the rest of this work will consist of proposing ways of improving these initial non-optimised autonomous cores directly extrapolated from reactors designed to be actively piloted.

The methodology used here to compare the four reactors is divided into two steps, presented in Sections 4.3 and 4.4. Firstly, the “reference designs” are compared, i.e. the reactors as designed in the

literature, but autonomously operated and all loaded with UO_2 fuel. Secondly, "equivalent designs" are compared, i.e. reactors all operating at the same power density level.

The approach of the autonomous core analysis consists of several steps. First, all reactors are loaded with UO_2 and the U-235 enrichment is adjusted to ensure a critical state of the reactor at Beginning Of Life (BOL). This is necessary because, in this first approach to the design of an autonomous reactor, the reactivity at BOL cannot be modified other than the core itself. In a second phase of the study, the reactivity feedback coefficients are calculated for each core designs. Then, the burn-up reactivity swing is analysed. Finally, with the KGH method, the temporal evolution of power is computed and analysed. This methodology will be applied from now on for all the cases of study in this work.

4.3. Comparison of reference designs

This paragraph presents the comparison between the reference designs. Table 4.1 summarises the main reactors characteristics.

Table 4.1 - Reference reactor designs characteristics.

Reactor	Power [MWth]	Power density [W/cm^3]	Spectrum
Heat Pipe Reactor	5	5.49	Fast
High Temperature Reactor	200	5.67	Thermal
Sodium-cooled Fast Reactor	3600	203	Fast
Pressurized Water Reactor	3817	101	Thermal

4.3.1. Fuel enrichment

The following Table 4.2 summarises the results of this initial analysis, with a comparison between the fuel enrichment of the literature designs and that considered for the reference designs in this work. As mentioned in Chapter 2, in the literature, all the reactors are already designed with UO_2 fuel, with the exception of the SFR, which is initially loaded with $UPuO_2$.

Table 4.2 - Reference reactors enrichment.

Reactor	U-235 enrichment[3] "reference design" [%]	U-235 enrichment "literature design" [%]
Heat Pipe Reactor	20.5	19.8
High Temperature Reactor	2.30	12.0
Sodium-cooled Fast Reactor	12.9	0.25 (in $UPuO_2$ fuel with Pu content: 15.8%)
Pressurized Water Reactor	1.05	3.70

[3] The U enrichment is defined as the ratio between the mass of U-235 and the total mass of U.

In this work, from now on, physical values of enrichments are considered not accounting for the different countries civil regulation. In the conclusions, the feasibility of each design will be discussed considering also the need for large fuel enrichments.

The Serpent 2 code was used for the HPR, HTR and PWR simulations. ERANOS was used for the SFR. The convergence process in the search for the necessary enrichment to get the criticality at BOL is stopped at $|\rho| < 500\ pcm$. This limit was considered adequate so as not to significantly influence the reactivity evolution results, as explained in the Annex IV.1.

With these reference enrichments, the energy spectra of the four reactors (33 groups) are compared in Figure 4.1. Furthermore, the "spectrum index" is calculated in Table 4.3. It is defined as follows:

$$x = \frac{\int_{0.025\ eV}^{1\ eV} \phi\ dE}{\int_{1\ eV}^{100\ MeV} \phi\ dE}\ \frac{(100e6-1)}{(1-0.025)}; \qquad (4.1)$$

This index represents the ratio between the integral of the "thermal" flux and the "fast" flux (the limit between the two being set at 1 eV).

Table 4.3 - Reference reactors spectrum index.

Reactor	Spectrum index [-]
Heat Pipe Reactor	1.0e-3
High Temperature Reactor	2.4e0
Sodium Fast Reactor	1.2e-3
Pressurized Water Reactor	6.3e-1

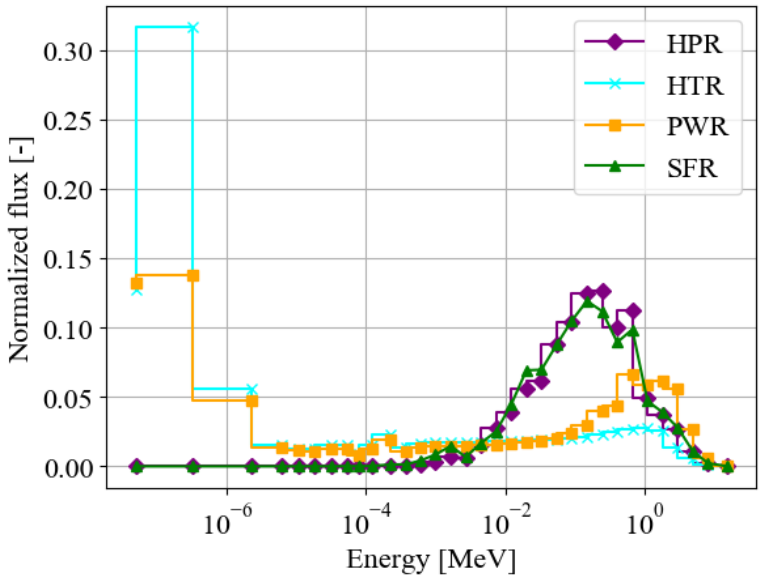


Figure 4.1 – Reference reactors spectrum comparison.

It can be seen that, of the four reference reactors, the HTR has the sharpest thermal spectrum, the PWR has a softer thermal spectrum and the HPR and SFR have a fast spectrum.

4.3.2. Reactivity feedback effects

In this section, the reactivity feedback coefficients of the four designs are evaluated. The designs are different in terms of neutronics characteristics, geometry, heat removal system, coolant and size, and the reactivity feedback effects therefore vary from design to design.

Table 4.4 shows the results of the calculation of reactivity feedback coefficients.

Table 4.4 - Reactivity feedback coefficients of the reference reactors.

HPR	Reactivity coefficient [pcm/K]
Fuel Doppler	-0.22
Fuel axial expansion	-0.63
HTR	
Fuel Doppler	-5.60
Graphite temperature	-2.08
Graphite radial expansion	-0.14
SFR	
Fuel Doppler	- 0.61
Fuel expansion	- 0.08
Structure expansion (clad + TH)	0.03
Sodium density	0.03
PWR	
Fuel Doppler	-2.43
Water density	-33.31

Different assumptions have been made for each design.

In Heat Pipe Reactors, which are fast spectrum reactors, the main effects are expected to include the Doppler effect, the fuel axial expansion, the radial expansion of the stainless steel matrix and the variation in sodium density. The effect of stainless steel expansion was assessed and found to be two orders of magnitude smaller than the other coefficients and is therefore considered negligible. The variation in sodium density was also analysed. The sodium density was varied by a corresponding titre from 0% (liquid) to 100% (completely vaporised). The associated variation in reactivity was less than 10 pcm. In heat pipes at nominal operation, the variation in sodium state is limited, so in conclusion, the effect of sodium density on reactivity is considered negligible in this work [83] [84].

In High Temperature Reactors, since the fuel consists of TRISO particles, fuel expansion is excluded by design. In addition, the helium coolant has a very weak interaction with neutrons, so the coolant density effect is considered negligible. The reactivity effects studied are the Doppler coefficient of the fuel and graphite as well as the graphite density variation [85].

In Sodium Fast Reactors, the effects on reactivity consist of the Doppler coefficient, fuel expansion, structure expansion and sodium density variation [86]. In this work, the relative variation in the axial insertion of the control rods is not taken into account due to the absence of active reactivity control systems. The effect of grid expansion is not taken into account here, as the core inlet temperature is assumed to be constant (as explained in the conclusions of Chapter 3).

Finally, the main effects in Pressurized Water Reactors are due to the fuel Doppler coefficient and the density of water [87]. The coolant coefficient has been computed considering a linear interpolation between 10°C variation in coolant temperature (and corresponding density) with respect to the nominal value.

The Serpent code is used for the HPR, HTR and PWR. The coefficients are calculated by linear regression with multiple simulations at different temperatures. The simulations were carried out with 10000 active cycles, 10000 simulated neutrons per cycle and 50 inactive cycles. The uncertainties on the results have been computed and considered acceptable for this preliminary analysis. A complete uncertainties study should be done if specific and detailed core design is done. In addition, the SFRs were analysed using a deterministic code and perturbation theory was applied to calculate the feedback coefficients. The Doppler coefficient of the SFRs is not linear with temperature, and in this table a linearized (at nominal temperature) coefficient has been displayed for quantitative comparison with the other coefficients.

The results in Table 4.4 show that the Doppler coefficient is larger for the more thermal neutron spectrum. In thermal reactors, neutrons are slowed down through the resonance energy range. In this energy range, the Doppler effect broadens the resonance peaks, leading to a reduction in reactivity. In fast reactors, neutrons are not thermalized and those that pass through the resonances are less numerous, which reduces the importance of the Doppler effect. In HTRs, the Doppler effect prevails over the others, while in PWRs, the most important effect is bound to the variation in water density. On the other hand, as far as fast reactors are concerned, the effect of fuel axial expansion is the most important in HPRs, while in SFRs, the Doppler effect is the most important negative effect, but the structure expansion and the sodium density variation contribute to the positive effect. In any case, the total feedback coefficient (sum of each coefficient multiplied by temperature variation) remains negative.

4.3.3. Burn-up reactivity swing

In this section, the reactivity evolution of the reference reactors is analysed. Assuming a state of zero reactivity at BOL, no active intervention, a constant material temperature and power, the “natural” evolution of the cores is illustrated in Figure 4.2.

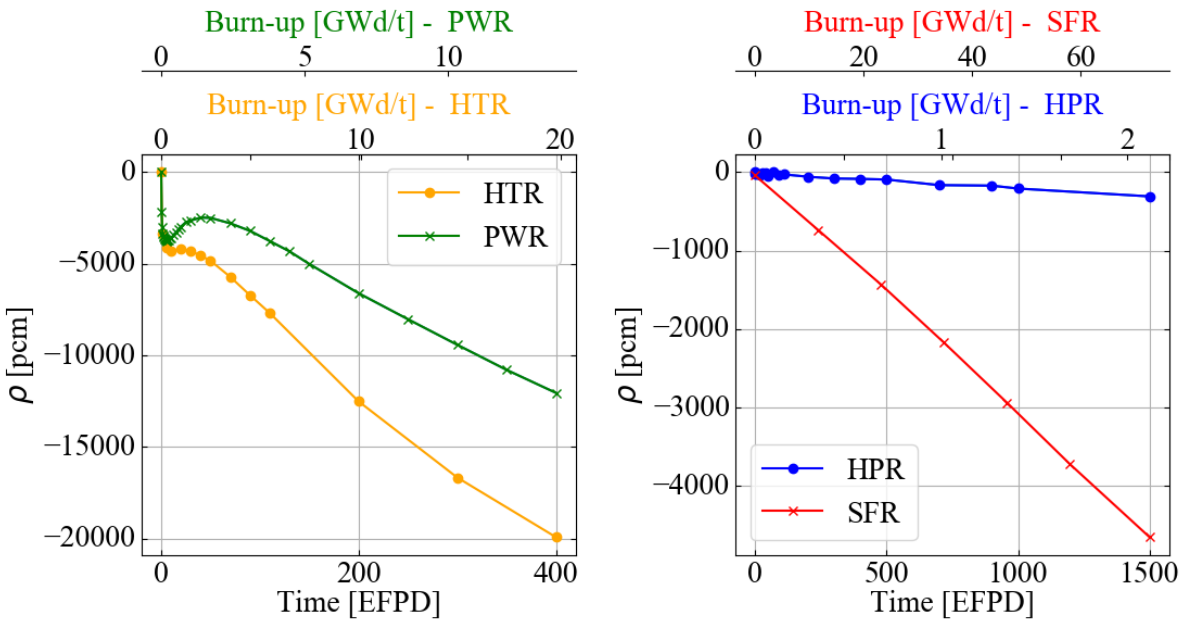


Figure 4.2 – Reactivity evolution for autonomous reference reactors.

The results, obtained for the Heat Pipe Reactors and Sodium-cooled Fast Reactors, show a linear reactivity loss. The coefficients representing the slope of the reactivity loss curve are -0.18 pcm/EFPD for the HPR, operating at a power density of 5.49 W/cm^3 and -3.1 pcm/EFPD for the reference SFR with a power density of 203 W/cm^3. The simulation is presented on a time scale of 1500 EFPD and the SFR simulation is limited by the condition imposed on the maximum radiation damage on the cladding material of 110 DPA.

The results for the thermal reactors, HTR and PWR, lead to a different observation. The reactivity loss does not exhibit linear behaviour over time. Both cases are characterised by a significant initial drop in reactivity during the first few hours. Thereafter, reactivity increases for both reactors until a trend reversal occurs at around 50-100 days, and finally a decreasing linear behaviour is established. The curve in Figure 4.2 is shown up to 400 EFPD, after which the behaviour is simply linear. These three intervals, which characterise a changing trend in the reactivity evolution, can be explained by various physical reasons. The Xe effect, the build-up of Pu-239 and the fuel depletion. The physical detailed analysis is shown in Annex IV.2.

In conclusion, the main difference between the reactivity evolution of the four reactors is due to the neutron spectrum. Fast reactors show a linear reactivity evolution, whereas thermal reactors are characterised by a variation in the slope of the curve. In the next section, the comparison of the reactors is made with the same power density. Indeed, the power density can be seen as a performance indicator. To limit the difference to the only design of each reactor, it is proposed to make a comparison based on the same power density objective for each of them.

4.4. Comparison of equivalent designs

In the previous section, the comparison was made between reference reactors, i.e. reactor designs fuelled by UO_2 and operated without active control on the reactivity. In any case, the power density level at which the reactor operates could have a first-order influence on the core the “lifetime” (as will

be defined in detail after). In this section, the reactors are compared in terms of the same power density defined, in this work, as equivalent design. The hypothesis for this comparison includes the geometry and dimensions of the reactors, which must remain constant, and the operational power, which must be adapted.

To define an equal power density value, the power density of micro-reactors was increased and that of the industrial-scale reactors was decreased for this specific comparison. While there is a less restrictive technical limit for decreasing the power density of large cores, increasing the power of micro-reactors is subject to possible operating limits. These are determined by the need to respect the constructive, physical and safety limits of the reactor cores. In fact, HPRs are characterised by specific operating limits concerning the power removal by heat pipes technology. As described in Chapter 2, the heat pipe operating ranges impose a limit on the heat that can be extracted by each pipe as a function of the specific operating temperature. Figure 4.3 shows the heat pipe limits chosen for the reference design, the nominal operating point and the maximum heat removal possible with this particular system.

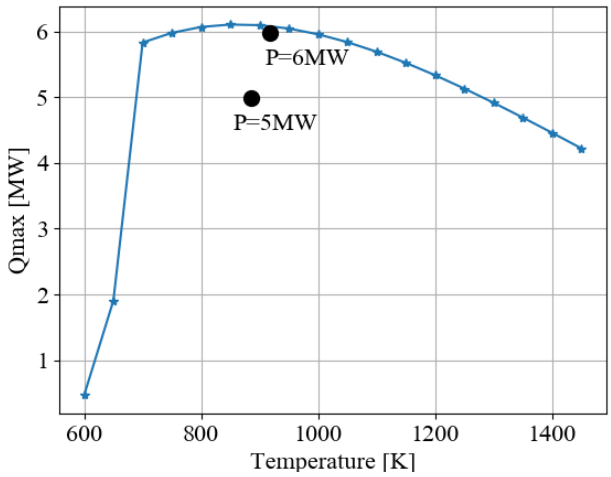


Figure 4.3 - Heat Pipe Reactor nominal and maximum operational power.

The maximum core fission power at which the HPR described in this work can be operated is 6 MW. In this configuration, each heat pipe removes 5.98 kW at an operating temperature of 906 K. In this work, a reference heat pipe model was considered. It consists of a simple annular wick adjacent to the pipe wall. In the literature [88], many different heat pipe configurations are proposed to improve the possible heat transfer of each pipe, as shown in Chapter 2. In this work, only the simplest concept has been analysed because the optimisation of the heat pipes technology was out of the scope of this work. However, an interesting perspective could be to analyse the optimisation of heat removal as a function of pipe design, models and geometry. The other HPR limitation on operating power density concerns the matrix temperature. Since, in the design envisaged, the core solid matrix is made of stainless steel, a limitation on the maximum temperature of this material is imposed. This maximum temperature is set at 1200 K for safety reasons linked to thermal stress [89]. In the configuration of the reactor operating at 6 MW, the average stainless steel temperature is 918 K, which is well below the limits. However, more precise 3-D calculations could be carried out to determine the hot spots and maximum temperatures reached in steady state and during any transients. This could be a perspective study for the design of a heat pipe micro-reactor.

With the constraint of heat pipes operation, the actual reactor power can be increased from 5 MW to 6 MW, which corresponds to a variation in power density from 5.49 W/cm^3 to 6.59 W/cm^3. The comparison will be based on this power density.

HTRs are also limited in terms of maximum fuel temperatures, due to the integrity of TRISO particles. The maximum fuel temperature is set at 1600 °C [90]. With this limitation, the 200 MW reference design (5.67 W/cm^3) achieves an average fuel temperature of 1018 K. If the power density is increased from 5.67 W/cm^3 to 6.59 W/cm^3 (corresponding to the power of 232.4 MW), the average fuel temperature rises to 1059 K, which is below the limits. The increase of the power density of HPR and HTR is clearly a theoretical case, not accounting for the safety margins, but that is used only in this section for the scope of theoretical comparison.

Finally, industrial-scale reactors can be operated at 6.59 W/cm^3 by reducing the core power. Although this power density target may seem rather low compared with the reference targets for PWR and SFR cores, it may help to highlight the potential behavior of these concepts as "passive" cores. If margins are found with respect to the initial purpose of this work, this will indicate that solutions may exist using such cores and that they are worth investigations.

The power and power density of the reference designs and the comparison case are listed in Table 4.5. With these adjustments, it is possible to make a comparison of these cores in terms of reactivity loss and autonomous lifetime.

Table 4.5 - Reference and comparison power density of different reactors.

	Reference design		**Equivalent design**	
Reactor	Power [MW]	Power density [W/cm^3]	Power [MW]	Power density [W/cm^3]
HPR	5	5.49	**6.0**	**6.59**
HTR	200	5.67	**232.4**	**6.59**
SFR	3600	203	**116.5**	**6.59**
PWR	3817	101	**248.5**	**6.59**

The comparison method is the same as that used for the reference reactors. In the next sections, the reactivity loss of equivalent designs is analysed. The power evolution is then calculated using the KGH method. Finally, the performance characteristics are listed and the comparison between the four autonomous reactors is presented.

4.4.1. Burn-up reactivity swing

In this paragraph, the results on the reactivity evolution are presented for the reference power density and the power density adapted for the comparison (6.59 W/cm^3). The evolution of reactivity is shown in Figure 4.4.

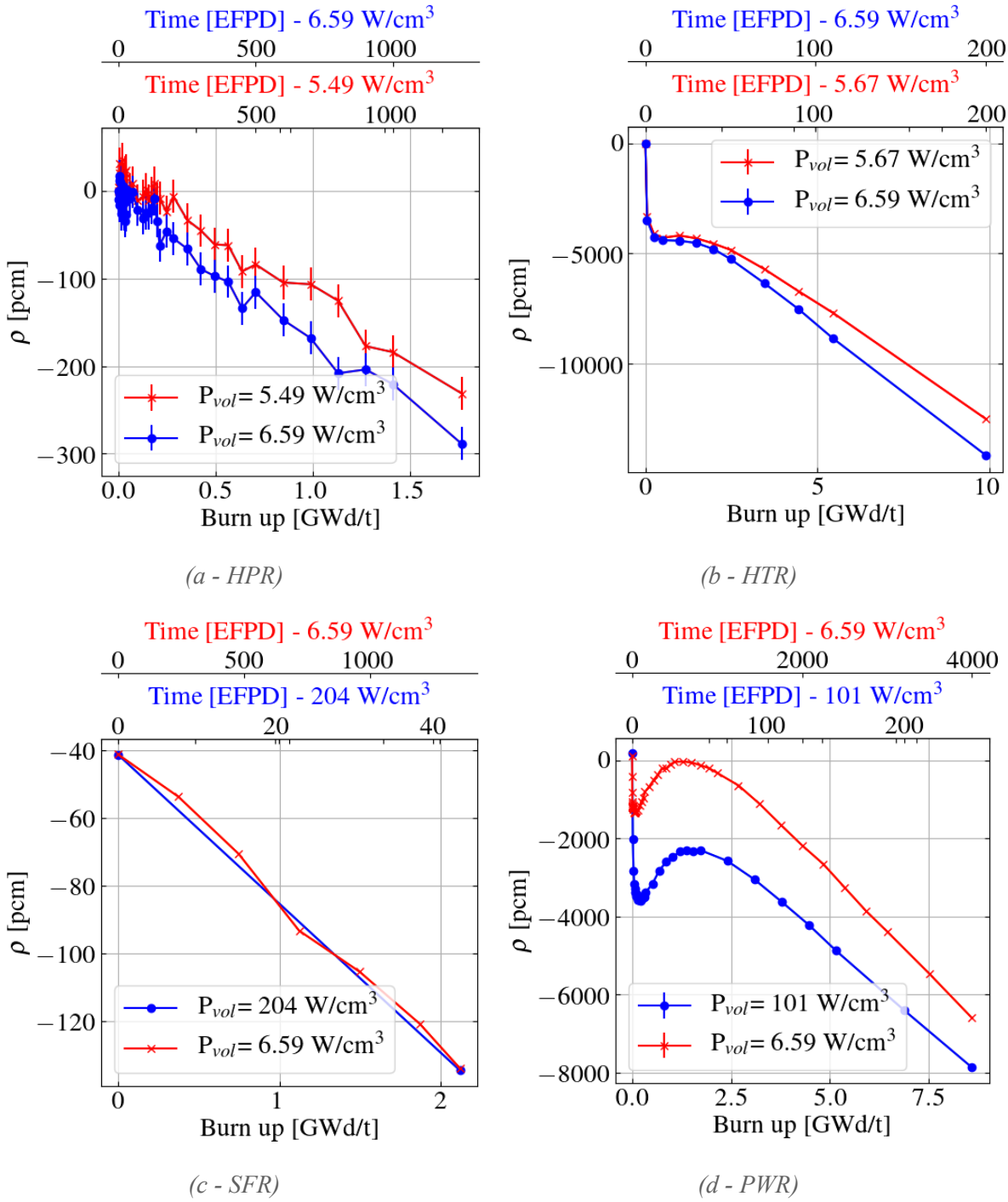


Figure 4.4 – Reactivity loss comparison for the same power density – HPR (a), HTR (b), SFR (c), PWR (d).

The evolution of the reactivity swing has been represented up to 2 GWd/t for fast reactors (that have a linear reactivity loss for all the burn-up), while up to about 10 GWd/t for the thermal reactors that show a linear behaviour after the first increase and then decrease of the reactivity.

The reactivity swing as a function of burn-up is, at first order, independent of the power density and power of the core. The only modification concerns the Xenon effect as it can be seen at the beginning of the reactivity curve of the PWR.

The reactivity evolutions curves for the 6.59 W/cm^3 power density are used in the following to calculate the corresponding power evolution and to evaluate the performance parameters of the equivalent designs.

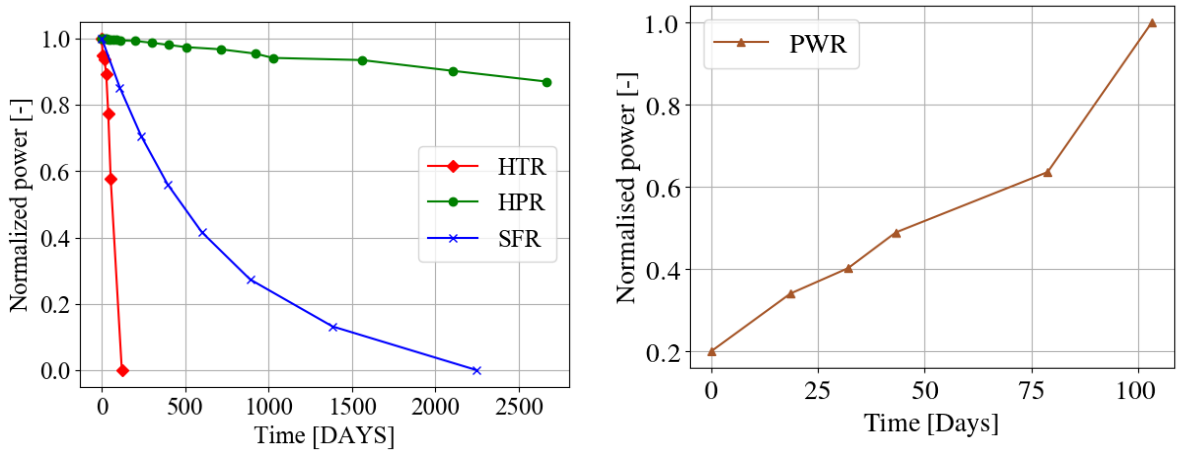
4.4.2. Power evolution

In this section, the KGH method is applied to the design of the four reactors to assess the power evolution. The HTR and PWR graphs are obtained excluding the initial Xe effect (this will be explained into details in the next section). The power evolution of the four reactors is compared in Figure 4.5.

With respect to the reactivity swing, evaluated in EFPD, this graph accounts for a different time scale. Here the time is plotted in days. A change of scale is made to shift from EFPD (days evaluated as if the reactor was operated at the same power level) to days, accounting for the actual power level with respect to the nominal one.

A specification is given here on the neutronics calculations made in this work. The reactivity swing is composed of two factors: $\Delta\rho = \Delta\rho_{BU} + \Delta\rho_{decay}$. The $\Delta\rho_{BU}$ represents the variation of the reactivity due to the irradiation of materials, while the $\Delta\rho_{decay}$ is due to the spontaneous decay of certain isotopes (as the Pu-241 to Am-241). This second term is considered in this work depending only on EFPD and not days, as it contributes in a very small part to the total reactivity in our study. Anyway, if more detailed calculations should be done, the $\Delta\rho_{decay}$ should be considered more precisely and independently of the $\Delta\rho_{BU}$ term. It is only dependent of the days of operation, so the total reactivity swing per burn-up would not anymore be independent of the power density.

SFR and HPR show a linear power decrease. The SFR is characterised by a power loss of approximately -0.070 %P_N/day, while the HPR is -0.002 %P_N/day, where %P_N represents the percentage of the initial nominal power. The HTR is characterised by a power slope of around -0.83 %P_N/day. The PWR, on the other hand, shows a sharp power increase in the first 6 days of around +1.28 %P_N/day.



(a) *(b)*

Figure 4.5 - Power evolution comparison between HPR, HTR and SFR (a) and PWR (b).

A preliminary comparison between reactors is summarised in Table 4.6.

Table 4.6 – Comparison of equivalent reactor designs.

Performance	HPR	HTR	SFR	PWR
Power density [W/cm^3]	**6.59**	**6.59**	**6.59**	**6.59**
Lifetime [years]	>10	0.27	2.97	0.28
Burn-up at EOL [GWd/t]	0.19	2.01	2.00	0.29

The design with the longest, autonomous behaviour is the HPR. However, this type of reactor is very limited in terms of achievable power density. This is because the heat pipes operate within a very narrow range of possible values of temperatures and powers values. For this reason, the HPR will be excluded for the rest of the work. Based on the current results, no conclusion can be drawn between the other three reactors. A specific methodology is proposed and explained in the next section in order to compare the achievable performance of HTR, PWR and SFR.

4.5. Criteria of definition of autonomous cores

In the rest of the work, the three selected reactors will be studied with the objective to increase their autonomous lifetime. In this section, the assumptions made are presented and the method chosen to compare the results is explained. This methodology will be applied in the rest of the work.

4.5.1. Definition of autonomous core operation

In this section, the criteria adopted for the operation of an autonomous core are presented.

The first criterion concerns the Xe reactivity loss effect. The thermal reactors (HTR and PWR) are characterised, at the beginning of the irradiation, by a significant reactivity loss due to the Xe effect. This phenomenon corresponds to a sharp power decrease, as shown in Figure 4.6 for the HTR, taken as an example. The power goes from initial values to zero in about 4 days; the reactor is therefore characterised by a very short lifetime. Since active reactivity control must be present in the reactor core during the start-up phase, it could also be used during the first 6 days to control the Xe effect. A hypothesis is put forward on the possibility of designing a start-up system that operates during the start-up phases and actively during the first few days of the reactor's lifetime to compensate for the Xe-effect. The possibility of designing this type of system should be the subject of further analysis, but is outside the scope of this work. In this case, the power autonomous evolution (from the end of the Xe reactivity loss) is shown in Figure 4.6.

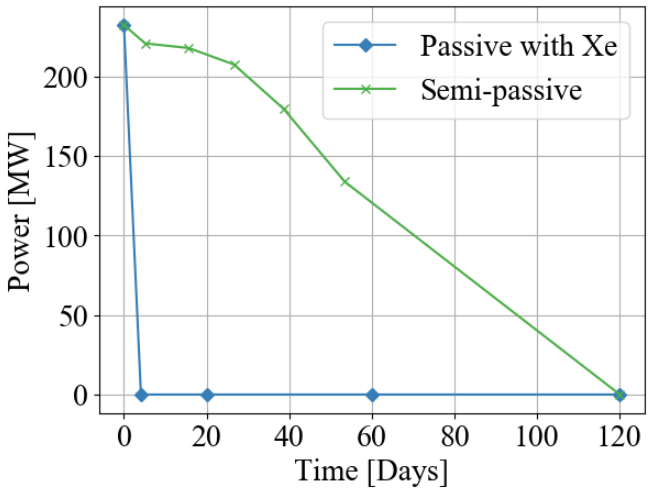


Figure 4.6 - HTR power evolution in completely autonomous operation and in semi-autonomous configuration, with compensation of Xe effect.

The lifetime is extended to around 120 days and the power drop is attenuated, which shows the advantage of using an active system to compensate for the Xe effect at BOL. So, for all the rest of the work, the thermal reactors will be considered with active control in the first few days of life to tackle the Xe effect, when necessary.

Even if the initial reactivity loss is compensated for, the effect of Xe production is present throughout the irradiation of the core. It must be taken into account in the equation of the power evolution as shown in Annex IV.3. Nevertheless, in this work, it is set aside as its impact is considered to be of second order effect in the thermal spectrum cores analysed in the following chapters. The cores will have hardened spectra and the xenon effect will disappear.

The other criterion for the autonomous core concerns the End Of Life and the power fluctuation.

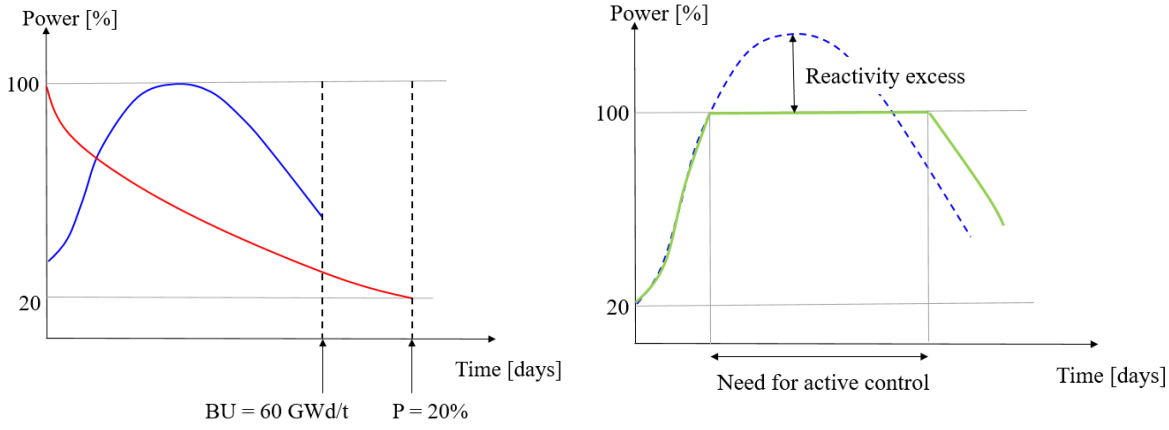


Figure 4.7 – Criteria for autonomous core operation.

The criterion of the End Of Life of the core is fixed at 60 GWd/t or the reach of 20% of the nominal power, as a minimum value. The burn-up criterion is chosen as it is a “reasonable” value of burn-up of fuel in the current PWR operating nowadays [91]. The threshold value of 20% of nominal power is chosen as corresponding to the minimum value of French PWR admissible for the load following [19]. This value is the theoretical technical minimum, imposed by regulation, defined as the minimum power that can be produced under stable conditions with the regulations in service, the steam bypass at the

condenser and the atmospheric discharge being closed. It defines the minimum load following threshold for French reactors [92].

As shown in Figure 4.7(a), the power can have two different trends, according to the reactivity swing. It can be monotonically decreasing, in this case the reactor is started-up at its nominal power. On the other hand, the power can be increasing first and then potentially decreasing. In this case, the reactor is started-up at a smaller value than its nominal power. This starting value is chosen so that the maximum power, reached by autonomous operation, corresponds to the design value. The minimum start-up value is 20% as for the EOL.

In the case of fluctuating power, the corresponding reactivity increase could lead to a power rise over the nominal one, even starting the power at 20%, as shown in Figure 4.7(b). This case is not viable as the nominal power is used to size the system and components and cannot be exceeded. Only in this case, an active control is foreseen to compensate the reactivity excess and keep the power constant on the nominal value for a period of time. This active control could be, for example, made by the control over the secondary system. However, these specific cases needing active control will be highlighted in the comparisons as a non-full autonomous reactors.

4.5.2. Performance evaluation

The comparison between the different cores will be summed-up in a graph radar, as shown in Figure 4.8.

The different axes represent:

- Actinide [%] is the content of actinides inserted into the fuel (this will be discussed in the following chapters); it can also be burnable poison;
- U-235 [%] is the U-235 enrichment required to reach criticality a BOL;
- RF [pcm/%P] is the reactivity feedback integral between 20% and 100% of nominal power. The core inlet temperature is considered constant. It quantifies the impact of the feedback coefficients. To facilitate the reading, it is expressed in pcm per percent of nominal power (considering a linear variation);
- $\Delta\rho$ [pcm/EFPD] is the maximum range of reactivity variation during the core lifetime (with a limit of 20% of nominal power or 60 GWd/t);
- BU [GWd/t] is the average burn-up reached at the end of life;
- $\bar{P}$ [%Pmax] is evaluated as the average power of operation during the lifetime considered; 100% corresponds to the ideal case;
- $\Delta\rho_{ECS}$ [%] is the maximum of the possible contribution of the ECS (described in the previous chapter), characteristic of different reactor types. This value (in pcm) is normalised by the burn-up reactivity loss during the lifetime, giving a percentage of the possible ECS contribution to maintain criticality at constant core power. If the value is equal to or greater than 100%, the reactor can be controlled throughout its lifetime by the ECS contribution. On the other hand, a value between 0% and 100% indicates the fraction of reactivity loss due to burn up that can be compensated by the ECS control.

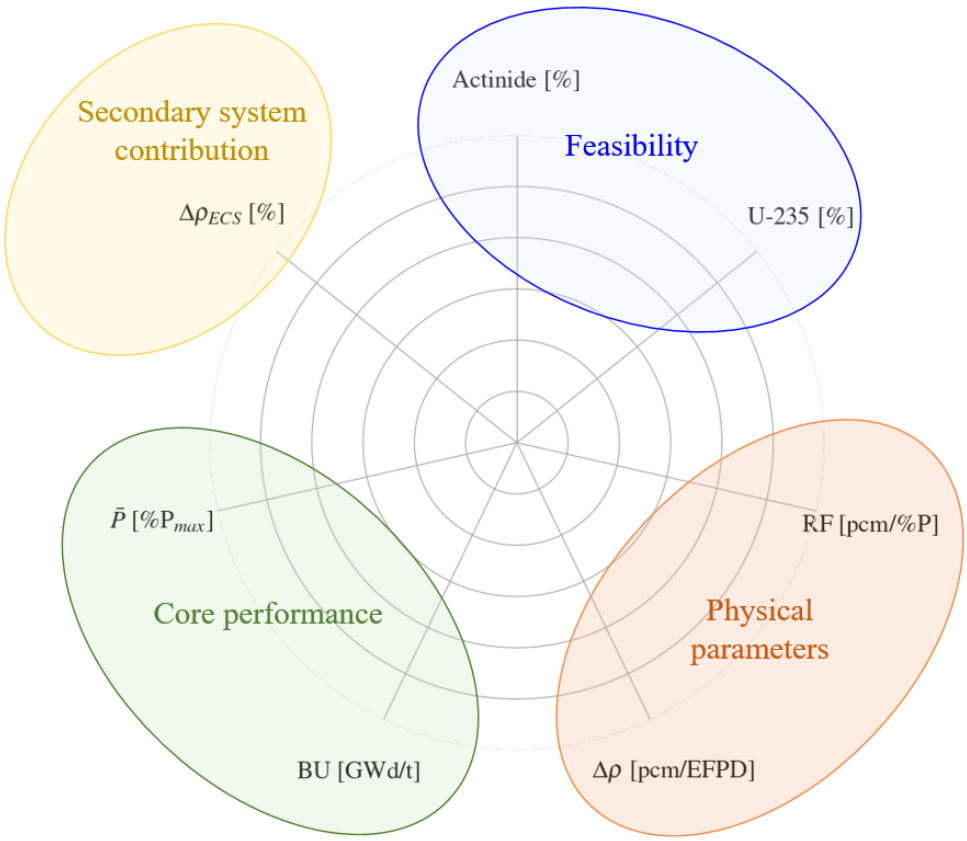


Figure 4.8 – Scheme of comparison of different autonomous cores.

The axes with actinides (for example, as explained in the next chapter) content and the U-235 enrichment are indicative of fuel manufacturability. The reactivity feedbacks and reactivity swing represent the physical parameters defining core behaviour during irradiation: the larger the RF, the larger the capacity of the core to counterbalance the reactivity loss. On the other hand, the lower the reactivity swing, the longer the core lifetime.

The reached burn-up at EOL and mean power of operation represent indicators of core "performance". The burn-up is also indicative of fuel utilisation and indicative of the fuel "cycle cost", while the average power gives an indication of the integral of the energy over the core lifetime and is strongly correlated with the power generation capital cost (in terms of $/kWh of energy produced).

The axis of $\Delta\rho_{ECS}$ is present only for graphs that compare different reactor types. It is an indicator of the possible "gain" by the secondary system and it is a characteristic of each technology.

Finally, the graphs also show the Xe effect. In particular, the limit at -500 pcm is chosen. Cases with a larger loss of reactivity, due to the Xe effect, are shown with a dashed line. On the other hand, cases with a smaller loss of reactivity are shown with a solid line and the Xe effect is assumed to be absent. It is considered that, design optimisation may lead to a further reduction in reactivity loss, or an initial active control may be used to compensate the reactivity up to 500 pcm.

4.6. Conclusions

In this chapter, the comparison between the previously selected reactors is made on the basis of autonomously operated cores. The objective is to study different reactor cores, designed to be driven by active reactivity control, but to evaluate, in this work, their performance in autonomous operation.

The methodology adopted provides for an initial comparison of literature designs of reactors, operated autonomously. In this first phase, the design was kept identical to that of the literature references, with the exception of the fuel material. The four reactors were fuelled with UO_2 in order to provide a simpler and more consistent comparison. The conclusion of this initial study highlights the difference between the reactivity swing of thermal and fast reactors (the first with a fluctuation and the second with monotonic decrease) and the time to get the same performance indicator of burn-up. This study also has presented the different reactivity feedback coefficient characteristics of each core design.

The comparison was then extended by extrapolating all the designs to the same power density. In this first approach, the core geometries remained the same and the power was adapted. The HPR has interesting characteristics when operated autonomously, but is very limited in terms of power density (due to the operation of the heat pipes). Because of its intrinsic limitations in terms of power density, the HPR will not be analysed in more detail in the following chapter.

The three designs considered potentially interesting are nevertheless characterised by very low performance compared with current industrial reactors. The average performance of existing PWRs (for example in the French fleet) consists of a power density of around 100 W/cm^3 a fuel cycle of between 12 and 18 months and a fuel burn-up on discharge of around 50 GWd/t [93]. The PWR autonomously operated is characterised by few month lifetime and very low burn-up of the order of 0.3 GWd/t. In the case of HTR and SFR, for autonomous operation, the lifetime is of the order of a few months or years, but the burn-up at the end of life is very low, of the order of 2 GWd/t. This overall performance is not competitive. The aim of the next part of the work is to explore different ways of increasing the performance of these autonomous concepts and to compare them with those of industrial reactors. As the power density is not of first-order influencing the core behaviour, the reactors studied in the next part will be the ‘reference design’, i.e. with the power density of the literature.

Chapter 5

Thermal spectrum autonomous reactors

Summary

5.2. Actinides and burnable poisons 109

5.2.1. Theoretical description of actinides under irradiation 109

5.2.2. Theoretical description of burnable poisons under irradiation 111

5.3. Autonomous HTR with actinides and burnable poisons 112

5.3.1. Actinides in HTR core 112

5.3.1.1. Parametric study on the americium insertion in HTR fuel 117

5.3.1.2. Parametric study on the neptunium insertion in HTR fuel 122

5.3.1.3. Parametric study on the plutonium insertion in HTR fuel 124

5.3.2. Conclusion on actinides insertion in HTR 126

5.3.3. Burnable absorbers in HTR core 127

5.3.3.1. Parametric study on the boron insertion in HTR core 128

5.3.3.2. Parametric study on the dysprosium insertion in HTR core 129

5.3.4. Conclusion on burnable absorbers insertion in HTR core 132

5.4. Autonomous PWR with actinides and burnable poisons 133

5.4.1. Actinides in PWR core 133

5.4.1.1. Parametric study on the americium insertion in PWR fuel 133

5.4.1.2. Parametric study on the neptunium insertion in PWR fuel 139

5.4.1.3. Parametric study on the plutonium insertion in PWR fuel 142

5.4.1.4. Parametric study on the thorium insertion in PWR fuel 145

5.4.2. Conclusions on actinides insertion in PWR core 148

5.4.3. Burnable absorbers in PWR core 149

5.4.3.1. Parametric study on the boron insertion in PWR fuel 149

5.4.3.2. Parametric study on the dysprosium insertion in PWR fuel 151

5.4.4. Conclusion on burnable absorbers insertion in PWR core 154

5.5. Conclusions 155

5.1. Introduction

In this chapter, an analysis of potential improvement of autonomous reactors is presented. Main efforts are focused on performance enhancement by tuning reactivity evolution due to fuel depletion. This chapter deals with such modification of core design.

In the actively operated reactors, reactivity is controlled by both active and passive systems. Active methods are used to compensate reactivity variation and to actively follow power demand from the secondary system. Passive methods are also applied to compensate the initial reactivity excess in the core (use of burnable poison materials for instance).

In this work, the potential use of burnable materials (or analogously actinides) in HTR, PWR and SFR cores is analysed. Although already done in many core concepts, they are used here as the only degree of freedom for reactivity loss compensation an autonomous core, thus to increase the core lifetime. In this chapter, only thermal cores will be analysed and compared, while the fast core case will be studied in the next chapter.

The study, from now on, is based on the selected reactor designs with their original design (with associated power densities: 5.67 W/cm^3 for HTR and 101 W/cm^3 for PWR). The first part of the chapter is dedicated to a literature review (the state of art of burnable poison and actinides under irradiation). The second part is dedicated to the analysis of the insertion of different actinides and burnable poisons in the HTR cores. Finally, in the third part of the chapter, the same methodology will be applied for the PWR and main outcomes will be highlighted.

The effect of actinides and burnable poisons in the core is analysed through four steps. First, the chosen isotope is inserted in the fuel and the reactor steady-state at BOL is analysed. The U-235 enrichment (or the Pu content, as explained in the following) is adapted to ensure core criticality at BOL. Second, the reactivity feedback coefficients are evaluated for each configuration. Then, the burn-up reactivity evolution is shown. Finally, the KGH method is applied to assess the power evolution of the different configurations.

In this section, all the burn-up simulations have been run with Serpent 2 with 5000 active neutrons cycles, 5000 neutrons simulated per cycle and 50 initial inactive cycles. On the other hands, the steady-state simulations have been run with 7000 active neutrons cycles, 7000 neutrons simulated per cycle and 50 initial inactive cycles. A specific uncertainties analysis is considered as a perspective if a specific detailed core design is foreseen.

5.2. Actinides and burnable poisons

This section describes the behaviour of actinides and burnable poisons under irradiation.

5.2.1. Theoretical description of actinides under irradiation

Actinides are elements with atomic number included between 89 and 103. They are produced following irradiation of heavy nuclei and their nuclear filiation. They are distinguished in major and minor actinides. The first ones include uranium (Z=92) and plutonium (Z=94) isotopes and are called major actinides because they are widely used in nuclear fuel for power production. The latter includes neptunium (Z=93), americium (Z=95) and curium (Z=96) isotopes and are defined as minor actinides because are produced in minor quantities by the fuel irradiation with respect to plutonium [94].

The depletion chain of the cited actinides is presented in Figure 5.1.

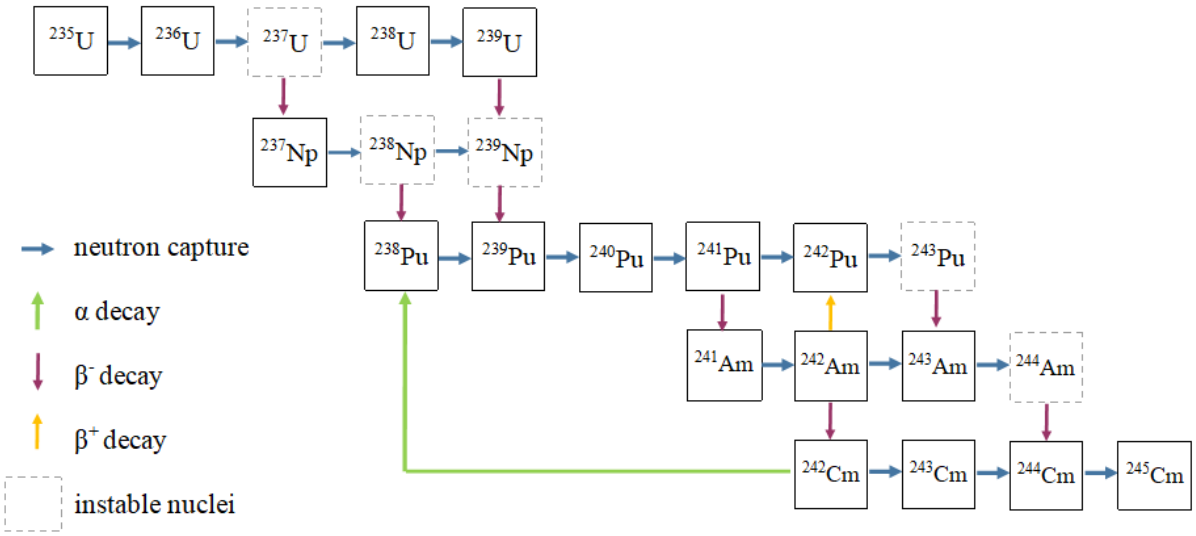


Figure 5.1 - Actinides irradiation chain.

The interest in inserting minor actinides in fuel, by substitution of some amount of uranium, is bound to their neutron capture cross sections. Inserting a minor actinide in fresh fuel provides a higher absorption rate at BOL with respect to the solely U-238. Progressively, with burn-up, minor actinides are consumed and this additional absorption contribution is reduced. So, the necessary U-235 enrichment at BOL has to be higher to account for larger absorption rate. There is an ideal ratio between the content of actinides and fissile materials that makes such consumption compensating the fissile depletion. The minor actinide isotopes selected in this work are Np-237, Am-241 and Am-243, being the actinides that show an absorption cross section larger that U-238 (for the thermal neutron spectrum). Curium is not considered in the study because no suitable absorption cross-section compared to U-238, (except for the Cm-244,which has high spontaneous fission rate and therefore difficult to shield and handle).

Insertion of plutonium could also be considered. The MOX (Mixed OXide) fuel is composed of the mix of the reactor grade Pu recycled from spent LWR fuel and depleted uranium. The interest of the use of MOX is related to the recycling of nuclear waste. Indeed, in a commercial nuclear UO_2 PWR, with U-235 content ranging between 3% and 5%, significant fraction of plutonium isotopes are formed with irradiation. Among them, Pu-239 and Pu-241 are the only fissile isotopes in thermal range. During the fuel cycle of a commercial reactor, only a limited fraction of these fissile isotopes are consumed, while the remaining are discharged from the reactor. To exploit this fraction of fissile material, it is possible to separate the plutonium and mixing it with depleted uranium, to recycle the fuel inside one or multiple new irradiation cycles.

Thorium is considered in this work, even if it is not included in the uranium fuel irradiation chain. The $UThO_2$ fuel has been studied at the beginning of the nuclear reaction era as the other uranium and plutonium based oxide fuels. The main interest in studying the thorium based fuel was related to the risk of uranium shortage. Indeed, thorium content on earth is estimated being three times larger than the uranium's one. Anyway, several reasons discouraged the thorium fuel exploitation such as low concern about the uranium worldwide stock consumption or high-energy gamma rays of U-232 produced by irradiation. In addition, Th-232 exhibits larger capture cross section than U-238 leading to higher U-235 content at the core start-up.

The thorium depletion chain is shown in Figure 5.2. As Th-232 is not a fissile isotope, the thorium-based fuel needs a fissile isotope or an important source of neutrons at the beginning of life. However, when irradiated, it decades into U-233 which is a fissile isotope. The advantage of U-233 with respect to U-235 and Pu-239 is its higher fission to capture ratio.

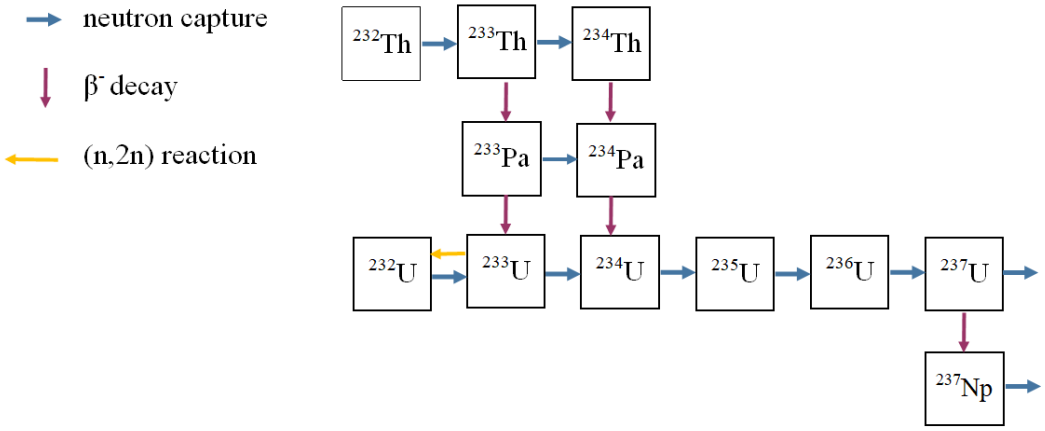


Figure 5.2 - Thorium irradiation chain.

5.2.2. Theoretical description of burnable poisons under irradiation

Burnable poisons (BP) are materials that contain isotopes characterised by a large capture cross section, that are not fissile and do not include fissile elements in their depletion chain. During the reactor operation, they are naturally depleted, decreasing their relative importance on neutron capture. They are inserted in fresh fuel cores allowing to load large fissile quantities for cycle length purpose and ensure a less core excess reactivity at the beginning of cycle. Progressively with irradiation, the fuel and the burnable poisons are consumed allowing the decrease of fissile material to be compensated by the decrease of the absorber. This feature is used to have longer life cores and avoid controlling this reactivity excess by other active means [40]. Ideally, they are chosen in such way that their depletion kinetic is of the same order of the fuel depletion [95]. The burnable poison, in commercial reactors are inserted for the compensation of the initial reactivity in thermal reactors. They are not used in fast reactors, where the initial reactivity is compensated by the control rods.

The most common burnable poison in thermal reactors includes boron and gadolinium [96]. Normally, the boron is inserted in its natural composition (19.9 % B-10 and 80.1 % B-11 in atomic contents). The only absorber isotope of boron in B-10. Other materials are considered as burnable absorbers, such as gadolinium, europium, hafnium, cadmium and dysprosium based materials. More information on absorber candidate materials can be found in [97].

In thermal reactors, the burnable poisons are typically loaded in the core according to three different options: merged in the fuel, inserted in the fuel cladding or inserted in dedicated pins situated in specific core locations. The first two configurations guarantee homogenised dispersion of the burnable material. On the contrary, insertion of dedicated pins with burnable poison can be used to locally modify the spectrum shape, for example to compensate some hot spots. Usually, the three configurations are used at the same time [97].

In this study, the insertion of boron is considered as an example of burnable absorber as the most common BP. Then, as it will be detailed afterward, in view of conceiving an autonomous reactor with

the longer autonomous life, also de dysprosium is tested because it has a depletion dynamic that is slower that boron.

5.3. Autonomous HTR with actinides and burnable poisons

In this section, insertion of minor actinides and burnable poisons in the fuel is proposed in HTR. Several choices of actinides, with different contents in the core, are considered. A physical analysis is provided to compare different configurations and some layouts are highlighted as promising configurations for an autonomous reactor design. The main parameters of the core are summed up in the next Table 5.1 and Figure 5.3.

Table 5.1 – Sum-up of the HTR core characteristics.

Core thermal power [MW]	200
Power density [W/cm^3]	6
Assembly pitch [cm]	36
Pins per assembly	108
TRISO packing fraction [%]	30
Fissile zone volume [m^3]	35

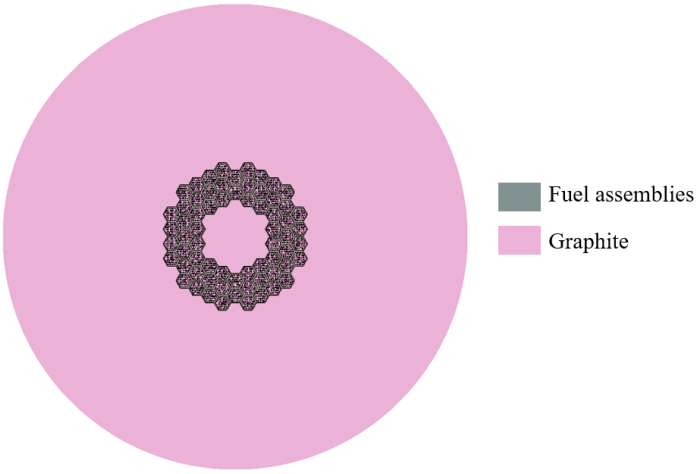


Figure 5.3 - Radial description of HTR core.

In the next paragraph 5.3.1, the insertion of the actinides in the core is analysed, while in paragraph 5.3.3 the insertion of burnable absorbers is analysed.

5.3.1. Actinides in HTR core

The study is organised with a first comparison of all the different actinides (in this paragraph 5.3.1) and then a sensitivity study with variable content of each actinide (paragraphs 5.3.1.1, 0 and 5.3.1.3). The considered isotopes are: Am, Np, Pu and Th.

Enrichment

First of all, BOL results on the steady-state conditions are presented. Actinides have been inserted homogeneously within the fuel material. The fissile content has been computed according to the criterion of criticality at BOL. The reference actinide contents values are taken as the upper limits based on safety criteria described in [41]. The Am has been considered composed of 75% of Am-241 and 25% of Am-243, the Np is Np-237 and the Th is Th-232.

The MOX case is slightly different with respect to the others. The U-235 enrichment has been fixed at 0.25 % (as in the usual MOX fabrication process involving depleted uranium) and the PuO_2 content has been adjusted in order to guarantee criticality at BOL. The MOX fuel is composed of a plutonium vector including Pu-238, Pu-239, Pu-240, Pu-241, Pu-242 and a residual content of Am-241 coming from Pu-241 decay. Am-241 is taken into account as the short Pu-241 half-life always leads to the production of a small amount of americium in the fresh fuel. Among these isotopes, the Pu-239 and Pu-241 are fissile elements in thermal spectrum. The plutonium isotopic composition considered, in this case, is summed up in Table 5.2. It corresponds to the predicted configuration of MOX fuel for a reference French nuclear scenario, named MOX-2035 [98].

Table 5.2 - MOX reference isotopic vector.

MOX isotope	Mass fraction [%]
Pu-238	3.57
Pu-239	47.39
Pu-240	29.66
Pu-241	8.23
Pu-242	10.37
Am-241	0.78

In Table 5.3, reference actinides content and relative fuel enrichments are shown. In all the analysis from now on, the content is defined as the ratio between the isotope mass and the whole fuel mass. On the contrary, the U-235 enrichment is defined as the ratio between the U-235 mass and the total uranium mass. The fissile in the table includes the sum of all the fissile isotopes in the fuels as the U-235, Pu-239 and Pu-241 (if present).

Table 5.3 - HTR actinides insertion configuration.

Configuration	Actinide or Pu content [%w]	U-235 enrichment [%w]	Fissile content [%w]
$UAmO_2$	5.2	34.0	32.2
$UNpO_2$	16.3	40.0	33.5
$UThO_2$ [99]	74.0	13.5	3.5
$UPuO_2$	51.0	0.25	28.5
UO_2	-	2.3	2.3

The neutron spectrum of the five different configurations is analysed in Figure 5.4. In this figure, spectrum has been represented at 315 energy groups. The "spectrum index" is reported in Table 5.4. This parameter allows a comparison between spectra of different reactors. The higher is the index value, the more neutrons are in the range of thermal energies. It is defined according to the following equation:

$$x = \frac{\int_{0.025\ eV}^{1\ eV} \phi(E)dE}{\int_{1\ eV}^{100\ MeV} \phi(E)dE} \frac{(100e6-1)}{(1-0.025)}; \qquad (5.1)$$

In Table 5.4 the value distinguishing thermal and fast energies is set at 1eV.

Table 5.4 – HTR actinides "spectrum index".

Configuration	Index [-]
$UAmO_2$	1.53
$UNpO_2$	1.51
$UThO_2$	16.90
$UPuO_2$	0.43
UO_2	2.30

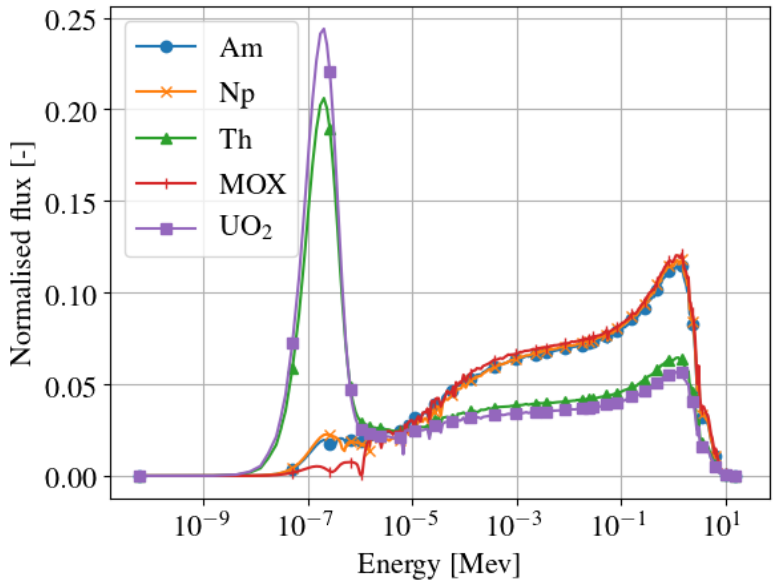


Figure 5.4 - HTR actinides fuel spectrum.

From Table 5.3 and Table 5.4 it is possible to compare the content of fissile elements and the relative neutron spectrum. The configurations that show a hardened spectrum (americium, neptunium and plutonium), needs a higher fissile content to achieve criticality as fission cross sections of U and Pu at higher energies are lower than in thermal energy range. The cases of insertion of Am and Np show comparable spectra and comparable fissile content in fuel. The case of $UPuO_2$ exhibits "fast spectrum", but needs a slightly lower total fissile content. This is due to the insertion of Pu inside the fresh fuel. Indeed, in fast spectrum, Pu-239 and Pu-241 (the fissile isotopes of Pu vector) have higher neutrons generation efficiency, because they are characterised by a higher number of neutrons produced by

fissions than U-235. The mean neutrons produced following a fission event are 2.44 by U-235, 2.88 by Pu-239 and 2.95 by Pu-241 [100]. On the contrary, configurations related to "thermal spectrum" ($UThO_2$ and the reference UO_2) need a lower fissile content due to the larger fission cross section of U-235 in thermal range.

Detailed analysis of the different spectra hardening can be found in Annex V.1.

Reactivity feedbacks

The reactivity feedbacks of each configuration are calculated and the results are shown in Table 5.5.

Table 5.5 – Reactivity feedbacks for different actinides configurations - HTR.

Configuration	Doppler coefficient [pcm/K]	Graphite coefficient [pcm/K]
$UAmO_2$	-2.52	-7.21
$UNpO_2$	-2.13	-7.25
$UThO_2$	-4.06	-1.21
$UPuO_2$	-2.17	-2.60
UO_2	-5.60	-2.08

As expected, Doppler coefficient decreases with spectrum hardening and the increase of the U-235 enrichment, as Doppler effect is mainly due to the U-238 resonances captures.

On the other hand, the graphite coefficient is increased, in particular, the case of Am and Np show a large increase of this coefficient. The thermal utilisation factor (referred to the four factors formula [60]) is shown in Figure 5.5. In Am and Np (and slightly Pu) case, the absorption in the actinides resonances decrease the factor and increase the coefficient.

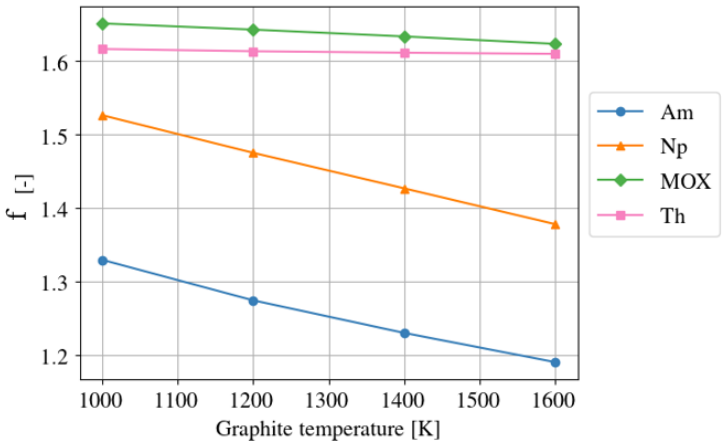


Figure 5.5 – Thermal utilisation factor variation as a function of graphite temperature - HTR.

For the objective of the present work, the larger are the reactivity feedbacks the larger is their contribution to counterbalance the reactivity loss of the fuel depletion. So, with respect to the UO_2 case, the reduction of Doppler and the increase of graphite coefficients are competing effects. These impacts will be analysed in the KGH model, together with the reactivity swing variation.

Burn-up reactivity swing

In this section, the configurations presented above are analysed in terms of reactivity evolution according to fuel burn-up (without accounting for reactivity feedbacks here at first). Figure 5.6 shows the reactivity evolution of each fuel considered.

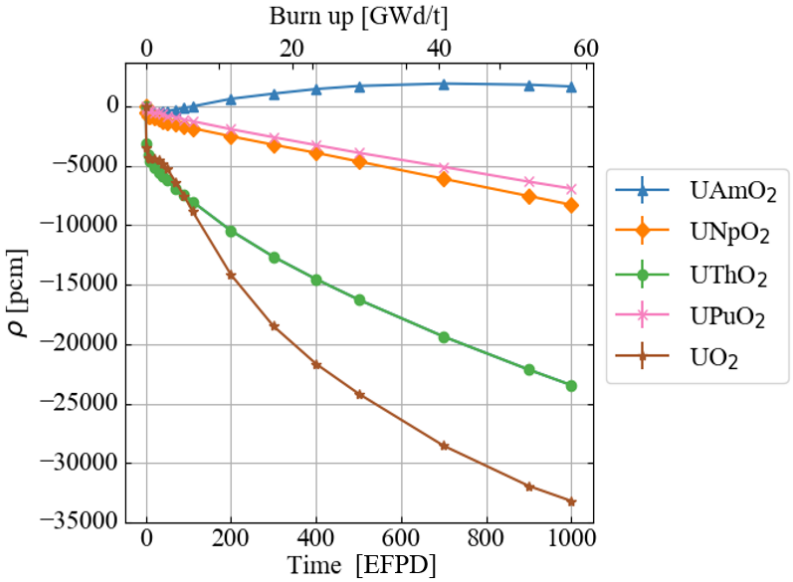


Figure 5.6 – Reactivity evolution of HTR core loaded with actinides.

The UO_2 and $UThO_2$ configurations are characterized (as explained above) by thermal spectrum and thus, they show a significant Xe-effect on the reactivity loss in the first days of the core life. The average slope of reactivity loss is around +2.74 pcm/EFPD for the $UAmO_2$, -7.58 pcm/EFPD for the $UNpO_2$, -6.70 pcm/EFPD for the $UPuO_2$, -15.9 pcm/EFPD for the $UThO_2$ and -22.8 pcm/EFPD for the UO_2. All these values were averaged between 0 and 1000 EFPD except for the $UThO_2$ and UO_2, which are averaged between 200 and 1000 EFPD, to consider a mean slope after the first days with the Xe reactivity drop and the effect of reactivity fluctuation due to low enrichment of UO_2.

The Am and Np configurations are characterised by almost the same fissile content and neutron spectrum, but show different trends for reactivity evolution. An investigation of the physics of this phenomena is given in Annex V.2. The conclusion highlights an effect of spectrum that differs between the two cases.

Power evolution

In this paragraph, the effect of the reactivity evolution and the reactivity feedbacks are simultaneously considered within the KGH calculations. The results in terms of power evolution are shown in Figure 5.7.

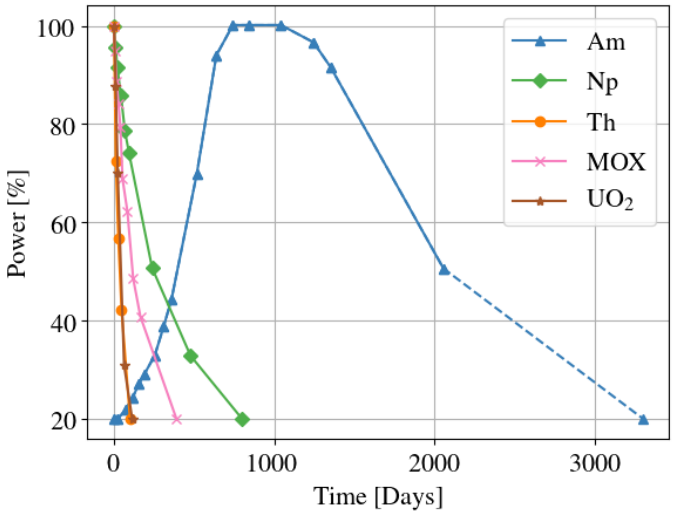


Figure 5.7 - Power evolution for different actinides configurations – HTR.

The trend of the power evolution follows the trend of the reactivity swing and the larger are the reactivity feedbacks, the larger is the compensation of the reactivity variation.

In conclusion, in this paragraph, a comparison between different actinides insertion in HTR fuel has been analysed highlighting a decrease in the reactivity loss with respect to the case of UO_2 core. In next paragraphs, all the different actinides but Th are analysed individually. The $UThO_2$ configuration is set aside as its potential to reduce the burn-up reactivity swing seems to be limited. The effect observed with a high Th content (74% in this case) is far less effective than the other actinides.

So, the $UAmO_2$, the $UNpO_2$ and the $UPuO_2$ configuration will be analysed individually, varying their content in fuel.

5.3.1.1. Parametric study on the americium insertion in HTR fuel

In this paragraph, the attention is focused on $UAmO_2$ configuration to assess the effect of the variation of the Am content.

Enrichment

The content of Am varies between 1 % and 10 % and the associated U-235 enrichment is calculated.

Table 5.6 – Variation of the content of americium in $UAmO_2$ HTR fuel.

Configuration	Am content [%]	U-235 enrichment [%]	Fissile content [%]
Am 1%	1.0	10.0	9.9
Am 5.2%	5.2	34.0	32.2
Am 10%	10.0	50.5	45.5

As shown in Table 5.6, as the actinide content increases (thus the core captures increased), U-235 enrichment is consequently increased to guarantee criticality at BOL.

The spectrum and the associated spectrum index variation is detailed Annex V.3.

Reactivity feedbacks

The reactivity feedback effects, associated to the previous configurations are shown in Table 5.7.

Table 5.7 - Reactivity feedbacks for different $UAmO_2$ configurations - HTR.

Configuration	Doppler coefficient [pcm/K]	Graphite coefficient [pcm/K]
UO_2	-5.60	-2.08
Am 1%	-4.74	-11.05
Am 5.2%	-2.52	-7.21
Am 10%	-1.68	-5.76

The strong decrease in U-238 content in the fuel (and the spectrum hardening) leads to a decrease of the Doppler coefficient with the addition of americium.

With small addition of americium, the graphite coefficient is increased thanks to the high americium thermal resonance. When the americium content increases, this coefficient tends to reduce with the increase of the fast neutron importance.

Burn-up reactivity swing

Figure 5.8 presents the reactivity evolution associated with the considered cases. For low Am content, the reactivity increases rapidly with time, reaches a peak and then decreases. A small addition of Am-241 in the fuel leads to a very small spectrum hardening (the Xe effect is still present) and a quick disappearance of this isotope. Within a reduced burn-up range, the reactivity gets back to its "natural" decreasing behaviour. Increasing the Am content, the reactivity peak reduces up to a configuration where the reactivity is almost flat up to about 1000 EFPD, for an Am content in fuel of 10%. Furthermore, the spectrum hardening leads to a significant reduction of the Xe effect.

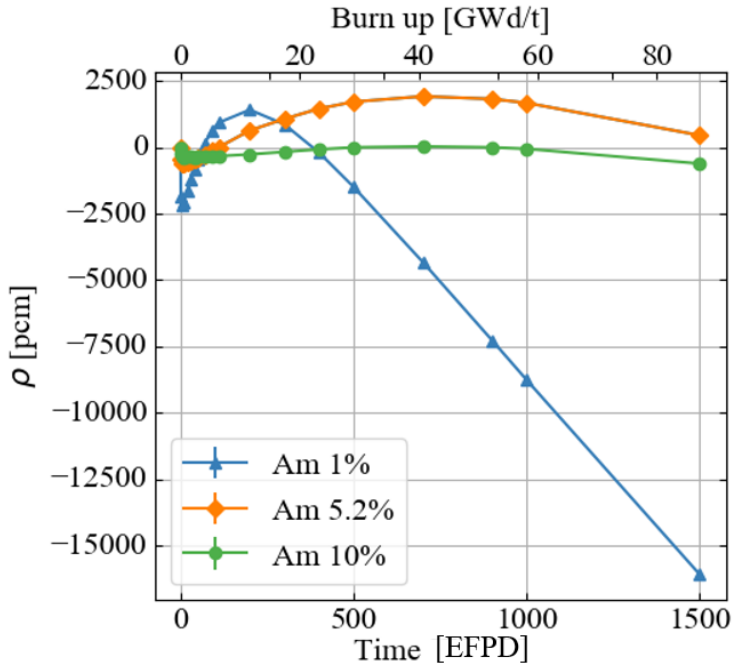
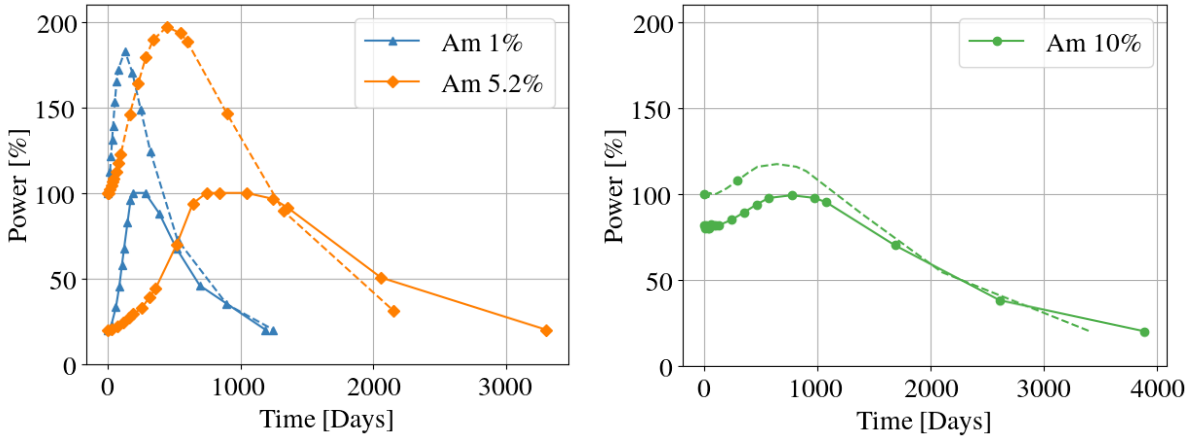


Figure 5.8 – Reactivity evolution according to variation of Am content in $UAmO_2$ HTR fuel.

In Annex V.3, a detailed analysis of the reactivity evolution according to the Am contents is performed. The conclusion highlights that the Am 10% configuration is the one that allows a compensation between the slight increase of the generation mean cross section and the slight decrease of the mean absorption cross section.

Power evolution

This section presents the power evolution associated to the previously presented reactivity swing and feedback. In all the three cases, the power increases over its initial value. For this reason, the reactor operation is started at lower value with respect to the nominal power. Figure 5.9 shows the evolution of the power of the considered cases, comparing the theoretical curve (dashed lines) with the curve starting from lower power values (solid line). In terms of cycle length, the adaptation of the core initial power enables an increase of cycle length, which is interesting for an autonomous reactor.



(a) *(b)*

Figure 5.9 - Power evolution for different $UAmO_2$ configurations with adapted initial value – HTR.

For the configurations of Am-1% and Am-5.2%, the core is started-up at 20% of the nominal power. Even started-up at the lowest admissible value, the power exceeds the nominal one during the evolution. This because the reactivity increase is so wide that the positive reactivity inserted with burn-up exceeds the feedback reactivity margin (integral of reactivity between the two states of 20% and 100% of nominal power). During the periods beyond nominal power, it is supposed that an active system (active control on the ECS for example) is used to keep the power to the maximum design value or that an optimization of the core could allow this design to go below the feedback reactivity margins. The exceeding reactivity is 487 pcm and 463 pcm respectively in case Am-1% and Am-5.2%. A more important exceed in reactivity would have made the design unviable.

Figure 5.10 compares the power evolution of the three cases. In the figure, the evolution of the power is represented by a continuous line up to 60GWd/t (chosen as the maximum burn-up value) and with dashed line beyond.

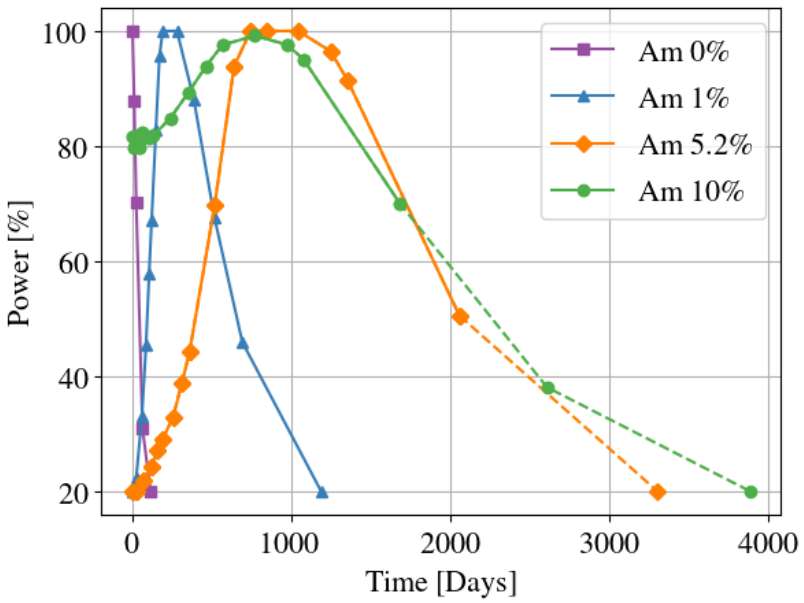


Figure 5.10 - Power evolution for different $UAmO_2$ configurations – HTR.

The narrow variation in reactivity in low Am content (1%) leads to a significant power variation in a short period of time. Increasing the Am content has two opposite effects: the reactivity swing is flattened (reduction of the reactivity swing by a factor of 10 to 100) and the reactivity feedbacks decrease. The Am-10% configuration shows a flattened power evolution compared to the two others.

To evaluate more globally each solution, a sum-up is presented in Figure 5.11. This type of graph was defined in paragraph 4.5.2 and will be used from now on to summarise the characteristics of the different configurations.

The reference case of core fuelled in UO_2 is not reported in the graph, because of readability reasons, but the values of the listed parameters are shown in the following Table 5.8.

Table 5.8 – Comparative parameter of autonomous UO_2 core – HTR.

Parameter	Value
U-235 [%]	2.3
RF [pcm/%P]	19.6
$\Delta\rho$ [pcm/EFPD]	50.1
BU [GWd/t]	1.2
$\overline{P}$ [$\%P_{max}$]	11.9

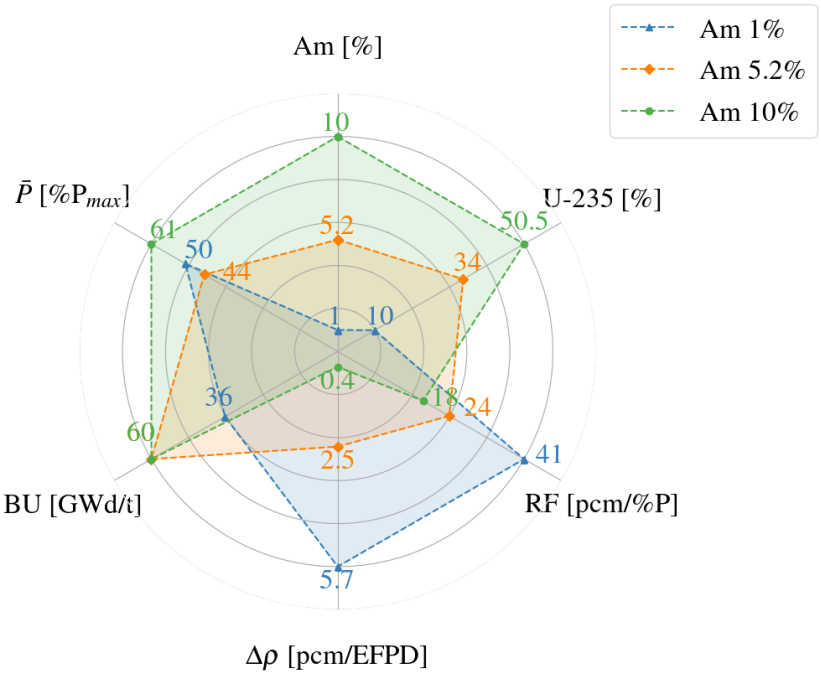


Figure 5.11 – Sum-up of the core performance for different $UAmO_2$ configurations – HTR.

First we focus on the core performance, looking at the axes of the mean power ($\bar{P}$) and the burn-up at EOL (BU). The targeted burn-up of 60 GWd/t could only be obtained with 5 or 10% range of Am content. Lower values lead to large reactivity loss. For "larger" americium content, the addition of more americium allows a better specific average power of operation. With 10% of americium, the average operating power is about 61% of the nominal power during the 1600 days of operation.

The second point to be noticed concerns the physical analysis, shown on the axis of the reactivity feedbacks (RF) and the reactivity swing ($\Delta\rho$). The impact of the reactivity swing modification is largely dominant compared to the reactivity feedback variation, in this range of americium addition. Indeed, the reactivity feedback between the case Am-1% and Am-10% is reduced by 57% (between 41 and 18 pcm/%P). On the other hand, the reactivity swing is reduced by 93% (between 5.7 and 0.4 pcm/EFPD).

Finally, it should be noted that the addition of americium highly increases the U-235 enrichment. With a HALEU compatible enrichment (in the analysed cases only the configuration Am-1%), it will be difficult to reach a mean power of more than 50% and a target burn-up of 60 GWd/t.

5.3.1.2. Parametric study on the neptunium insertion in HTR fuel

The same study is made on different content of Np-237 in the fuel.

Enrichment

In this section, the U-235 enrichment is computed. Table 5.9 shows that the higher is the content of the actinide, the higher is the U-235 enrichment needed for criticality as the spectrum is hardened. This effect is similar to the one observed in the americium insertion case.

Table 5.9 - Variation of the content of neptunium in $UNpO_2$ HTR fuel.

Configuration	Np content [%]	U-235 enrichment [%]	Fissile content [%]
Np 1%	1.00	4.00	3.96
Np 5%	5.00	13.0	12.4
Np 16.3%	16.3	40.0	33.5
Np 20%	20.0	48.0	38.4
Np 40%	40.0	93.0	55.8

Reactivity feedbacks

The reactivity feedbacks are computed in this paragraph, the explored configurations can reach Np content of 16.3%. Higher contents presented in Table 5.9 are used in the next paragraph to assess a threshold effect on the reactivity swing, but not considered further due to the high U enrichment needed. The results are presented in Table 5.10.

Table 5.10 - Reactivity feedbacks for different $UNpO_2$ configurations - HTR.

Configuration	Doppler coefficient [pcm/K]	Graphite coefficient [pcm/K]
UO_2	-5.60	-2.08
Np 1%	-5.75	-10.52
Np 5%	-4.19	-11.42
Np 16.3%	-2.13	-7.25

Burn-up reactivity swing

Figure 5.12 shows the reactivity evolution as function of initial Np content in the core. The reactivity loss becomes linear with the increase of the Np content. The higher is the content of Np-237, the lower is the reactivity loss. The reactivity loss variation shows a saturation effect, as the slope of the curve does not go linearly to zero when increasing the neptunium content. The configuration with 40% of Np-237 already implies a large U-235 enrichment, of about 93 %, and excludes the possibility to reach a “flat” reactivity curve increasing the Np content.

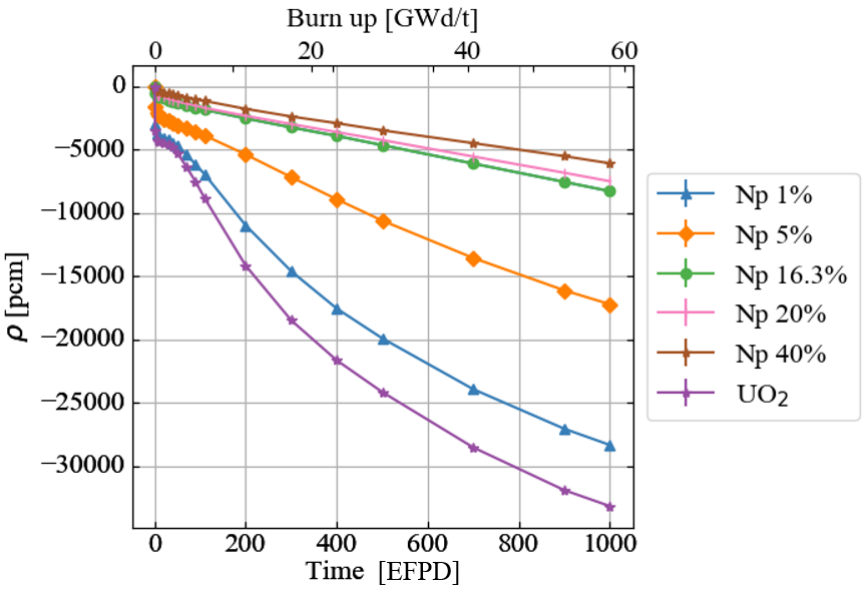


Figure 5.12 - Reactivity evolution according to the variation of Np content in $UNpO_2$ HTR fuel.

The behaviour of the $UNpO_2$ has been compared to the one of $UAmO_2$ in 5.3.1.1 and the detailed analysis is made in Annex V.3. Indeed, it is interesting to show why the two configurations, characterised by similar physical behaviour, show different reactivity swing when increasing the actinide content. The explanation is based on the modification of spectrum during irradiation as detailed in Annex V.3.

Power evolution

The concurrent effects of the reactivity swing and feedbacks coefficients are analysed with the KGH method. The power evolution of the three considered configurations is represented in Figure 5.13.

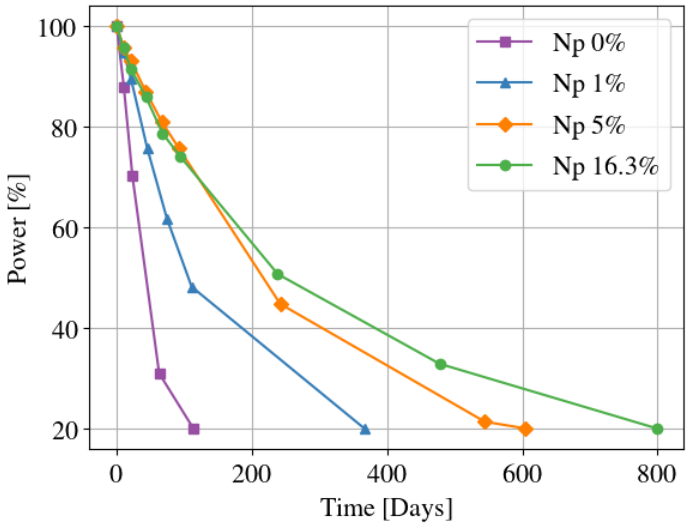


Figure 5.13 - Power evolution for different $UNpO_2$ configurations – HTR.

The results of the core performance are summed up in Figure 5.14.

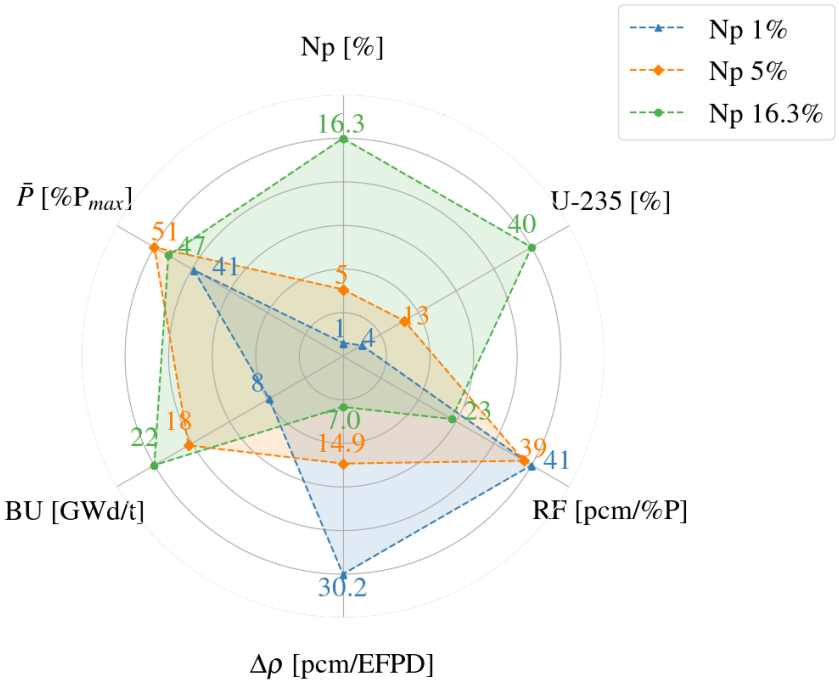


Figure 5.14 - Sum-up of the core performance for different $UNpO_2$ configurations – HTR.

The increase of the Np content in HTR fuel shows an increase of the core lifetime but does not provide significant power flattering compared to the addition of Am. Even with high content of neptunium (and high U-235 enrichment), the burn-up stays at lower values, up to 22 GWd/t. In parallel, the average effective power stays below 50%.

As in the case of Am, the reactivity swing reduction prevails on the reduction of the reactivity feedbacks. When increasing the neptunium content from 1% to 16.3%, the RF is reduced by 44%, while the reactivity loss per EFPD is reduced by 76%.

The configurations up to 5% of Np content show a U-235 enrichment that is compatible with HALEU requirements.

5.3.1.3. Parametric study on the plutonium insertion in HTR fuel

Enrichment

The case of plutonium has been analysed in a slightly different way. The U-235 enrichment was varied (starting from depleted uranium used with MOX) and the plutonium content was adapted to ensure the criticality condition at BOL. The plutonium vector has been, in a first stage, considered constant and its composition is summed up in Table 5.2.

In Table 5.11, the configurations analysed are summed up. It is reminded that the content is defined as the ratio between the isotope mass and the whole fuel mass. On the contrary, the enrichment is defined as the ratio between the U-235 mass and the total uranium mass. The fissile in the table takes into account the sum of all the “fissile” isotopes in the fuel (U-235, Pu-239 and Pu-241). The more the uranium is enriched, the less is the content of Pu needed to have a critical core, the fissile isotopes of Pu are replaced by the U-235. Indeed, the total fissile content (sum of U-235, Pu-239 and Pu-241) is quite constant.

Table 5.11 - Variation of the uranium enrichment in $UPuO_2$ HTR fuel.

Configuration	U-235 enrichment [%]	Pu content [%]	Fissile content [%]
Pu-51%	0.25	51.0	28.5
Pu-49%	2.00	49.0	28.3
Pu-40%	10.0	40.0	28.2

Reactivity feedbacks

The associated reactivity feedback coefficients are shown in Table 5.12. The insertion of Pu in the fuel decreases the Doppler effect and increases the graphite coefficient.

Table 5.12 - Reactivity feedbacks for different $UPuO_2$ configurations - HTR.

Configuration	Doppler coefficient [pcm/K]	Graphite coefficient [pcm/K]
Pu-51%	-2.17	-2.60
Pu-49%	-2.26	-2.68
Pu-40%	-2.40	-2.83

Burn-up reactivity swing

Figure 5.15 shows the evolution of the different configurations mentioned above. In the range of variation of U-235 enrichment considered, the effect on the reactivity evolution is not significant considering the total fissile material content constant.

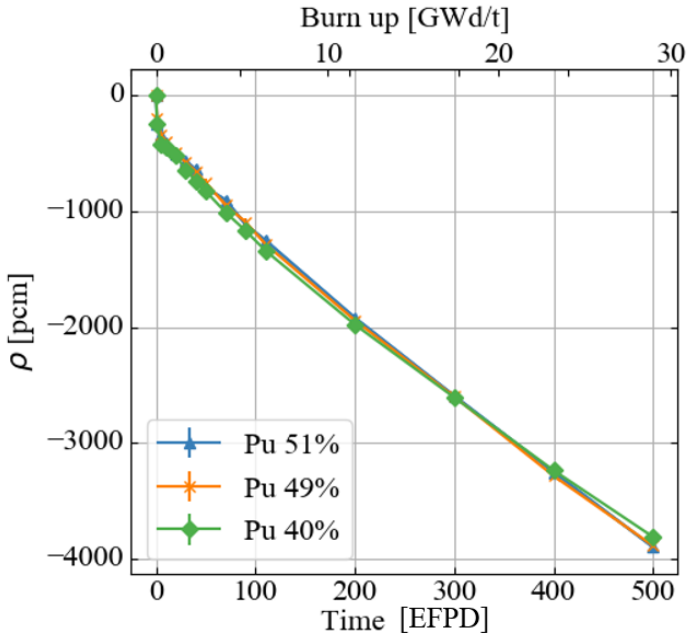


Figure 5.15 - Reactivity evolution according to the variation of Pu content in $UPuO_2$ fuel.

Power evolution

The effect of the reactivity swing and thermal feedbacks on the power are assessed and represented in Figure 5.16.

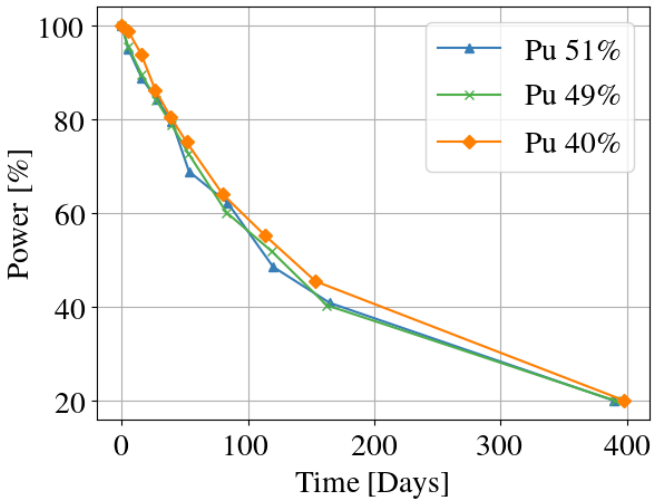


Figure 5.16 - Power evolution for different $UPuO_2$ configurations – HTR.

The variation of the U-235 enrichment and the consequent variation of Pu content does not lead to major variation of the power evolution, which was expected as the fissile content in all three configurations is similar. Further analysis could be made changing the Pu vector. In Annex V.4, a detailed study is presented to show the trends of the reactivity variation with different Pu vectors.

5.3.2. Conclusion on actinides insertion in HTR

The analysis of the insertion of actinides into HTR has been presented. The actinides that have been analysed are the Am, Np, Pu and Th. In the case of $UThO_2$ fuel, despite inserting a high content of thorium in the fuel, no large contribution in the reactivity evolution has been observed. For this reason, only the other three actinides have been analysed into further details.

The insertion of Am and Np increases the core performance with respect to the UO_2 core that is characterised by very low burn-up (1.2 GWd/t) and mean power (12%). The $UAmO_2$ case shows configurations that allow a significant improvement in terms of performance with a burn-up of 60 GWd/t and an average specific power from 44 to 60 %. However, these designs require high enriched uranium fuel (between 10 and 50.5%). The addition of neptunium shows improvement of performance, but even with a large neptunium content, the achievable burn-up seems limited around 20 GWd/t. The addition of classical plutonium vectors has a negligible effect. The separation of plutonium isotopes would be necessary to obtain a significant gain as it is observed with the neptunium or the americium.

In Figure 5.17, a comparison between the Am and Np cases is presented. The Am-1% and Np-5% cases are chosen as they show a similar U-235 enrichment (respectively 10% and 13%). Starting with the analysis of physical parameters, the reactivity feedback effects are comparable but the Am case shows lower reactivity swing. The reason is due to the reactivity evolution that is monotonically decreasing for the Np and increasing in a first period and then decreasing for the Am. Because of that, the burn-up reached in the Am case is twice as high as the one in the Np case. When it comes to average power, they both show a similar average value, although it should be reminded that the power profile overtime is not the same as it follows the same trend as the reactivity swing.

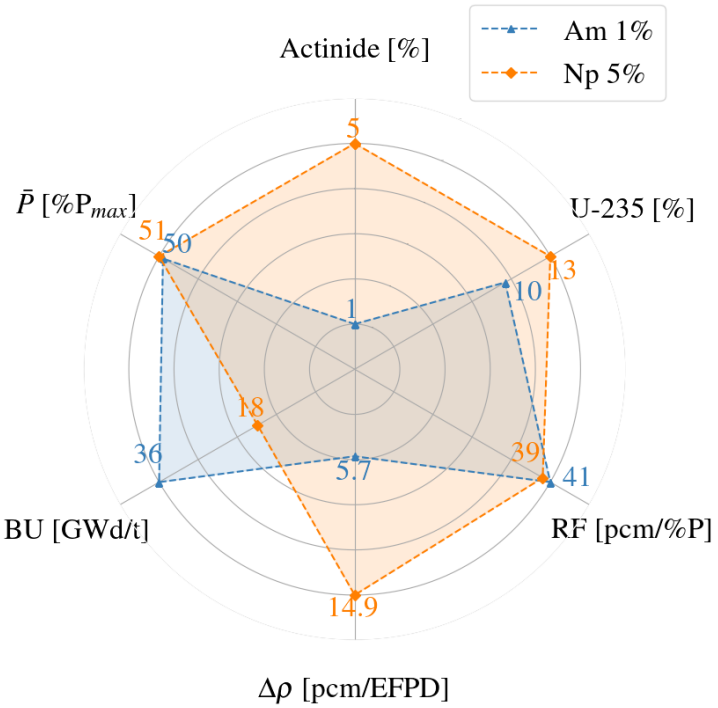


Figure 5.17 – Comparison of core performance loaded with $UamO_2$ and $UNpO_2$ – HTR.

5.3.3. Burnable absorbers in HTR core

Different burnable poisons (BP) are available for thermal spectrum cores and they are characterised by different kinetics of disappearance. The burnout rate of the burnable poison is dependent on the BP cross section and the neutron flux as described by the following equation:

$$BR = N\ \sigma_a(E)\ \Phi(E); \tag{5.2}$$

where: BR is the poison burnout rate [s^{-1} cm^{-3}]: N is the burnable poison atom density [cm^{-3}]; $\sigma_a(E)$ is the absorption cross section (dependent on the energy spectrum [b]; $\Phi(E)$ is the neutron flux, also energy-dependent [neutrons s^{-1} cm^{-2}].

The average absorption cross section (in thermal spectrum) of the major used burnable poisons is summed up in Table 5.13.

Table 5.13 – Mean absorption cross section of major burnable poisons [101].

Isotope	$\sigma_{a,thermal}$ [b]
B-10	3844
Cd-113	19969
Sm-149	40150
Eu-151	9185
Gd-155	60737
Gd-155	252912
Dy-164	2653

In this section, the insertion of burnable poison in HTR cores is analysed. At first, the insertion of boron has been considered as the most employed material as burnable poison. It has been chosen as reference material as it shows a slow kinetic of disappearance suitable to large time scale reactivity compensation.

In the literature studies, the addition of burnable poison in the core is widely studied, as a way to compensate the initial reactivity excess, but additional reactivity control systems are still required during the core lifetime. For this reason, larger content of poisons is considered in this work with respect to the HTR literature.

In Annex V.5, a study on different possible configurations of insertion of burnable poison is presented. Insertion in fuel or in TRISO external layer have been compared and no large difference is highlighted in core power evolution. In the following, only the configuration with the BP homogeneously inserted in the fuel is considered.

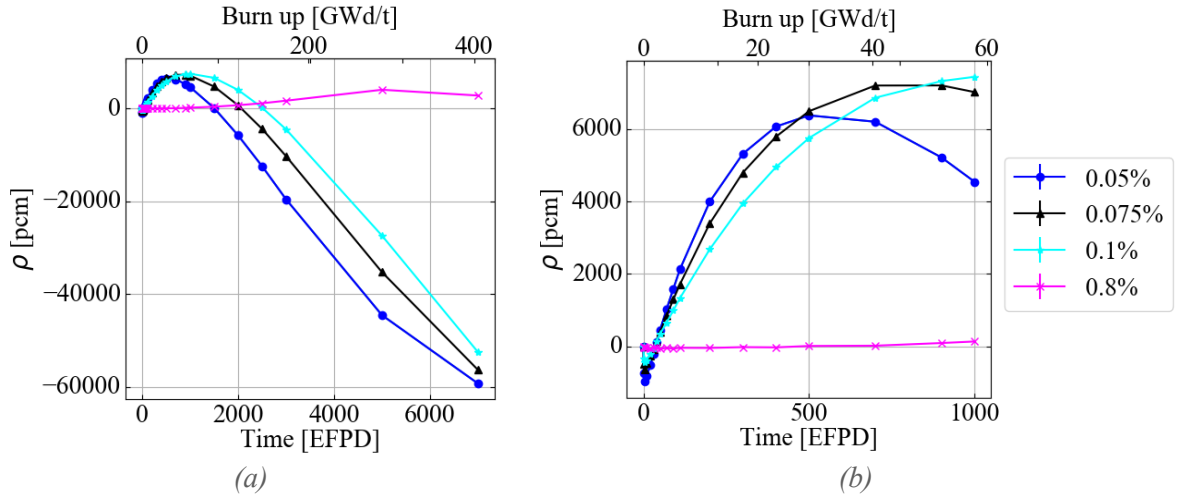
5.3.3.1. Parametric study on the boron insertion in HTR core

In next lines, various B-10 content inside the fuel has been studied. Based on literature and on preliminary results, presented in the Annex V.5, a range from 0.05 % to 0.80 % B-10 content inside the fuel kernel has been simulated. In Table 5.14, configurations are summed up with the respective U-235 enrichment necessary to ensure criticality at BOL.

Table 5.14 – Variation of the content of B-10 merged inside UO_2 fuel and relative U-235 enrichment.

B-10 content [%]	U-235 enrichment [%]
0.050	19.5
0.075	25.5
0.100	31.0
0.800	92.0

Figure 5.18 represents the reactivity evolution of the different configurations.

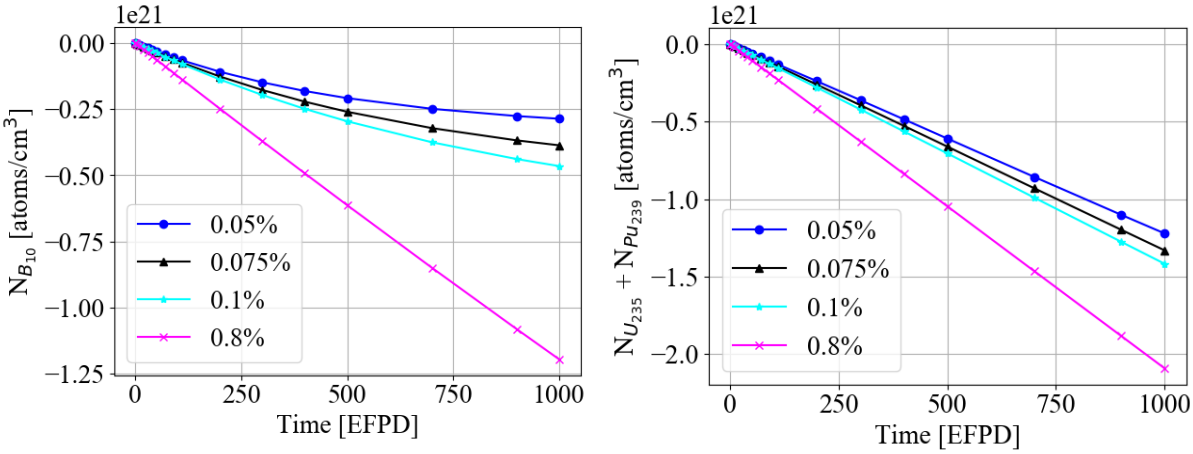


(a) *(b)*

Figure 5.18 – HTR reactivity evolution with boron in fuel with various contents of B-10 (a) – zoom on the first 1000 EFPD (b).

When the B-10 content increases, the U-235 enrichment increases and the peak of the reactivity curve seems to be displaced to the right of the graph. The initial Xe effect decreases when boron content is increased, due to the spectrum hardening (see Figure 5.18(b) where a zoom is made on the first 1000 EFPD).

The reason for the different reactivity evolution resides in the kinetic of boron consumption. As presented in Figure 5.19(a), the relative B-10 content shows a flatter slope for configurations up to 0.1 % of the B-10 content in fuel. On the other hand, when the B-10 content is increased, its evolution up to 1000 EFPD becomes linear. Figure 5.19(b), shows the time evolution of the sum of the main fissile isotopes in the core (U-235 and Pu-239). In all the cases, it is linear and sharper for configurations that need higher U-235 enrichment (thus configurations with higher B-10 content). The reactivity evolution is thus influenced primarily by the different kinetic of B-10 consumption according to the initial content.



(a) *(b)*

Figure 5.19 – Atomic content evolution relative to the initial value of B-10 (a) and U-235+Pu-239 fissile isotopes (b) in different B/fuel HTR configurations.

The configuration with 0.8% content of B-10 shows a reactivity evolution quite constant during the first 1000 EFPD and a peak around 5000 EFPD of about 4000 pcm. This configuration shows a flatter reactivity evolution but the needed U-235 enrichment is too high, making impossible to use this kind of fuel.

Nevertheless, other isotopes are proposed in the literature [97] [102] [103]. An analysis of an isotope with a slower kinetic of depletion could lead to flatter reactivity curves. According to Table 5.13, the dysprosium shows a slower kinetic and could be interesting in this application.

5.3.3.2. Parametric study on the dysprosium insertion in HTR core

A deeper analysis is made here for the Dy-164 insertion in HTR fuel.

Enrichment

The Dy content and relative U-235 enrichment are shown in Table 5.15.

Table 5.15 - Variation of the content of Dy merged in UO_2 fuel - HTR.

Configuration	Dy content [%]	U-235 enrichment [%]
Dy-0.4%	0.4	8
Dy-1.1%	1.1	15
Dy-2%	2	21.4

The progressive insertion of dysprosium, lead to the increase of the U-235 enrichment.

Reactivity feedbacks

The Table 5.16 shows the variation of the coefficients increasing the Dy content. Both the Doppler and graphite coefficient increases with the insertion of Dy.

Table 5.16 - Reactivity feedbacks for different Dy in UO_2 configurations - HTR.

Configuration	Doppler coefficient [pcm/K]	Graphite coefficient [pcm/K]
Dy-0.4%	-5.12	0.84
Dy-1.1%	-4.24	1.33
Dy-2%	-3.68	1.34

All the configurations are characterised by a global KGH coefficient that is negative and so the method can be applied ensuring the existence of the result, as explained in Section 2.2.3.3.

Burn-up reactivity swing

The reactivity swing is represented in Figure 5.20.

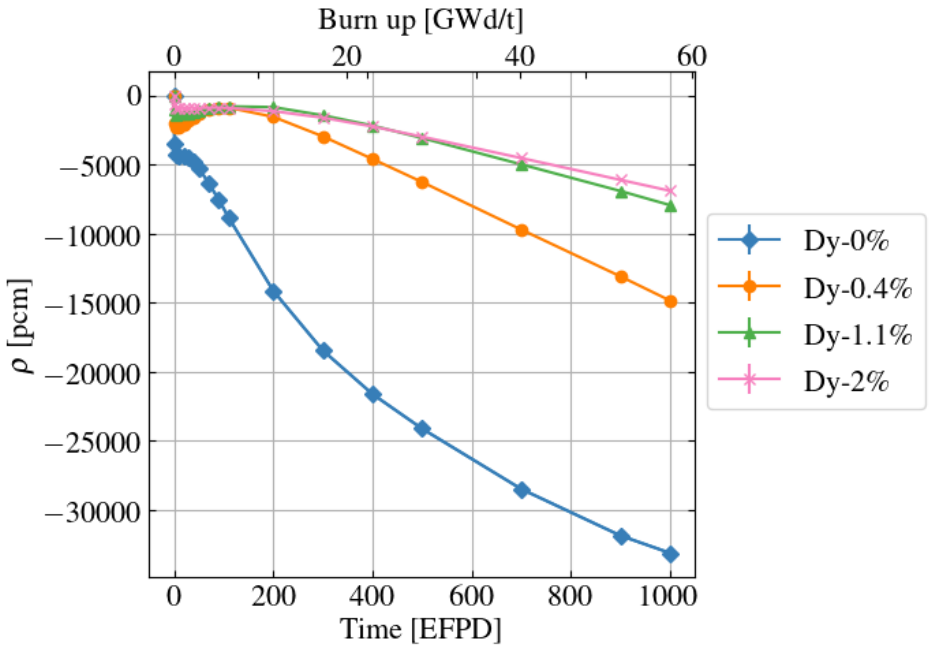


Figure 5.20 - Reactivity evolution according to the variation of Dy content in UO_2 fuel - HTR.

The configuration of Dy higher than 1.1% shows a flatter reactivity with a lower Xe initial effect.

Power evolution

The effect on the power evolution is shown in Figure 5.21.

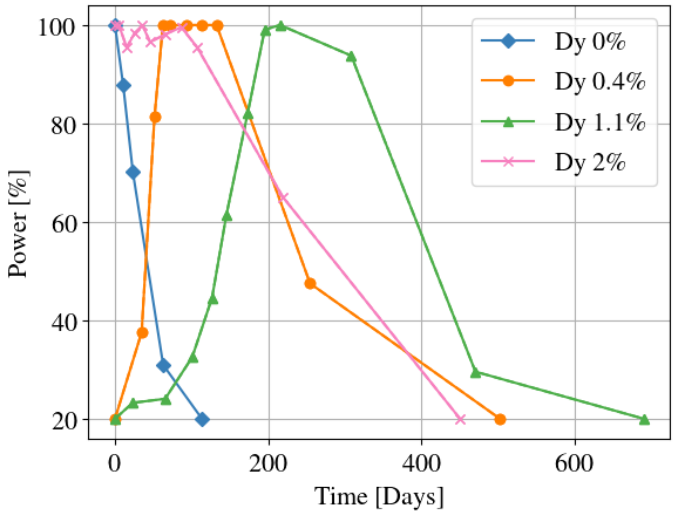


Figure 5.21 - Power evolution for different Dy in UO_2 configurations – HTR.

The case Dy-0% shows a monotonically decreasing power. On the other hand, for Dy content between 0.4% and 1.1%, the reactivity swing shows an increase and then a decrease, so the core has to be started-up at lower values with respect to the nominal one. Furthermore, the case Dy-0.4% need an active control for the compensation of a reactivity excess. Finally, the case Dy-2% shows an initial flat power evolution. The fluctuations in the graph are due to the uncertainties in the neutronic simulations, but they are considered acceptable for this level of analysis.

The comparison between the different cases is summed up in Figure 5.22.

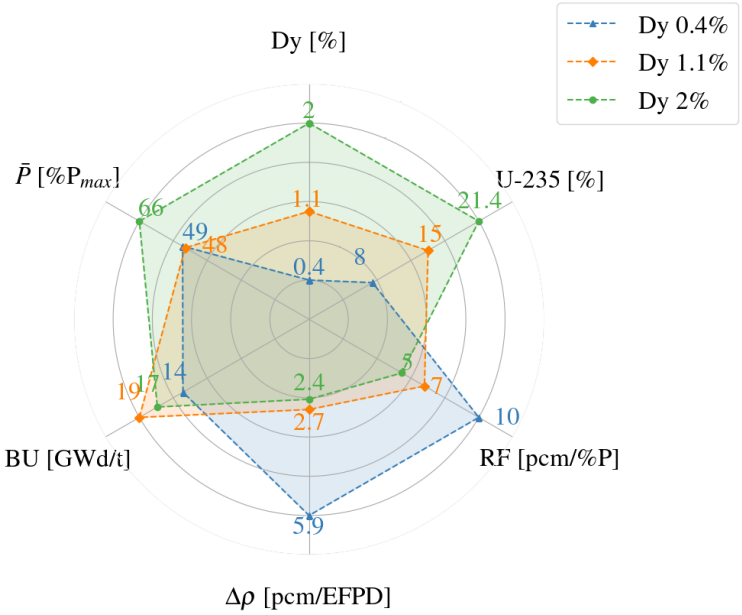


Figure 5.22 - Comparison of core performance loaded with Dy in UO_2 – HTR.

The results show an increasing U-235 enrichment for increasing Dy content, up to 21.4% for the configuration that lead to the flatter reactivity curve. The associated reactivity feedback integral effect decreases and simultaneously also the reactivity swing decreases. Anyway, the decrease of the reactivity swing prevails and lead to higher performance. The burn-up at EOL is increased between 14 and

19 GWd/t with the insertion of the poison up to 2%. Finally, for increasing Dy content, the mean power is increased between 48% and 66%. All the three configurations are characterised by an initial important Xe effect and thus requires initial control on the reactivity.

5.3.4. Conclusion on burnable absorbers insertion in HTR core

In conclusion, the boron has been inserted in the HTR, homogeneously mixed in the fuel. Results on the reactivity evolution show that, in order to reach a flat curve, an insertion of about 0.8% of B-10 is needed, but also leads to high U-235 enrichments (over 90%). Then, an isotope with slower disappearance kinetic has been analysed, such as the dysprosium. The insertion of Dy allows to reach higher burn-up (up to 19 GWd/t) and mean power of the order of 66%. The results highlight the improvement of the core performance with respect to the UO_2 core. It is indeed characterised by very low burn-up (1.2 GWd/t) and mean power (12%).

The same study is made on PWR core, with the insertion of the same actinides and burnable poison. In the next section, the results are presented and compared to the HTR, to highlight the advantages of each design for an autonomous operation: spectrum, temperature range, materials.

5.4. Autonomous PWR with actinides and burnable poisons

The same study of actinides and burnable poisons is made on PWR. First, the actinides are analysed. The Am, Np, Pu and Th are homogeneously inserted in the fuel in Section 5.4.1. The same reference contents have been considered as for the HTR study and then a sensitivity analysis is made varying these contents. Successively, the burnable poisons are inserted in the core in the configuration of absorber homogeneously distributed in the fuel, in Section 5.4.3. For all these cases, it is reminded that the study foresees: the research of the U-235 enrichment to ensure criticality at BOL; the computation of the associated reactivity feedback effects; the analysis of the burn-up reactivity swing and the power evolution calculation via the KGH method.

5.4.1. Actinides in PWR core

In this section, the different actinides are homogeneously inserted in fuel and a parametric study is performed, changing the content of the isotope.

5.4.1.1. Parametric study on the americium insertion in PWR fuel

The americium is inserted in the fuel. The material considered is made of Am-241 and Am-243 respectively 75% and 25% of mass content, as in the previous study on HTR.

Enrichment

The Table 5.17 shows the considered Am content and the associated U-235 enrichment.

Table 5.17 - Variation of the content of americium in PWR fuel.

Configuration	Am content [%]	U-235 enrichment [%]
Am-0% (reference)	0	1.05
Am-2%	2	8
Am-5.2%	5.2	16.5
Am-10%	10	24.5

As for HTR, U-235 content must be increased for higher content of Am in the fuel. This is due to the larger neutron captures due to the Am and the hardening of the neutron spectrum. The spectrum of the different configurations is shown in Figure 5.23.

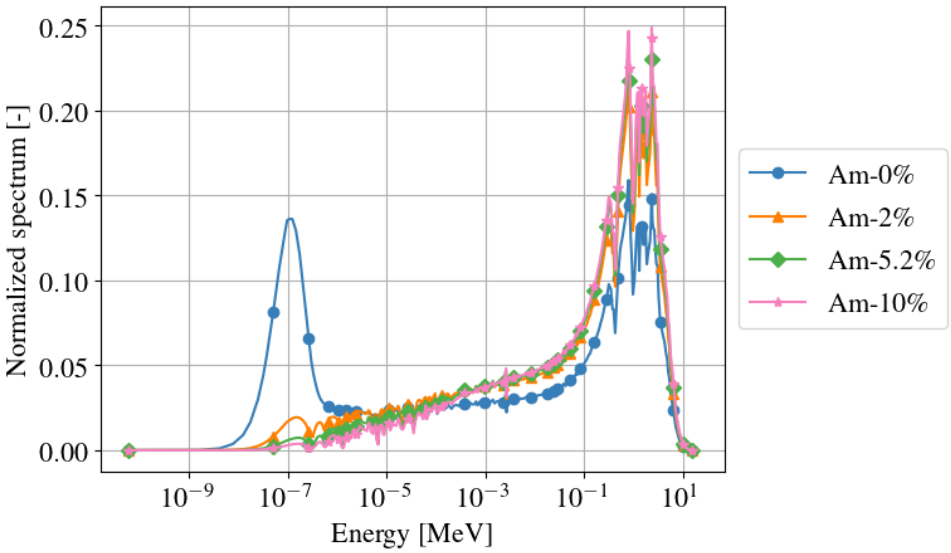
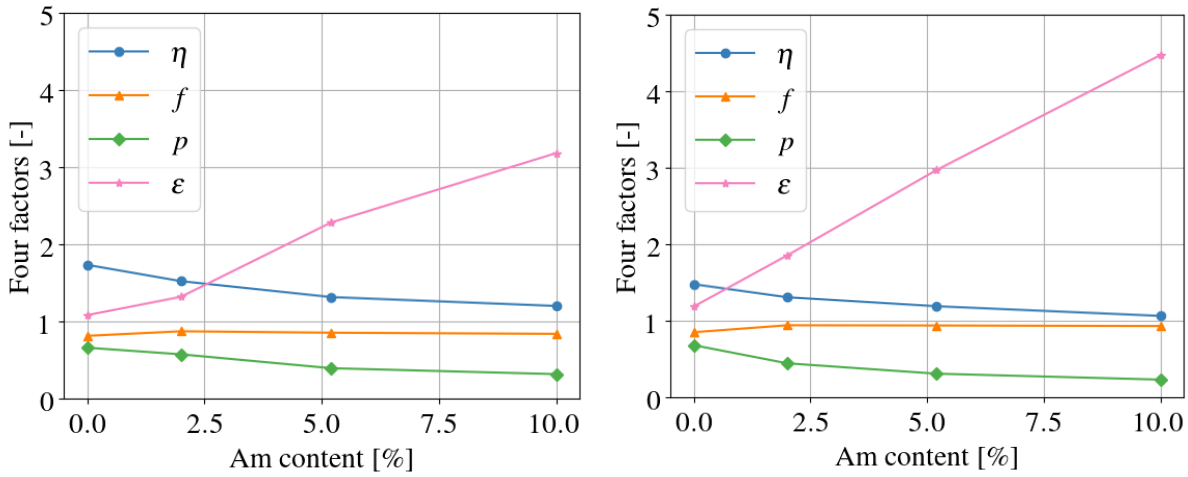


Figure 5.23 – Neutron spectrum in different $UAmO_2$ configurations - PWR.

It can be noticed that associated enrichments are lower, about the half, compared to the HTR. The four factors formula is shown in Figure 5.24, comparing HTR and PWR. These results have been obtained by Serpent calculations and are valid for thermal reactors, they are shown here to display the trend of the four factors. Anyway deeper analysis should be carried on for fast cores calculations.



(a - HTR) *(b - PWR)*

Figure 5.24 – Four factors formula for different UAmO2 configurations – HTR (a); PWR (b).

In both reactors, the importance of fast fission increases (ε), while the one of thermal fissions decreases (η). The PWR are characterised by a larger increasing importance of fast fission. In HTR, due to the heterogeneous fuel dispersion, the neutrons thermalisation is higher and so, for harder spectra (with Am), higher enrichment is required.

Reactivity feedbacks

The reactivity feedback coefficients of the previous configurations are computed. Table 5.18 sums up the Doppler coefficients.

Table 5.18 – Doppler coefficient for different UAmO2 configurations - PWR.

Configuration	Doppler coefficient [pcm/°C]
Am-0% (reference)	-2.43
Am-2%	-2.80
Am-5.2%	-2.29
Am-10%	-1.81

The addition of Am in fuel causes an initial increase of the Doppler effect and then a decrease. Adding americium causes a spectrum hardening and the insertion of Am corresponds to a decrease of the U-238 atoms, mainly responsible for the Doppler effect. These two effects are concurrent and lead to the Doppler initial increase and then decrease.

In Figure 5.25, the moderator coefficient has been analysed in function of temperature and Am content. Each value has been computed considering a linear interpolation between 10°C variation in coolant temperature (and corresponding density) with respect to the central value.

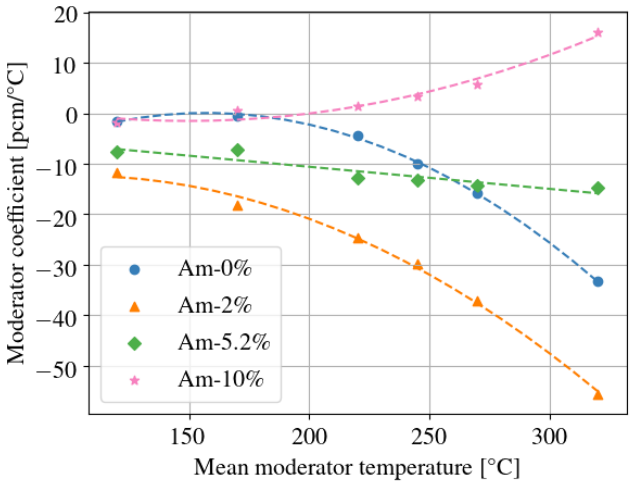


Figure 5.25 - Moderator coefficient for different Am contents depending on temperature – PWR.

For low Am contents, the moderator coefficient tends to decrease with temperature. Increasing the Am content, the coefficient tends to increase with temperatures, up to positive values for the case of Am-10%. For higher temperatures, the water expansion is larger. Furthermore, for larger Am contents, the spectrum is hardened and the moderation effect becomes less and less efficient.

As the Am-10% configuration shows a positive coefficient, the KGH method has been verified, according to the hypotheses made in Chapter 2, Section 2.2.3.3. The global coefficient, computed according to the present hypothesis is negative and so the KGH equation can be applied, ensuring the existence of the results.

Now, following the hypothesis of constant core inlet temperature set in Section 3.6, the attention is focused on the coefficient at 320°C. Indeed, the core inlet temperature considered for the PWR is 290°C, so 320°C is considered a suitable value to compute the coefficient corresponding to the mean core temperature. Figure 5.26 shows the moderator coefficient trend according to the Am content and the associated U-235 enrichment.

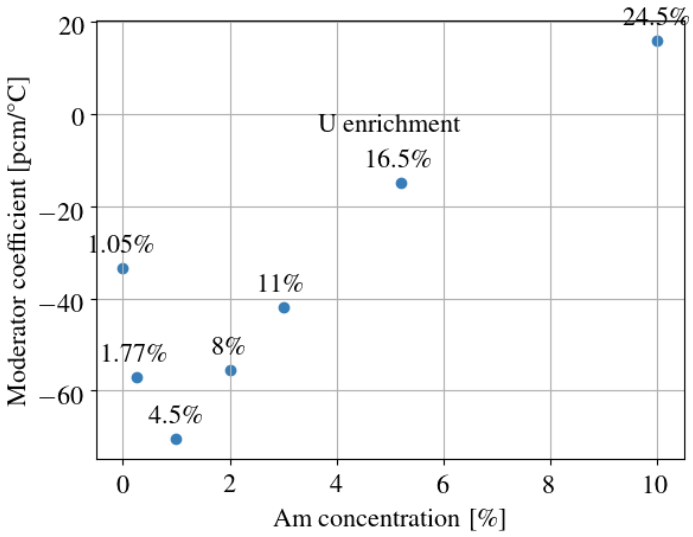


Figure 5.26 - Moderator coefficient for different Am contents at 320°C – PWR.

This variation of the moderator coefficient is related to both effects of increasing the U-235 content and the Am-241 content. The η factor contribution in case of water temperature variation (amplified by the p factor variation) is the main contributor when reducing Am content. As soon as the Am content reaches 2% (and U-235 4%), the ε factor becomes the main contributor with an increase of the fast fissions in the case of reduction of the moderation. More details are available in Annex V.6.

The increase (in absolute value) of the moderator coefficient between 0% and 1% of americium is linked to the negative effect of the η and p factors. However, their negative contribution is counterbalanced by the fast fission factor increase with more Am.

Burn-up reactivity swing

The different configurations of $UAmO_2$ are analysed in terms of reactivity evolution with burn-up, in Figure 5.27.

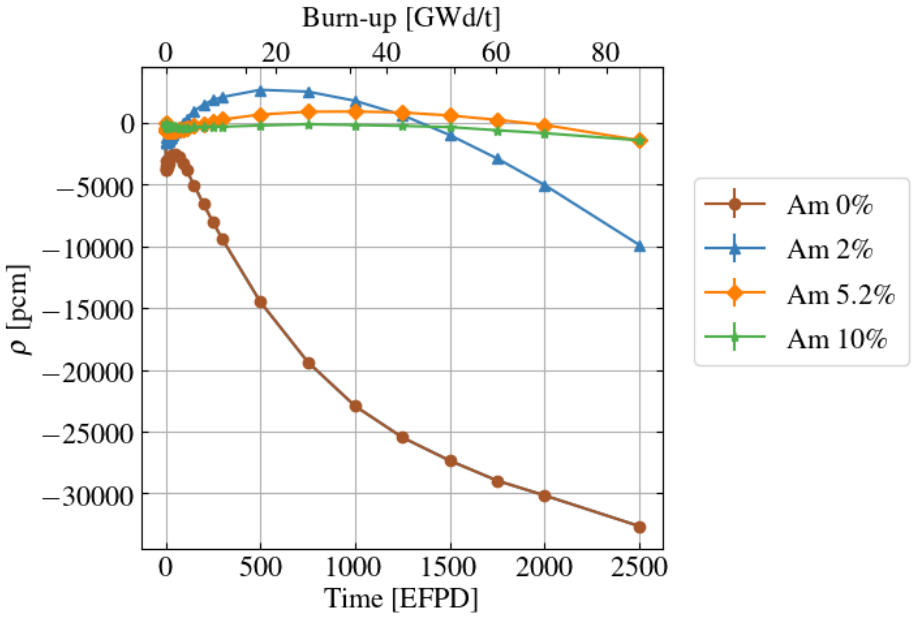


Figure 5.27 – Burn-up reactivity swing for different $UAmO_2$ configurations - PWR.

The insertion of Am reduces the initial Xe effect due to the hardening of the spectrum and allows to decrease the reactivity swing with irradiation. The physics of the Am consumption is the same as the HTR. The Am-10% configuration is the one that allows a flatter reactivity due to the concurrent effect of Pu-239 built-up (that increases the generation rate), the U-235 consumption (that decreases the generation rate) and the Am-241 depletion (that decreases the capture rate).

Power evolution

The concurrent contribution of the burn-up reactivity evolution and the reactivity feedbacks are computed via the KGH method. Figure 5.28 shows the evolution of the power according to the different configurations.

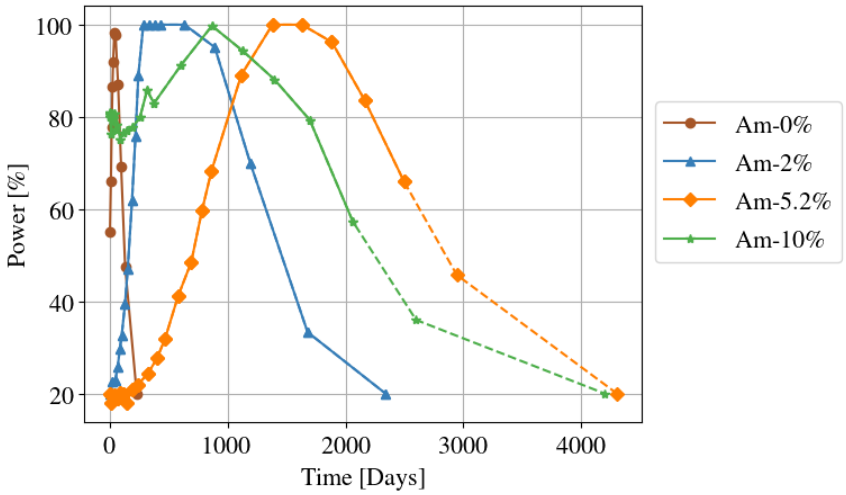


Figure 5.28 – Power evolution for different $UAmO_2$ configurations - PWR.

The initial Xe effect is supposed actively controlled at the beginning of life. It is then not represented in the core autonomous behaviour. The core is started up at a fraction of the nominal power in order to reach the peak during operation corresponding to the design power. In the cases Am-2% and Am-5.2% the reactivity increase is larger than the possible power excursion and so even starting up at low power, the peak would overcome the design value. As in the HTR case, in this interval, the power is considered actively controlled and limited at its maximum value. In the case of Am-2%, excess reactivity to be controlled over 350 days is around 1700 pcm. In the case Am-5.2%, the excess of reactivity is around 250 pcm, over 250 days.

The power evolution of the three cases is characterised by the same trend as the reactivity swing. For low Am contents, the core reaches 20% of the nominal power for burn-ups lower that 60 GWd/t. For higher Am content, this burn-up is reached for larger powers (indicated in the figure with a solid line up to 60GWd/t and dashed after).

The results of the comparison of the different cases are summed up with a radar graph, in Figure 5.29. The reference values for the case of core loaded with UO_2 is summed up in Table 5.19.

Table 5.19 - Comparative parameter of autonomous UO_2 core – PWR.

Parameter	Value
U-235 [%]	1.05
RF [pcm/%P_n]	23.4
$\Delta\rho$ [pcm/EFPD]	28.8
BU [GWd/t]	4.6
$\bar{P}$ [%P_{max}]	60

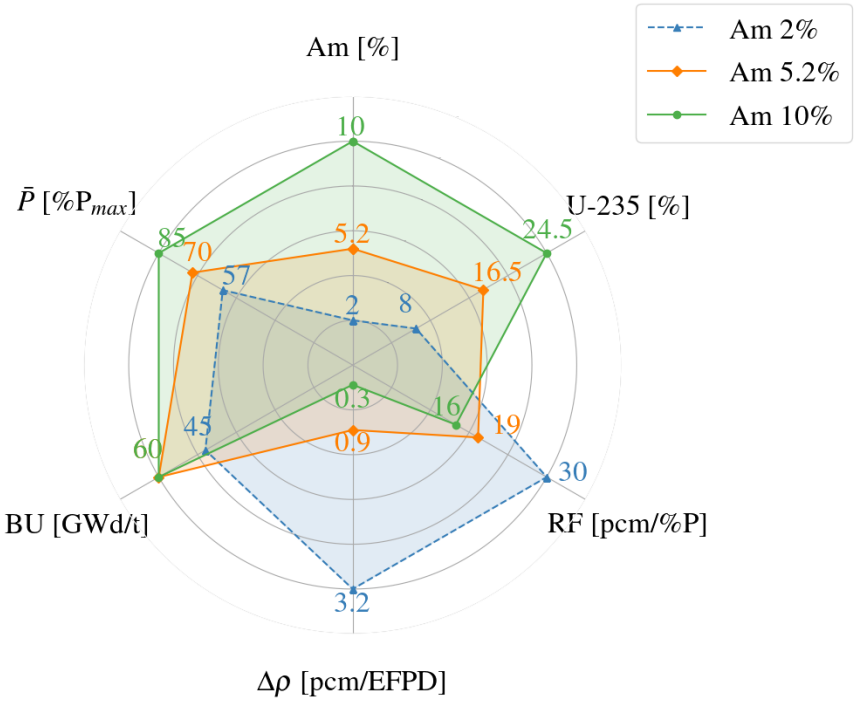


Figure 5.29 - Sum-up of the core performance for different $UAmO_2$ configurations – PWR.

First we focus on the core performance, looking at the axes of the mean power ($\bar{P}$) and the burn-up at EOL (BU). For lower Am values, the EOL happens when reaching 20% of the nominal power (for the case Am-2%). When increasing the Am content, the burn-up reaches the value of 60 GWd/t before the power reaching 20% of the nominal value. When increasing the Am content, the mean power is increased until reaching high values (85% in the Am-10% case). There is then a strong relation between performance and Am content.

The second point to be noticed concerns the physical analysis, shown on the axis of the reactivity feedbacks (RF) and the reactivity swing ($\Delta\rho$). When increasing the americium content from 2% to 10%, the associated reactivity feedback integral effect decreases by 47%, while the reactivity swing decreases by 91%. In addition, increasing the americium content leads to a decrease of the Xe effect because of spectrum hardening. For the configurations 5.2% and 10% (solid line), there is no initial reactivity loss and the reactor can be considered completely autonomous, while for low americium contents (dashed line), an initial control is needed for the initial reactivity loss due to the Xe effect.

Finally, the insertion of americium requires an increase of U-235 enrichment up to 24% for the configuration Am-10%.

5.4.1.2. Parametric study on the neptunium insertion in PWR fuel

The same study is made inserting Np-237 in fuel.

Enrichment

The needed enrichment for criticality at BOL has been calculated and showed in Table 5.20. The Np contents chosen are the same as for the HTR study.

Table 5.20 - Variation of the content of neptunium in PWR fuel.

Configuration	Np content [%]	U-235 enrichment [%]
Np-0% (reference)	0	1.05
Np-1%	1	1.87
Np-5%	5	6.8
Np-16.3%	16.3	21
Np-40%	40	49

As for the americium case, the insertion of neptunium hardens the spectrum (see Figure 5.30) and thus higher U-235 enrichments are required. Even in this case, they are lower with respect to the ones required in HTR, for the same reason as explained before, in Section 5.4.1.1.

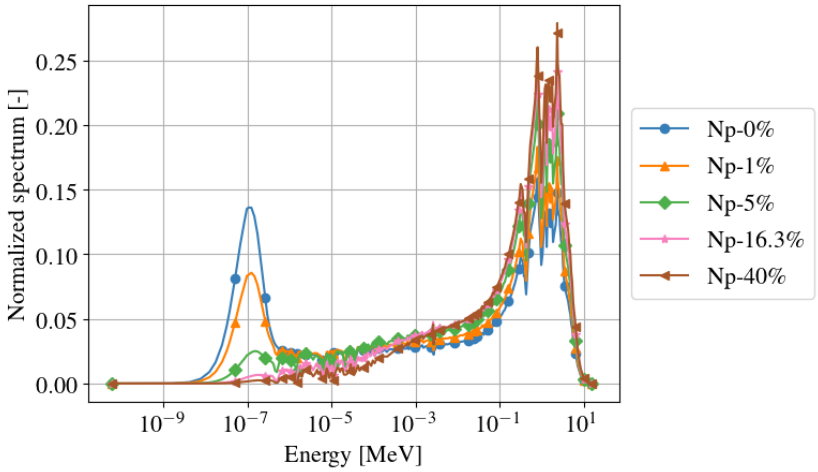


Figure 5.30 - Neutron spectrum in different $UNpO_2$ configurations - PWR.

Reactivity feedbacks

The Doppler coefficients of different configurations are shown in Table 5.21.

Table 5.21 - Doppler coefficient for different $UNpO_2$ configurations - PWR.

Configuration	Doppler coefficient [pcm/°C]
Np-0% (reference)	-2.43
Np-1%	-2.70
Np-5%	-2.64
Np-16.3%	-2.46
Np-40%	-1.75

The variation of the Doppler coefficient is the same as the case of Am. The concurrent effects of an increase of capture resonances and an U-238 decrease make the coefficient increase and then decrease.

The same study, as in the Am case, is made on the moderator coefficient dependent on the temperature, shown in Figure 5.31.

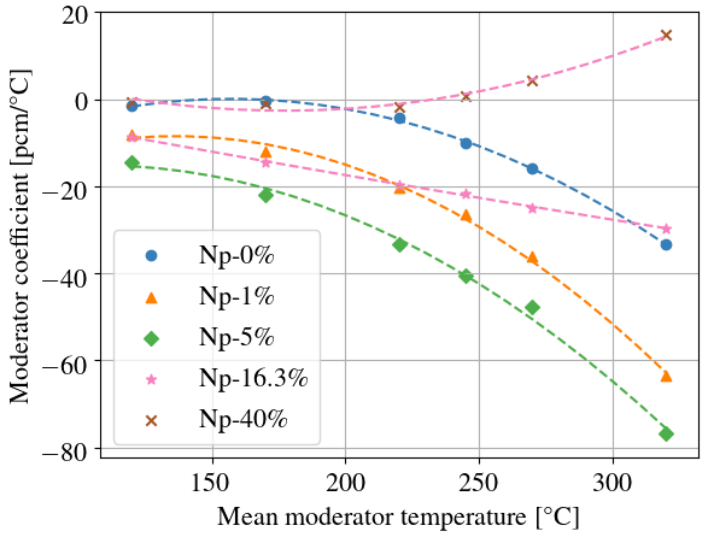


Figure 5.31 - Moderator coefficient for different Np contents depending on temperature – PWR.

The physics of the core with increasing Np content is the same as the Am case. The moderator coefficient decreases with temperature for low Np content and increases for higher ones. The coefficient at nominal temperature (320°C) decreases for lower Np content and increases after 5% Np contents. The case of Np-40%, characterised by a positive value, has been verified in the application of KGH, as explained in Chapter 2, Section 2.2.3.3 and the existence of the solution is guaranteed by a total negative feedbacks coefficient.

Burn-up reactivity swing

The previous configurations are analysed in evolution. The burn-up reactivity swing of the different cases is shown in Figure 5.32.

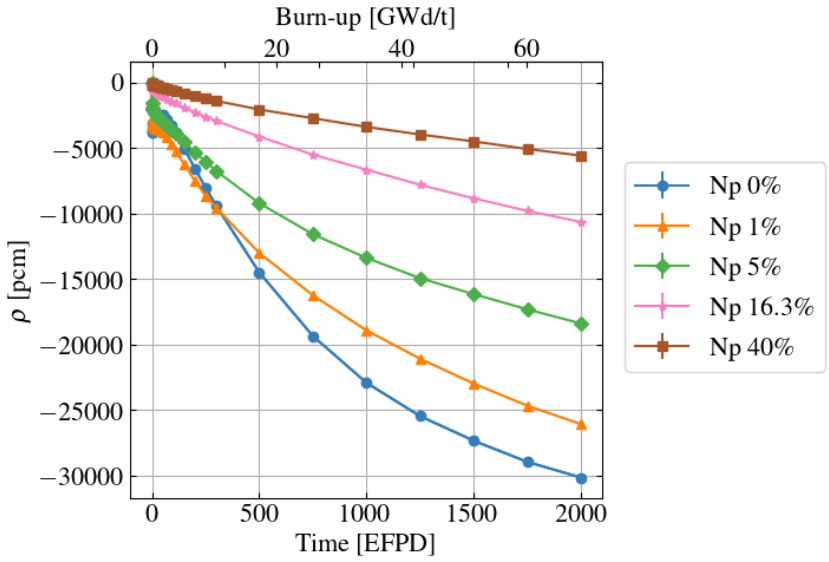


Figure 5.32 - Burn-up reactivity swing for different $UNpO_2$ configurations - PWR.

The results show the same trend as for the HTR, increasing the Np content decreases the Xe effect and reduces the reactivity swing up to the configuration of Np-40%. Higher values of Np content have not been explored as the Np-40% corresponds already to very high U-235 enrichment.

Power evolution

The effect of reactivity swing and reactivity feedbacks have been analysed with the KGH method. The power evolution is shown in Figure 5.33.

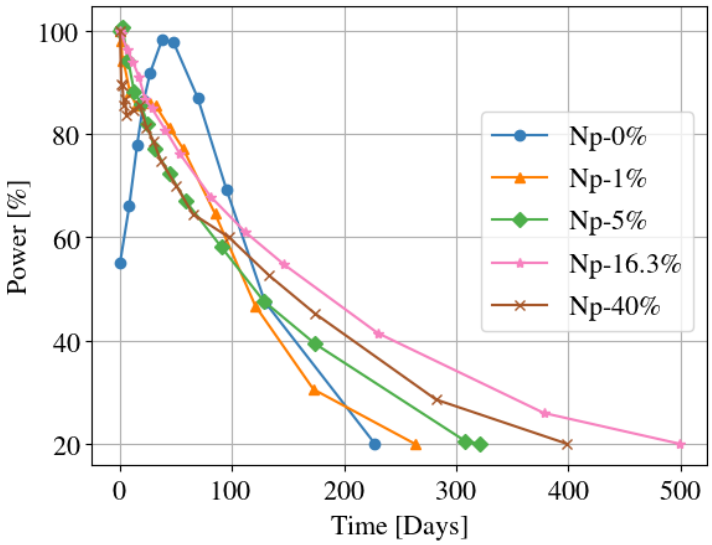


Figure 5.33 - Power evolution for different UNpO2 configurations - PWR.

For increasing Np content, the simultaneous effects of the reactivity swing reduction and reactivity feedbacks coefficients decreases, make the power evolve with a similar behaviour for all the cases.

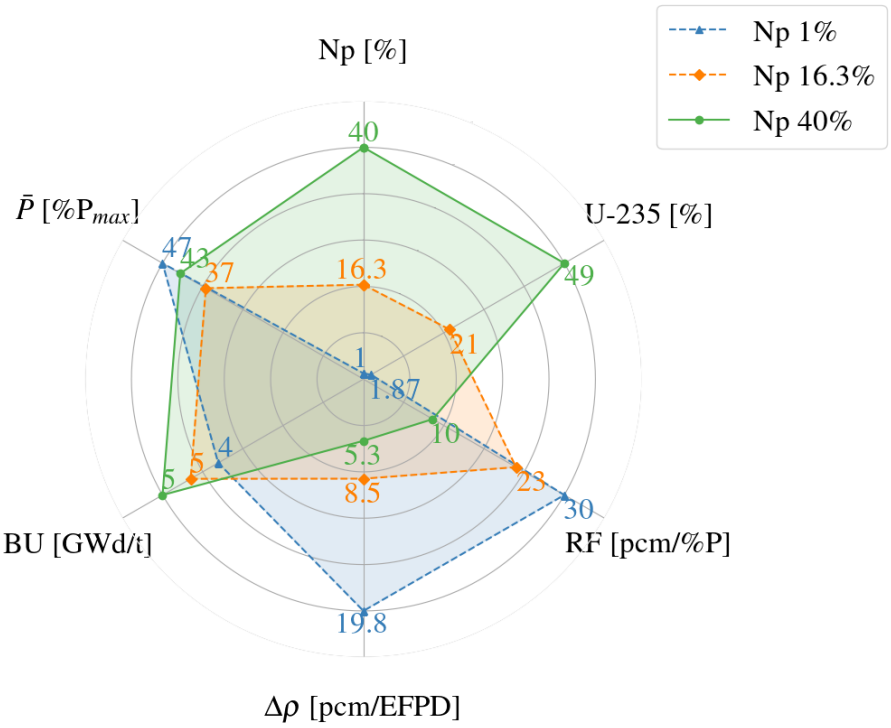


Figure 5.34 - Sum-up of the core performance for different $UNpO_2$ configurations – PWR.

Figure 5.34 sums up of the core performance for different $UNpO_2$ configurations. First we focus on the core performance, looking at the axes of the mean power ($\bar{P}$) and the burn-up at EOL (BU). For all different Np contents, the average power is of the same order of magnitude (between 37% and 47% of the nominal power). Moreover, the maximum achievable burn-up is about 5 GWd/t for all configurations, which means that neptunium content does not impact the burn-up significantly. As a reminder, the core is shutdown when its power reaches 20% of the nominal value. Here, the power decreases rapidly towards 20% of its nominal value, which explains why the burn-up is low.

The second point to be noticed concerns the physical analysis, shown on the axis of the reactivity feedbacks (RF) and the reactivity swing ($\Delta\rho$). When increasing the neptunium content from 1% to 40%, the reactivity loss decreases by 73% while the reactivity feedbacks decrease by 67%. These values quite proportionally, so the power evolution is similar and so the performance in terms of burn-up.

Only in the case Np-40%, the Xe effect is annulled, anyway, this case has a U-235 enrichment that is too high, making this case not viable.

5.4.1.3. Parametric study on the plutonium insertion in PWR fuel

The study has been pursued with $UPuO_2$ fuel. The composition of the Pu vector has been chosen as the one reference for the HTR study, named MOX-2035 (see Table 5.2).

Enrichment

Table 5.22 and Figure 5.35 shows the U-235 enrichments and relative neutron spectra for different Pu content in fuel. As in the HTR study, the plutonium has been inserted in a configuration with depleted uranium (configuration Pu-1.7%) and then the U-235 enrichment has been varied.

Table 5.22 - Variation of the content of plutonium in PWR fuel.

Configuration	Pu content [%]	U-235 enrichment [%]
Pu-0% (reference)	0	1.05
Pu-1.1%	1.1	0.5
Pu-1.7%	1.7	0.25

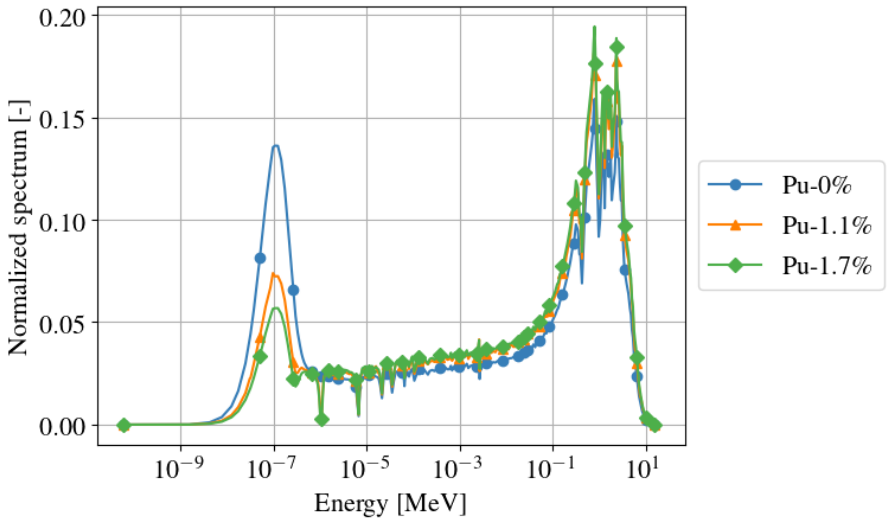


Figure 5.35 - Neutron spectrum in different $UPuO_2$ configurations - PWR.

Unlike the HTR case, the insertion of plutonium in depleted UO_2 does not need high Pu content to ensure criticality. In the HTR, the moderator capacity of the graphite is lower than the hydrogen one. The Pu-240 has a large absorption resonances that, in HTR, absorbs all the neutrons before they reach thermal energies. For example, in Annex V.4, different theoretical Pu vectors are tested in the HTR configuration and the one with only PU-8 and Pu-9 shows much lower U-235 enrichments.

Reactivity feedbacks

The reactivity feedback coefficients, relative to the previous configurations are presented in Table 5.23 and Table 5.24. Here, the moderator coefficient has been analysed directly at 320°C.

Table 5.23 - Doppler coefficient for different $UPuO_2$ configurations - PWR.

Configuration	Doppler coefficient [pcm/°C]
Pu-0% (reference)	-2.43
Pu-1.1%	-2.97
Pu-1.7%	-2.93

Table 5.24 - Moderator coefficient for different $UPuO_2$ configurations at 320°C - PWR.

Configuration	Moderator coefficient [pcm/°C]
Pu-0% (reference)	-33.31
Pu-1.1%	-66.19
Pu-1.7%	-74.66

Burn-up reactivity swing

The reactivity swing associated with the analysed configuration is shown in Figure 5.36.

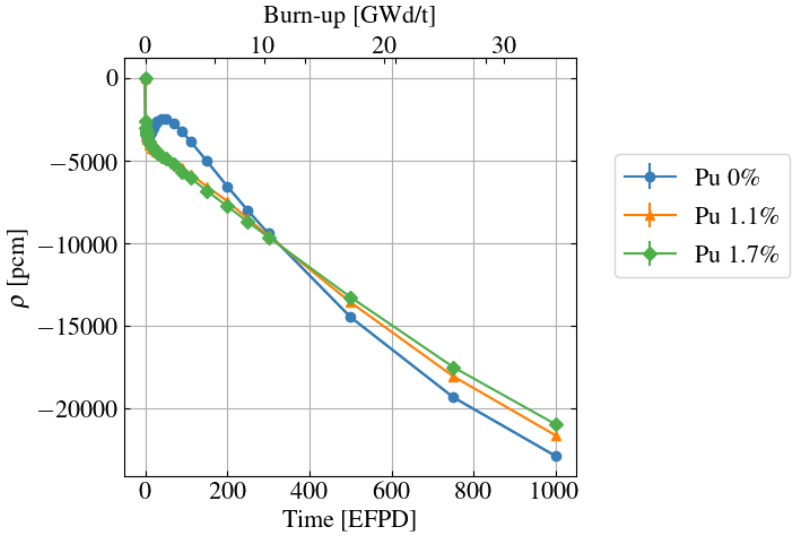


Figure 5.36 - Burn-up reactivity swing for different $UPuO_2$ configurations - PWR.

The insertion of Pu in fuel shows about the same Xe initial reactivity loss. On the other hand, the reactivity increase in the first days is not any more present where Pu is inserted. It was due (for low U-235 enrichments) to the large quantity of U-238, as explained in Annex V.3.

Power evolution

The associated effects of reactivity feedbacks and burn-up reactivity swing are analysed with the KGH method and Figure 5.37 shows the evolution of the associated reactor power.

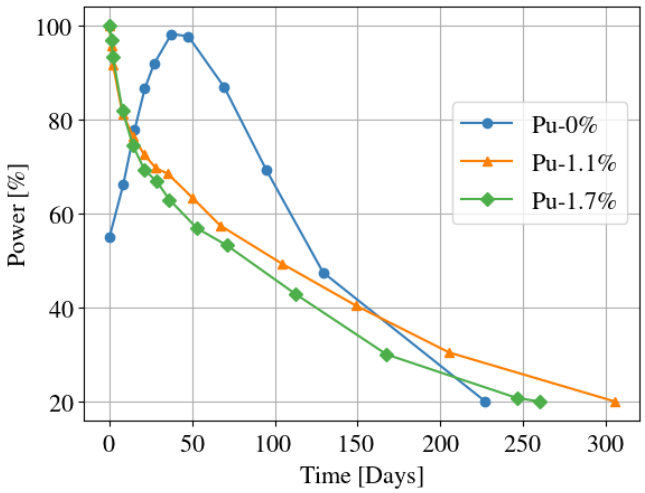


Figure 5.37 - Power evolution for different $UPuO_2$ configurations - PWR.

The insertion of Pu in the core eliminates the initial power increase. Anyway, the power is rapidly decreasing, reaching 50% of the nominal power within a period of about 100 days. This configuration is similar to the Np case and the core performance is comparable.

5.4.1.4. Parametric study on the thorium insertion in PWR fuel

The Th-232 is analysed with the same content as the HTR study.

Enrichment

The enrichment of the uranium is shown in Table 5.25 and the neutron spectrum in Figure 5.38 in comparison with the UO_2 case.

Table 5.25 - Variation of the content of thorium in PWR fuel.

Configuration	Th content [%]	U-235 enrichment [%]
Th-0% (reference)	0	1.05
Th-74% [99]	74	8.5

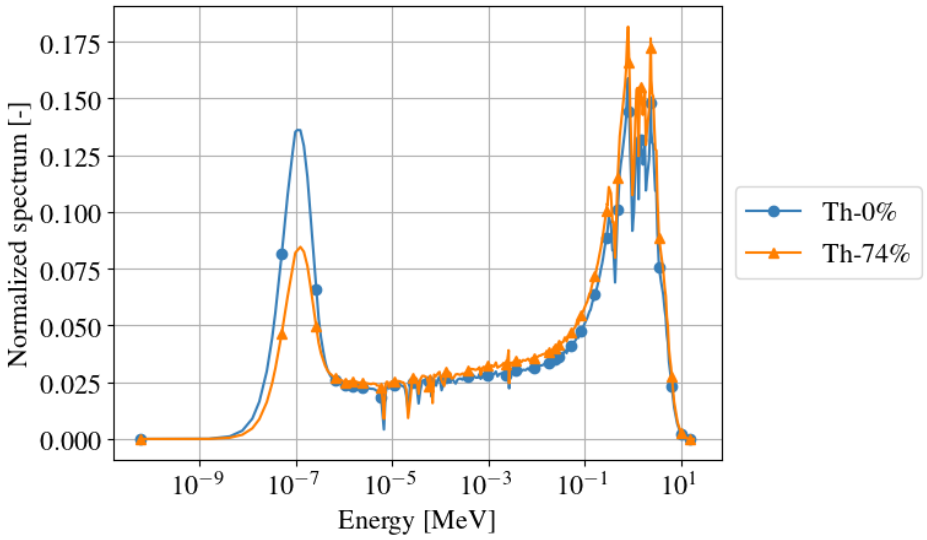


Figure 5.38 - Neutron spectrum in different $UThO_2$ configurations - PWR.

The needed U-235 enrichment is considerably lower with respect to the case of HTR.

Reactivity feedbacks

The associated reactivity feedback coefficients are shown in Table 5.26 and Table 5.27, considering the moderator coefficient at the nominal temperature of 320°C.

Table 5.26 - Doppler coefficient for different $UThO_2$ configurations - PWR.

Configuration	Doppler coefficient [pcm/°C]
Th-0% (reference)	-2.43
Th-74%	-4.09

Table 5.27 - Moderator coefficient for different $UThO_2$ configurations at 320°C - PWR.

Configuration	Moderator coefficient [pcm/°C]
Th-0% (reference)	-33.31
Th-74%	-54.65

Burn-up reactivity swing

The reactivity evolution is presented in Figure 5.39.

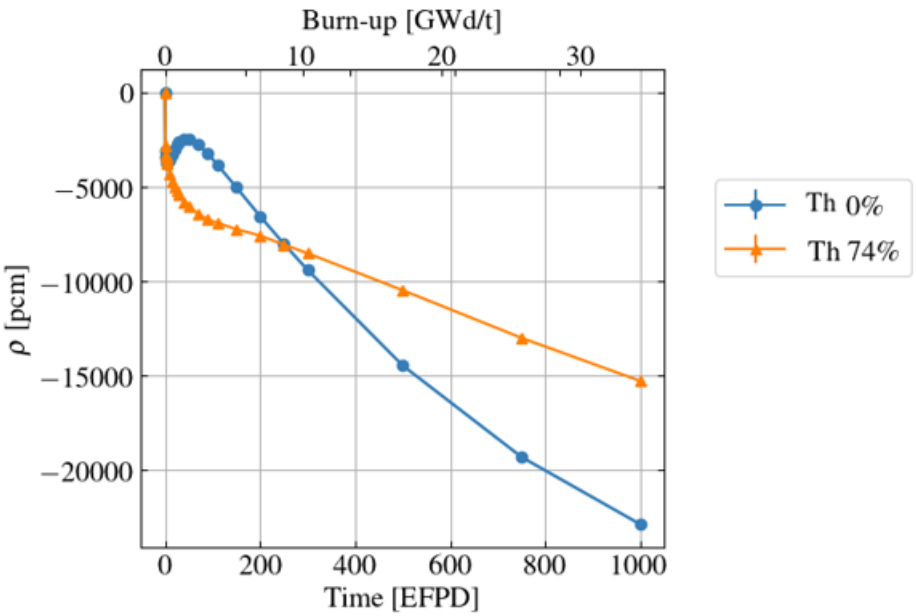


Figure 5.39 - Reactivity evolution for $UThO_2$ configuration - PWR.

Power evolution

The power evolution is shown in Figure 5.40.

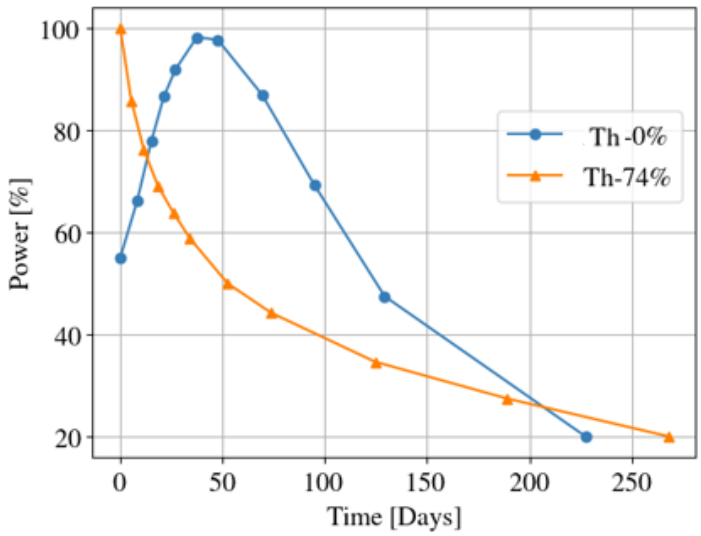


Figure 5.40 - Power evolution for different $UThO_2$ configurations - PWR.

The Th configuration shows the same trend as the Pu configuration but an enhanced power decrease. Half of the nominal value is reached after about 50 days. The performance of Th configuration is at first approach comparable to the Pu one and the Np one. Anyway, in this case, the Th content is already very elevated and its increase is limited, as the improvement of the reactivity swing.

5.4.2. Conclusions on actinides insertion in PWR core

The insertion of Am an Np increases the core performance with respect to the UO_2 core that is characterised by very low burn-up (4.6 GWd/t) and mean power (60%). The $UAmO_2$ case shows configurations that allow a significant improvement in terms of performance with a burn-up of 60 GWd/t and an average specific power from 57 to 85 %. The addition of neptunium shows improvement of obtained performance, but even with a large neptunium content, the achievable burn-up seems limited around 5 GWd/t. The addition of classical plutonium vectors seems to have a negligible effect. The separation of plutonium isotopes would be necessary to obtain a significant gain as it is observed with the neptunium or the americium.

The Np, Pu and Th configurations show similar trends in power evolution. The Np case has been considered into details and here compared to the Am case. In Figure 5.41, Am-10% and Np-16.3% cases are compared as they both have a similar U-235 enrichment.

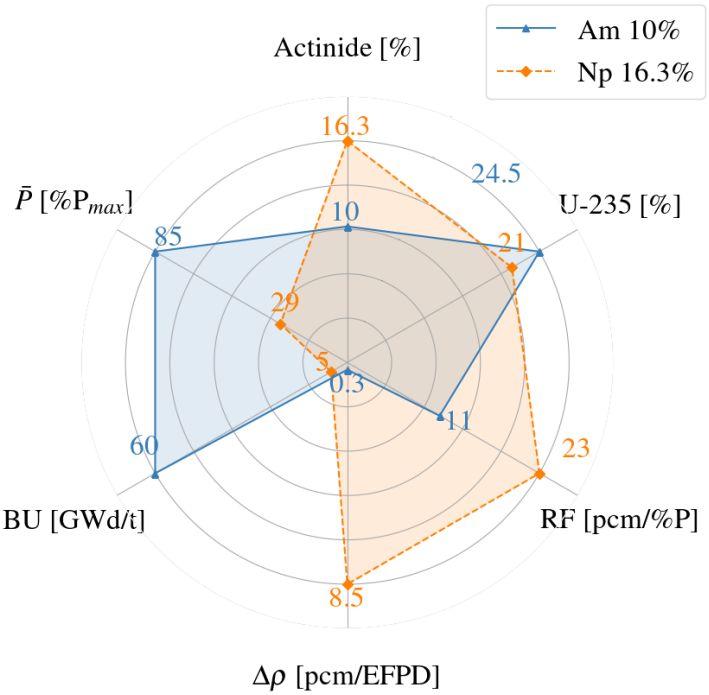


Figure 5.41 - Comparison of core performance loaded with $UamO_2$ and $UNpO_2$ – PWR.

Starting with the analysis of physical parameters, the reactivity feedbacks are two times higher in the case of neptunium insertion than in the case of americium insertion. However, the Am-10% case shows an average reactivity swing that is almost flat, whereas the one of the Np-16.3% case decreases monotonically. For this reason, the Am-10% case reaches the targeted burn-up of 60 GWd/t with a high average power (85%). On the other hand, the Np-16.3% case shows a very low burn-up of 5 GWd/t and a low average power of 29%. In this situation, the reduction of reactivity swing is the best available lever to maximize the performance.

To complete this analysis, it is recalled that in the Am-10% configuration, the initial reactivity loss due to xenon effect is reduced (lower than 500 pcm), so that the core could be considered here as completely autonomous. On the other hand, the Np-16.3% configuration has an initial reactivity loss that would need an initial active control.

5.4.3. Burnable absorbers in PWR core

In this section, the insertion of burnable poison is presented, analogous to the HTR study. The study starts from boron insertion and, for the same reason than in HTR (slower kinetics), also the insertion of dysprosium is analysed.

5.4.3.1. Parametric study on the boron insertion in PWR fuel

The burnable poison is studied in comparison with the HTR in the fuel configuration. So, the boron is inserted homogeneously in the fuel and the content of B-10 is varied.

Enrichment

The U-235 enrichment for criticality at BOL is shown in Table 5.28, with the associated neutron spectrum in Figure 5.42.

Table 5.28 - Variation of the content of boron in PWR fuel.

Configuration	B-10 content [%]	U-235 enrichment [%]
B_{10}-0% (reference)	0.00	1.05
B_{10}-0.02%	0.02	7.10
B_{10}-0.10%	0.10	19.20

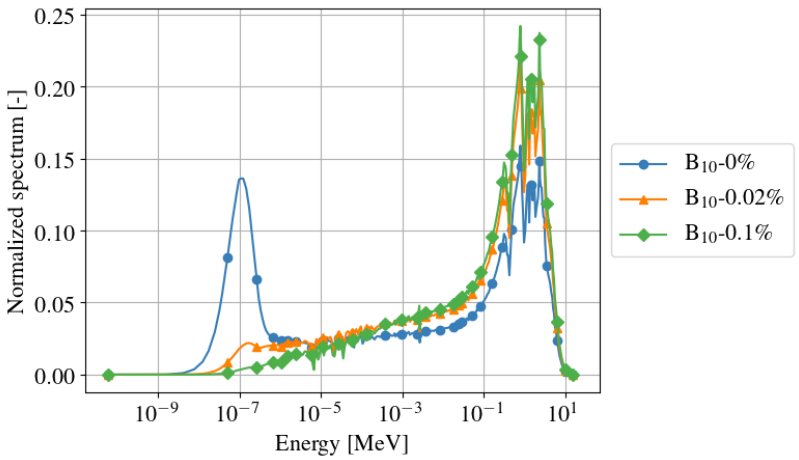


Figure 5.42 - Neutron spectrum in different UO_2 with B configurations - PWR.

Reactivity feedbacks

The Doppler coefficients relative to the previous configurations are summed up in Table 5.29.

Table 5.29 - Doppler coefficient for different UO_2 with B configurations – PWR.

Configuration	Doppler coefficient [pcm/°C]
B_{10}-0% (reference)	-2.43
B_{10}-0.02%	-1.80
B_{10}-0.1%	-0.91

On the other hand, the moderator coefficients, computed for 320°C are shown in Table 5.30.

Table 5.30 - Moderator coefficient for different UO_2 with B configurations at 320°C - PWR.

Configuration	Moderator coefficient [pcm/°C]
B_{10}-0% (reference)	-33.31
B_{10}-0.02%	-37.01
B_{10}-0.1%	10.64

The global coefficient of the KGH method (see Chapter 2, Section 2.2.3.3) ensures the existence of a solution for the first two cases but not for the configuration of B_{10}-0.1%, in which the overall reactivity feedbacks coefficient is positive. For these reasons, other configurations with higher B-10 contents are not explored.

Burn-up reactivity swing

The reactivity evolution of the analysed configurations is shown in Figure 5.43.

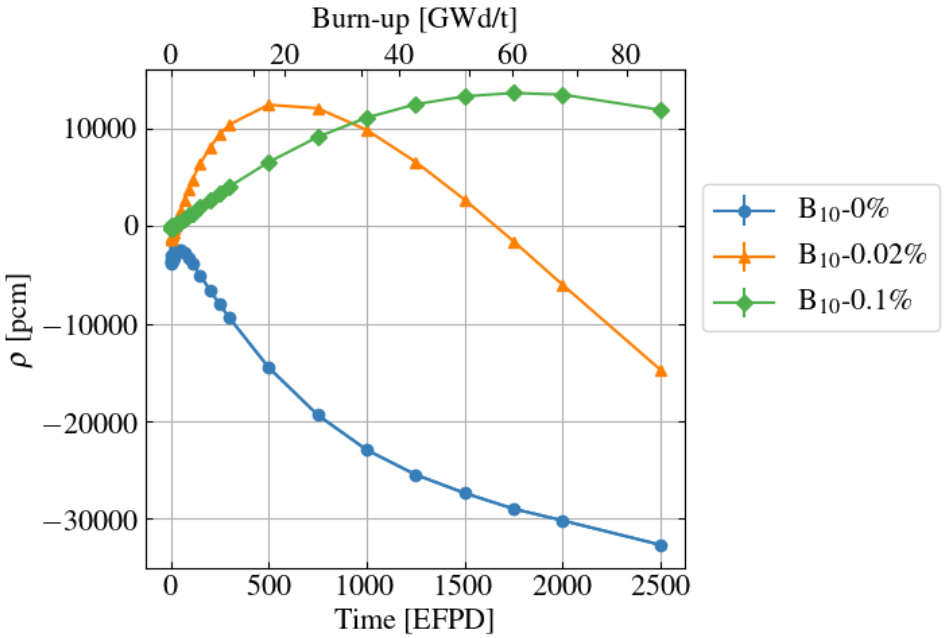


Figure 5.43 - Burn-up reactivity swing for different UO_2 with B configurations - PWR.

Power evolution

The power evolution of the configuration B-0.02% (the only with an admissible global coefficient for the KGH method) is shown in Figure 5.44.

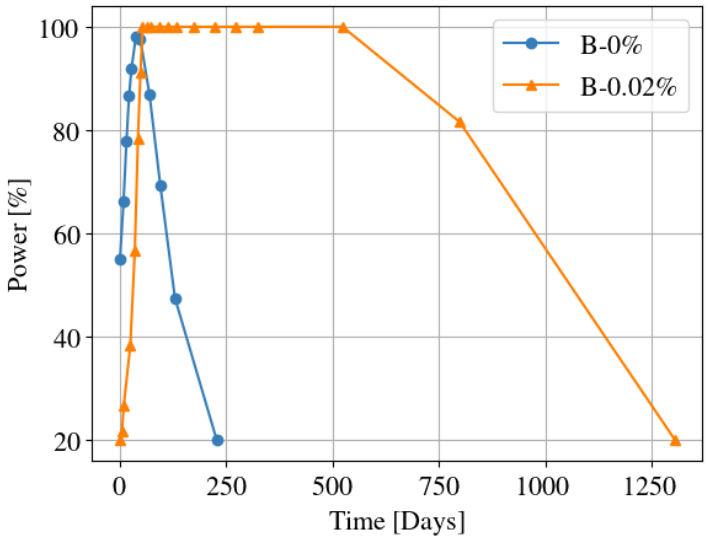


Figure 5.44 - Power evolution for different UO_2 with B configurations – PWR.

As the reactivity has a large swing, the initial core power corresponds to the minimum value of 20% of the nominal power. Then, it is observed that the power would exceed the nominal value in the case of a core autonomous operation. To avoid this excess of power, an active control is needed for a period of about 470 days. This period of controlled operation represents about 40% of the core lifetime, which could be problematic considering the objective of designing a completely autonomous core. Furthermore, the observed reactivity excess reaches 12109 pcm, which is a considerably high amount. This issue could be solved by using a poison with a slower kinetic of consumption. That is why the use of dysprosium is analysed in the following section.

5.4.3.2. Parametric study on the dysprosium insertion in PWR fuel

As discussed in paragraph 5.3.3, the different burnable poisons are characterised by different kinetic of disappearance. In this case of an application of a BP that is used to compensate the reactivity loss, the boron shows a relatively fast kinetic and a slower poison could be better in this case. Table 5.13 shows that the Dy-146 is a burnable poison characterised by a lower cross section in thermal energies and slower disappearance kinetics with respect to the boron.

Enrichment

Table 5.31 sums-up the variation of Dy content and the associated U enrichment. In Figure 5.45 the associated neutron spectrum is shown.

Table 5.31 - Variation of the content of dysprosium in PWR fuel.

Configuration	Dy content [%]	U-235 enrichment [%]
Dy-0% (reference)	0	1.05
Dy-0.02%	0.02	1.25
Dy-0.4%	0.40	4.40
Dy-1.1%	1.10	8.40

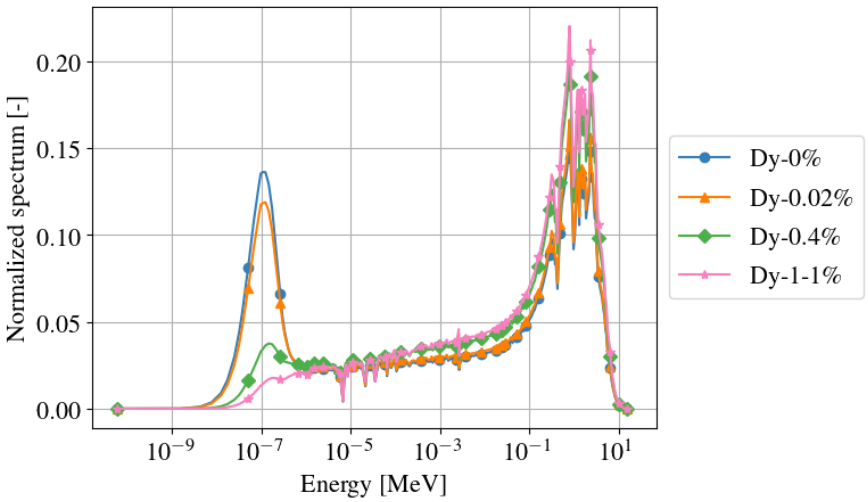


Figure 5.45 - Neutron spectrum in different UO_2 with Dy configurations - PWR.

Reactivity feedbacks

Table 5.32 and Table 5.33 show the reactivity feedback coefficients bound to the configurations previously described.

Table 5.32 - Doppler coefficient for different UO_2 with Dy configurations – PWR.

Configuration	Doppler coefficient [pcm/°C]
Dy-0% (reference)	-2.43
Dy-0.02%	-2.25
Dy-0.4%	-1.98
Dy-1.1%	-1.66

Table 5.33 - Moderator coefficient for different UO_2 with Dy configurations at 320°C - PWR.

Configuration	Moderator coefficient [pcm/°C]
Dy-0% (reference)	-33.31
Dy-0.02%	-33.83
Dy-0.4%	-30.20
Dy-1.1%	-6.23

All the configurations are characterised by a global KGH coefficient that is negative and so the method can be applied ensuring the existence of the result, as explained in Section 2.2.3.3.

Burn-up reactivity swing

Figure 5.46 shows the reactivity evolution bounded to the different Dy configurations.

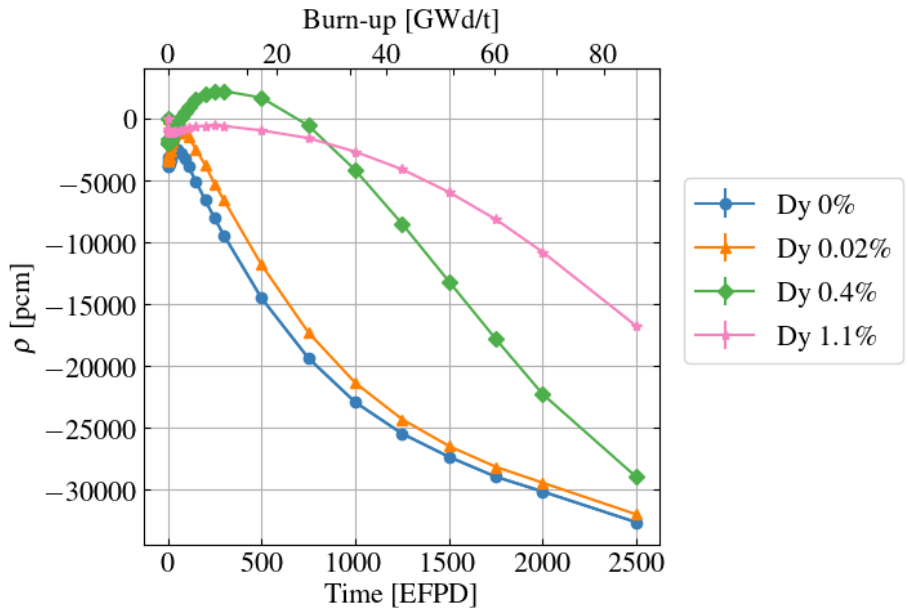


Figure 5.46 - Burn-up reactivity swing for different UO_2 with Dy configurations - PWR.

The Dy-1.1% configuration shows a flattened reactivity.

Power evolution

The effect of the reactivity feedbacks and reactivity burn-up swing is accounted with KGH method. Figure 5.47 shows the power evolution.

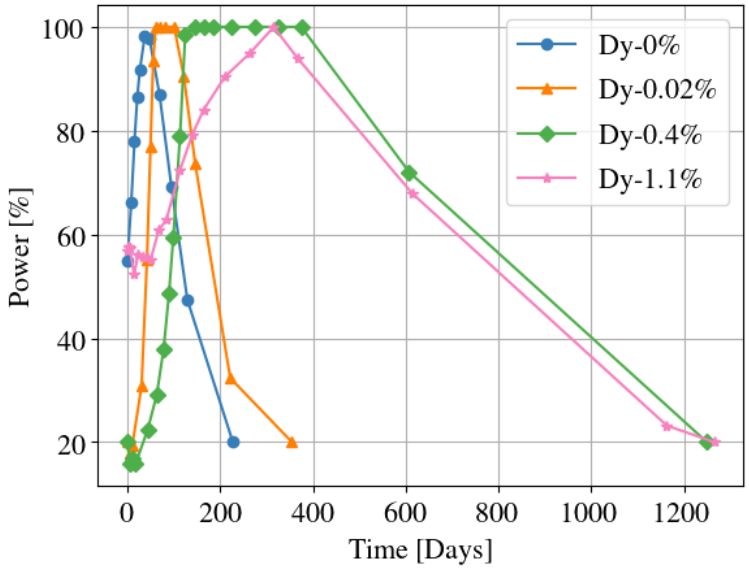


Figure 5.47 – Power evolution for different UO_2 with Dy configurations - PWR.

In all the cases, the reactivity swing shows an increase and then a decrease, so the core has to be started-up at lower values with respect to the nominal one. For lower values of Dy content (Dy-0.02% and

Dy-0.4%), an active control is necessary to prevent the power overcome the nominal value. The reactivity excess is around 670 pcm and 160 pcm for about 40 days and 230 days, respectively for the Dy-0.02% and Dy-0.4%. The comparison between the different cases is summed up in Figure 5.48.

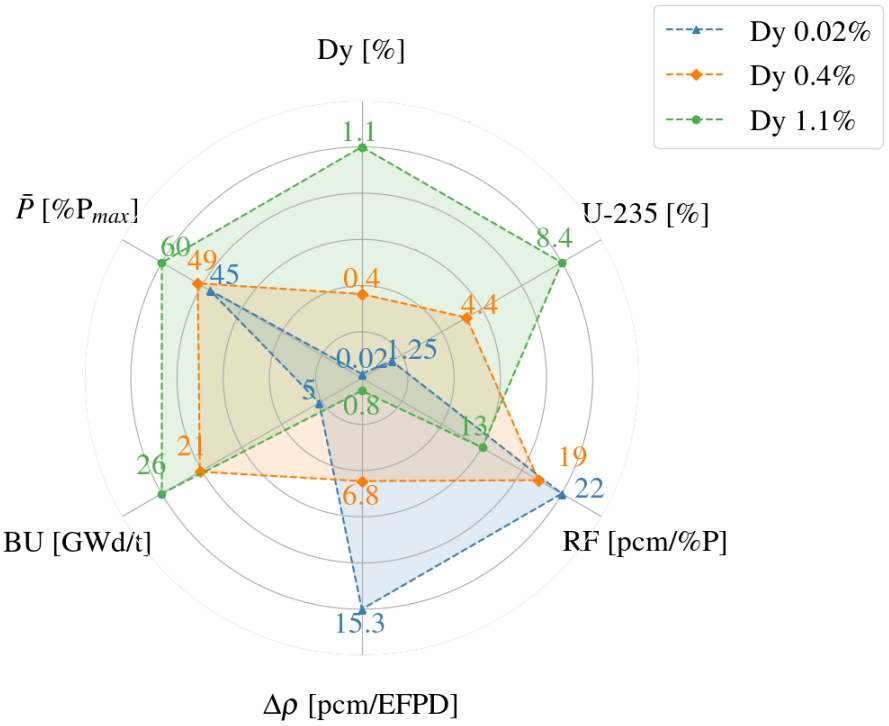


Figure 5.48 - Sum-up of the core performance for different Dy configurations – PWR.

First we focus on the performance of the cores, looking at the axes of the mean power ($\bar{P}$) and the burn-up at EOL (BU). The insertion of dysprosium leads to an increase of the maximum burn-up, from 5 GWd/t in the case Dy-0.02% to 26 GWd/t in the case Dy-1.1%. The average power obtained is also better, going from 45% to 60%. The behaviour is significantly better than with the boron insertion.

The second point to be noticed concerns the physical analysis, shown on the axis of the reactivity feedbacks (RF) and the reactivity swing ($\Delta\rho$). When increasing the dysprosium content from 0.02% to 1.1%, the reactivity loss decreases by 95% while the reactivity feedbacks decrease by 41%. This shows the great potential of dysprosium to flatten the reactivity loss and thus improving core performance.

The Dy-0.4% case leads to a U-235 enrichment need of 4.4%, which is close to the one of actively controlled PWR. It is then possible to stay within classical U-235 enrichment values and multiply by 5 the burn-up in an autonomous configuration. The maximum U-235 enrichment reaches 8.4% in the Dy-1.1% case. This value is rather low in comparison with the maximum enrichment of HALEU fuels, which means that it would be possible to investigate further higher dysprosium content. It has to be noticed that all three configurations are characterised by an initial xenon effect that would require an active reactivity control system for the reactor BOL (reactivity to be controlled during the first days from
1000 pcm to 3600 pcm).

5.4.4. Conclusion on burnable absorbers insertion in PWR core

In conclusion, with the boron, the kinetic of absorption is too high and too large and thus the excess of reactivity leads to the need of an active control over a long period of time. On the other hand, the

dysprosium is a better candidate as burnable poison for autonomous PWR. The core performance is increased up to 26 GWd/t and 60% of mean power. In Figure 5.49, a radar graph compares dysprosium and americium insertion in PWR, as they have shown the best performance respectively for burnable poisons and actinides. The cases compared are the ones characterised by the largest content of Am and Dy studied in this chapter.

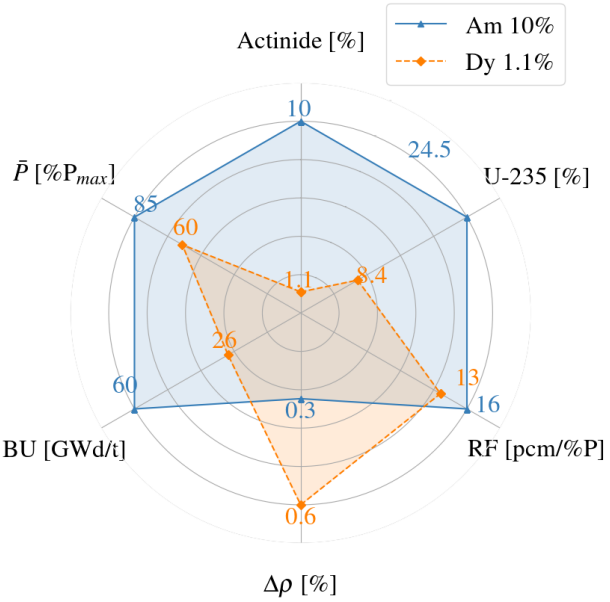


Figure 5.49 - Comparison between $UAmO_2$ and Dy configurations in PWR.

Americium insertion shows the best results in terms of performance. Actually, the Am-10% configuration reaches the maximum burn-up of 60 GWd/t while having a high average power of 85%. On the other hand, the Dy-1.1% configuration shows a decent average power of 60%, but a reduced burn-up of 26 GWd/t. These results are explained by the more favourable reactivity feedbacks and reactivity loss in the Am-10% case. Even if these estimators are of the same order of magnitude, reactivity loss is 50% lower and reactivity feedbacks are 23% higher in the Am-10% case.

However, this performance is obtained at the cost of a higher U-235 enrichment (24.5% for the americium insertion against 8.4% for the dysprosium insertion). Americium content is also ten times higher than dysprosium content studied here. It could be interesting to compare both of them at the same U-235 enrichment.

Finally, the Am-10% configuration reduces the Xe effect to be considered controlled in the start-up phase. On the contrary, the Dy-1.1% need an active control of the Xe reactivity loss, larger than 500 pcm.

5.5. Conclusions

In this chapter, an analysis of possible strategies to increase the lifetime of an autonomous core is presented. The attempt to decrease the reactivity swing due to fuel depletion is done via the insertion of actinides and burnable poisons. In both HTR and PWR, the actinides studied are americium, neptunium, plutonium and thorium, while the burnable poisons studied are boron and dysprosium.

The plutonium and thorium insertion in the HTR have been considered less interesting than the other cases due to the high plutonium or U-235 content needed. On the other hand, configurations in PWR

showed similar results to the neptunium case, but less relevant than the americium case. In addition, boron insertion has led to lower performance than dysprosium insertion. This is why only americium, neptunium and dysprosium insertion are discussed in these conclusions. For each element considered, a comparison of their effect is done between HTR and PWR so that a link can be made between reactor technology and element insertion. For each element, the highest content has been chosen. Then, the best configurations of each technology are compared and their feasibility is discussed.

An axis dedicated to the ECS is also shown in the following graphs in order to assess its possible contribution in maintaining core criticality at constant power. $\Delta\rho_{ECS}$ is the maximum theoretical ECS contribution in pcm normalized by the total reactivity loss during the autonomous lifetime. As a reminder, the autonomous lifetime corresponds to the time until the burn-up reaches 60 GWd/t or the power goes lower than 20% of its nominal value. The contribution of the PWR has been computed in Chapter 3, Section 3.4. The maximum temperature variation is 283 °C while the integral coefficient bounded to the ECS is K=-28.9 pcm/°C. On the other hand, the temperature difference for the HTR is computed considering a direct Brayton cycle. The maximum temperature, corresponding to nominal core outlet temperature, is 850°C. The minimum temperature is the one on the cold leg considering the temperature rise due to the compressor. It is considered of 26°C. This gives a maximum temperature variation of 824 °C and a K=-7.7 pcm/°C. The maximal ECS contribution is 8179 pcm for the PWR and 6328 pcm for the HTR. This contribution is however theoretical and if technologically achievable would necessarily lead to a strong reduction of the reactor efficiency.

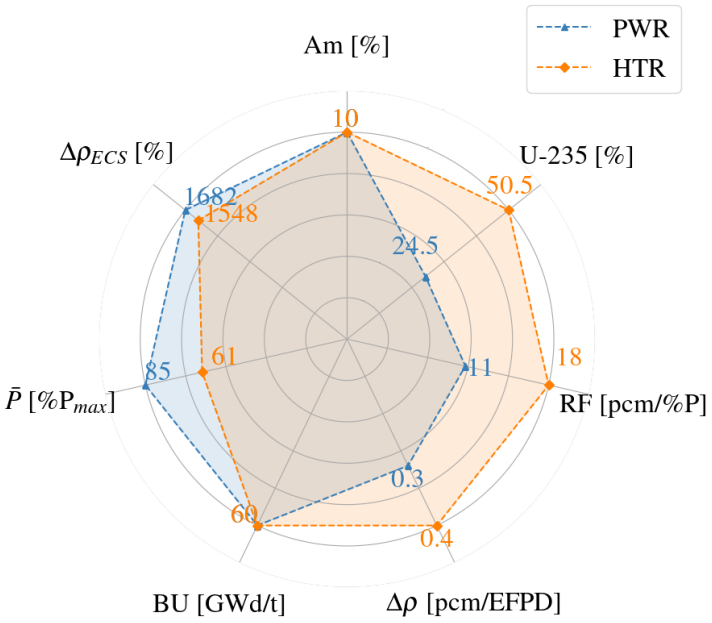


Figure 5.50 – Comparison between $UAmO_2$ HTR and PWR.

Figure 5.50 shows the comparison of the effect of americium insertion between a PWR and a HTR. In both cases, the burn-up reaches the maximum value of 60 GWd/t. However, the PWR case shows an average power 39% higher than the HTR one (85% against 61%). When it comes to reactivity indicators, the HTR has a reactivity feedback effect 63% higher and a burn-up reactivity swing 33% higher. Meanwhile, the HTR case needs a U-235 enrichment twice as high than the PWR, which means that in this case, the HTR is not in range of HALEU fuels while the PWR is almost there. Finally, the ECS could provide a lot of manoeuvrability within a low temperature variation as its maximum theoretical contribution represents about 1600% of the reactivity loss at constant power.

Figure 5.51 shows the comparison of the effect of neptunium insertion between a PWR and a HTR. The HTR performance is higher than the PWR ones. Actually, the burn-up reached is more than 4 times higher in the case of HTR (22 GWd/t vs. 5 GWd/t) and the average power is 62% higher. When it comes to reactivity indicators, both reactors have the same reactivity feedback effect, but the burn-up reactivity swing is 17% lower. Similarly to the americium insertion case, the HTR needs a U-235 enrichment twice as high than the PWR. Once again, the PWR is still in range of HALEU fuels while the HTR is not. Finally, the ECS contribution in the case of PWR is twice as high as the HTR one, meaning that it would be easier to compensate the reactivity loss in a PWR.

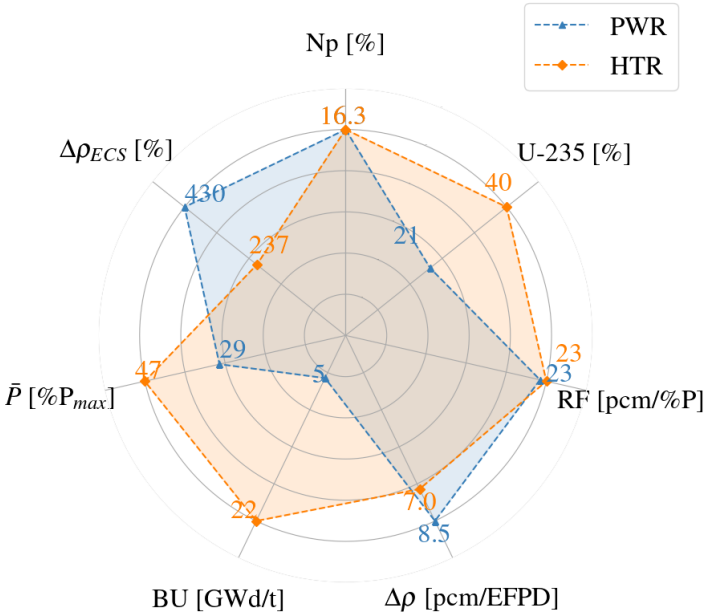


Figure 5.51 - Comparison between $UNpO_2$ HTR and PWR.

Finally, the cases of dysprosium insertion in HTR and PWR are compared in Figure 5.52. The PWR shows a reactivity feedback effect 86% higher and a reactivity swing 70% lower than the HTR. For this reason, the PWR reaches better performance with a burn-up 37% higher and an average power 25% higher. Moreover, the PWR needs lower U-235 enrichment and has more manoeuvrability margin from the ECS.

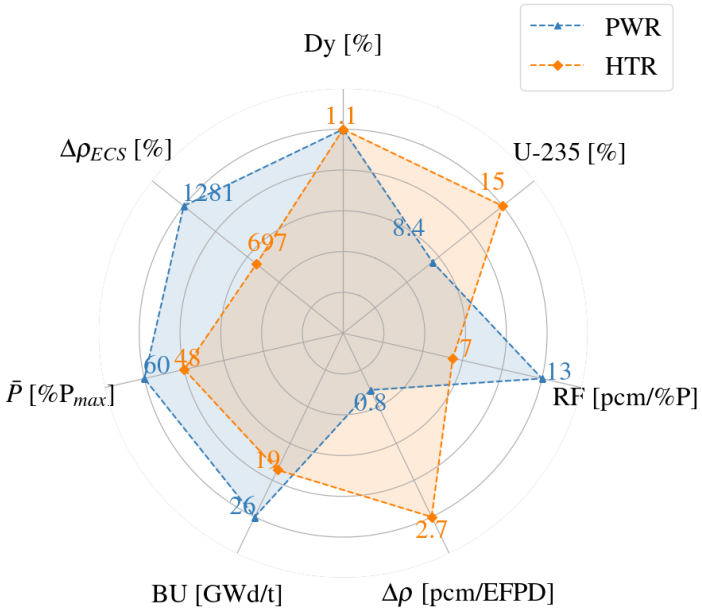


Figure 5.52 - Comparison between Dy in UO_2 in HTR and PWR.

To sum up these observations, the insertion of americium is effective for both technologies as it strongly decreases the reactivity loss, although the performance is slightly higher in the PWR case. Dysprosium insertion seems more suitable for the PWR as it simultaneously reduces the burn-up reactivity swing and increases the reactivity feedback effects, leading to higher performance. In the end, neptunium insertion is more effective in the HTR, even if is it necessary to keep in mind that a saturation effect has been witnessed. In other word, it would not be possible to increase the performance a lot further with neptunium.

Now that the tendencies depending on the technology and the element inserted have been identified, it is interesting to set criteria in order to highlight the best configurations available. Two types of criteria are chosen.

First of all, performance criteria are set. French PWRs are chosen as the reference. They have an average load factor of 71% [104], a maximum target burn-up of 52 GWd/t and a cycle length of one year / one year and a half [105]. It should be noticed that the load factor of PWR takes into account events like stops for reloading or load-following periods, while no such considerations are taken into account for the autonomous reactor. Despite this observation, 71% of average power and a burn-up higher than 52 GWd/t are chosen for performance criteria.

Secondly, a parameter is set on the feasibility of the fuel chosen for the reactor. Based on the HALEU criterion (maximum U-235 enrichment of 20%), the configurations above 25% of U enrichment are considered not reachable and so excluded in the final choice in this work. The value of 25% is chosen, slightly higher than the HALEU because a study of fine optimisations on the configurations could be done to still decrease the enrichment while optimising the performance.

With this new set of criteria, the best configuration of the insertion of americium, neptunium and dysprosium in the two cores is analysed.

The HTR shows larger performance with the insertion of Am with respect to Np and Dy. The case Am-1% is the only one with admissible U-235 enrichment limit (10%) and corresponds to 36 GWd/t and 50% of mean power. The Np-5% is the last admissible case in terms of U enrichment (13%) and

corresponds to 18 GWd/t and 51% of mean power. Increasing the content (up to the HALEU limit) with an optimisation process the performance in the two cases would be increased, but the Am is the most promising among the two. The case Dy-2% shows the performance of 17 GWd/t and 66% of mean power and is characterised already by an enrichment of 21.4%. The performance is considered inferior to the Am potentiality.

In PWR, the Am-10% lead to an enrichment of 24.5% (with a performance of 60 GWd/t and 85% mean power). The Np-16.3% need 21% of U enrichment and lead to a performance of 5 GWd/t and 47% of mean power. A more precise study should be done on the two configurations to optimise the enrichment. Anyway, the performance of the Am case is larger than Np and larger than Am-HTR case. On the other hand, the Dy-1.1% in PWR lead to an enrichment of 8.4% (with 26 GWd/t and 60% mean power). The increase of the Dy in PWR could be a potential way to investigate further.

Furthermore, all the cited configurations in HTR and PWR are characterised by an initial Xe effect, except for the one of Am in PWR. On the other hand, the Am-1% in HTR and Am-10% in PWR are the only configurations that need an active control to compensate an excess of reactivity (that would increase the power over the nominal value). In HTR is around 460 pcm while in PWR is around 250 pcm. This excess could be reduced (or even eliminated) with a process of optimisation on the configurations.

In the end, the insertion of americium in PWR seems to be the best candidate that has been found within the scope of this study, as the Am-10% case shows the best performance and respect the limit on U-235 enrichment. Dysprosium insertion in PWR could be also investigated, but further studies are needed to optimise the configuration.

Finally, another available lever to maximize performance is the control of the ECS. An example is given below in Figure 5.53 in the Am-10% insertion case. For both cores, the power can be maintained at its nominal level until the burn-up reaches 60 GWd/t/. Indeed, the theoretical contribution of the ECS is large enough to compensate the reactivity loss. Theoretical calculations have been made on the reactivity values, while the simulations of the ECS by CYCLOP could compute the efficiency of the system on a 15% of power variation.

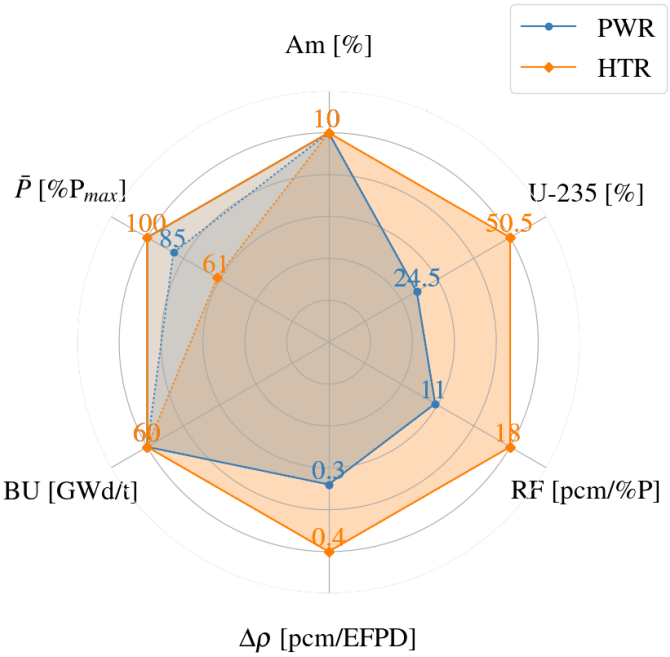


Figure 5.53 - Comparison of PWR and HTR $UAmO_2$ performance with the theoretical contribution of the ECS.

Chapter 6

Fast spectrum autonomous reactors

Summary

6.1. Introduction 162
6.2. Autonomous SFR with actinides 162
6.2.1. Actinides in SFR core 163
6.2.2. Parametric study on the americium insertion in SFR fuel 166
6.2.3. Parametric study on the neptunium insertion in SFR fuel 170
6.2.4. Parametric study on the plutonium insertion in SFR fuel 173
6.2.5. Conclusions on actinide insertion in SFR fuel 176
6.3. Autonomous SMSFR with actinides 178
6.3.1. Parametric study on the americium insertion in SMSFR fuel 178
6.3.2. Parametric study on the neptunium insertion in SMSFR fuel 181
6.3.3. Parametric study on the Np and Pu insertion in SMSFR fuel 184
6.3.4. Conclusions on actinides insertion in SMSFR fuel 187
6.4. Discussion on burnable poison in SFR 187
6.5. CADOR core 189
6.6. Conclusions 191

6.1. Introduction

In this chapter, an analysis on the possibility of improving the autonomous reactor performance is made for SFR. The study, here, is based on the designs of the reactors with their design of 203 W/cm^3 SFR. The objective is to perform the same study as for the thermal spectrum core and to compare the results according to the different reactors spectra.

First, the insertion of actinides in the fuel is considered. As for the thermal reactors, the analysis focuses on a comparison between the Am, Np, Th and Pu. Then, the configurations of interest are analysed in more detail with parametric study varying the actinide content. The same study is made on a small SFR core. The reference design for the smaller SFR core is a Small Modular SFR, based on the reduced volume of the V2B design [41]. This SMSFR concept is characterised by a volume of about 1/10 of the original V2B core.

Then, an analysis of the insertion of burnable poison in the SFR core is made based on literature. The BP in SFR are not efficient as in the thermal cores and need specific and optimised designs. Studies have been made on optimised configurations and are compared here to the other case of study.

Finally, a specific core based on 'CADOR' concept is considered [106]. It has been designed with the objective of increasing the reactivity feedback effects (the Doppler). It is compared to the SFR-V2B, to analyse the impact of the increase of RF on an autonomous core.

The analysis of each configuration is made with the same approach as in thermal cores. The enrichment is calculated in order to guarantee criticality at BOL, then the associated reactivity feedbacks are evaluated, together with the burn-up reactivity swing. Finally, the power evolution is computed, via the KGH method and the results are presented with radar graphs to compare the different configurations.

6.2. Autonomous SFR with actinides

In this paragraph, the analysis of the insertion of minor actinides in SFR fuel is conducted. The methodology is analogous to the one applied to the thermal cores. The various actinides, described at the beginning of this chapter, are inserted in the fuel and their effects are compared. Successively, the content of each actinide is varied in order to analyse the effect on the reactivity evolution and to find the most suitable configuration for an autonomous core.

The core parameters are summed up in the next Figure 6.1 and Table 6.1.

Table 6.1 – Sum-up of the SFR core characteristics.

Core thermal power [MW]	3600
Power density [W/cm^3]	203
Assembly pitch [cm]	21.2
Pins per assembly	217
Pin outer diameter [mm]	10.8
Fissile zone volume [m^3]	17.7

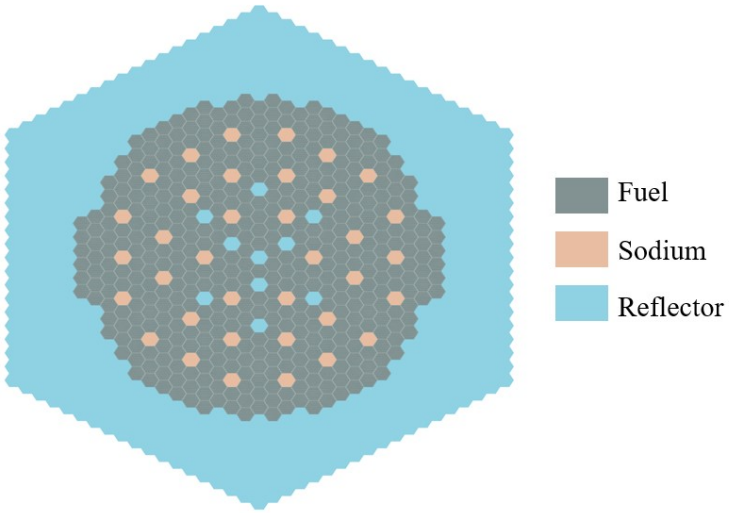


Figure 6.1 – Radial description of SFR core.

6.2.1. Actinides in SFR core

As in the analysis of thermal cores, four actinides were selected: Am, Np, Th and Pu. As a first approach, the Am, Np and Th are inserted in the fuel with reference content (based on [41]) and the U-235 enrichment is adapted to ensure criticality at BOL. On the other hand, the Pu is inserted considering depleted uranium and adapting the MOX content for the initial criticality.

Enrichment

Table 6.2 shows the reference actinides contents and the associated U-235 enrichment for the critical configuration at BOL. As a reminder, the U-235 enrichment is the ratio between the mass of U-235 and the total mass of U, while the fissile content is the ratio between the total mass of fissile isotopes and the total mass of fuel.

Table 6.2 – SFR actinides insertion configuration.

Configuration	Actinide/Pu content [%]	U-235 enrichment [%]	Fissile content [%]
$UAmO_2$	5.20	14.6	13.9
$UNpO_2$	16.3	17.0	14.2
$UThO_2$	74.0	62.3	16.2
$UPuO_2$	14.7	0.25	8.38
UO_2	-	12.9	12.9

The equivalent content of fissile in the core, to ensure criticality at BOL, is of the same order of magnitude for all the configurations. Figure 6.2 shows that all the configurations have a similar neutron spectrum. The necessary fissile content depends on the capture and fission rates of the inserted actinide compared to U-238 and the neutron production of the different fissile isotopes (U-235 or Pu-239 and Pu-241 in the case of MOX).

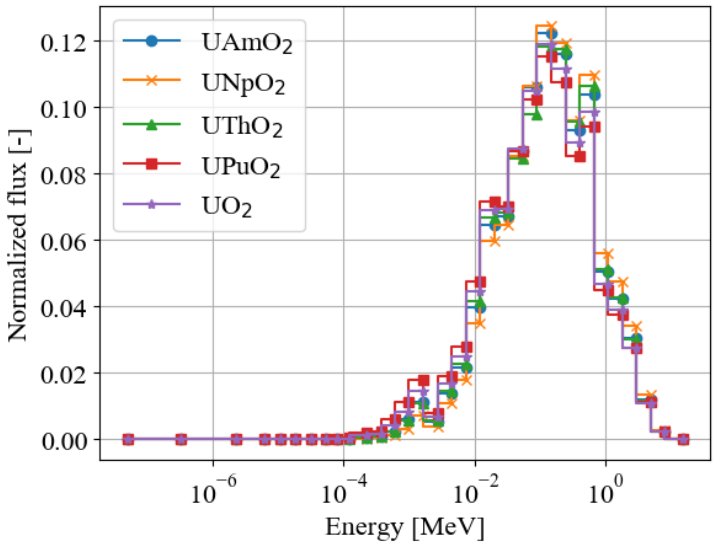


Figure 6.2 - SFR actinides fuel spectrum.

Reactivity feedbacks

In this paragraph, the reactivity feedbacks associated to the different configurations are presented. In Table 6.3, the Doppler constants are compared, while in Table 6.4 the other reactivity feedbacks are summed-up.

Table 6.3 – Doppler constant of SFR core with actinides.

Configuration	Doppler constant [pcm]
$UAmO_2$	-642
$UNpO_2$	-216
$UThO_2$	-756
$UPuO_2$	-1294
UO_2	-1194

Table 6.4 – Reactivity feedback coefficients of SFR core with actinides.

Configuration	Fuel expansion [pcm/K]	Structure expansion (clad + TH) [pcm/K]	Sodium density [pcm/K]
$UAmO_2$	-0.090	0.041	0.190
$UNpO_2$	-0.125	0.055	0.510
$UThO_2$	-0.057	0.022	0.055
$UPuO_2$	-0.126	0.058	0.403
UO_2	-0.080	0.030	0.027

As it is observed in the literature, with the use of dense fuels like metal or carbide, the spectrum hardening (Am, Th, Np) leads to a reduction of the Doppler constant, due to a reduction of the epithermal

flux. Furthermore, comparing the capture cross sections of U-238, Am-241 and Np-237, in the energy interval between 20 keV and 0.15 keV, the U-238 has resonances in the cross section, while both Am-241 and Np-237 have a capture cross section larger than the average one of the U-238. The insertion of these actinides in the fuel contributes to the absorption of neutrons and decreases the number of neutrons absorbed in the resonances intervals and thus decreasing the Doppler effect [107]. On the other hand, the insertion of Pu in the fuel increases the Doppler effect with respect to the UO_2 case. Indeed, in $UPuO_2$ configuration, the U-238 is partially replaced by some fissile isotopes of Pu but also the fertile ones, that also contributes to the Doppler effect. Furthermore, the Pu isotopes show resonances that starts at 5.5 keV, and for lower energies the mean cross section is lower than Am and Np.

Also the U-238 content impacts directly this feedback coefficient as it is widely reduced in some cases, especially for the Th.

Burn-up reactivity swing

In this section, the reactivity variation according to burn-up is considered. Initially, the configurations with the actinides are compared to the reference case of the reactor loaded with UO_2. Figure 6.3 shows the different reactivity evolution according to the actinide insertion.

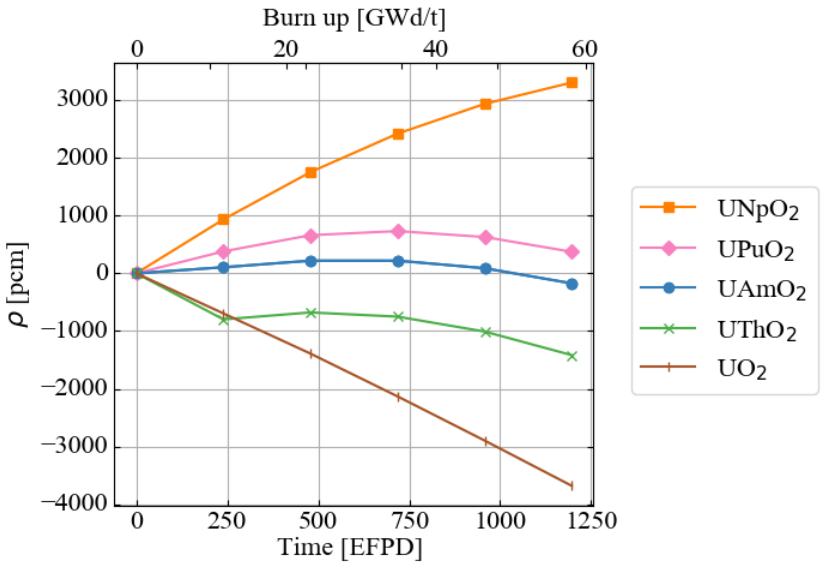


Figure 6.3 – Reactivity evolution of SFR core loaded with actinides.

The analysis of the different evolutions is made via the study of the macroscopic cross sections in Annex VI.1. The depletion chain of the different actinides inserted mainly drives the behaviour of the core: breeder or burner.

Power evolution

In this section, the coupled effect of the reactivity evolution and reactivity feedbacks is considered in the KGH method. The power evolution of the core is calculated and represented in Figure 6.4.

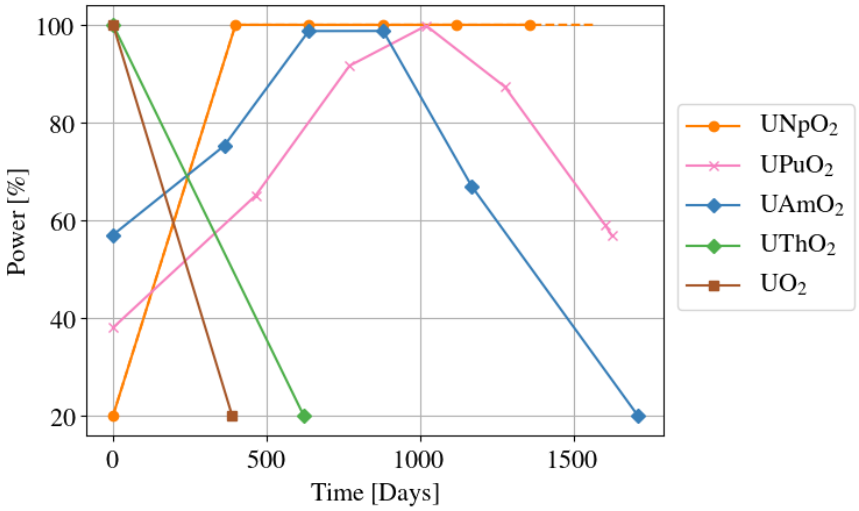


Figure 6.4 - Power evolution of SFR core loaded with actinides.

The insertion of the Th in the core does not lead to major contribution due to the initial large reactivity loss (of the same order of the UO_2 configuration), before the production of U-233. The configurations of Am and Pu show similar reactivity curves and similar power trends. In these configurations, the core is started-up at lower values (57% and 38% of the nominal power, respectively for Am and Pu). The maximum power is not overcome and no active control is necessary. The EOL of the Am core is determined by reaching 20% of the nominal power at about 1700 days, while the EOL of Pu core is determined by reaching 60 GWd/t at about 1625 days. Finally, the configuration containing Np in fuel is characterised by a very large reactivity swing (about 3330 pcm over the core lifetime). For this reason, the core is started-up at 20% of the nominal power and also an active control is needed over nearly the whole core life (or shut down after 400 days).

An analysis of the variation in the influence of the different isotopes as a function of the change in the initial actinide content is given in the following sections.

6.2.2. Parametric study on the americium insertion in SFR fuel

In this paragraph, the insertion of Am in the SFR core is analysed varying the Am content in the core.

Enrichment

The Table 6.5 sums-up the studied configurations, the Am content and the relative U-235 enrichment necessary to ensure criticality at BOL.

Table 6.5 - Variation of the content of americium in $UAmO_2$ SFR fuel.

Configuration	Am content [%]	U-235 enrichment [%]	Fissile content [%]
Am-0%	0.0	12.9	12.9
Am-1%	1.0	13.2	13.1
Am-2%	2.0	13.6	13.3
Am-5.2%	5.2	14.6	13.9

The higher is the actinide content, the higher is the needed U-235 enrichment. However, as the core has already fast spectrum, the uranium enrichment variation is quite limited (compared for example to the thermal core of the HTR). It only compensates the difference of captures and fissions between U-238, Am-241 and Am-243.

Reactivity feedbacks

In Table 6.6 and Table 6.7, the Doppler constant and the other reactivity coefficients are summed-up.

Table 6.6 - Doppler constant of SFR core with $UAmO_2$.

Configuration	Doppler constant [pcm]
Am-0%	-1194
Am-1%	-1045
Am-2%	-920
Am-5.2%	-642

Table 6.7 – Reactivity feedback coefficients of SFR core with $UAmO_2$.

Configuration	Fuel expansion [pcm/K]	Structure expansion (clad + TH) [pcm/K]	Sodium density [pcm/K]
Am-0%	-0.080	0.030	0.027
Am-1%	-0.074	0.034	0.065
Am-2%	-0.078	0.036	0.099
Am-5.2%	-0.090	0.041	0.190

The insertion of Am in the fuel causes a decrease in the absolute value of the Doppler effect and an increase of the positive coefficients of structures and coolant expansion caused by a spectrum hardening (fission threshold at a lower energy than U-238). All these effects decrease the possibility to counterbalance the reactivity loss of the core. On the other hand, the insertion of Am causes an increase of the absolute value of the fuel expansion coefficient by increasing the mean neutron free path.

Burn-up reactivity swing

Figure 6.5 shows the evolution of the different configurations. With the insertion of the Am, the reactivity loss is reduced, up to the content of 5.2%, where the reactivity slightly increases, with a peak around 650 EFPD and then decreases.

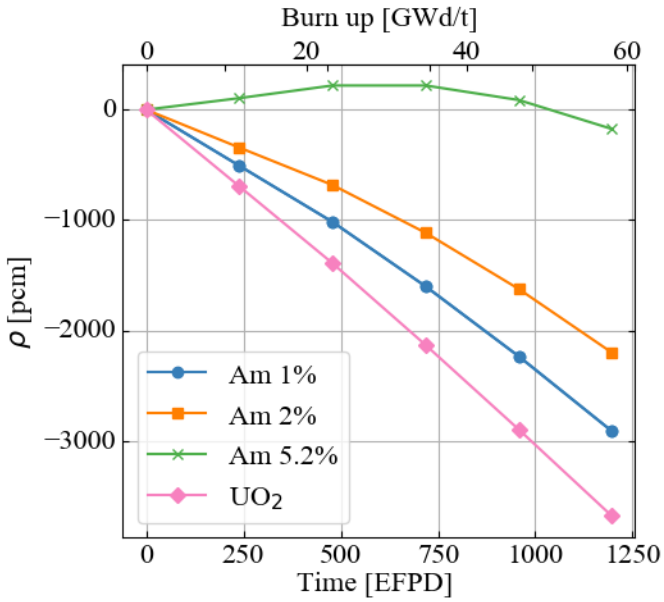


Figure 6.5 - Reactivity evolution according to the variation of Am content in $UAmO_2$ SFR fuel.

The evolution of the reactivity according to the different Am content is analysed via the examination of the major isotopes cross section evolution. In Figure 6.6, the macroscopic cross sections of the capture and fission of americium, uranium and plutonium major isotopes are shown. In particular, the configuration of Am 1% and Am 5.2% are analysed to compare two cases with different trends in the reactivity evolution.

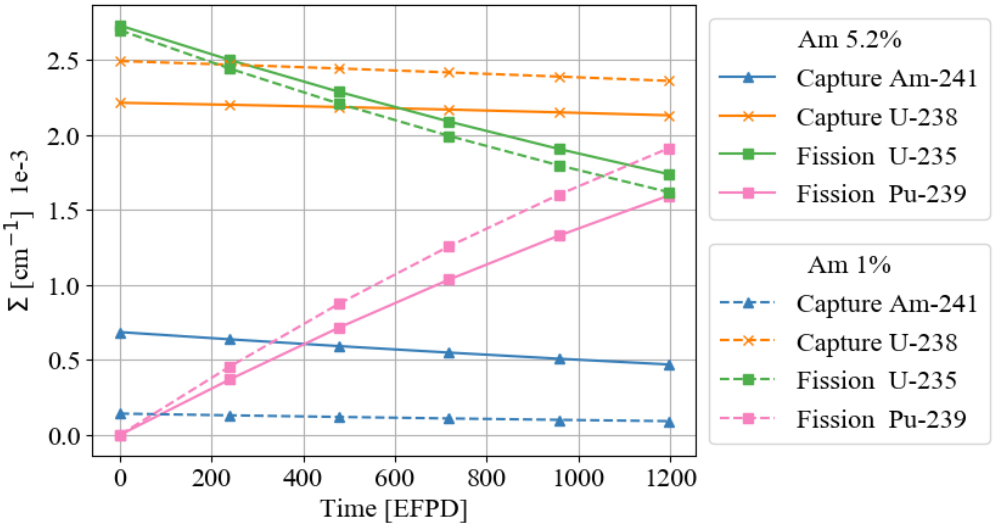


Figure 6.6 – Macroscopic cross sections of the main isotopes in the UAmO2 configurations with 5.2% and 1% Am insertion.

The higher is the Am content, the faster is the kinetics of disappearance. The case of Am 5.2% shows a larger variation of its content during the evolution with respect to the case of 1% Am content. On the other hand, the larger is the Am content, the lower is the content of U-238. The case of 1% Am shows a faster kinetic of absorption of U-238 that determines a larger and faster Pu-239 build-up. The reactivity evolution is determined by the concurrent effects of Am disappearance (larger with higher Am content) and Pu-239 build-up (larger for lower Am contents). The increase of the Am content involves an increase

of the contribution of the Am disappearance over the Pu-239 creation and thus reduces the reactivity loss slope.

Power evolution

In Figure 6.7, the power evolution of the different Am configurations is shown.

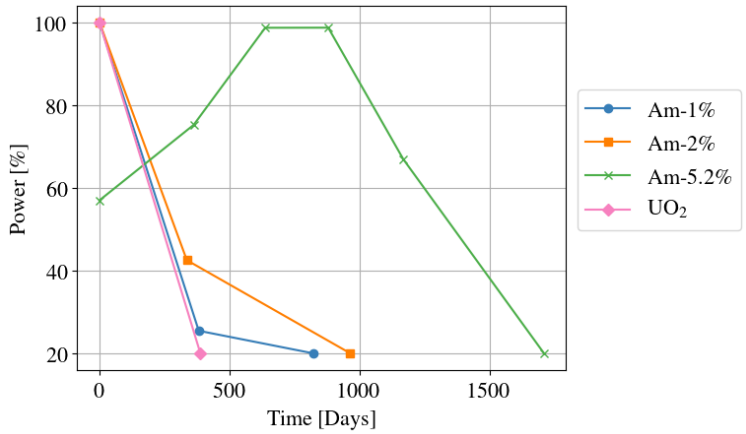


Figure 6.7 - Power evolution of SFR core loaded with $UAmO_2$.

The insertion of Am, in low content, decreases slightly the reactivity loss and consequently increases slightly the core lifetime. With higher Am content (5.2%) the reactivity curve shows an initial increase and then a decrease. The power shows the same behaviour, for this reason the core is started-up at about 58% of the nominal power.

A precision here is made: in the Am-5% case, there is only one reactivity calculated at 600 days and one at 900 days. Between the two, the power is considered to be 'flat'. In reality, the reactivity is probably bell-shaped and so is the power. This could therefore change the initial power and the effective power value (because the 100% value would be reached at another time and would be 'higher' than the current 100%. But this is considered acceptable at this level of comparison. In Figure 6.8 the performance of the different configurations is compared.

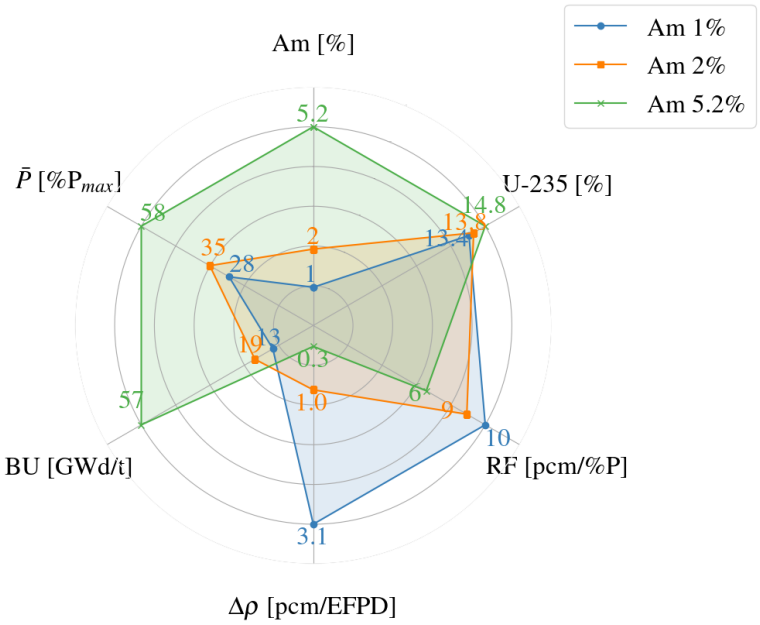


Figure 6.8 - Sum-up of the core performance for different $UAmO_2$ configurations – SFR.

First we focus on the core performance, looking at the axes of the mean power ($\bar{P}$) and the burn-up at EOL (BU). Between the configurations Am-1% and Am-5.2%, the burn-up at EOL is increased from 13 GWd/t to 57 GWd/t and the mean power is increased from 28% to 58%.

The second point to be noticed concerns the physical analysis, shown on the axis of the reactivity feedbacks (RF) and the reactivity swing ($\Delta\rho$). The reactivity feedbacks have decreased up to 60%, while the reactivity swing decreases up to 90%. The large reactivity loss decrease leads to the performance increase.

The insertion of americium in SFR fuel slightly increases the need in U-235 enrichment that is around 14%.

6.2.3. Parametric study on the neptunium insertion in SFR fuel

In this section, a study, analogous to the previous one, is made for the insertion of neptunium in SFR core.

Enrichment

The Np content is varied and the needed U-235 enrichment is computed for criticality at BOL. The results are shown in Table 6.8.

Table 6.8 - Variation of the content of neptunium in $UNpO_2$ SFR fuel.

Configuration	Np content [%]	U-235 enrichment [%]	Fissile content [%]
Np-0%	0.0	12.9	12.9
Np-1%	1.00	13.1	13.0
Np-2%	2.00	13.5	13.2
Np-5%	5.00	14.4	13.7
Np-16.3%	16.3	17.0	14.2

As with the insertion of Am, the insertion of Np implies a limited variation in fissile content.

Reactivity feedbacks

Table 6.9 and Table 6.10 sum-up the reactivity feedback coefficients for the different Np configurations.

Table 6.9 - Doppler constant of SFR core with $UNpO_2$.

Configuration	Doppler constant [pcm]
Np-0%	-1194
Np-1%	-1043
Np-2%	-917
Np-5%	-645
Np-16.3%	-216

Table 6.10 – Reactivity feedback coefficients of SFR core with $UNpO_2$.

Configuration	Fuel expansion [pcm/K]	Structure expansion (clad + TH) [pcm/K]	Sodium density [pcm/K]
Np-0%	-0.080	0.030	0.027
Np-1%	-0.075	0.034	0.075
Np-2%	-0.079	0.036	0.117
Np-5%	-0.091	0.040	0.226
Np-16.3%	-0.125	0.055	0.510

The insertion of Np in fuel causes the same effects on the reactivity feedbacks as the Am. Increasing the Np content, the Doppler constant decreases (in absolute values) and the positive coefficients of coolant and structure expansion increases their positive values. The only beneficial effect is on the fuel expansion coefficient.

Burn-up reactivity swing

The corresponding reactivity variations are shown in Figure 6.9. Increasing the neptunium content, the reactivity loss decreases.

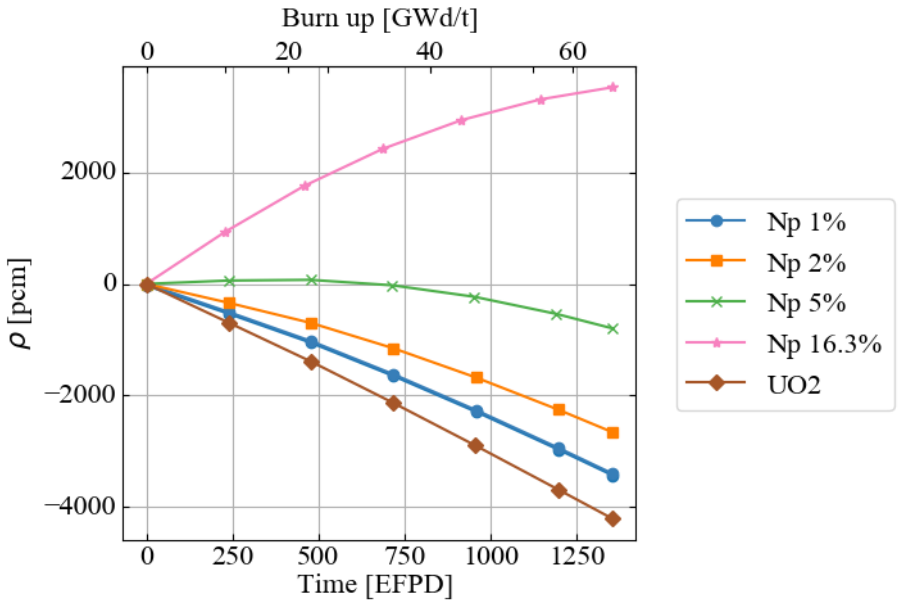


Figure 6.9 - Reactivity evolution according to the variation of Np content in $UNpO_2$ SFR fuel.

The analysis of the reactivity variation is deepened with the examination of the cross sections of the core isotopes. The evolution of the cross sections of the major isotopes is shown in Figure 6.10. The two configurations of Np 1% and Np 5% are compared. The largest contribution to the reactivity is given by the U-238 and Np-237 absorptions and the U-235 and Pu-239 fissions. Analogously to the Am case, studied in the previous paragraph, the reactivity of the $UNpO_2$ core is driven by the counterbalancing effects of Pu-239 build-up and Np-237 disappearance. The higher is the Np content, the faster is its disappearance kinetic and the slower is the Pu-239 build-up (and the disappearance of U-238). In the

case of Np 5%, the two effects counterbalance the U-235 depletion and make the reactivity loss variation slightly around zero in the first 750 EFPD.

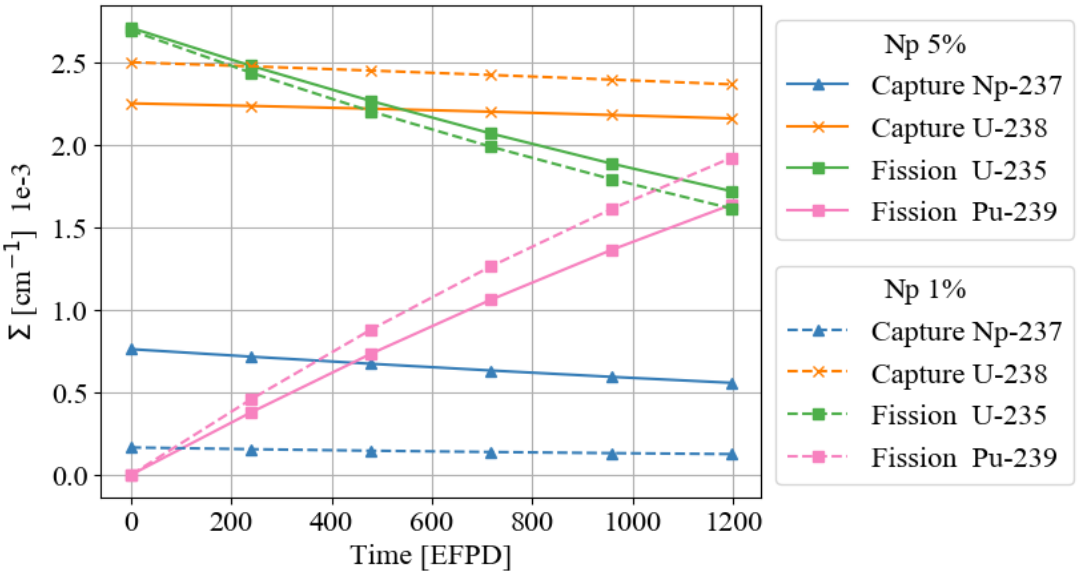


Figure 6.10 - Macroscopic cross sections of the main isotopes in the UNpO2 configurations with 5% and 1% Np insertion.

The configuration of Np 5% shows a slightly varying reactivity up to 750 EFPD and then it decreases.

Power evolution

In this section, the KGH method is used to evaluate the concurrent effect of the reactivity loss and the reactivity feedbacks. Figure 6.11 shows the power evolution of the different configurations and Figure 6.12 sums-up the core performance.

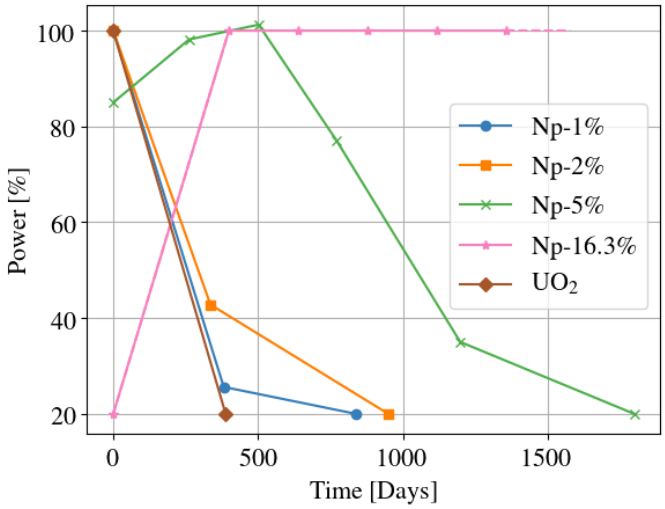


Figure 6.11 - Power evolution of SFR core loaded with $UNpO_2$.

The insertion of low quantity of Np increases the core lifetime (about 850 days), with respect to the configuration of UO_2 fuel (about 400 days). The power trend is monotonically decreasing. With Np content of 5%, the core is started-up at lower power and the lifetime is increased to about 1800 days. Increasing further the Np content, the reactivity increase becomes larger and the core is started-up at lower and lower power. With a content of 16.3% the core is started at 20% of the nominal power and an

active control is needed, up to the fuel burn-up of 60 GWd/t, for a period of 957 days, corresponding to a reactivity excess of 2371 pcm. The other solution would be to stop the core after 400 days of operation, with a burn-up equivalent to the case without Np. In conclusion, this last configuration is considered out of the scope of this work as it needs a too large active control, or presents no advantage compared to the reference case.

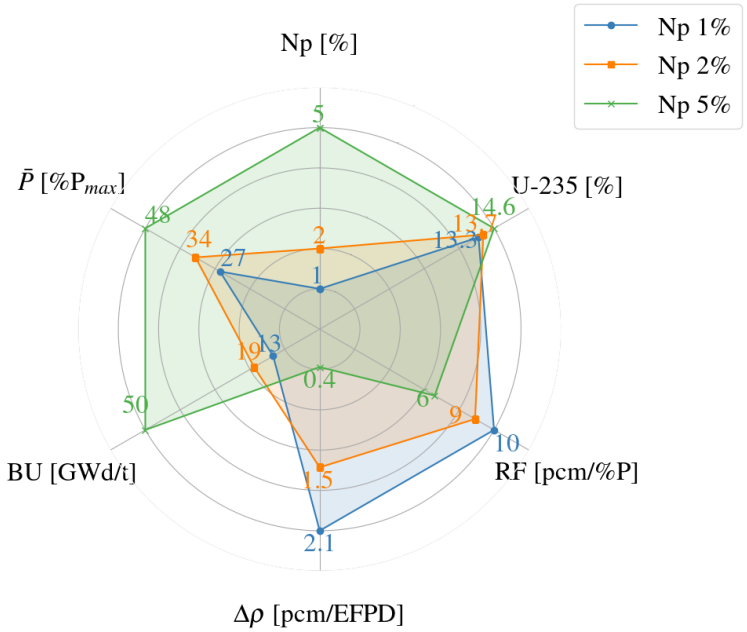


Figure 6.12 - Sum-up of the core performance for different $UNpO_2$ configurations – SFR.

First we focus on core performance, looking at the axes of the mean power ($\bar{P}$) and the burn-up at EOL (BU). Between the configurations Np-1% and Np-5%, the burn-up at EOL is increased from 13 GWd/t to 50 GWd/t and the mean power is increased from 27% to 48%.

The second point to be noticed concerns the physical analysis, shown on the axis of the reactivity feedbacks (RF) and the reactivity swing ($\Delta\rho$). The reactivity feedbacks have decreased up to 60%, while the reactivity swing decreases up to 81%. The large reactivity loss decrease leads to the performance increase.

Finally, the insertion of neptunium in SFR fuel slightly increases the need in U-235 enrichment that is around 14%.

6.2.4. Parametric study on the plutonium insertion in SFR fuel

The study of variation of actinide content is made also in the plutonium case. As for the thermal cores, in this case, the uranium enrichment has been varied and the associated Pu content has been computed.

Enrichment

In Table 6.11, the Pu content is calculated according to the uranium enrichment of each configuration. The Pu vector has been kept the same as the one used in section 6.2.1.

Table 6.11 - Variation of the content of plutonium in $UPuO_2$ SFR fuel.

Configuration	Pu content [%]	U-235 enrichment [%]	Fissile content [%]
Pu-0%	0.0	12.9	12.9
Pu-9.7%	9.7	5	9.9
Pu-12.9%	12.9	2	8.9
Pu-14.7%	14.7	0.25	8.4

The decrease of the U-235 enrichment is compensated by higher Pu content. However, increasing the Pu content, the total mass of fissile needed for the criticality decreases. Indeed, in fast spectrum, Pu-239 and Pu-241 (the fissile isotopes of Pu vector) have higher neutrons generation efficiency, because they are characterised by a higher number of neutrons produced by fissions than U-235. The mean neutrons produced following a fission event are 2.44 by U-235, 2.88 by Pu-239 and 2.95 by Pu-241 [100].

Reactivity feedbacks

In next Table 6.12 and Table 6.13, the Doppler constant and feedback coefficients are summed-up.

Table 6.12 - Doppler constant of SFR core with $UPuO_2$.

Configuration	Doppler constant [pcm]
Pu-0%	-1194
Pu-9.7%	-1275
Pu-12.9%	-1286
Pu-14.7%	-1294

Table 6.13 - Reactivity feedback coefficients of SFR core with $UPuO_2$.

Configuration	Fuel expansion [pcm/K]	Structure expansion (clad + TH) [pcm/K]	Sodium density [pcm/K]
Pu-0%	-0.080	0.030	0.027
Pu-9.7%	-0.105	0.049	0.267
Pu-12.9%	-0.119	0.055	0.353
Pu-14.7%	-0.126	0.058	0.403

The insertion of Pu decreases the Doppler and fuel expansion effect and increases the structure and sodium density effect. With respect to the other actinides, the Pu insertion has a beneficial effect on the Doppler coefficient.

Burn-up reactivity swing

In Figure 6.13, the burn-up reactivity swing is presented, for each analysed configuration. The increase of the Pu content decreases the reactivity swing, thanks to the addition of fertile elements of the plutonium leading to fissile isotopes.

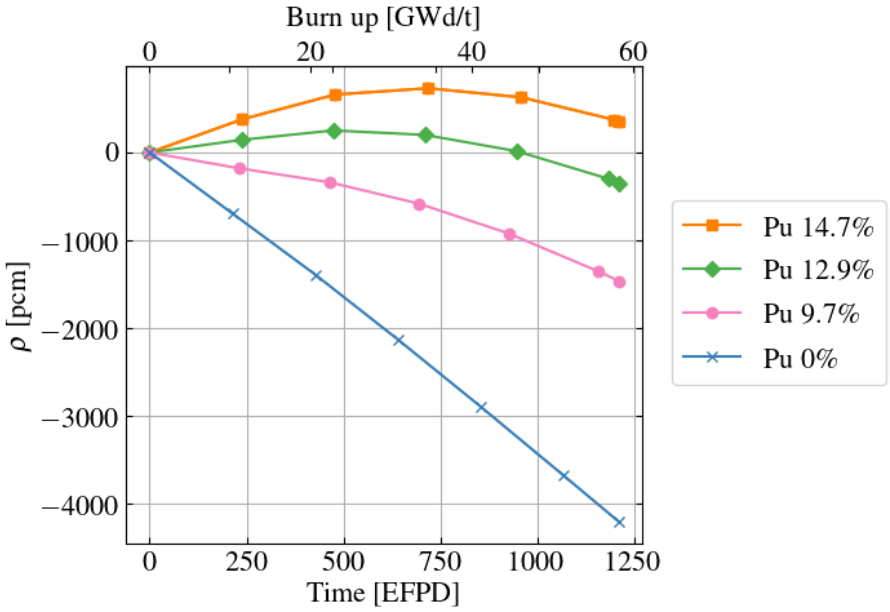


Figure 6.13 - Reactivity evolution according to the variation of Pu content in $UPuO_2$ SFR fuel.

More detailed analysis of the effect of Pu on the reactivity evolution can be found in Annex VI.2.

Power evolution

The simultaneous effect of reactivity swing and reactivity feedbacks variation is computed with the KGH method and the power evolution is presented in Figure 6.14.

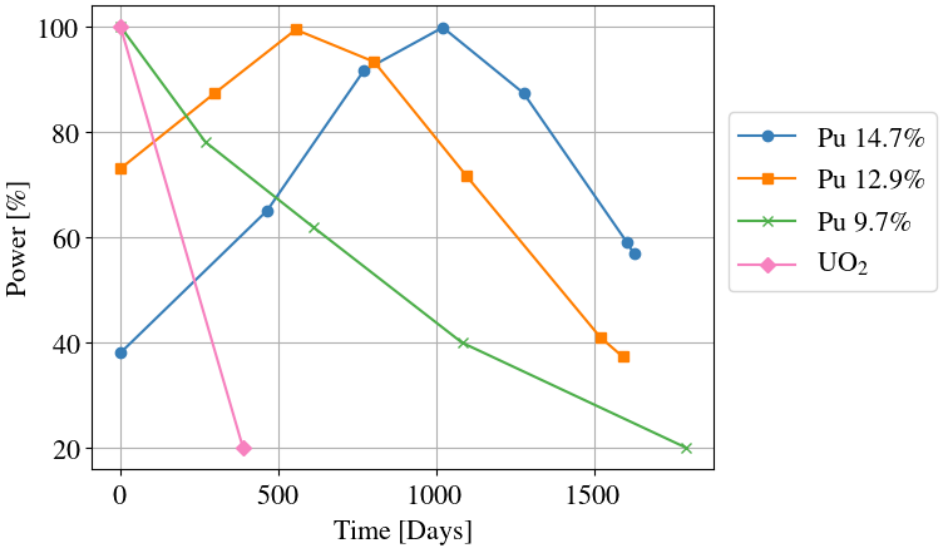


Figure 6.14 - Power evolution of SFR core loaded with $UPuO_2$.

For low content of Pu, the power decreases monotonically, following the reactivity curve. The EOL of the core is achieved when the power reaches 20% of the nominal value. Increasing the Pu content (12.9% and 14.7%), the reactivity increases and then decreases and the power follows this trend. The initial power is lower than the nominal one and reaches the maximum design value at the peak of the curve. No active control is needed for these configurations. The EOL of the core is defined by the achievement of 60 GWd/t of burn-up.

Figure 6.15 allows a comparison between the different configurations.

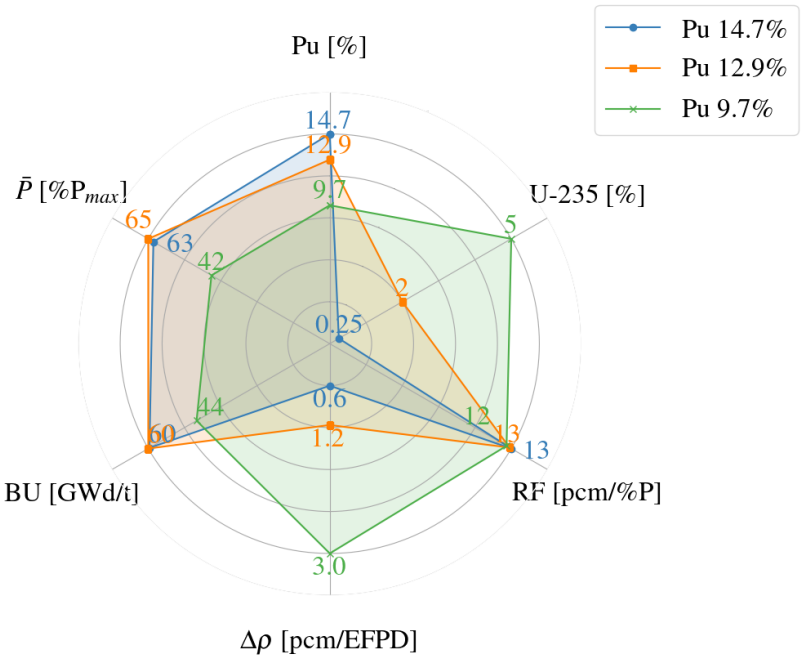


Figure 6.15 - Sum-up of the core performance for different $UPuO_2$ configurations – SFR.

First we focus on core performance, looking at the axes of the mean power ($\bar{P}$) and the burn-up at EOL (BU). For lower Pu content, the increase of Pu increases the burn-up at EOL, up to the saturation at
60 GWd/t, when the reactor is chosen to be shutdown (case Pu-12.9% and beyond). The mean power is increased for lower Pu content and is around 60% for the configurations with Pu higher than 12.9%.

Concerning the physical analysis, the reactivity feedbacks and reactivity loss are compared now. The benefits of the Pu insertion is the small variation of the reactivity feedback effect, corresponding to a large variation of the reactivity swing (1 pcm/%P with respect to the gain of 2.4 pcm/EFPD between the case Pu-9.7% and Pu-14.9%). This is due to the decrease of the fuel effect (Doppler and expansion), which partially compensate the increase of the other effects.

The insertion of Pu in the SFR core allows to find configurations with small U-235 enrichments that can guarantee the criticality at BOL.

6.2.5. Conclusions on actinide insertion in SFR fuel

Inserting actinides in the SFR core allows increasing the lifetime and the burn-up of the reactor. Insertion of Am and Np has similar impact on the core. The progressive insertion of these two actinides decreases the reactivity swing and decreases the main reactivity feedbacks. The reactivity loss decrease allows finding configurations characterised by effective power larger than 55% and EOL burn-up higher

than 55 GWd/t: for instance, Am-5.2%. On the other hand, Pu insertion leads to different impact on the core. Indeed, the increase in Pu content causes a decrease of reactivity swing, but only a very slight degradation of reactivity feedbacks. This allows reaching configurations with an effective power larger than 65% and EOL burn-up of 60 GWd/t.

Figure 6.16 compares the cores with different actinides. The configurations Am-5.2%, Np-5%, Pu-12.9% are chosen for the comparison.

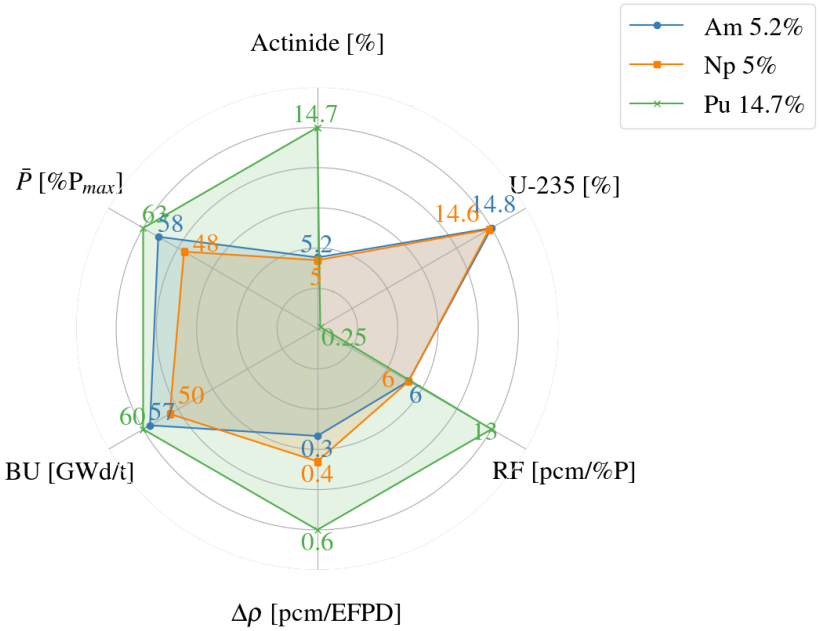


Figure 6.16 - Comparison of core performance loaded with Am, Np and Pu – SFR.

The Am and Np configuration are characterised by similar reactivity swing and reactivity feedbacks. The Pu configuration has about the double of the reactivity loss and the double of the reactivity feedbacks values. So, the burn-up at EOL and mean operation power of the three configurations are of the same order of magnitude and improvements could probably be reached with a fine optimisation calculation. The main difference is that the same core performance can be reached with U-235 enrichments around 14.7% for Am and Np configurations and lower enrichments are needed for the Pu insertion (0.25% in the case of Pu-14.7%).

One can also mention that the impact of the uncertainties of the reactivity loss will be reduced in the Pu case, thanks to a larger reactivity loss over the cycle.

To broaden the analysis of the insertion of actinide in a SFR core like, in the next section, the effect of actinides in a Small Modular SFR (SMSFR) is studied. Indeed, the SFR-V2B core is characterised by a very soft reactivity loss (compared to other SFR designs). It could be interesting to analyse the effect of actinides insertion on a core with larger reactivity loss. For this reason, the study on a Small Modular SFR is proposed in the next section, indeed the geometric leakages on a small core are much more important and increase the reactivity loss reducing the core breeding capability.

6.3. Autonomous SMSFR with actinides

In this section, the insertion of actinides in fuel is analysed on a small size reactor. As presented in Annex VI.3, the core volume variation influences the reactivity (in steady state and autonomous evolution) of fast spectrum cores, while does not cause major variation on the reactivity of thermal spectrum cores. For this reason, insertion of actinides is evaluated also on a small SFR core size (small modular version of the V2B core as described in Annex VI.3.

The core and its main parameters are presented in the next Figure 6.17 and Table 6.14.

Table 6.14 – Sum-up of the SMSFR core characteristics.

Core thermal power [MW]	350
Power density [W/cm^3]	206
Assembly pitch [cm]	13.4
Pins per assembly	127
Pin outer diameter [mm]	9.70
Fissile zone volume [m^3]	1.72

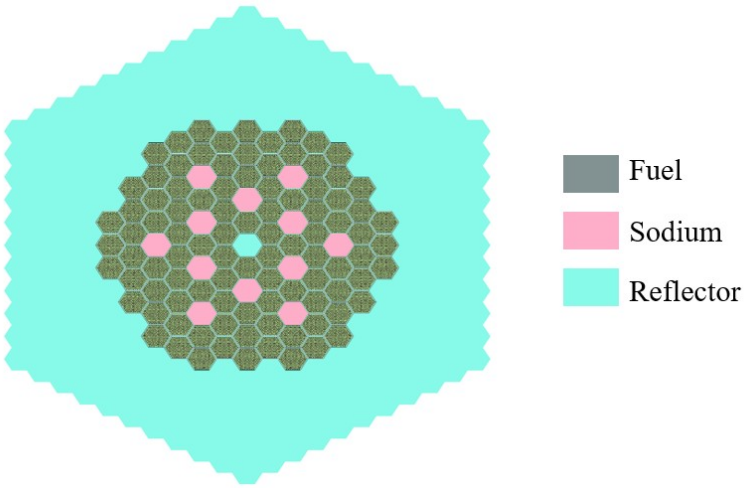


Figure 6.17 - Radial description of SMSFR core.

The americium, neptunium and plutonium insertion in the core is analysed. The same reference values are studied as for the large SFR core and parametric studies are made, varying the actinide contents.

6.3.1. Parametric study on the americium insertion in SMSFR fuel

The insertion of americium in the SMSFR is here analysed, with variable configurations.

Enrichment

In the Table 6.15, americium contents are reported for the different analysed configurations.

Table 6.15 – SMSFR americium insertion configurations.

Configuration	Am content [%]	U-235 enrichment [%]	Fissile content [%]
Am 0%	0	17.33	17.33
Am 5.2%	5.2	19.60	18.58
Am 20%	20	24.58	19.66

Enrichment needed for the criticality of the core at BOL is growing for higher contents of Am because of the insertion of "absorber" isotopes. The need for higher enrichments is due to the substitution of the U-238 with the actinide that has larger capture cross sections.

Compared to the large SFR-V2B core, the need for the U-235 enrichment is higher. For example, in the case of UO_2 fuel (Am-0%), the SFR-V2B has an enrichment of 12.9%, while the SMSFR-V2B of 17.3%. By inserting the Am with a content of 5.2%, enrichment is increased by around 2% for both cores.

Reactivity feedbacks

In this paragraph, reactivity feedbacks are summed up for the different Am configurations. The Doppler constant is presented in Table 6.16, while the other coefficients are summed-up in Table 6.17.

Table 6.16 - Doppler constant of SMSFR core with $UAmO_2$.

Configuration	Doppler constant [pcm]
Am 0%	-830
Am 5.2%	-467
Am 20%	-132

Table 6.17 – Reactivity feedback coefficients of SMSFR core with $UAmO_2$.

Configuration	Fuel expansion [pcm/K]	Structure expansion (clad + TH) [pcm/K]	Sodium density [pcm/K]
Am 0%	-0.229	0.008	-0.245
Am 5.2%	-0.233	0.015	-0.084
Am 20%	-0.251	0.043	0.222

As for the large core SFR, the increase in Am content increases the Doppler, sodium density and structure expansion coefficients. On the other hand, the fuel expansion coefficient is decreased.

Burn-up reactivity swing

The evolution of the reactivity is analysed and shown in Figure 6.18. As in the large SFR core, the increase in the actinide content determines a decrease of the reactivity loss slope. The main difference is in the slope variations. In the large SFR core a nearly flat reactivity was reached with the content of

5.2% of Am in $UAmO_2$ (see Figure 6.5). In this smaller core case, the content needed to flatten the reactivity curve is about 20% of Am.

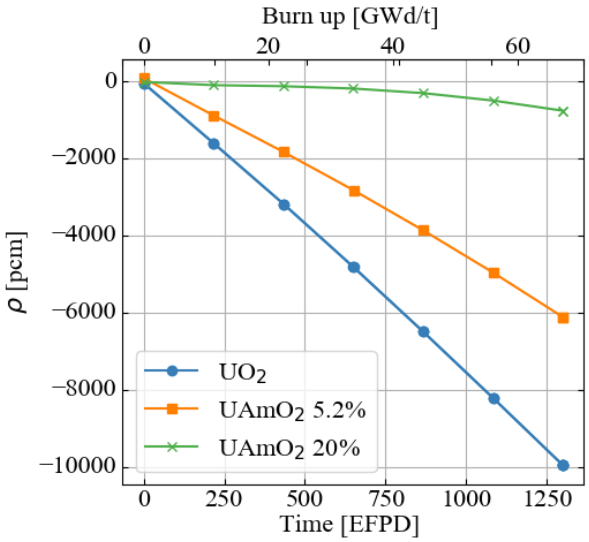


Figure 6.18 - Reactivity evolution according to the variation of Am content in $UAmO_2$ SMSFR fuel.

The reactivity loss decreases with the addition of the minor actinides. The addition of 5.2% of Am causes a reduction of around 40% of the reactivity loss. To double this gain, a content of around 15% is necessary. So the gain in pcm needs more and more actinide content.

Power evolution

The effects of the reactivity swing and reactivity feedbacks are analysed with KGH method. The power evolution is shown in Figure 6.19.

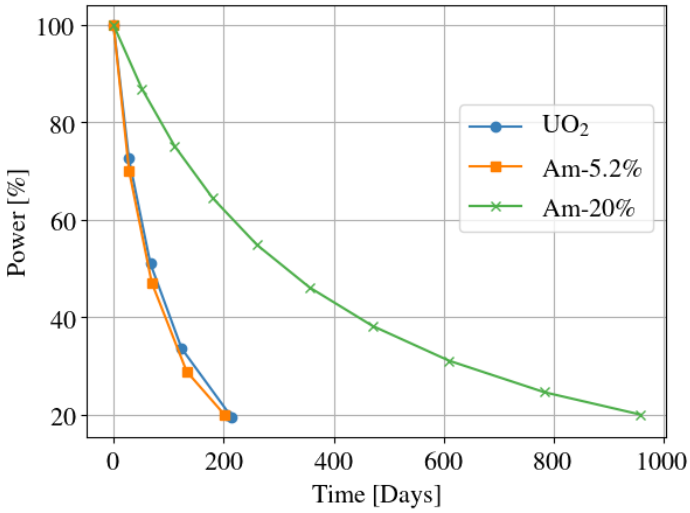


Figure 6.19 - Power evolution of SMSFR core loaded with $UAmO_2$.

The beneficial effect of the reduction of the reactivity loss is almost entirely counterbalanced by the decrease of the reactivity feedbacks for low Am content. The increase of Am content increases the lifetime beyond 900 days for 20% of Am. Increasing further the Am content, a curve of reactivity swing that increases first and decreases later, could be found. However, the feedbacks coefficient will approach zero or even a positive value. Anyway, the Am content and the associated U-235 enrichment presented

here are already large and an optimisation process is considered as a perspective but not implemented in this work.

The core performance is compared in Figure 6.20.

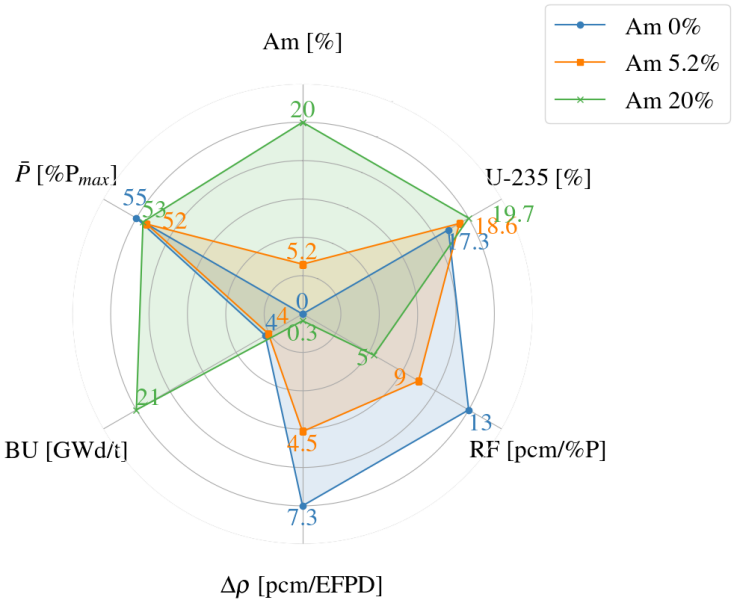


Figure 6.20 - Sum-up of the core performance for different $UAmO_2$ configurations – SMSFR.

First we focus on core performance, looking at the axes of the mean power ($\bar{P}$) and the burn-up at EOL (BU). The larger decrease of the reactivity loss leads to longer core lifetime and fuel burn-up. Anyway, even for high Am content, the performance of such a SMSFR core is lower than the SFR in terms of fuel burn-up (up to 21 GWd/t for the case Am-20%) and mean power (about 50%) due to the fast decrease of the power to 20% of its nominal value. The leaking term is much more penalizing the neutron balance in this small core and does not allow to increase the mean operating power.

The second point to be noticed concerns the physical analysis, shown on the axis of the reactivity feedbacks (RF) and the reactivity swing ($\Delta\rho$). The larger is the Am content, the lower are the reactivity feedback effects and the reactivity swing. For low content of Am (between 0% and 5%), the reactivity loss and the reactivity feedbacks decrease proportionally. Indeed, for Am-5% the reactivity contribution decreases of 31% and the reactivity loss of 38% (with respect to the case Am-0%). On the other hand, increasing the Am content (up to 20%), the reactivity feedbacks contribution decreases of 62%, while the reactivity loss of 96% (with respect to the case Am-0%).

6.3.2. Parametric study on the neptunium insertion in SMSFR fuel

The same study, as the previous one, is made here on $UNpO_2$ fuel.

Enrichment

The enrichment of U-235 is calculated and shown in Table 6.18.

Table 6.18 - SMSFR neptunium insertion configurations.

Configuration	Np content [%]	U-235 enrichment [%]	Fissile content [%]
Np 0%	0	17.33	17.33
Np 5.0%	5.00	19.18	18.22
Np 16.3%	16.3	22.46	18.80
Np 20%	20.0	23.47	18.78
Np 24%	24.0	24.47	18.60

Above 16% of Np, the fissile content is stabilizing: the spectrum gets to an asymptotic value.

Reactivity feedbacks

The reactivity feedbacks associated to the previous configurations are shown in Table 6.19 and Table 6.20.

Table 6.19 - Doppler constant of SMSFR core with $UNpO_2$.

Configuration	Doppler constant [pcm]
Np 0%	-830
Np 5.0%	-476
Np 16.3%	-175
Np 20%	-130
Np 24%	-97

Table 6.20 – Reactivity feedback coefficients of SMSFR core with $UNpO_2$.

Configuration	Fuel expansion [pcm/K]	Structure expansion (clad + TH) [pcm/K]	Sodium density [pcm/K]
Np 0%	-0.229	0.008	-0.245
Np 5.0%	-0.236	0.017	-0.060
Np 16.3%	-0.251	0.035	0.230
Np 20%	-0.255	0.039	0.304
Np 24%	-0.259	0.045	0.378

The same trend of the coefficient is shown for the Np as for the Am insertion, so the decrease of the fuel expansion coefficient and the increase of the others. The penalty on the Doppler is limited after 16% of Np insertion, because the spectrum no longer changes much above this value.

Burn-up reactivity swing

Figure 6.21 shows the reactivity swing for the different Np analysed configurations.

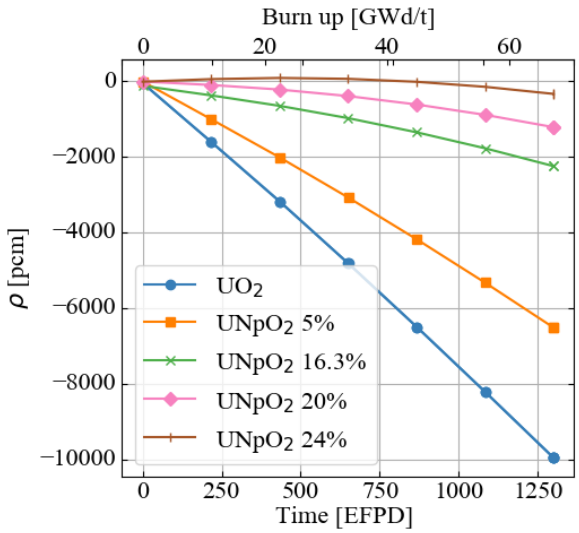


Figure 6.21 - Reactivity evolution according to the variation of Np content in $UNpO_2$ SMSFR fuel.

The reactivity loss decreases with the addition of the minor actinide. The addition of 5% of Np causes a difference of about 4000 pcm at around 1250 EFPD. To decrease the reactivity loss of other 4000 pcm a content of around 16.3% is necessary. So the gain in pcm need more and more actinide content, as it was the case for the Am insertion. The curve that allows to have a flattened reactivity requires a content of around 24% of Np.

Power evolution

The power evolution of the different configurations is shown in Figure 6.22.

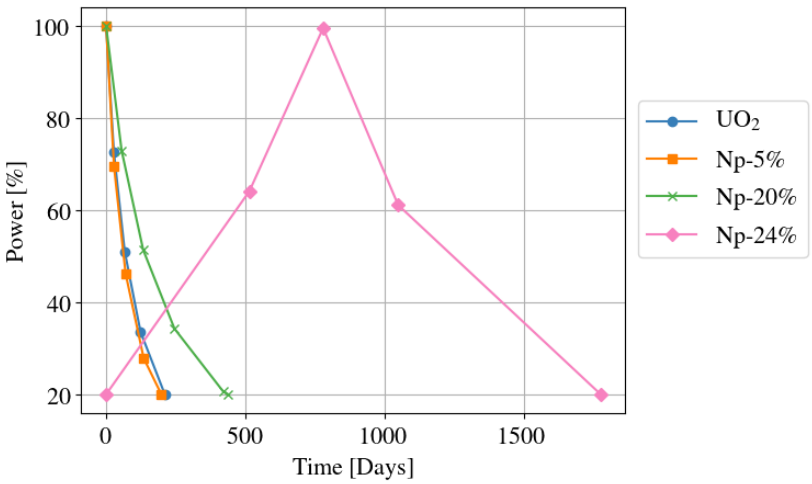


Figure 6.22 - Power evolution of SMSFR core loaded with $UNpO_2$.

The configurations of Np content lower than 20% show a monotonic decreasing power. For higher Np content, the power starts at lower values (20% in the case Np-24%), increases in the first 800 days and decreases up to 1770 days, following the reactivity curves.

Figure 6.23 sums-up the Np core performance.

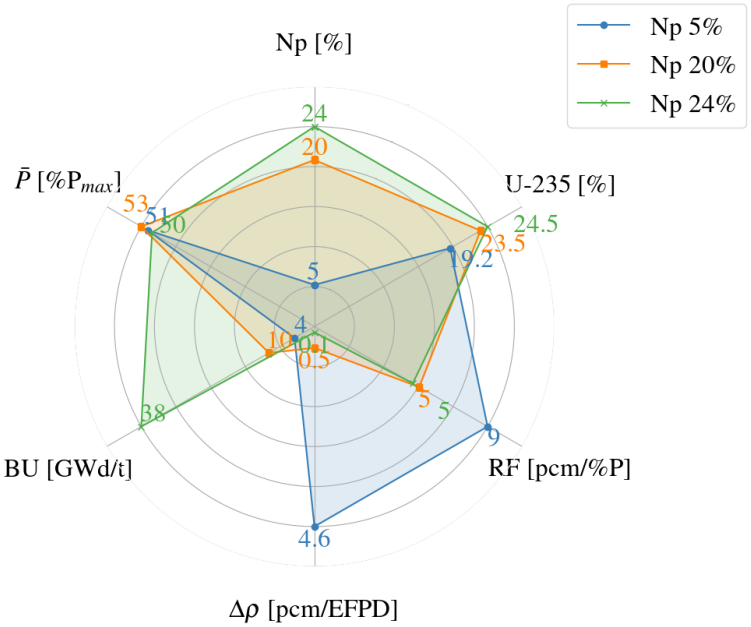


Figure 6.23 - Sum-up of the core performance for different $UNpO_2$ configurations – SMSFR.

First we focus on core performance, looking at the axes of the mean power ($\bar{P}$) and the burn-up at EOL (BU). The Np-24% allows to increase the lifetime and burn-up of fuel (38 GWd/t with respect to 10 GWd/t) with respect to the Np-20% that is characterised by similar reactivity feedbacks and reactivity swings of the same order of magnitude. The mean power is of the same order in the monotonic curve or the increasing-decreasing one. An optimisation process could be applied to find the best reactivity curve to increase the core burn-up.

The second point to be noticed concerns the physical analysis, shown on the axis of the reactivity feedbacks (RF) and the reactivity swing ($\Delta\rho$). The insertion of Np in the core decreases the reactivity swing and the reactivity feedbacks, as in the case of large SFR. The configuration of Np-24% shows a power behaviour that increases and then decreases, with respect to the Np-20% that is monotonic decreasing.

6.3.3. Parametric study on the Np and Pu insertion in SMSFR fuel

As it is well known that a flatten reactivity loss curve will be not possible on a SMSFR only with classical plutonium vector, it could be interesting to analyse the case of lower content of Am and Np and the addition of the Pu to compensate the remaining reactivity loss. For example, the case of Np 5% has been studied with the addition of Pu. The Pu vector used is the one taken as reference in this work and described in Paragraph 5.3.1. The approach has been the one used for the insertion of the plutonium in the fuel in this work. The uranium is considered as the same as the depleted one (0.25% enrichment), the Np content is fixed at 5% and the Pu content is adjusted to ensure criticality at BOL.

Enrichment

The two configurations are summed up in Table 6.21.

Table 6.21 - SMSFR neptunium and plutonium insertion configurations.

Configuration	Np content [%]	U-235 enrichment [%]	Pu content [%]
Np 5.0%	5.0	19.2	0
Np 5.0% Pu	5.0	0.25	20.6

Reactivity feedbacks

The reactivity feedbacks associated to the configurations are shown in Table 6.22 and Table 6.23.

Table 6.22 – Doppler constant of SMSFR core with neptunium and plutonium.

Configuration	Doppler constant [pcm]
Np 5.0%	-476
Np 5.0% Pu 21%	-565

Table 6.23 - Reactivity feedback coefficients of SMSFR core with neptunium and plutonium.

Configuration	Fuel expansion [pcm/K]	Structure expansion (clad + TH) [pcm/K]	Sodium density [pcm/K]
Np 5.0%	-0.236	0.017	-0.060
Np 5.0% Pu 21%	-0.290	0.048	0.360

As shown in the case of large SFR, the insertion of Pu in fuel causes a decrease of the Doppler and fuel expansion coefficient and an increase of the structure and coolant expansion ones. The sum of the coefficients G+H is -9 pcm/%P in the case of Np and -11 pcm/%P in the case of Np-Pu.

Burn-up reactivity swing

In Figure 6.24, the reactivity swing is shown.

The combination of the two actinides (Np and Pu) is possible and allows to reduce the reactivity loss. The content of 5% of Np needs an insertion of around 20% of Pu for the criticality at BOL. The reactivity slope is reduced but this specific configuration is not optimised. Adjustment on the ratio between the Np and Pu content could be made to improve the reactivity loss. Furthermore, the Pu vector taken as reference could be varied to increase the contribution of the Pu to the reactivity loss decrease. The optimisation of this configuration is considered as a perspective to evaluate the neptunium content needed, but will not be analysed in detail in this work.

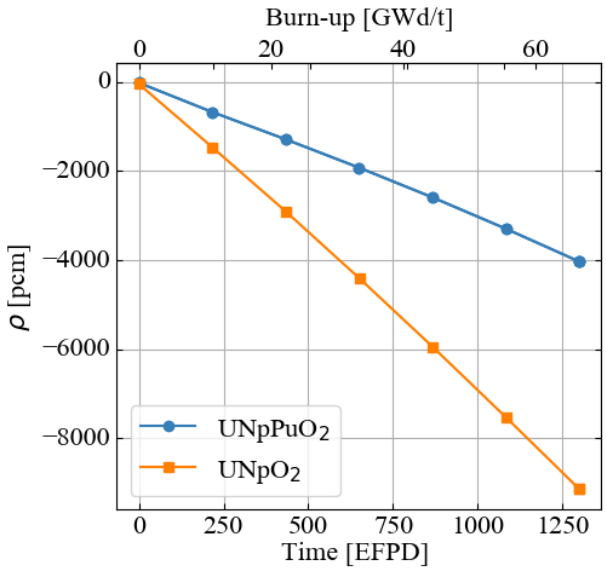


Figure 6.24 – Reactivity evolution according to the Np and Pu insertion in SMSFR fuel.

Power evolution

The power evolution of the two configurations is shown in Figure 6.25.

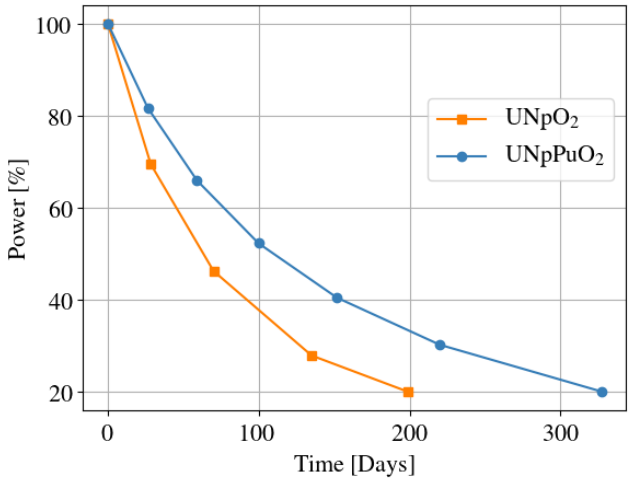


Figure 6.25 - Power evolution of SMSFR core loaded with $UNpPuO_2$.

The insertion of Pu in Np configuration is beneficial for the core performance. The insertion of 20% of Pu increases the core lifetime of about 120 days and the burn-up of the fuel of about 4.4 GWd/t. Anyway, further calculations should be made to optimise the configuration.

6.3.4. Conclusions on actinides insertion in SMSFR fuel

The configurations of Am and Np have been analysed in a Small Modular SFR, as summed-up in Figure 6.26.

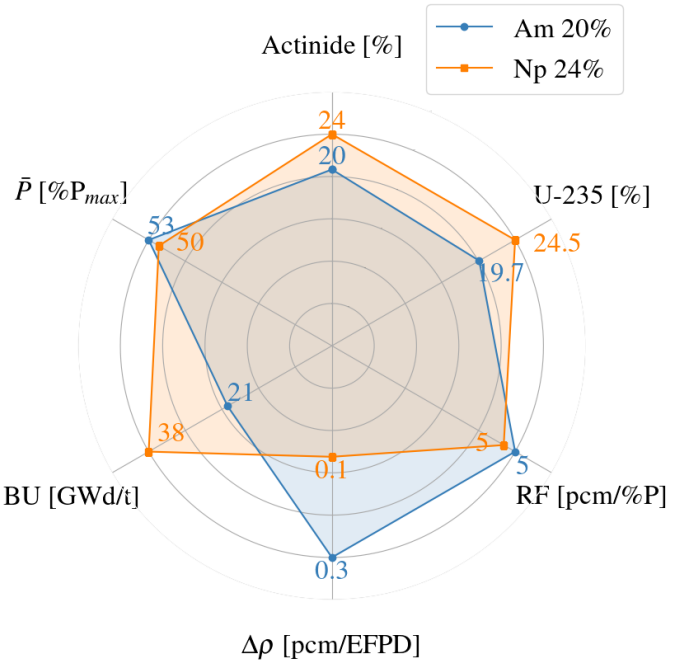


Figure 6.26 - Comparison of core performance loaded with Am and Np – SMSFR.

The insertion of the two actinides has a similar effect on the autonomous core. The reactivity feedback effects are degraded, but the reactivity swing is improved. The case of Np is better than the Am in terms of lower reactivity loss and burn-up of fuel at EOL because of the insertion of higher Np content that causes the reactivity curve to increase in a first period and decrease in a second one, so decreasing the reactivity swing. The increase of the Am content could be explored and is expected to show the same trends in the results. A work of fine optimisation is expected to increase the performance. Anyway, in the two cases, the U-235 enrichment is already considered elevated (20%) and higher values are considered not possible regarding proliferation and HALEU limitations.

The addition of Pu is considered as a possibility to increase the core performance. It decreases the U-235 enrichment needed, it increases slightly the reactivity feedbacks and it decreases the reactivity loss. A fine work of optimisation could find the best configuration to maximise the performance of such a core. However, and as expected, the performance of such a small fast core is more difficult to improve compared to a large core. Similar performance would be difficult to obtain only with actinide insertion.

6.4. Discussion on burnable poison in SFR

Usually in SFR, burnable poisons (BP) are not considered due to the too low cross sections in fast spectrum. Anyway, in literature, some possible designs have been proposed for the insertion of BP in fast cores. The work of Guo [41] proposes an optimisation of a configuration for burnable poisons in V2B core. The BP assembly is composed of B_4C pins and $ZrH_{1.72}$ pins to moderate neutrons and increase the BP efficiency.

The framework of the study includes a core fuelled by batch of the duration of 400 EFPD and MOX fuel. The difference with this work is that the core foresees a cycle of refuelling. Furthermore, the configuration of the burnable poisons has been optimised for the configuration of the core fuelled heterogeneously by MOX. The poisoned configuration is optimised with a, both axial and radial, heterogeneous geometry.

As the optimisation process to define an efficient burnable poison for a specific core is time consuming, it is proposed in a preliminary approach to test the multi-batch core defined in the study from Guo et al. [41]. If performance of a single cycle is promising, the search of dedicated BP to autonomous reactor needs could be seen as a perspective of this work.

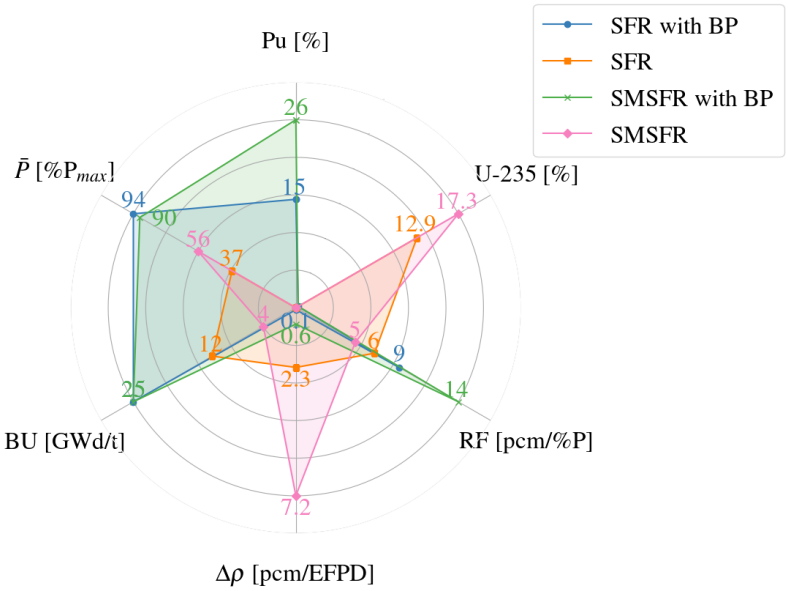


Figure 6.27 - Comparison of core performance loaded with optimised configuration of BP from literature – SFR.

Figure 6.27 shows the performance of the insertion of BP in optimised configuration. The large and small cores are compared between the ones with burnable poison and loaded with MOX and the ones without BP and loaded with UO_2. The BP configurations show larger reactivity feedbacks and a very low reactivity loss (thanks to the optimisation of the configuration). This could lead to a burn-up of 25 GWd/t with a very large mean power (corresponding to one cycle of this multi-batch core).

The BP could be potential candidates to increase the autonomous SFR performance. However, their application requires specific configurations design with heterogeneous geometries. Furthermore, the possibility to design efficient BP for such 1-batch cores has to be demonstrated. It is considered as a perspective of the work but not included in this preliminary study.

Up to now, methods headed for the decrease of the reactivity loss are analysed. The increase of the reactivity feedbacks is useful to increase the core lifetime. Anyway, it would imply a deep modification of the core design. For comparison, in the next paragraph, a specific core is analysed, designed with the objective of increasing the Doppler effect.

6.5. CADOR core

In literature, some methods to increase the reactivity feedback effects have been proposed for the SFR cores. This section analyses the operation of an autonomous core, with a design that increases the Doppler reactivity feedback, as one of the main components acting in an autonomous operation.

The CADOR [106] core is an example of a possible SFR design with an important increase of the Doppler effect. The approach is based on the principle of "inherent safety" to avoid core meltdown accident when prompt reactivity insertion is considered. The main objective of the CADOR concept was to increase the Doppler integral between nominal power and the fuel melting point to preclude this type of accident.

Two approaches are possible to increase this Doppler effect: the softening of the neutron spectrum (to increase the number of neutrons passing through resonances) and the increase of the fuel temperature variation between nominal and maximum allowable temperature (Doppler integral). The CADOR concept combines both methods.

To enhance Doppler integral, the nominal fuel temperature at nominal power is to be lowered. This is done by a lower the linear heat rating, increasing the assemblies height. The softening of the spectrum is achieved by inserting Beryllium pins with a volume that represents a compromise between the increase of the Doppler Effect and the advantages of fast spectrum (such as breeding capability or reactivity loss during fuel burn-up).

In this section, the CADOR core is analysed following the methodology illustrated up to now, except that only the Doppler effect increase is kept: the fuel temperature is not reduced. It is loaded with UO_2 and the enrichment is calculated to ensure criticality at BOL.

Enrichment

Two configurations of CADOR are explored, corresponding to a large and a small core. The first characterised by 3600 MWth and the second by 400 MWth. Table 6.24 sums-up the initial U-235 enrichments of the two configurations.

Table 6.24 – CADOR and SFR-V2B comparison of UO_2 configurations.

Configuration	U-235 enrichment [%]
CADOR-3600	13.9
SFR-V2B-3600	12.9
CADOR-400	19.4
SMSFR-V2B-350	17.3

The needed enrichment is slightly higher than the V2B SFR and SMSFR. Indeed, the spectrum is slightly thermalized and the insertion of beryllium in CADOR increases the neutron captures at BOL.

Reactivity feedbacks

The reactivity feedbacks of the two configurations are summed up in Table 6.25.

Table 6.25 - Reactivity feedback coefficients of CADOR core.

Configuration	Doppler coefficient [pcm/K]	Fuel expansion [pcm/K]	Structure expansion (clad + TH) [pcm/K]	Sodium density [pcm/K]
CADOR-3600	-1.40	-0.10	0.09	0.25
CADOR-400	-1.07	-0.14	0.07	-0.08

The Doppler effect is increased with respect to the SFR-V2B and SMSFR-V2B.

Burn-up reactivity swing and power evolution

The reactivity loss of the two configurations shows a linear trend. The coefficient of the slope of the curve is shown in Table 6.26, compared to the V2B cores.

Table 6.26 – Reactivity loss comparison between CADOR and V2B cores.

Configuration	Reactivity loss slope [pcm/EFPD]
CADOR-3600	-8.2
SFR-V2B-3600	-2.3
CADOR-400	-12.6
SMSFR-V2B-350	-7.2

The CADOR configurations show larger reactivity loss than the V2B. But on the other hand are characterised by larger reactivity feedbacks. The concurrent effects on the reactivity are accounted with the KGH method. In Figure 6.28, the power evolution of the autonomous cores is shown.

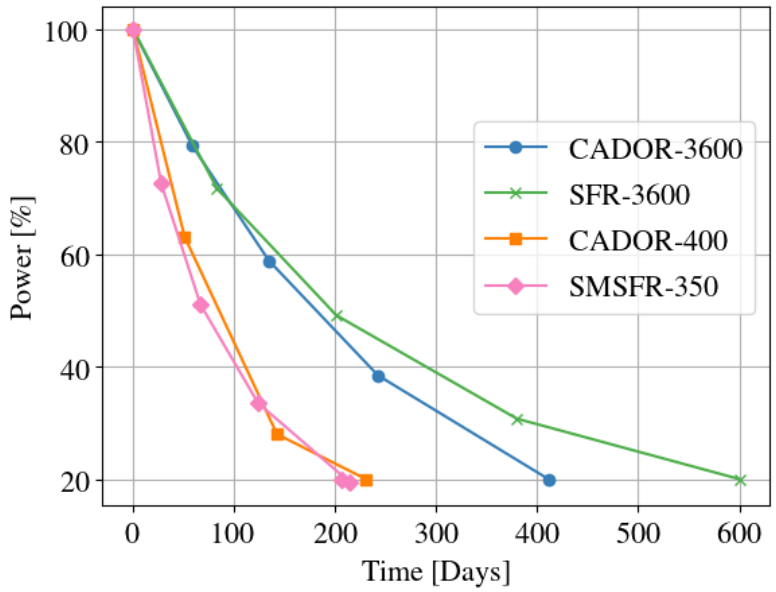


Figure 6.28 - Power evolution comparison between CADOR and V2B cores.

The power evolutions of the two large and small cores are respectively comparable. The radar graph of Figure 6.29 compares the parameters of the configurations.

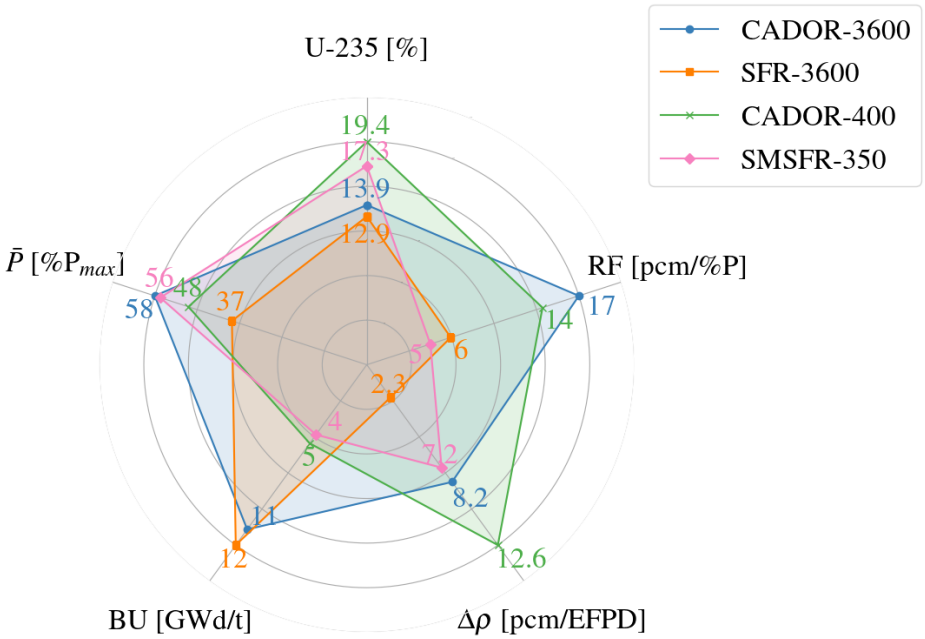


Figure 6.29 - Comparison of CADOR and V2B core performance.

The enrichment needed for small size cores (SMSFR-350 and CADOR-400) is higher than those needed for larger ones, due to enhanced neutron leakage. The CADOR cores show increased reactivity feedback integrals (of the order of 14 and 17 pcm/%P) with respect to the SFR configurations (of the order of 5 and 6 pcm/%P). On the other hand, the reactivity loss of the CADOR cores are higher than the SFR configurations, following an equivalent ratio.

Comparing the two largest size configurations (CADOR-3600 and SFR-3600), the reactivity feedback of the CADOR are 2.8 times larger than SFR, while the reactivity is 3.6 times larger. The lifetime of the SFR is longer of about 180 days while the fuel burn-up is comparable (slightly larger). The mean power is slightly larger in the CADOR core.

The two smaller configurations are CADOR-400 and SMSFR-350. The CADOR is characterised by reactivity feedback integral 2.8 times larger than SMSFR, but also 1.75 times the reactivity loss. The core performance is comparable.

In conclusion, the effort to increase the reactivity feedback coefficients in SFR by softening the spectrum seems to produce results comparable to the ones of the reference design. The benefits on the reactivity feedbacks is counterbalanced by the penalties on the reactivity loss.

6.6. Conclusions

This chapter presents a detailed analysis of the insertion of actinides and burnable poisons in sodium-cooled fast reactors. The study is divided into three steps. Firstly, the effect of the insertion of americium, neptunium, plutonium and thorium is analysed in 3600 MWth SFR and in 11 MWth SMSFR. Secondly, the theoretical possibility to insert burnable poisons in a fast spectrum core is discussed. Finally, design modifications have been considered in order to discuss the possibility of increasing reactivity feedbacks to enhance core performance.

The results of the first study highlight the increase of the core lifetime with the insertion of actinides. Thorium configuration has been discarded since performance is not improved noticeably even with a

large thorium content. The other configurations are studied, varying the content of actinides. The study highlights the following features:

- the need for higher U-235 enrichments for higher actinide content (except for the Pu case, that already contains fissile isotopes);
- the reduction of the reactivity swing with the insertion of the actinides;
- the decrease of the Doppler Effect with the insertion of Am and Np. The fuel expansion reactivity coefficients are decreased and the structure and coolant expansion coefficients increases, with the insertion of all the isotopes.

The cases for each isotope on reactivity swing have been compared (see Figure 6.16). To sum-it up, the Am-5.2% case shows a burn-up of 57 GWd/t and an average power of 58%. The Np-5% case is characterised by a burn-up of 50 GWd/t and an average power of 48%. Finally, the Pu-14.7% case leads to a burn-up of 60 GWd/t and an average power of 63%. Further studies could be done in order to optimise these configurations. The Pu case still seems to be more promising in terms of performance, as it shows a lower need for U-235 enrichment and higher reactivity feedback effects.

In terms of U-235 enrichment, in the analysis of the thermal spectrum reactor, a criterion is set on the feasibility of the fuel chosen for the reactor. Based on the HALEU criterion (maximum U-235 enrichment of 20%), the configurations above 25% are considered not reachable and so need to be excluded in the final choice in this work. The value of 25% is chosen, slightly higher than the HALEU to account for margin for further fine optimisations on these configurations. In this analysis of fast spectrum cores, all the cases are below the HALEU limit.

The use of the ECS to improve performance has also been quantified. In Figure 6.30, the Pu case is analysed with the contribution of the secondary system. It is shown that it would be possible to reach the maximum burn-up while increasing the mean power from 63% to 76%. This contribution is however theoretical and if technologically achievable would necessarily lead to a strong reduction of the reactor efficiency. Theoretical calculations have been made on the reactivity values, while the simulations of the ECS by CYCLOP could compute the efficiency of the system on a 15% of power variation.

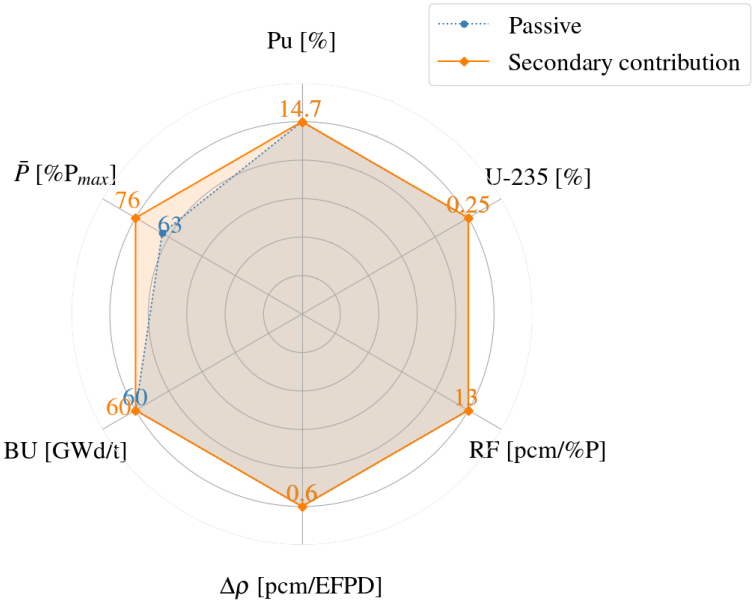


Figure 6.30 – Comparison of SFR $UPuO_2$ performance with the possible contribution of the ECS.

In a second part, design variations have been studied to assess the possibility to manage the reactivity loss. The same study has been made with a 350 MWth Small Modular SFR (SMSFR). The study highlights the same trend as the large SFR with the insertion of actinides. A comparison between the SFR and SMSFR is made in Figure 6.31 for the case of Np.

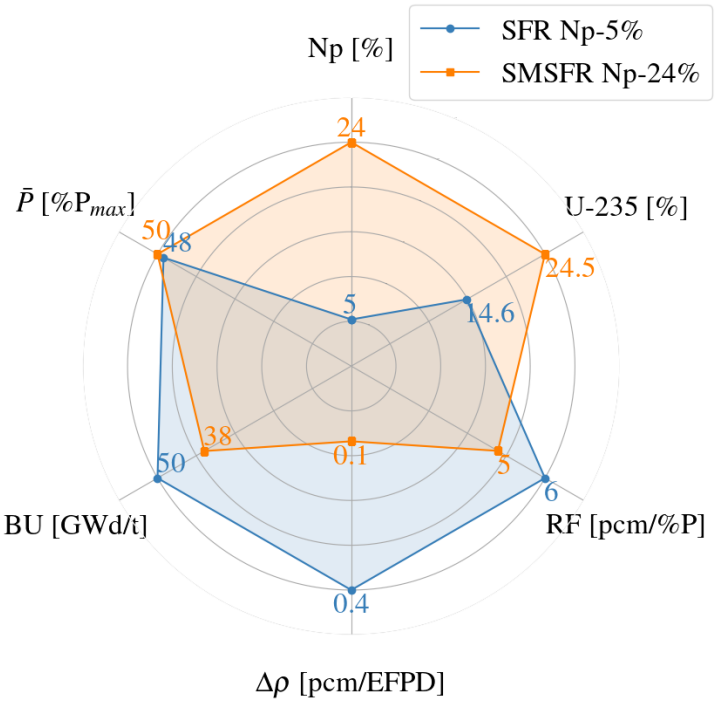


Figure 6.31 - Comparison of SFR and SMSFR core performance loaded with Np.

The comparison highlights that, in order to obtain comparable mean power and quite comparable burn-up at EOL (50 GWd/t for the SFR and 38 GWd/t for the SMSFR), SFR needs lower both Np content and U-235 enrichments. Such different configurations (Np-5% for the SFR and Np-24% for the SMSFR) lead to similar reactivity feedback effects and reactivity loss. Indeed, the physics of a small core is largely influenced by the level of neutron leakage.

Insertion of burnable poisons has been considered, but with respect to the thermal cores, they are less efficient in fast spectrum systems. Anyway, in literature, a proposition is made to insert Boron together with ZrH in dedicated assemblies of in SFR MOX core. The effect of local neutron moderation leads to reduce the relativity swing, considering refuelling every 400 EFPD. The performance of such a core is comparable to the ones obtained with the insertion of actinides. But, the insertion of BP in SFR requires a specific radial and axial heterogeneous optimization of the design and is considered in a core refuelled per batches. A homogenous insertion of BP in fuel would not provide a significant effect on the power on the lifetime of the core, so compared to the actinides, the BP needs more specific studies. In this work, such an optimisation is not analysed and considered as a perspective.

Finally, the comparison with a core characterised by increased reactivity feedback effects is made. The reference core is based on the CADOR concept, considered in two configurations: 3600 MWth and 400 MWth. The results are compared to the design of the SFR and SMSFR, loaded with UO_2. The results highlight that the effort to increase the reactivity feedbacks leads to an increase in the reactivity loss. The performance of the autonomous cores are comparable. For this reason, the effort in the reduction of the reactivity loss is considered as a better way to increase the autonomous core performance.

Conclusions and perspectives

7.1. Conclusions

The growing concern about climate change has led to the need of moving towards carbon free energy sources. In this context, the energy mix tends to the elimination of the fossil fuels and the increasing introduction of renewable source of energy in the global mix. In this framework, the nuclear energy sees its role changing. The NPPs have adopted more and more the role of accommodating the variation of the grid needs, to substitute gradually the fossil fuel plants. For this reason, the design and operation have been made more and more complex with the addition of systems for active control and load-following optimisation. This thesis is positioned backwards and investigates the possibility to simplify the reactor design. The load-following objective is set aside and a methodology to reach a design of an "autonomously operated" reactor is proposed. The objective is a reactor as an energy source, which is connected to the grid or to specific applications, switched on and produces energy autonomously.

An "autonomous reactor" has been defined as a reactor that is started-up, left to its own autonomous evolution and shutdown at the end of life. Except for start-up and shutdown, no control system at the primary side is activated during operation. In other words, the fuel initial content is chosen to have a null reactivity at BOL. The physics of such a reactor is characterised by a core that produces a power driven by the coupled effects of fuel depletion and reactivity feedbacks. The study is focused on the core physics and thus a physical model has been implemented to study the reactivity and power evolution of such reactor. It is based on an adiabatic method that couples the neutronic and thermal-hydraulic fields, known as KGH.

The approach is based on the choice of some reactor designs in literature in order to perform qualitative and quantitative comparisons between them in terms of autonomous operation. In the literature context, the choice was made to start the analysis from the micro-reactors category, for their simplified and enhanced autonomous characteristics. The Heat Pipe Reactor (HPR) and High Temperature Reactor (HTR) have been chosen accordingly. They have been compared, to some extent, to the industrial size reactors such as Pressurized Water Reactor (PWR) and Sodium-cooled Fast Reactor (SFR).

Two parameters have been identified as governing the power of an autonomous core: the burn-up reactivity swing and the thermal reactivity feedbacks. The reactivity feedbacks are driven by the core power variation or the control over the cooling system. Two approaches are possible for this kind of problem: an integrated approach taking into account simultaneously the core evolution and the ECS control, or a simplified approach done by an individual analysis of each contribution. The first approach is more complex and time-consuming, as it requires to build a detailed coupled system. The main focus of this work is to deeply understand the impact only based on core modifications. The second approach was then chosen. The potential contribution of the ECS has been analysed independently. The maximum possible gain on the performance has been assessed, considering a theoretical control on the ECS system. Then Rankine and Brayton cycle have been designed and coupled to PWR and SFR. The efficiency and related electric produced power have been calculated and compared. Once the ECS possible contribution

has been quantified, the problem has been simplified by considering a constant core inlet temperature and the focus has been set on the core autonomous behaviour.

The approach consists in considering the reactivity feedbacks bounded to the core power evolution and compare them to the burn-up reactivity loss. An initial comparison shows that the HPRs are characterised by enhanced autonomous features, as the primary cooling system based on natural circulation. On the contrary, they are characterised by a very limited flexibility of possible operation due to their cooling system and thus they are limited to operating at very low power densities. Although it is recognised that this type of reactor may be useful for specific applications (such as space applications), the design is not extendable to a more general large power application. For this reason, this design has been set aside and the HTR, PWR and SFR have been considered. In order to compare the remaining cores, some quantified estimators have been compared to assess the reactivity contribution due to power variation and fuel depletion:

- RF [pcm/%P] as the reactivity feedback integral between 20% and 100% of nominal power. The core inlet temperature is considered constant. It quantifies the impact of the feedback coefficients. To facilitate the reading, it is expressed in pcm by percent of nominal power (considering a linear variation);
- $\Delta\rho$ [pcm/EFPD] as the maximum range of reactivity variation during the core lifetime (with a limit of 20% of nominal power or 60 GWd/t).

Then, performance estimators have been built. They give an overview of the service that can bring the reactor in terms of energy produced and power provided over time:

- BU [GWd/t] as the average burn-up reached at the end of life;
- $\bar{P}$ [%Pmax] is evaluated as the average power of operation during the lifetime considered;

The core "autonomous behaviour" is characterised by much lower performance than when actively operated. Consequently, the insertion of actinides and burnable poisons have been considered to increase the performance. Such modifications have a noticeable impact on the fuel, so two more estimators are needed:

- Actinide [%] is the content of actinide inserted in the core;
- U-235 [%] is the U-235 enrichment to reach criticality a BOL, the cores with enrichment lower than 25% has been considered feasible. Indeed, a further optimisation of the design could reduce the enrichment to the HALEU limit of 20%.

Finally, a dedicated estimator has been added to quantify the possible contribution of the secondary system:

- $\Delta\rho_{ECS}$ [%] is the theoretical maximum reactivity "gain" possible by the control over the secondary system), characteristic of different reactor technologies. It is expressed in pcm and normalised by the pcm loss due to burn-up during the autonomous core lifetime.

The cores studied in this work are characterized by thermal or fast spectrum. Thermal reactors generally exhibit larger reactivity feedbacks with respect to fast reactors. On the other hand, fast reactors are characterised by lower reactivity loss due to fuel depletion than thermal ones. Based on that observation, it was decided to study thermal and fast reactors separately as their respective physics is different and then to compare the viable solutions of the two. A particular effort is made to improve the

reactor performance decreasing the reactivity swing due to fuel depletion with the insertion of actinides or burnable poisons in the fuel.

In the case of thermal reactors, significant insertion of actinides or burnable poison has as major consequence a neutron spectrum hardening. This spectrum shift has two main consequences: the decrease of Xenon effect and a higher fissile content needed to be critical at BOL. The latter leads to a global decrease of both reactivity loss and reactivity feedbacks. It is observed that the combined effect leads to a global performance increase. In other words, the decrease of reactivity loss due to depletion prevails on the decrease of reactivity feedbacks. However, for an equivalent spectrum hardening, the effect on the reactivity evolution still depends on the isotopes inserted at BOL.

Among the possible actinides available in literature, the americium shows the most promising performance increase, due to its large reactivity swing reduction effect. The neptunium increases the performance but it is less efficient than americium, because it is characterised by a threshold effect on reactivity loss reduction. The thorium and plutonium cases do not significantly increase the performance in thermal spectrum, indeed their effect on the core reactivity is lower than the previous ones Concerning the burnable poisons, the boron has been initially considered in thermal spectrum, but the study highlight that its kinetic of disappearance is too fast for the compensation of the reactivity loss due to fuel depletion. Among the burnable poisons in literature, the dysprosium is the one showing a slower kinetic than boron. For this reason, it shows larger performance in autonomous cores, comparable to the actinides ones. In the end, the americium and dysprosium elements are the most promising to maximize core performance.

In the case of fast reactors, only the case of actinides insertion has been studied. Actually, burnable poison are not that effective in fast spectrum when inserted without any explicit optimization. A study from the literature in which such optimization has been done is taken as reference to assess the expected performance for burnable poison insertion. It shows that it can provide good autonomous performance, but with a fine optimisation process on the core design. Indeed, the effect of BP homogeneous insertion is not efficient enough to reach our initial goal. When it comes to actinide insertion, the initial enrichment necessary to have a critical core at BOL is higher due to the increase of neutron captures. The global effect is a decrease of the reactivity loss due to a compensation between the fissile depletion and the actinide consumption, and a decrease of the reactivity feedbacks contribution (except for plutonium insertion). Again, the performance is increased, meaning that the effect of fuel depletion prevails.

Among the possible actinides available in literature, the americium shows again promising performance increase, due to its large reactivity swing reduction effect. In fast cores, the neptunium has a behaviour similar to the americium one. Anyway, this preliminary analysis shows slightly lower performance in this second case, a fine optimisation study could determine the precise difference between the two performance values. The thorium has been discarded as it provides lower performance than the others. Finally, the plutonium has been identified as the most promising of the analysed actinides as it allows to decrease the reactivity loss and increase slightly the Doppler coefficient.

Also the impact of the reactivity feedback coefficients has been assessed. For the thermal reactors, the two analysed cores are characterised by different thermal spectra. The HTR is characterised by lower energy spectrum than PWR. The analysis highlights that the more the spectrum is thermalized, the larger are the reactivity feedbacks, but this does not result in an increase of autonomous performance. For the fast cores, the SFR has been analysed in a special configuration designed to increase the reactivity feedback effects. The autonomous operation of such a configuration does not show increased

performance, confirming that the reactivity loss reduction is more determinant on autonomous behaviour than reactivity feedbacks increase. As it will be mentioned in the perspectives, it could be interesting to study a PWR with a slightly hardened spectrum (under-moderated PWR [108]), which would characterise the behaviour of an intermediary core between thermal and fast ones. It could be interesting to assess the effect of the reactivity loss reduction and contemporary reactivity feedbacks reduction (hardening the PWR spectrum) and to compare it to a fast SFR core.

A comparison of all promising core configurations is done with americium in HTR and PWR and plutonium in SFR in Figure 7.1. Further investigations could also be interesting loading PWR with Dy that seems to give possible interesting performance and varying the Pu vector in SFR to optimise the configuration.

The comparison here is made considering configurations leading to a burn-up of 60 GWd/t while satisfying the requirement of U-235 enrichment as close as possible of 25% in order to stay in range of HALEU fuels (feasibility concern).

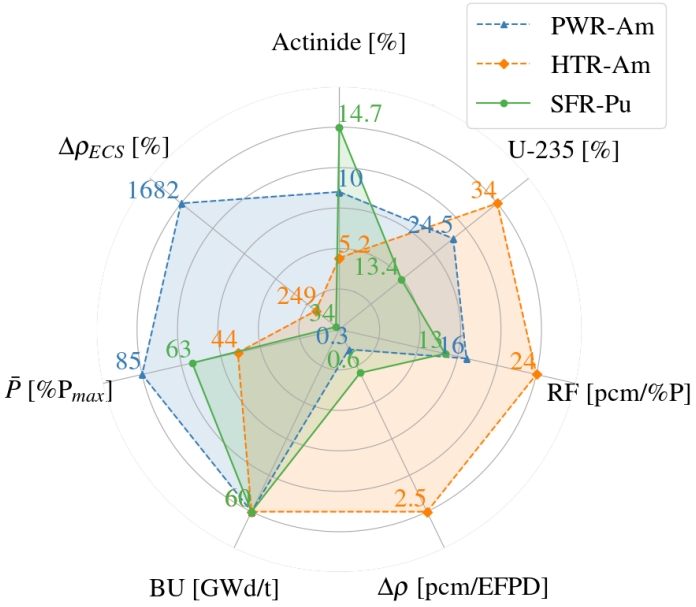


Figure 7.1 – Comparison of HTR-Am, PWR-Am and SFR-Pu autonomous cores.

Globally, looking at the axis of the burn-up at EOL and the mean power of operation, for the same burn-up of fuel, the mean power is the highest in PWR (85%), is 63% in SFR and the lowest in HTR (44%), as a larger reduction of reactivity swing can be reached in PWR and SFR with respect to HTR. The specific economic analysis is not performed, but the analysis of the burn-up axis gives information of the efficiency of the fuel utilisation and thus an indication of the fuel cost. On the other hand, the mean power is the equivalent of a lifetime averaged capacity factor and gives an indication of the capital cost of investment of the reactor (in terms of $/kWh of energy produced). This means that for the same burn-up of 60 GWd/t, the power generation capital cost (represented by the mean power of operation) will be the lowest in the case of PWR and the highest in HTR.

Then a comparison of the physical parameters is made here, in terms of reactivity feedback and burn-up reactivity swing. The reactivity feedback integral is larger in the thermal spectrum. In particular the HTR shows the highest reactivity feedback effect. On the other hand, the reactivity loss is larger in HTR and lower in PWR and SFR.

Then, the theoretical contribution of the ECS is compared. The secondary system of thermal reactor can give a theoretical contribution larger than SFR, due to the larger reactivity feedback coefficient. Indeed, the control of the ECS of a PWR-Am configuration could insert reactivity level in the core that allows to guarantee about 1700% of the core lifetime. The HTR-Am configuration could be maintained at constant power by managing the secondary system control up to 249% of the lifetime. Finally, it can be seen that the SFR could be maintained at constant power for approximately the 34% of its lifetime. This indicates that it could be very interesting to exploit a control on the ECS in thermal reactors, while it would potentially result in a less significant performance increase in fast reactors. With a deeper analysis, the ECS efficiency has been calculated with the tool CYCLOP. Anyway this calculation is possible only in a limited power variation range (15%), beyond that, a proper feasibility and impact study would be required.

From the fuel point of view, the HTR needs the highest content (34%) due to its most thermalized neutron spectrum. On the other hand, the same burn-up can be reached with an enrichment below the limit of 25% in PWR and SFR. For the SFR, the U-235 enrichment is noticeably lower as the plutonium contains fissile isotopes. The limits on the enrichment of U-235 is chosen to be less than 25%, comparable to the HALEU, estimating that an optimisation can be done to get 20%. For this reason, the enrichment of HTR, shown in Figure 7.1, is not allowed and configurations with lower Am content should be chosen, but would lead to lower performance. The HTR is considered less promising with respect to other reactors, when autonomously operated due to the higher enrichment need for performance comparable to the PWR and SFR.

Upon synthesis of the comparison between thermal and fast spectrum cores and considering conclusions on the different possibilities to enhance autonomous performance, a first selection can be made on the most promising designs:

- **The PWR-Am core configuration is found to be the best candidate for autonomous operation among the considered designs. This core is selected as the reference basis for the design of an autonomous core.** Indeed, with the PWR-Am, an average power of 85% can be attained, considering a U-235 enrichment in the HALEU limits. This value is comparable to the one of nowadays reactors, accounting for the maintenance and refuelling periods. This conclusion allows the preliminary selection of a reactor design and the establishment of a basis for a subsequent, more detailed study of the specific characteristics of the selected design, as highlighted in the perspectives.
- The SFR-Pu shows lower performance in terms of average power in operation, but is considered equally promising candidates for the design of autonomous core. Indeed, these results are derived from a preliminary study and without any optimisation. It is therefore expected that an in-depth analysis of the design may allow further optimisation of performance.
- Finally, the PWR-Dy configuration also shows promising performance, anyway further optimisation is required to increase performance and, in principle, it does not seem possible to achieve the same level as the PWR-Am.

In conclusion:

- this work enabled the identification of preliminary rejection and selection of candidate reactors to be autonomous;
- contrary to what one might expect, this work highlights that the potential performance of the final selected cores is not too far away from the one of an active industrial-size reactor;
- a compromise is needed to be found among the design criteria to be able to improve the core found at the end of this work;
- the engineering design of such a core is an open perspective.

7.2. Future work

The perspectives of this work can be distinguished in seven main points:

- implementing an improved calculation scheme, to complete the study of the selected designs;
- studying an intermediary design between the PWR thermal and SFR fast spectrum;
- implementing a finer optimisation tool of the selected designs;
- reconsidering some assumptions or constraints chosen at the beginning of the work;
- defining and analysing possible applications of an autonomous reactor;
- widening the approach used in the work to go to a deeper level of physical analysis;
- improving the computational models used, to enable additional specific studies.

The first point is now analysed. As mentioned in the conclusion, the PWR-Am was chosen as the reference autonomous core. This opens up the main perspective of implementing an improved calculation model to define the design in more detail. First, the Am content will be optimised to improve as much as possible the performance. The dependence of reactivity feedbacks on burn-up will be included in the calculation. The model will also include a study of material flows in terms of fuel needs and radioactive waste (front and back end cycle).

Specific studies could be also be performed on the fuel cycle and the reactor safety. Such a fuel with actinides insertion should be analysed in terms of feasibility, manufacturability and manipulation. The $UAmO_2$ in PWR, for example, is not a common fuel. The specific mechanical and thermal behaviour should be assessed, together with the type and amount of nuclear waste deriving from its irradiation and limitations on the Am content could be considered. On the other hand for the SFR charged with $UPuO_2$, larger knowledge is acquired and applications have already been put in place. The feasibility of this fuel and its insertion in the fuel cycle is better known. Finally, all the assessment of safety criteria and limits should be considered. The flux distribution and the hot points in the core have to be analysed. Also the behaviour of structural material during irradiation should be also analysed. Finally, accidental conditions should be recognised and studied-for example the Loss Of Cooling Accident in a boron-free PWR could have a minor impact on an autonomous core.

The second point concerns the possibility to analyse in the same way as done in this work, an under-moderated PWR design [108]. This concept foresees a decrease of the space between the fuel elements in the core, reducing the moderation ratio. This allows the reactor operating with epithermal spectrum intermediary between the PWR and SFR configuration to benefit potential margins regarding reactivity loss.

The third point concerns the possible optimisation of the chosen design. Further investigations could improve the design characteristics and optimise the nominal operation (heterogeneous fuel distribution of fuel, etc…). Insertion of different actinides and burnable poison in could be considered, as Am and Dy in PWR for example, characterised by a different kinetic of disappearance and a different effect on the neutron spectrum, could provide an optimisation of the performance. Also the core geometry could be modified, to optimise the moderator-to-fuel ratio in PWR.

Furthermore, this work was based on a "macroscopic" analysis of autonomous reactor designs, highlighting the main axes of study. Starting from the main outcomes of the present work, it could be possible to make a "microscopic" analysis, setting up a mathematical model for a multi-parametric optimisation. Using an optimising method, a reference design could be identified and then a more detailed analysis could be carried out. The safety and cost analysis should be evaluated on such a design. For this scope, an improvement in the physical model should be foreseen.

The fourth point of the perspectives concerns the reconsideration of certain assumptions. This thesis presents a description of an autonomous reactor, which was developed by putting a series of assumptions and fixing some constraints. In particular, the framework of the work is outlined as follows:

- An autonomous reactor is defined as a reactor with autonomous core and primary cooling system. It may also include an active control on the ECS.
- The core is not refuelled over the lifetime, it is charged with new fuel and discharged at the EOL. This approach is consistent with the objective of designing a core that is as autonomous and simple as possible.
- The initial reactivity loss, due to the xenon effect when present, is considered to be compensated by an active initial control. This control system could be the same one designed for the reactor start-up and shutdown.

The reconsideration of these assumptions may result in a change in the analysis. The previous list is reconsidered in terms of perspectives:

- The autonomous reactor could be studied by initially examining an autonomous ECS and subsequently designing the core to adapt its behaviour, with an active control on the reactivity if necessary (still no control rods acting but adapted secondary flow instead). This approach would necessitate focusing on the ECS system, calculating the power produced autonomously and then designing of the core to produce this required power.
- The refuelling could be re-introduced in the framework of the problem. This would increase the degree of complexity of the core and reduce its autonomous operation. However, it could allow an increase in the overall performance (improved the core lifetime and fuel cycle).
- This work quantifies the initial reactivity loss due to the xenon effect and assumes that it could be compensated by an initial active control. However, this control is not designed here. A further analysis could be made on the possible reactor start-up and shutdown system and their reactivity margins. The specific design could determine whether it is worthwhile to compensate for the Xe effect, or whether only the concepts with a small or no effect should be selected.

The fifth point of the perspectives concerns the possible applications of an autonomous reactor and the possible gains with respect to an active design. Different applications could be foreseen, for example electricity production for the national grid or for localised applications, heat production or others. According to the specific application, the "gain" with respect to an active reactor could be assessed. And

eventually some assumptions of autonomous core reconsidered, as explained before. For example, the possible flexibility given by the ECS control could be included in the design and assessed in terms of benefits for different applications, such as the grid stability. Anyway, deeper and detailed studies should be performed to evaluate the real capacities and performance of a secondary system dedicated to the piloting function.

The sixth item of perspective is here analysed. It concerns the method and the approach used in the thesis. The approaches to the problem could be different: an integrated approach that models all the reactor, including core and the entire cooling system; or an individual approach, that studies each system separately. This study focuses on the second approach. The cooling primary and secondary cooling system is analysed in a first study and its possible operation is suggested. Then the attention is focused on the core behaviour. A perspective of this work includes the integrate modelling of the entire reactor system. This would give a larger view on the points discussed upward.

The last point to discuss about the work perspectives concerns the computational model implemented. Improvement could be made in the coupling method and the single physics schemes. A completely coupled model could be used to evaluate fast transients, which accounts for the transient inertia of neutronic and thermal fields. In particular, the effect of the delayed neutron emissions and the effect of thermal inertia characteristics of the core materials. Furthermore, the neutronic calculations are made on the entire core, while the thermal-hydraulic implemented solver is based on 1D solver that returns the results for a mean material, averaged in radial and axial directions. The thermal solver could be implemented in 3D geometry, in order to be coupled on the entire core geometry. This approach would be advantageous to analyse the core power distribution and to highlight any possible hotspot. Moreover, the thermal model is based on the solution of conductive and convective equations. Ranges of amelioration could be foreseen using a solver that includes dynamic features of the problem, as the coolant flowing in the core. The use of Computational Fluid Dynamics (CFD) methods, for example, could improve the precision of the results.

References

[1] IEA International Energy Agency, 'Net Zero by 2050 - A Roadmap for the Global Energy Sector', Directorate of Sustainability, Technology and Outlooks International Energy Agency, Paris.

[2] J. M. Chen, 'Carbon neutrality: Toward a sustainable future', *The Innovation*, vol. 2, no. 3, p. 100127, Aug. 2021, doi: 10.1016/j.xinn.2021.100127.

[3] A. Savolainen, 'The Role Of Nuclear And Other Conventional Power Plants In The Flexible Energy System', Lappeenranta University of Technology, Finland, Report, 2015.

[4] A.-L. Mazauric, 'Démarche innovante de conception de réacteurs nucléaires flexibles capables d'accommoder les forts taux de productions d'électricité variables', Université Grenoble Alpes, Grenoble, 2022.

[5] H. Gerhardus, 'Model based predictive control for load following of a pressurised water reactor', Randse Afrikaanse Universiteit, Report, 2009.

[6] C. Tucker, *How to Drive a Nuclear Reactor*. Cham: Springer International Publishing, 2019. doi: 10.1007/978-3-030-33876-3.

[7] Y. Oka, Ed., *Nuclear Reactor Design*, vol. 2. in An Advanced Course in Nuclear Engineering, vol. 2. Tokyo: Springer Japan, 2014. doi: 10.1007/978-4-431-54898-0.

[8] J. Vujić, R. M. Bergmann, R. Škoda, and M. Miletić, 'Small modular reactors: Simpler, safer, cheaper?', *Energy*, vol. 45, no. 1, pp. 288–295, Sep. 2012, doi: 10.1016/j.energy.2012.01.078.

[9] B. Zohuri, *Nuclear Micro Reactors*. Cham: Springer International Publishing, 2020. doi: 10.1007/978-3-030-47225-2.

[10] Nuclear Energy Institute, 'Cost Competitiveness of Micro-Reactors for Remote Markets', Nuclear Energy Institute, U.S.A., Apr. 2019.

[11] C. Matthews, R. Wilkerson, R. Johns, H. Trellue, and R. Martineau, 'Task 1: Evaluation of M&S tools for micro-reactor concepts', LA-UR--19-22263, 1505953, Mar. 2019. doi: 10.2172/1505953.

[12] H. Guo, K. Y. Feng, H. Y. Gu, X. Yao, and L. Bo, 'Neutronic modeling of megawatt-class heat pipe reactors', *Annals of Nuclear Energy*, vol. 154, p. 108140, May 2021, doi: 10.1016/j.anucene.2021.108140.

[13] H. C. Lee, T. Y. Han, H. S. Lim, and J. M. Noh, 'An accident-tolerant control drum system for a small space reactor', *Annals of Nuclear Energy*, vol. 79, pp. 143–151, May 2015, doi: 10.1016/j.anucene.2015.02.001.

[14] K. Kugeler and Z. Zhang, *Modular High-temperature Gas-cooled Reactor Power Plant*. Berlin, Heidelberg: Springer Berlin Heidelberg, 2019. doi: 10.1007/978-3-662-57712-7.

[15] P. Gauthe and P. Sciora, ‘Sensitivity studies of sfr unprotected transients with global neutronic feedback coefficients’, *International Conference on Fast Reactors and Related Fuel Cycles Next Generation Nuclear Systems for Sustainable Development (FR17)*, Yekaterinburg, Russia., 2017.

[16] L. Carlson, J. Miller, and Z. Wu, ‘Implications of HALEU fuel on the design of SMRs and micro-reactors’, *Nuclear Engineering and Design*, vol. 389, p. 111648, Apr. 2022, doi: 10.1016/j.nucengdes.2022.111648.

[17] L. Liu *et al.*, ‘The role of nuclear energy in the carbon neutrality goal’, *Progress in Nuclear Energy*, vol. 162, p. 104772, Aug. 2023, doi: 10.1016/j.pnucene.2023.104772.

[18] IEA International Energy Agency, ‘IEA – International Energy Agency - Data and statistics’, IEA. [Online]. Available: https://www.iea.org/data-and-statistics.

[19] C. Cany, ‘Interactions entre énergie nucléaire et énergies renouvelables variables dans la transition énergétique en France: adaptations du parc électrique vers plus de flexibilité’, Université Paris Saclay (COmUE), Paris, 217AD.

[20] R. Prăvălie and G. Bandoc, ‘Nuclear energy: Between global electricity demand, worldwide decarbonisation imperativeness, and planetary environmental implications’, *Journal of Environmental Management*, vol. 209, pp. 81–92, Mar. 2018, doi: 10.1016/j.jenvman.2017.12.043.

[21] IAEA, ‘Non-baseload Operation in Nuclear Power Plants: Load Following and Frequency Control Modes of Flexible Operation’, International Atomic Energy Agency, Vienna, NP-T-3.23.

[22] S. M. Goldberg and R. Rosner, ‘Nuclear Reactors: Generation to Generation’, *Nuclear Reactors, AMERICAN ACADEMY OF ARTS & SCIENCES,* 2011.

[23] T. Murakami, ‘A historical review and analysis on the selection of nuclear reactor types and implications to development programs for advanced reactors; A Japanese study’, *Energy Reports*, vol. 7, pp. 3428–3436, Nov. 2021, doi: 10.1016/j.egyr.2021.05.049.

[24] U.S. Department of Energy, ‘NUCLEAR PHYSICS AND REACTOR THEORY, Reactor Theory (Reactor Operations)’, Module 4, Department of Energy Fundamentals Handbook.

[25] P. Mohanakrishnan and K. Umasankari, ‘Fuel burnup, fuel management, and fuel cycle physics’, in *Physics of Nuclear Reactors*, Elsevier, 2021, pp. 331–372. doi: 10.1016/B978-0-12-822441-0.00005-4.

[26] IAEA Report, Ed., *Modern instrumentation and control for nuclear power plants: a guidebook*. in Technical reports series, no. 387. Vienna: International Atomic Energy Agency, 1999.

[27] IAEA, ‘Interaction of Grid Characteristics with Design and Performance of Nuclear Power Plants A Guidebook’, International Atomic Energy Agency, Vienna, Technical reports series 224, 1983.

[28] N. Kerkar and P. Paulin, *Exploitation des coeurs REP*. in Génie atomique. Les Ulis: EDP sciences, 2008.

[29] IAEA, ‘Passive Safety Systems and Natural Circulation in Water Cooled Nuclear Power Plants’, International Atomic Energy Agency, Vienna, Thecnical reports series IAEA-TECDOC-1624, 2009.

[30] S. Qvist and E. Greenspan, ‘An Autonomous Reactivity Control system for improved fast reactor safety’, *Progress in Nuclear Energy*, vol. 77, pp. 32–47, Nov. 2014, doi: 10.1016/j.pnucene.2014.06.003.

[31] T. Lindström, 'SPARC fast reactor design - Design of two passively safe metal-fuelled sodium-cooled pool-type small modular fast reactors with Autonomous Reactivity Control', Uppsala Universitet, UPTEC F15060, Sep. 2015. Accessed: Sep. 03, 2024. [Online]. Available: https://uu.diva-portal.org/smash/get/diva2:862225/FULLTEXT01.pdf

[32] K. Tirel, 'Méthodologie de couplage de la conception de cœurs avec les scénarios électronucléaires: application au cas des RNR-Na', Université Grenoble Alpes, Grenoble, 2022.

[33] R. A. Moore, M. E. Kantor, H. L. Brey, and H. G. Olson, 'HTGR experience, programs, and future applications', *Nuclear Engineering and Design*, vol. 72, no. 2, pp. 153–174, Sep. 1982, doi: 10.1016/0029-5493(82)90212-6.

[34] NEI Nuclear Energy Institute, 'Roadmap for the Deployment of Micro-Reactors for U.S. Department of Defense Domestic Installations', NEI Nuclear Energy Institute, Washington, D.C., 2018.

[35] IAEA, 'Advances In Small Modular Reactor Technology Developments. A Supplement to: IAEA Advanced Reactors Information System (ARIS)', *International Atomic Energy Agency*, 2020.

[36] J. Leppanen, 'Serpent – a Continuous-energy Monte Carlo Reactor Physics Burnup Calculation Code', *VTT Technical Research Centre of Finland*, Jun. 2015.

[37] G. Rimpault, D. Plisson, J. Tommasi, R. Jacqmin, J.-M. Rieunier, and D. Verrier, 'The ERANOS Code And Data System For Fast Reactor Neutronic Analyses', *PHYSOR 2002 - International Conference on the New Frontiers of Nuclear Technology: Reactor Physics, Safety and High-Performance Computing*, Seoul, South Korea, 2002.

[38] G. Valocchi, 'Modélisation neutronique de coeurs complexes en cinétique multidimensionnelle : application au coeur ASTRID faible vidange et à la préparation d'expériences de validation', Aix-Marseille Université, Aix-en-Provence, 2020.

[39] B. H. Yan, C. Wang, and L. G. Li, 'The technology of micro heat pipe cooled reactor: A review', *Annals of Nuclear Energy*, vol. 135, p. 106948, Jan. 2020, doi: 10.1016/j.anucene.2019.106948.

[40] J.-P. A. Renier and M. L. Grossbeck, 'Development Of Improved Burnable Poisons For Commercial Nuclear Power Reactors', 2021, *Department of Energy (DOE)*.

[41] H. Guo, 'Conception De Systèmes Innovants Pour Le Contrôle Optimal De La Réactivité Des Réacteurs À Neutrons Rapides De Quatrième Génération', Aix-Marseille Université, Aix-en-Provence, 2019.

[42] J.-F. Parisot and et Al., *Neutronics*. Monographie nucléaire, Commissariat à l'énergie atomique et aux énergies alternatives CEA, 2015.

[43] J.-F. Parisot and France, Eds., *Neutronics*. in DEN monograph. Paris: Editions Le Moniteur, 2015.

[44] J. Wang, Q. Wang, and M. Ding, 'Review on neutronic/thermal-hydraulic coupling simulation methods for nuclear reactor analysis', *Annals of Nuclear Energy*, vol. 137, p. 107165, Mar. 2020, doi: 10.1016/j.anucene.2019.107165.

[45] D. C. Wade and Y. I. Chang, 'The Integral Fast Reactor Concept: Physics of Operation and Safety', *Nuclear Science and Engineering*, Dec. 1988, doi: 10.13182/NSE88-2.

[46] M. W. Rosenthal, P. R. Kasten, and R. B. Briggs, 'Molten-Salt Reactors—History, Status, and Potential', *Nuclear Applications and Technology*, vol. 8, no. 2, pp. 107–117, Feb. 1970, doi: 10.13182/NT70-A28619.

[47] J. A. Lake, ‘Foundations for the fourth generation of nuclear power’, *Nuclear Energy*, vol. 40, no. 3, pp. 153–157, Jun. 2001, doi: 10.1680/nuen.40.3.153.40061.

[48] R. Testoni, A. Bersano, and S. Segantin, ‘Review of nuclear microreactors: Status, potentialities and challenges’, *Progress in Nuclear Energy*, vol. 138, p. 103822, Aug. 2021, doi: 10.1016/j.pnucene.2021.103822.

[49] M. Kambe and M. Uotani, ‘Design and Development of Fast Breeder Reactor Passive Reactivity Control Systems: LEM and LIM’, *Nuclear Technology*, vol. 122, no. 2, pp. 179–195, May 1998, doi: 10.13182/NT98-A2861.

[50] B. Zohuri, *Heat Pipe Applications in Fission Driven Nuclear Power Plants*. Cham: Springer International Publishing, 2019. doi: 10.1007/978-3-030-05882-1.

[51] P. Nemec, A. Čaja, and M. Malcho, ‘Mathematical model for heat transfer limitations of heat pipe’, *Mathematical and Computer Modelling*, vol. 57, no. 1–2, pp. 126–136, Jan. 2013, doi: 10.1016/j.mcm.2011.06.047.

[52] F. Damian, ‘Analyse des capacités des réacteurs à haute température (HTR) sous l’aspect de l’utilisation des matières fissiles’, Grenoble INPG, 2001.

[53] D. Jacquemain, Ed., ‘Chapitre 2 Conception et fonctionnement d’un réacteur à eau sous pression’, in *Les accidents de fusion du coeur des réacteurs nucléaires de puissance*, EDP Sciences, 2020, pp. 11–46. doi: 10.1051/978-2-7598-1846-4.c005.

[54] P. Coppolani and et Al., *La chaudière des réacteurs à eau sous pression*. in Colletion Génie Atomique. EDP Sciences, 2013.

[55] J. Guidez and P. Gérard, *Superphenix Technical and Scientific Achievements*. Atlantis Press, 2017.

[56] J.-P. Cretté, ‘Réacteurs à neutrons rapides refroidis au sodium’, Énergies | Génie nucléaire, Saint-Denis, France, BN3170V1, 2005.

[57] J. W. Sterbentz *et al.*, ‘Preliminary Assessment of Two Alternative Core Design Concepts for the Special Purpose Reactor’, *Idaho National Laboratory Nuclear Science and Technology Division*, 2018.

[58] S. Sihlangu, ‘A neutronic model of the PMR200 prismatic modular reactor using MCNP5’, North-West University, Degree Magister Scientiae in Nuclear Engineering, 2016.

[59] G. Rimpault *et al.*, ‘A Search for Improved SFR Cores Using Carbide Fuel’, *GLOBAL 2009 Congress: The Nuclear Fuel Cycle: Sustainable Options and Industrial Perspectives*, 2009.

[60] G. I. Bell and S. Glasstone, *Nuclear Reactor Theory*, Van Nostrand Reinhold Company, 1970.

[61] W. M. Stacey, *Nuclear Reactor Physics, Second Edition*, 2nd ed. Federal Republic of Germany: WILEY-VCH Verlag GmbH & Co. KGaA, 2007.

[62] J. Leppänen, M. Pusa, T. Viitanen, V. Valtavirta, and T. Kaltiaisenaho, ‘The Serpent Monte Carlo code: Status, development and applications in 2013’, *Annals of Nuclear Energy*, vol. 82, pp. 142–150, Aug. 2015, doi: 10.1016/j.anucene.2014.08.024.

[63] J. Leppänen, ‘Development of a New Monte Carlo Reactor Physics Code’, VTT Technical Research Centre of Finland, 2007.

[64] M. Pusa, ‘Numerical methods for nuclear fuel burnup calculations’, Aalto University, Otakaari 1 M, Espoo, Finland, 2013.

[65] J. Leppänen, ‘Burnup calculation methodology in Serpent’, *International Conference on the Physics of Reactors 2012: Advances in Reactor Physics, PHYSOR*, 2012.

[66] V. HUY, ‘Contribution to nuclear data improvement by assimilation of integral experiments for the ASTRID core neutronic characterizationecco-eranos.pdf’, Université d'Aix-Marseille, 2018.

[67] IAEA, ‘Summary Review on the Application of Computational Fluid Dynamics in Nuclear Power Plant Design’, International Atomic Energy Agency, Vienna, No. NR-T-1.20, 2022.

[68] M. Ma *et al.*, ‘A pure-conduction transient model for heat pipes via derivation of a pseudo wick thermal conductivity’, *International Journal of Heat and Mass Transfer*, vol. 149, p. 119122, Mar. 2020, doi: 10.1016/j.ijheatmasstransfer.2019.119122.

[69] J. E. Hansel, R. A. Berry, D. Andrs, M. S. Kunick, and R. C. Martineau, ‘Sockeye: A One-Dimensional, Two-Phase, Compressible Flow Heat Pipe Application’, *Nuclear Technology*, vol. 207, no. 7, pp. 1096–1117, Jul. 2021, doi: 10.1080/00295450.2020.1861879.

[70] M. Mansour, ‘Heat Transport Limitations and Overall Heat Transfer Coefficient for a Heat Pipe’, *International Journal of Engineering and Advanced Technology (IJEAT),* Volume-5 Issue-4, April 2016.

[71] Z. J. Zuo and A. Faghri, ‘A network thermodynamic analysis of the heat pipe’, *International Journal of Heat and Mass Transfer*, vol. 41, no. 11, pp. 1473–1484, Jun. 1998, doi: 10.1016/S0017-9310(97)00220-2.

[72] Y. Ma *et al.*, ‘Heat pipe failure accident analysis in megawatt heat pipe cooled reactor’, *Annals of Nuclear Energy*, vol. 149, p. 107755, Dec. 2020, doi: 10.1016/j.anucene.2020.107755.

[73] D. Plancq *et al.*, ‘STATUS OF THE ASTRID GAS POWER CONVERSION SYSTEM OPTION’, *GIF Symposium 2018 - The Generation IV International Forum*, 2018.

[74] H. D. Nguyen, N. Alpy, D. Haubensack, and D. Barbier, ‘Insight on electrical and thermal powers mix with a Gen2 PWR: Rankine cycle performances under low to high temperature grade cogeneration’, *Energy*, vol. 202, p. 117518, Jul. 2020, doi: 10.1016/j.energy.2020.117518.

[75] D. Haubensack, C. Thévenot, and P. Dumaz, ‘The COPERNIC/CYCLOP computer tool: pre-conceptual design of generation 4 nuclear systems’, *2nd International Topical Meeting on HIGH TEMPERATURE REACTOR TECHNOLOGY*, China, Jan. 2005.

[76] H. S. Pham *et al.*, ‘Mapping of the thermodynamic performance of the supercritical CO2 cycle and optimisation for a small modular reactor and a sodium-cooled fast reactor’, *Energy*, vol. 87, no. C, pp. 412–424, 2015.

[77] J. Floyd *et al.*, ‘A numerical investigation of the sCO2 recompression cycle off-design behaviour, coupled to a sodium cooled fast reactor, for seasonal variation in the heat sink temperature’, *Nuclear Engineering and Design*, vol. 260, pp. 78–92, Jul. 2013, doi: 10.1016/j.nucengdes.2013.03.024.

[78] J. A. Nelder and R. Mead, ‘A Simplex Method for Function Minimization’, *The Computer Journal*, vol. 7, no. 4, pp. 308–313, Jan. 1965, doi: 10.1093/comjnl/7.4.308.

[79] A. Dragunov, E. Saltanov, I. Pioro, P. Kirillov, and R. Duffey, 'Power cycles of generation III and III+ nuclear power plants', *Journal of Nuclear Engineering and Radiation Science*, vol. 1, p. 021006, Apr. 2015, doi: 10.1115/1.4029340.

[80] J. Guidez and B. Bonin, 'Réacteurs nucléaires à caloporteur sodium', CEA Saclay; Groupe Moniteur, 2014.

[81] J. Didier, *Les accidents de fusion du cœur des réacteurs nucléaires de puissance*. Collection sciences et techniques. France, 2013.

[82] C. Coquelet-Pascal, M. Tiphine, G. Krivtchik, D. Freynet, R. Girieud, and R. Eschbach, 'COSI6: a Tool for Nuclear Transition Scenarios Studies', *Global 2015*, Paris France, 2015.

[83] H. Sun *et al.*, 'Conceptual design and analysis of a multipurpose micro nuclear reactor power source', *Annals of Nuclear Energy*, vol. 121, pp. 118–127, Nov. 2018, doi: 10.1016/j.anucene.2018.07.025.

[84] Y. Ma *et al.*, 'Neutronic and thermal-mechanical coupling analyses in a solid-state reactor using Monte Carlo and finite element methods', *Annals of Nuclear Energy*, vol. 151, p. 107923, Feb. 2021, doi: 10.1016/j.anucene.2020.107923.

[85] Javier Ortensi and Abderrafi M. Ougouag, 'Improved Prediction of the Temperature Feedback in TRISO-Fueled Reactors', INL/EXT-09-16494, 966171, Aug. 2009. doi: 10.2172/966171.

[86] C. Bouret, 'Etudes des contre-réactions dans un réacteur à neutrons rapides à caloporteur sodium: impact de la conception et de la neutronique sur les incertitudes', Université Blaise Pascal-Clermont-Ferrand II, Clermont-Ferrand, 2014.

[87] S. Marguet, *The Physics of Nuclear Reactors*. Cham: Springer International Publishing, 2017. doi: 10.1007/978-3-319-59560-3.

[88] B. Zohuri, *Heat Pipe Design and Technology: Modern Applications for Practical Thermal Management*. Cham: Springer International Publishing, 2016. doi: 10.1007/978-3-319-29841-2.

[89] P. R. Mcclure, D. I. Poston, V. R. Dasari, and R. S. Reid, 'Design of megawatt power level heat pipe reactors', LA-UR--15-28840, 1226133, Nov. 2015. doi: 10.2172/1226133.

[90] H. Nickel, 'HTR Coated particles and fuel elements', presented at the High Temperature Reactor School HTR/ECS 2002, Cadarache, France, Nov. 04, 2002.

[91] X. Zhiwen and et Al., 'Impact of High Burnup on PWR Spent Fuel Characteristics', *Nuclear Science and Engineering*, vol. 151, 2005, [Online]. Available: https://dspace.mit.edu/bitstream/handle/1721.1/71263/22-251-fall-2005/contents/readings/impact.pdf

[92] H. Grard, *Physique, fonctionnement et sûreté des REP - Le réacteur en production*. in Collection Génie Atomique. 17, avenue du Hoggar Parc d'activitie´s de Courtaboeuf, BP 112 91944 Les Ulis Cedex A, France: EDP Sciences. [Online]. Available: https://laboutique.edpsciences.fr/produit/738/9782759817009/physique-fonctionnement-et-surete-des-rep

[93] CEA, 'Les combustibles nucléaires', Monographie nucléaire, Commissariat à l'énergie atomique et aux énergies alternatives, France.

[94] T. Kooyman, ‘Amelioration Des Performances De Transmutation Des Actinides Mineurs Dans Les Reacteurs De Quatrieme Generation : Aspects Cycle Et Cœurs’, Aix-Marseille Université, Aix En Provence, France, 2017.

[95] V. S. Volkov, A. S. Luk’yanov, V. V. Chapkunov, V. P. Shevyakov, and V. S. Yamnikov, ‘Use of burnable poisons in nuclear reactors’, *The Soviet Journal of Atomic Energy*, vol. 11, no. 2, pp. 745–757, Mar. 1962, doi: 10.1007/BF01626442.

[96] J. L. Kloosterman, ‘Application of boron and gadolinium burnable poison particles in UO2 and PUO2 fuels in HTRs’, *Annals of Nuclear Energy*, vol. 30, no. 17, pp. 1807–1819, Nov. 2003, doi: 10.1016/S0306-4549(03)00134-8.

[97] J. A. Evans, M. D. DeHart, K. D. Weaver, and D. D. Keiser, ‘Burnable absorbers in nuclear reactors – A review’, *Nuclear Engineering and Design*, vol. 391, p. 111726, May 2022, doi: 10.1016/j.nucengdes.2022.111726.

[98] K. Tirel, T. Kooyman, C. Coquelet-Pascal, and E. Merle, ‘Coupling reactor design and scenario calculations: a promising method for scenario optimization’, *EPJ Nuclear Sci. Technol.*, vol. 8, p. 7, 2022, doi: 10.1051/epjn/2022002.

[99] B. Ade and et Al., ‘Safety and Regulatory Issues of the Thorium Fuel Cycle’, United States Nuclear Regulatory Commission, Oak Ridge National Laboratory, NUREG/CR-7176 ORNL/TM-2013/543, 2014.

[100] A. Nichols, E. McCutchan, and P. Dimitriou, ‘INDC International Nuclear Data Committee’, BNL--114827-2017-IR, 1413963, Dec. 2017. doi: 10.2172/1413963.

[101] Jordan A. Evans and et Al., ‘Burnable Absorbers in Nuclear Reactors - A Review’, Idaho Falls, Idaho 83415, May 2022. [Online]. Available: https://www.osti.gov/servlets/purl/1908247

[102] M. Kauchi and Y. Shimazu, ‘Optimal Burnable Poison-Loading in a PWR with Carbon Coated Particle Fuel’, *Journal of Nuclear Science and Technology*, vol. 40, no. 1, pp. 22–29, Jan. 2003, doi: 10.1080/18811248.2003.9715328.

[103] J. Zou, S. Liu, C. Jin, Y. Cai, L. Wang, and Y. Chen, ‘Optimization method of burnable poison based on genetic algorithm and artificial neural network’, *Annals of Nuclear Energy*, vol. 192, p. 109985, Nov. 2023, doi: 10.1016/j.anucene.2023.109985.

[104] IAEA, ‘PRIS Power Reactor Information System’, Country Statistics. [Online]. Available: https://pris.iaea.org/PRIS/CountryStatistics/CountryDetails.aspx?current=FR

[105] J. Couturier, *Eléments de sûreté nucléaire - Les réacteurs à eau sous pression*, IRSN. Collection sciences et techniques. 2020. [Online]. Available: https://www.irsn.fr/sites/default/files/documents/larecherche/publications-documentation/collection-ouvrages-irsn/IRSN-livre-libman_PDF-web-NB-s.pdf

[106] A. Zaetta *et al.*, ‘CADOR “Core with Adding DOppleR effect” concept application to sodium fast reactors’, *EPJ Nuclear Sci. Technol.*, vol. 5, p. 1, 2019, doi: 10.1051/epjn/2018049.

[107] J. Wallenius, ‘PHYSICS OF AMERICIUM TRANSMUTATION’, *Nuclear Engineering and Technology*, vol. 44, no. 2, pp. 199–206, Mar. 2012, doi: 10.5516/NET.01.2012.505.

[108] J.-P. Millot, ‘Réacteur nucléaire du type sous-modéré’, EP0153240B1, Dec. 07, 1988 [Online]. Available: https://patents.google.com/patent/EP0153240B1/fr

[109] G. I. L. van Oudenaren, J. A. Ocadiz-Flores, and A. L. Smith, 'Coupled structural-thermodynamic modelling of the molten salt system NaCl-UCl3', *Journal of Molecular Liquids*, vol. 342, p. 117470, Nov. 2021, doi: 10.1016/j.molliq.2021.117470.

[110] F.-Y. Ouyang, C.-H. Chang, and J.-J. Kai, 'Long-term corrosion behaviors of Hastelloy-N and Hastelloy-B3 in moisture-containing molten FLiNaK salt environments', *Journal of Nuclear Materials*, vol. 446, no. 1, pp. 81–89, Mar. 2014, doi: 10.1016/j.jnucmat.2013.11.045.

[111] X. Liu *et al.*, 'Core thermal-hydraulic evaluation of a heat pipe cooled nuclear reactor', *Annals of Nuclear Energy*, vol. 142, p. 107412, Jul. 2020, doi: 10.1016/j.anucene.2020.107412.

[112] N. Tak, M.-H. Kim, and W. J. Lee, 'Numerical investigation of a heat transfer within the prismatic fuel assembly of a very high temperature reactor', *Annals of Nuclear Energy*, vol. 35, no. 10, pp. 1892–1899, Oct. 2008, doi: 10.1016/j.anucene.2008.04.005.

[113] Xavier Ficquet et al., 'International Congress on Advances in Nuclear Power Plant（ICAPP'10）', *atomos*, vol. 52, no. 11, pp. 761–761, 2010, doi: 10.3327/jaesjb.52.11_761.

[114] J. J. Duderstadt and L. J. Hamilton, *Nuclear Reactor Analysis*, John Wiley&Sons, Inc. U.S.A.: John Wiley & Sons, Inc., 1942.

[115] K. Herbreteau, 'Développement d'un outil physique orienté conception pour la simulation des excursions de puissance non protégée dans un RNR-Na', Université Grenoble Alpes (ComUE), Grenoble, 2018.

[116] NEA, 'JANIS', Nuclear Energy Agency (NEA). [Online]. Available: https://www.oecd-nea.org/jcms/pl_39910/janis

[117] B. Rouben, 'CANDU In-Core Fuel-Management', in *CANDU In-Core Fuel-Management Course*, McMaster University & University of Ontario Institute of Technology (UOIT), 2016.

[118] CANDU Owner Group, 'Nuclear Theory - Effect of fuel burn-up', in *Nuclear Theory Course - 277,* July 1979.

[119] S. Glasstone and A. Sesonske, *Nuclear Reactor Engineering*. Princeton, New Jersey: D. Van Nostrand Company, INC., 1963.

[120] A. Talamo, 'Conceptual design of quadriso particles with europium burnable absorber in HTRS', ANL-10/14, 979897, May 2010. doi: 10.2172/979897.

ANNEXES

Annex II

Annexes to chapter 2

II.1. Approach for the study of an autonomous MSR

In this annex, the methodology applied in Chapter 2 is discussed related to the possibility of application to the case of a Molten Salt Reactor (MSR).

Design of a reference MSR

A MSR is a reactor characterised by the fuel dissolved in the coolant, circulating in the circuit that is composed of the core, the pumps and the heat-exchangers. The main beneficial characteristic of the MSR is the large coefficients of the reactivity feedback effects (due to the Doppler and the effect of coolant expansion). They ensure an auto-stabilizing behaviour even in prompt critical conditions. On the other hand, the MSR show technological obstacles that still need further validations concerning the chemical behaviour of the salt and the corrosion aspects.

In this framework, a simplified model of MSR core is analysed. It has been represented as a cylindrical core of $1m^3$ with a fast neutron spectrum. The core characteristics are summed up in Table 9.1 and are taken as example of a representative molten salt design.

Table 9.1 - Characteristics of the reference MSR core.

Salt	$NaCl - UCl_3$ [109]
Cl enrichment [4][$\%_{mass}$]	99
Reflector/neutronic protection	Hastelloy N [110]
Volumetric power [W/cm^3]	6.59
Ratio core height/radius	1.85
Mean core temperature [K]	900
Reflector temperature [K]	900
Volume flow rate [m^3/s]	1

The volumetric power has been taken as the one used in Chapter 3 for the comparison among the other reactor design. The fast spectrum has been chosen to simplify the approach, setting aside the study of the addition of a moderator. In MSR, mainly two types of salts are used: the fluoride and the chloride.

[4] Defined as the ratio between Cl-37 mass content and the total Cl mass.

For reasons of solubility, the former is mainly used with the Th/U fuel cycle and the latter for the U/Pu cycle. The choice in this thesis is to focus the attention more on the second type of fuel, so in the MSR approach the chloride coolant has been chosen. The fuel is uranium, according to the comparison that is made in Chapter 4. Therefore, the salt used in this study is $NaCl - UCl_3$. As we are aiming for an autonomous operating condition of the reactor, no online refueling is envisaged.

The core has been represented as a cylinder for the circulation of salt surrounded by a reflector. The specific core geometrical dimensions are reported in Table 9.2.

Table 9.2 – Geometrical dimensions of the reference MSR core.

Core radius [cm]	55.64
Reflector radius [cm]	75.64
Core height [cm]	102.8
Reflector height [cm]	142.8

Application of the KGH method to the case of study of a MSR

The KGH method described in Chapter 2 is reminded briefly in the following equation:

$$\Delta\rho_{core} = H\ \Delta P_{core} + G\ \Delta(\Delta T_{core}) + K\ \Delta T_{in} + \Delta\rho_{fuel} = 0; \qquad (9.1)$$

where: ΔP_{core} is the variation of the core power [W]; $\Delta(\Delta T_{core})$ is the variation of the core temperature difference between outlet and inlet [K]; ΔT_{in} is the variation of the inlet core temperature [K]; $\Delta\rho_{fuel}$ is the variation of the reactivity due to the fuel depletion (or possibly the variation due to burnable poisons or other passive control methods) [pcm]. Finally, the H, G, K terms are specific coefficients that account for the reactivity feedback effects. In particular H accounts for the effect of the variation of the core power (keeping ΔT_{core} and T_{in} costant), G for the effect of the variation of the difference of temperature in the core (keeping P_{core} and T_{in} costant) and K for the effect of the variation of the core inlet temperature (keeping ΔT_{core} and P_{core} constant).

In this study, the hypothesis of constant core inlet temperature has been made (as explained at the end of Chapter 3), thus the equation is reformulated:

$$\Delta\rho_{core} = H\ \Delta P_{core} + G\ \Delta(\Delta T_{core}) + \Delta\rho_{fuel} = 0; \qquad (9.2)$$

In this specific case of application to the MSR, the equation has to be slightly reformulated. Indeed, the H and G coefficients are computed changing the core power and keeping the core temperature difference constant (for H) and vice versa (for G). In a MSR, it is not possible to compute separately these two terms because the core power is directly related to the fuel temperature variation in the core (as the fuel and the coolant are the same material). In this case the equation is re written as:

$$L\ \Delta(\Delta T_{core}) + \Delta\rho_{fuel} = 0; \qquad (9.3)$$

where L is the coefficient that accounts for the power and the simultaneous variation of the core temperature difference. This coefficient is computed as follows:

$$L = \alpha_{Doppler}\ \Delta T_{fuel} + \alpha_{coolant}\Delta T_{coolant}\ \left[\frac{pcm}{K}\right]; \qquad (9.4)$$

where: $\alpha_{Doppler}$ is the Doppler coefficient, $\alpha_{coolant}$ is the coefficient related to the coolant expansion effect.

The formulation between a time *t* and the following *t+dt* is thus re written as:

$$\Delta T_{core}(t+dt) = -\frac{\Delta\rho_{fuel}}{L} + \Delta T_{core}(t) \ ; \tag{9.5}$$

In this case of study the L coefficient has been determined as the variation of the reactivity between 900 K and 1000 K:

$$L = -8.6 \ \left[\frac{pcm}{K}\right];$$

The reactivity loss due to the fuel depletion has been computed with the Monte-Carlo code Serpent 2 and is linear with a value of:

$$\Delta\rho_{fuel} = -0.32 \ \left[\frac{pcm}{EFPD}\right];$$

The initial core temperature difference is computed as:

$$\Delta T_{core}(t=0) = \frac{P_{core}}{\rho \, \dot{V} c_p} = 0.35 \ K \ ;$$

where: P_{core} is the core power, set to 6.59 MW; ρ is the salt density computed at 900 K (3.31 g/cm^3); $\dot{V}$ is the volume flow rate (1 m^3/s) and c_p is the salt specific heat (5.69 J/g/K). This temperature variation is very small because this design has been deduced from a large power core, without modifying the flow rate.

With these data, the evolution of the core temperature difference is computed via the formulation (9.5). For a reactivity loss corresponding to ten EFPD of operation the temperature becomes:

$$\Delta T_{core}(t+dt) = -\frac{3.2}{8.6} + 0.35 = -0.022 \tag{9.6}$$

The result is not physical (as it represents a core outlet temperature inferior to the inlet one). This means that the reactor power goes to zero very fast (in the first days of operation).

It is possible to imagine some changes in the proposed design, such as:

- To impose a decreased salt flow rate. However, it will probably not be possible to reduce it so much because of limits on the natural circulation (and so on the minimum salt flow rate);
- To increase the nominal core power, in order to increase the value of the core temperature difference, but this would entail a consequent increase in the reactivity loss;
- To let the inlet temperature varying and maybe consider adding an active control in the secondary loop.

Further analysis are necessary to assess the possibility of designing an autonomous MSR by taking into account the whole system.

II.2. Validation of thermal models

The temperature steady state distribution in the core materials have been evaluated for each reactor with the thermal models described in Chapter 2. The obtained mean temperatures are compared to the literature values to validate the models.

Figure 9.1 represents the temperature distribution on a heat pipe in nominal working conditions. The temperature gradient is not very large along the pipe and the temperatures are mainly dependent on the secondary system heat exchange. These values have been compared to values in the literature, that show mainly the same results for a sodium cooled heat pipe reactor [111]. In the present HPR, the mean fuel temperature, corresponding to this heat pipe functioning, is *730 K*.

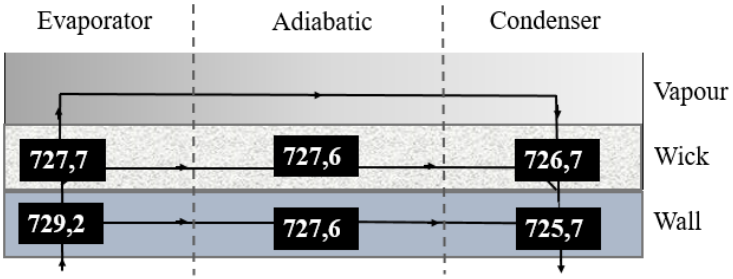


Figure 9.1 – Temperature distribution in one averaged heat pipe.

Figure 9.2 shows the temperature distribution in a reference geometry of HTR corresponding to graphite matrix and fuel channel. The mean fuel temperature in nominal operating conditions is *1017.65 K* in accordance with the literature results [112] [113].

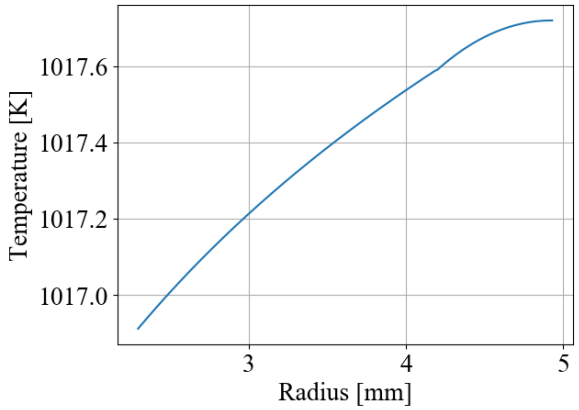


Figure 9.2 – Temperature distribution in a thermal cell of HTR.

Figure 9.3 shows the PWR temperature distribution, the mean fuel temperature is around *1150 K*. The results has been compared to the literature in [114].

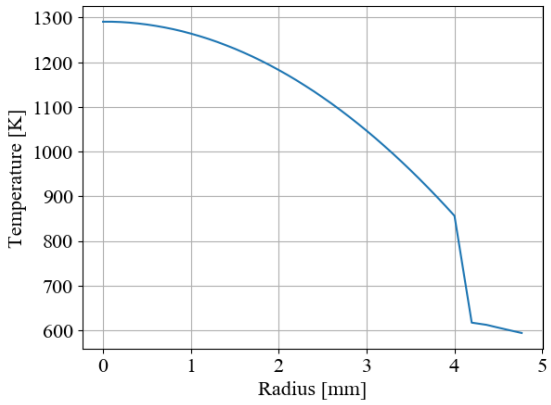


Figure 9.3 - Temperature distribution in a thermal cell of PWR.

Figure 9.4 shows the temperature distribution in a mean assembly of a SFR, in accordance with the literature reference[115]. The mean fuel temperature is around *1750 K* for the nominal operation of the selected sodium cooled reactor.

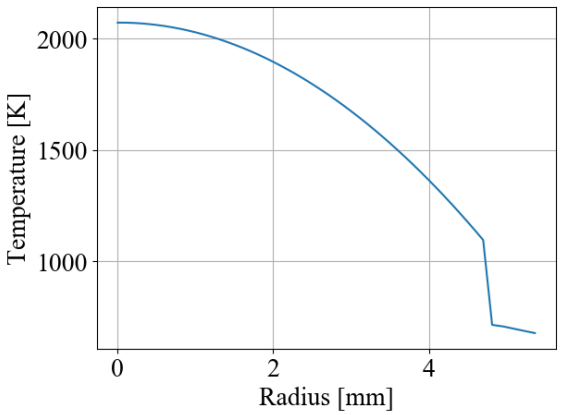


Figure 9.4 - Temperature distribution in a thermal cell of SFR.

Annex IV

Annexes to chapter 4

IV.1. Verification of the criteria for criticality

The aim of this annex is to show that a criterion can be set on the precision of the search of the critical state at BOL. Indeed, with Monte Carlo simulations, the fuel enrichment is modified, the simulation is launched and the reactivity evaluated. This process is repeated until the reactivity is equal to zero minus a defined uncertainty. Here it is demonstrated that, up to 500 pcm, the uncertainty does not influences reactivity evolution for the level of analysis needed in this work. Thus, the search for fuel enrichment at BOL can be stopped when this criterion is met.

To verify the criterion, of $|\rho| < 500\ pcm$, imposed at BOL to define a critical reactor, a sensitivity study was carried out on the HTR, taken as an example. The fuel enrichment was modified to increase the reactivity at BOL, as shown in Table 9.3. Successively, the reactivity evolution is simulated in Figure 9.5 and the mean deviation between the curves is compared.

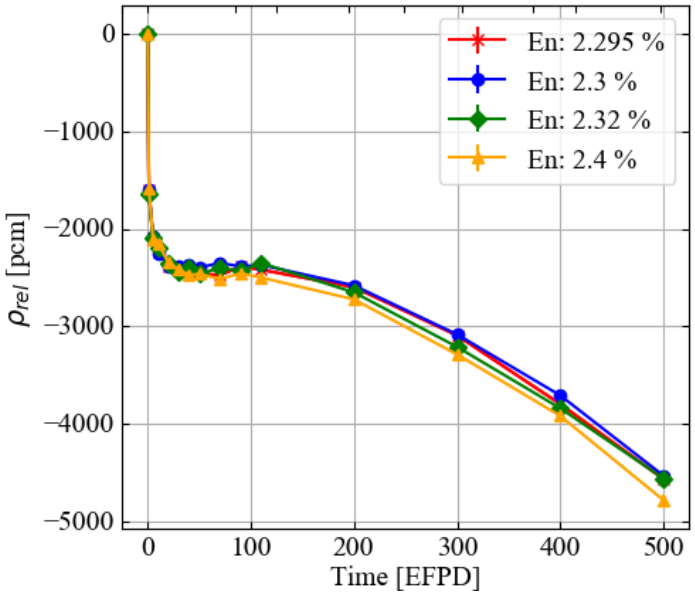


Figure 9.5 – Sensitivity analysis on the criterion chosen for the criticality state at BOL.

The effect of the criterion chosen for criticality is analysed. Figure 9.5 shows the relative (compared with the value at t=0) reactivity evolution for different initial enrichments. The case of 2.295% enrichment is considered as the reference one. The gap between the reference case and the others is evaluated by the mean difference *MD* between the curves as follows:

$$MD(\rho) = \frac{1}{N}\sum_{i=0}^{N}\left|\rho_i - \rho_{ref\ i}\right|; \qquad (9.7)$$

where: ρ_i are the values of the evolution of the relative reactivity, N is the number of time steps considered, $\rho_{ref\ i}$ are the values of the evolution of the reactivity reference curve (enrichment 2.295%).

The reactivity mean differences results are shown Table 9.3.

Table 9.3 - Sensitivity of the HTR fuel enrichment on the reactivity at BOL.

Enrichment [%]	Reactivity at BOL [pcm]	Mean difference [pcm]
2.295	175 ± 25	Reference case
2.300	228 ± 25	38
2.320	436 ± 25	39
2.400	1262 ± 25	69

The mean difference between the curves is below 40 pcm for cases up to 436 pcm deviation at BOL (corresponding in this case to enrichments up to 2.32 %) and from 70 pcm average difference during evolution for deviations at BOL greater than 500 pcm. The reactivity evolution is of the order of thousands of pcm variation, thus one order of magnitude larger than the deviation obtained by imposing the criterion of 500 pcm at BOL. This discussion leads to the conclusion that for a tolerance of up to 500 pcm at the BOL, the fuel evolution is not affected for the level of analysis needed in this work. Therefore, in this work, the criterion for defining reactor criticality has been arbitrarily set at $|\rho| < 500\ pcm$ and the search for fuel enrichment is pursued to an accuracy that satisfies this criterion.

IV.2. Thermal cores reactivity evolution insight

By way of illustration, the PWR case is analysed in more details, but the same physical behaviour is observed for HTR cores, so the discussion is valid for both designs. The reactivity loss curve is characterised by three intervals of different slope. In this section, they are analysed separately.

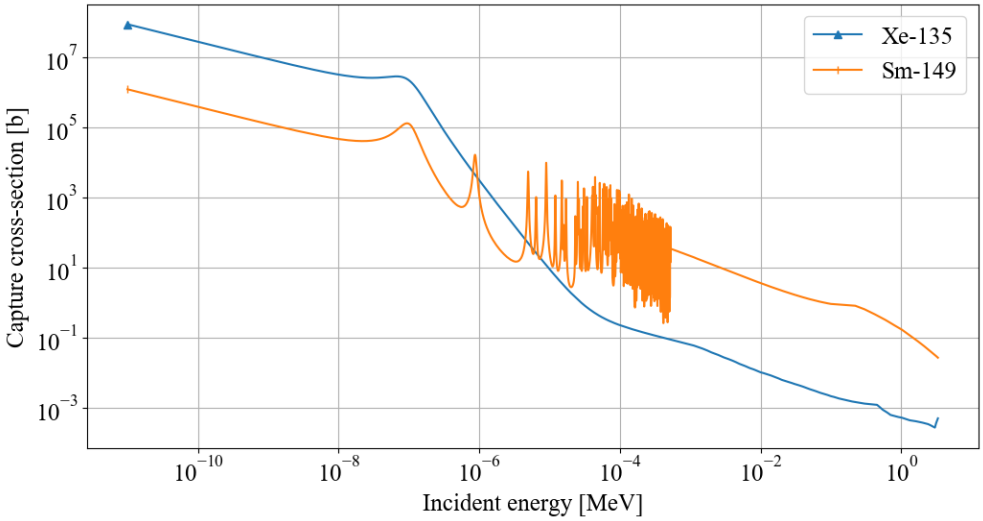
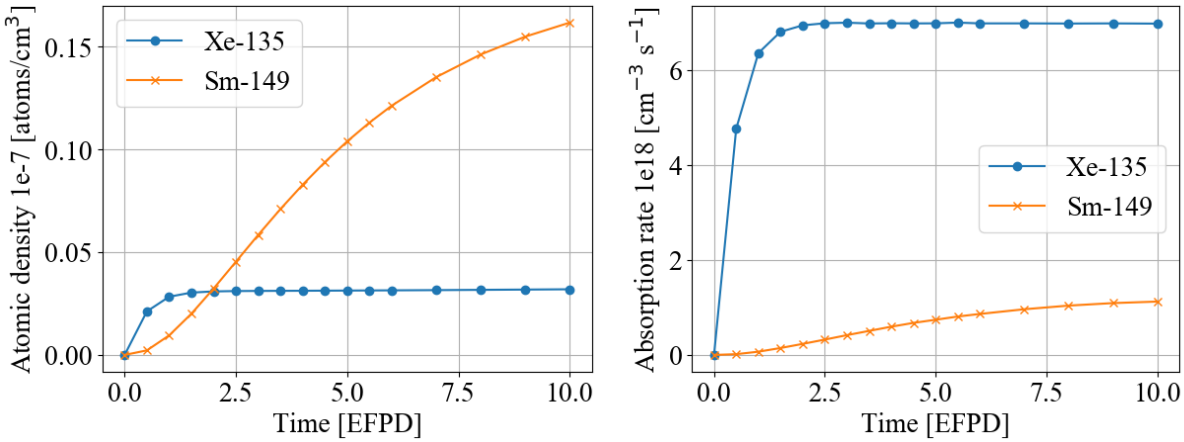


Figure 9.6 - Xe-135 and Sm-149 capture cross section [data from JANIS NEA, JEFF-3.1.1 [116]].

The first sharp drop in reactivity is due to the accumulation of xenon and samarium fission products. They appear during the first few hours of reactor operation and are characterised by a large effective absorption cross-section in the thermal spectrum, as shown in Figure 9.6.

The evolution of Xe-135 and Sm-149 contents and their absorption rate are shown in Figure 9.7.



(a) *(b)*

Figure 9.7 – Xe-135 and Sm-149 content (a) and absorption rate (b) evolution.

Figure 9.7(a) shows the content of the two capturing isotopes. Xe-135 is produced in the first few hours and then the content reaches a plateau, while Sm-149 is produced in the first days and the content increases steadily. Nevertheless, Xe-135 has a higher neutron capture cross section and its contribution to the absorption rate is larger and stabilises in the first few hours, as shown in Figure 9.7(b), which explains the initial reactivity loss.

The reason why the reactivity loss in the first few days of PWR and HTR is different is related to the difference in neutron flux. The PWR operates at higher power density and with a higher neutron flux. This increases the production of Xe-135, as shown in Figure 9.8. This explains why the PWR losses more reactivity than the HTR in the first few days of operation.

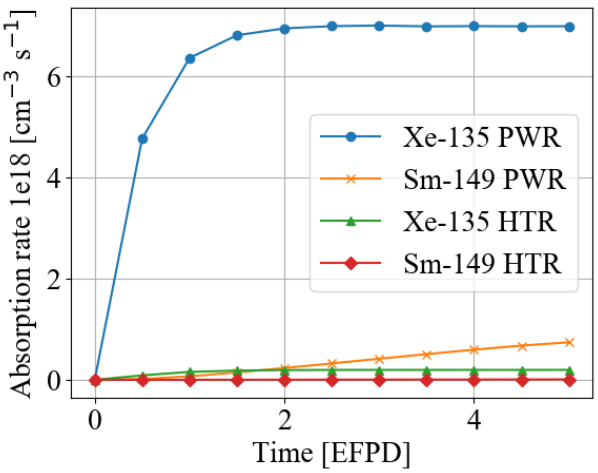


Figure 9.8 – Xe-135 content (a) and absorption rate (b) evolution comparison between PWR and HTR.

For the second interval of the reactivity evolution, in which the reactivity trend shows an increase, different fuel enrichments have been simulated in order to compare the effect on the reactivity in Figure 9.9. The PWR design is taken as an example for the analysis.

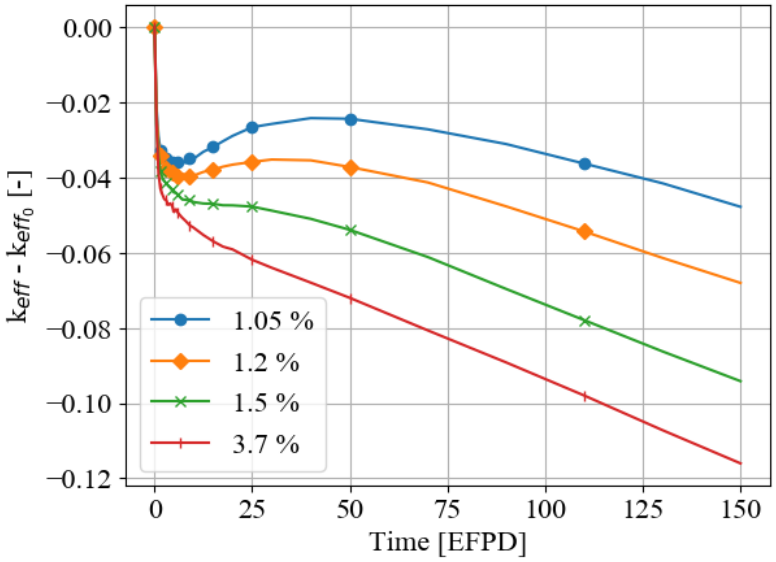


Figure 9.9 – PWR reactivity evolution according to different U-235 enrichments.

Figure 9.9 shows that reactivity varies according to the fuel enrichment. The less enriched the fuel, the more the reactivity increases before decreasing linearly. The focus is on the enrichment cases of 1.05% and 3.7%, the former being the reference case considered in this work, the latter being a reference value in industrial PWRs (a French 900 PWR taken as a reference) [93]. These two cases are analysed in more details.

The simulations were carried out with a normalised power which imposes a constant fission power throughout the evolution. For this reason, the macroscopic cross section is analysed, as it is not influenced by the normalisation parameter and considering the following formulation:

$$P_{fiss} = \sum_i \int E_{fiss_i} \tau_{fiss_i} = \sum_i \int E_{fiss_i} \Sigma_{fiss_i} \Phi \; ; \qquad (9.8)$$

where: P_{fiss} is the fission power [W], E_{fiss_i} is the energy released at each fission [eV], ν_i is the neutrons fraction produced following each fission event [-], τ_{fiss_i} is the fission rate [cm^{-3} s^{-1}], Σ_{fiss_i} is the macroscopic cross section [cm^{-1}], Φ is the neutronics flux [cm^{-2} s^{-1}]. The sum refers to the sum over all the fissile isotopes *i* and the integral refers to the integral over space, directions and neutron energies.

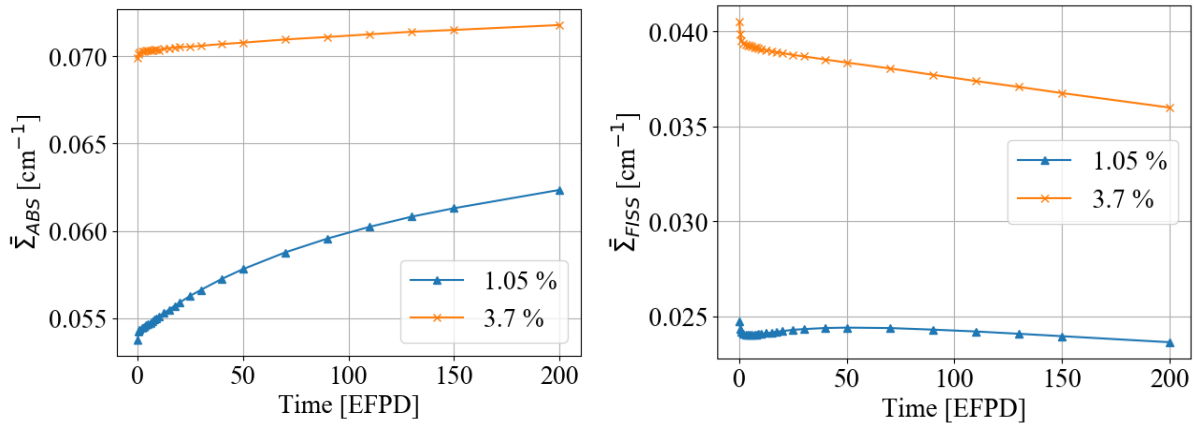
Power normalisation corresponds to a correction of the flux norm at each time step. In this analysis, the focus is on a parameter that is not influenced by the normalisation, and the macroscopic cross section is considered. Its definition is the following:

$$\Sigma_{fiss_i} = \sigma_{fiss_i} N_i \; ; \qquad (9.9)$$

where σ_{fiss_i} is the microscopic cross section of the isotope *i* [cm^{-2}], N_i is the isotope *i* content [cm^{-3}]. These two parameters are influenced by the normalisation factor during the evolution (in the Bateman equation), but not in the steady-state calculation. In the Bateman equation, the actinides, to a first

approximation, depend linearly on the flux. Normalisation should therefore influence the results on the evolution of the macroscopic cross section to second order.

In Figure 9.10, the mean macroscopic cross sections, integrated over the fuel volume, are shown for the fission and absorption events.



(a) *(b)*

Figure 9.10 - Comparison of absorption (a) and fission (b) macroscopic cross sections.

The curves of the mean absorption macroscopic cross section are shown in Figure 9.10(a). They show a monotonic increase, which is due to the accumulation of Pu from the U-238 irradiation and the fission products. Figure 9.10(b) shows the mean fission cross section. For higher enrichments, there is a linear decrease in the curve, due to the U-235 consumption. On the other hand, for lower enrichments, the fission cross section shows an increase over the first 50 days, followed by a linear decrease. This phenomenon is linked to the concurrent consumption of U235 and the accumulation of Pu-239.

As the fission cross sections show different behaviours between the various enrichments, the fissions evolution is further analysed in more details below. The macroscopic fission cross sections for the main isotopes are shown in Figure 9.11.

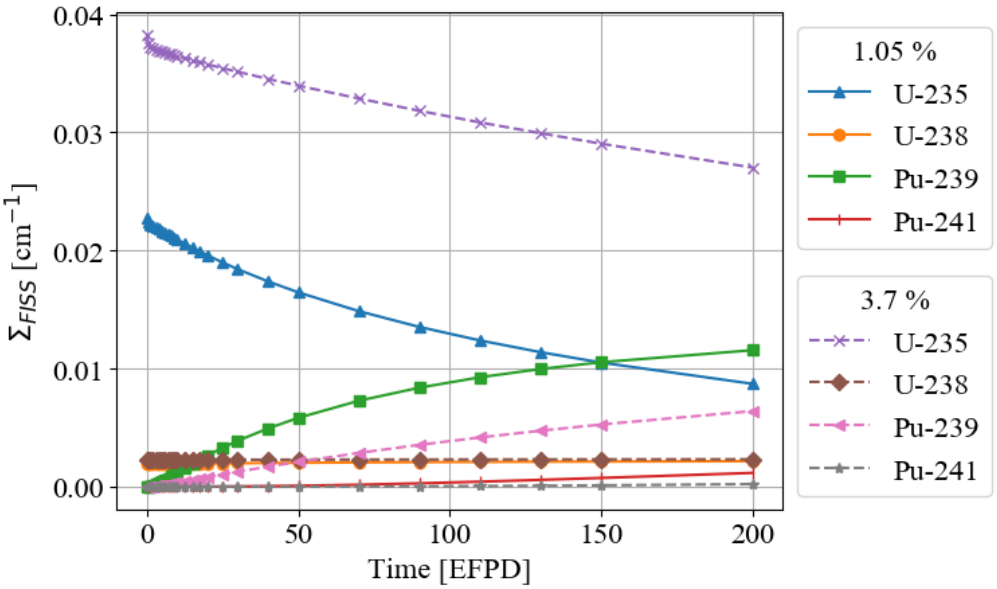


Figure 9.11 – Fission macroscopic cross section of the major fissile isotopes in PWR loaded with UO_2.

The lower the enrichment, the larger the decrease in U-235 and the increase in Pu-239. On the contrary, for higher enrichments, the respective decrease and increase are linear. It can be concluded that the behaviour of the reactivity evolution differs between the two enrichments, due to the faster relative consumption of U-235 and the faster accumulation of Pu-239 for a lower fuel enrichment. To prove this, the sum of the macroscopic fission cross sections of U-235 and Pu-239 is shown in Figure 9.12.

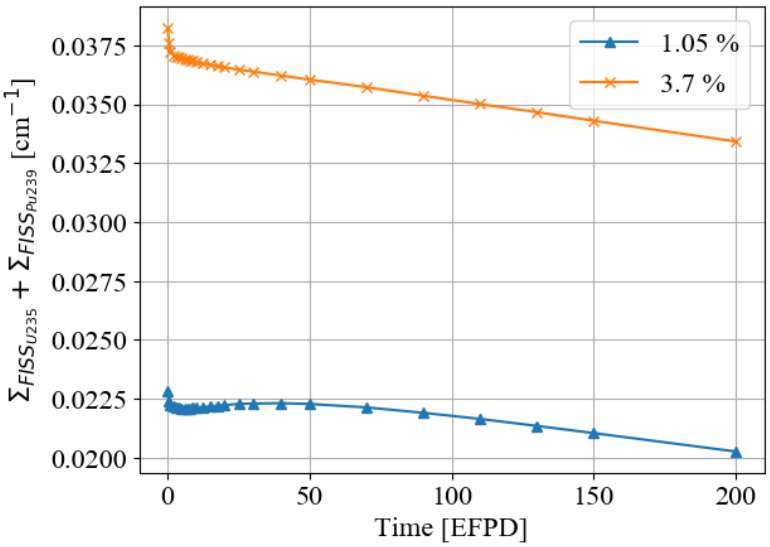


Figure 9.12 – Sum of U-235 and Pu-239 fission macroscopic cross sections.

The behaviour of the sum of macroscopic cross sections of U-235 and Pu-239 shows the same trend in the reactivity evolution in the different enrichment cases. In conclusion, for low enrichments, plutonium fissions are more important than U-235 consumption and make the reactivity increase during the first reactor period.

This variation in reactivity (which occurs at low uranium enrichments) is characteristic of CANDU reactor cores, which are cooled by heavy water and fuelled with natural uranium. The natural uranium enrichment is 0.72 % and the reactivity loss trend (as presented in this work for lower enrichments) is observed in this type of reactor. In the literature, the physical explanation is attributed to the accumulation of Pu-239 [117] [118].

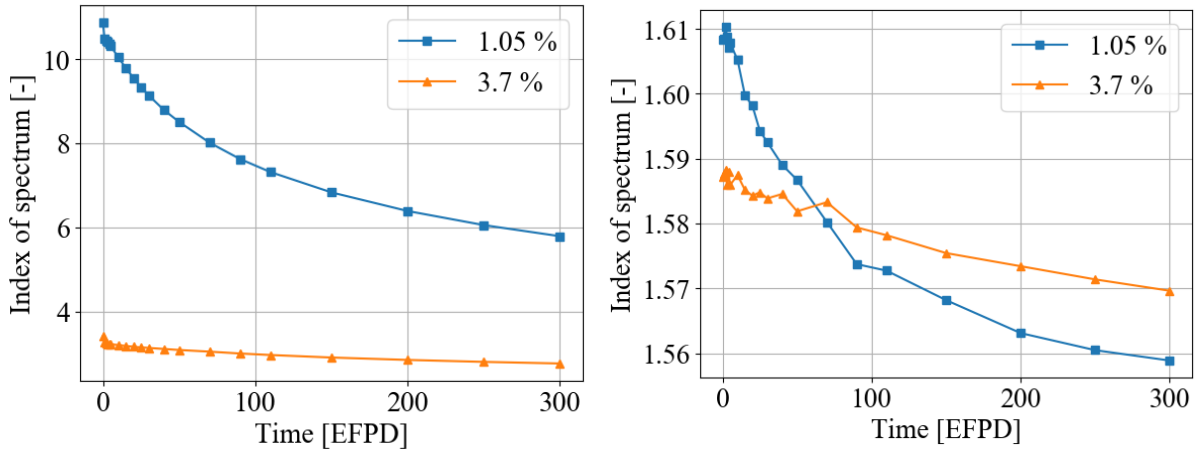
In the case of lower enrichment, the flux is more thermalized. In both cases, the spectrum is hardened during burn-up, due to the build-up of plutonium, which produces faster neutrons than uranium.

The parameter index of spectrum, described in (4.1), is calculated here accounting for the thermal and epithermal components of the spectrum. The represented index of spectrum is obtained considering the range up to 1 eV - in Figure 9.13(a) - for the thermal spectrum and between 1 eV and 1 keV - in Figure 9.13(b) - for the resonances zone:

$$x_{therm} = \frac{\int_{1e-10\ MeV}^{1e-7\ MeV} \phi\ dE}{\int_{\Delta E_{TOT}} \phi\ dE} \quad \frac{(\Delta E_{TOT})}{(1e^{-7} - 1e^{-10})} \tag{9.10}$$

$$x_{epith} = \frac{\int_{1e-7\ MeV}^{1e-2\ MeV} \phi\ dE}{\int_{\Delta E_{TOT}} \phi\ dE} \quad \frac{(\Delta E_{TOT})}{(1e^{-2} - 1e^{-7})} \tag{9.11}$$

Its variation of the spectrum is represented in the next Figure 9.13 for the two enrichments 1.05 % and 3.70 %. The two figures refers to the thermal and epithermal spectra, the fast spectrum is not represented as it is complementary to the other two.



(a - thermal) *(b - resonance)*

Figure 9.13 – PWR index of spectrum evolution with burn-up, for different U-235 enrichments in thermal interval (a) and resonance interval (b).

Between the two enrichments, the spectrum hardens with burn-up. For lower enrichments, the index shows a steeper slope. This effect can be explained by the plutonium production: the higher the content of U-238 at BOL, the larger the plutonium production and the harder the spectrum.

In conclusion, for lower uranium enrichments, the U-238 content is higher and, consequently, Pu production is greater. The higher Pu content implies a spectrum hardening, because the neutrons produced by Pu-239 (the main fissile isotope of Pu in this configuration) are emitted at higher energies than the neutrons produced by U-235. Furthermore, the amount of neutrons produced per fission event is higher for Pu-239 than for U-235. For these reasons, the simultaneous consumption of U-235 and the increasing fission rate of Pu-239 lead to an increase in reactivity during the first few days of reactor operation at low fuel enrichments.

IV.3. Xe contribution in the KGH method

The Xe contribution to the neutrons equilibrium depends on the core power (specifically on the neutron flux). In this section, the Xe effect is added to the KGH model to account for its contribution to the power evolution.

First the reactivity loss due to the Xe build-up is computed looking at the reactivity loss during the first days of core evolution for reactors operated at different powers. In Figure 9.14, the amplitude of the reactivity loss is shown for the HTR core presented in Chapter 4. The values of the loss computed at 5 days are summed up in Table 9.4.

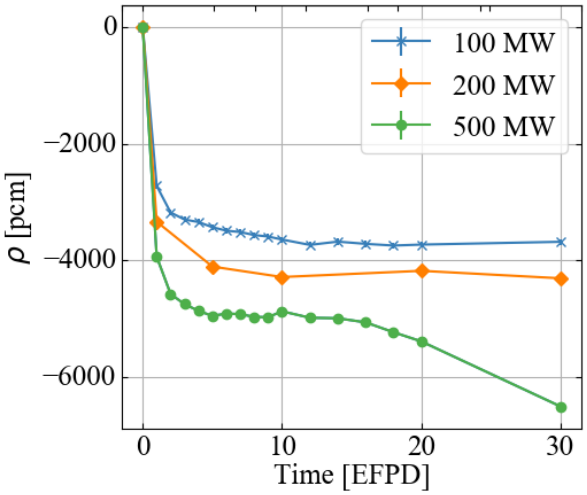


Figure 9.14 – Xe effect according to different core powers in HTR.

Table 9.4 – Xe effect on the initial reactivity loss according to different core powers in HTR.

Core power [MW]	Xe effect [pcm]
100	-3435
200	-4111
500	-4958

The contribution to the reactivity loss is not linear with the power and it is graphically represented in Figure 9.15. A logarithmic trend has been identified in a preliminary approach (represented by the pointed line in the figure) and the associated trend curve is evaluated:

$$\Delta\rho = 7{,}85\ e2 * ln(P) - \ 3{,}78\ e1; \qquad (9.12)$$

where $\Delta\rho$ is the reactivity loss in pcm and P is the power in MW.

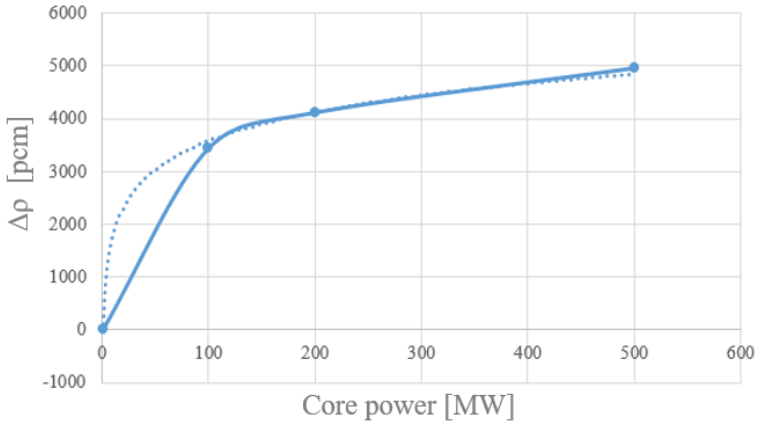


Figure 9.15 – Reactivity loss due to Xe-effect in function of core power.

Now let's consider a HTR reactor with a start-up phase actively controlled until the end of the Xe apparition. Then the autonomous operating mode starts. When the power will decrease with the time, the Xe effect will be reduced and will help to slow the reduction in power. To evaluate this contribution, one specific term is thus added to the KGH formulation:

$$\Delta\rho_{core} = H\,\Delta P_{core} + C_{Xe}\,\Delta P_{core} + G\,\Delta(\Delta T_{core}) + \Delta\rho_{fuel} = 0; \qquad (9.13)$$

where the term C_{Xe} is the power-dependent contribution to the reactivity due to the Xe-effect, expressed in pcm/%P_n.

The evolution of the power for a reference HTR with 232 MW of nominal power is analysed. In Figure 9.16, the case that does not account for the Xe contribution is compared to the one that accounts for that.

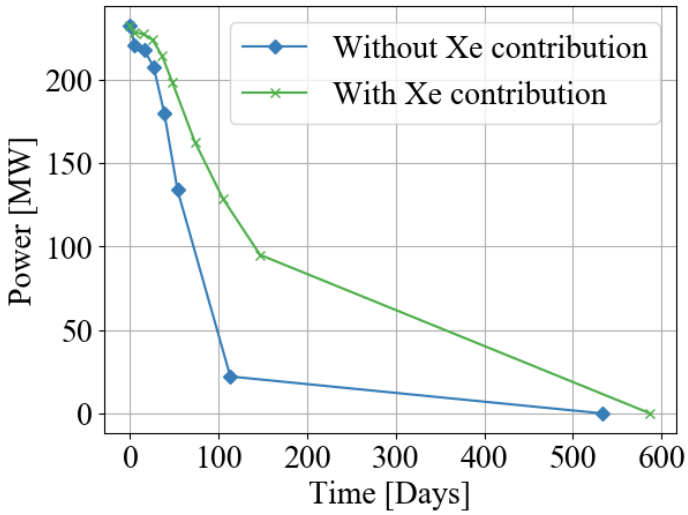


Figure 9.16 – Power evolution of HTR, comparison with the curve with the Xe contribution.

The two curves shows differences, the Xe effect contributes as expected in a beneficial way on the power evolution, decreasing the power loss rate and increasing the reactor lifetime. Its contribution is more important mainly for low powers. In this work this has not been taken into account mainly because the analysis has been focused on HTR reactors that has a neutron spectrum shifted through the fast energies (due to the insertion of actinides or burnable poison in fuel), where the Xe-effect is not present. It is noted that deeper theory on this can be found in [119].

Annex V

Annexes to chapter 5

V.I. Spectrum hardening of HTR with actinides

In this section, the attention is focused on an HTR core fuelled with actinides. The physical explanation of the different spectrum hardening is given.

First, the $UAmO_2$, $UNpO_2$ and $UThO_2$ cases are analysed. Figure 9.17 shows the capture cross sections for the absorbing isotopes in the three cases.

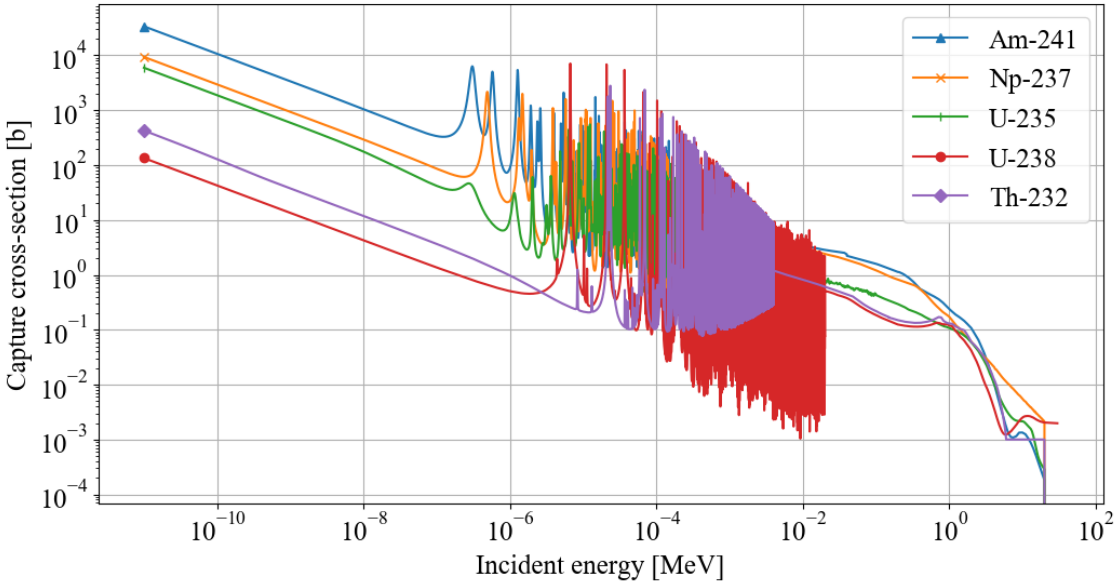


Figure 9.17 – Capture cross section of Am, Np and Th actinides compared to the U [data from JANIS NEA, JEFF-3.1.1 [116]].

The Am-241 and Np-237 exhibit large resonances captures around 1eV. Even U-235 shows resonance peak around 1eV and in the case of insertion of actinides, the enrichment of U-235 is increased. Thus, the thermal neutrons are mainly absorbed in this energy range, contributing to the spectrum hardening. The configuration of Th based fuel is characterized by lower capture cross section and resonances in higher energy range with respect to the previous actinides (the resonance peak of Th-232 is around 8e-4 MeV). Furthermore, the configuration includes a very large amount of Th that hardens slightly the spectrum, compared to UO_2 configuration. Indeed, the insertion of Th requires a slightly higher content of fissile material at BOL, with respect to the reference case of UO_2.

In Figure 9.18, the capture cross section of MOX fuel major isotopes are shown.

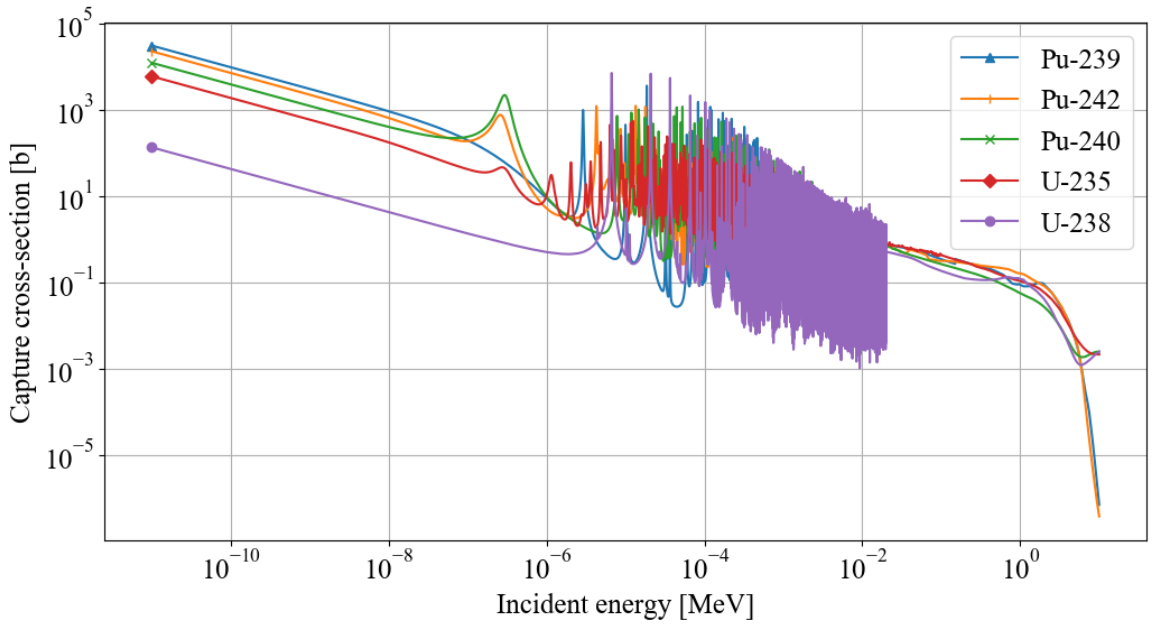


Figure 9.18 - Capture cross section of major Pu isotopes in MOX vector compared to the U sections[data from JANIS NEA, JEFF-3.1.1 [116]].

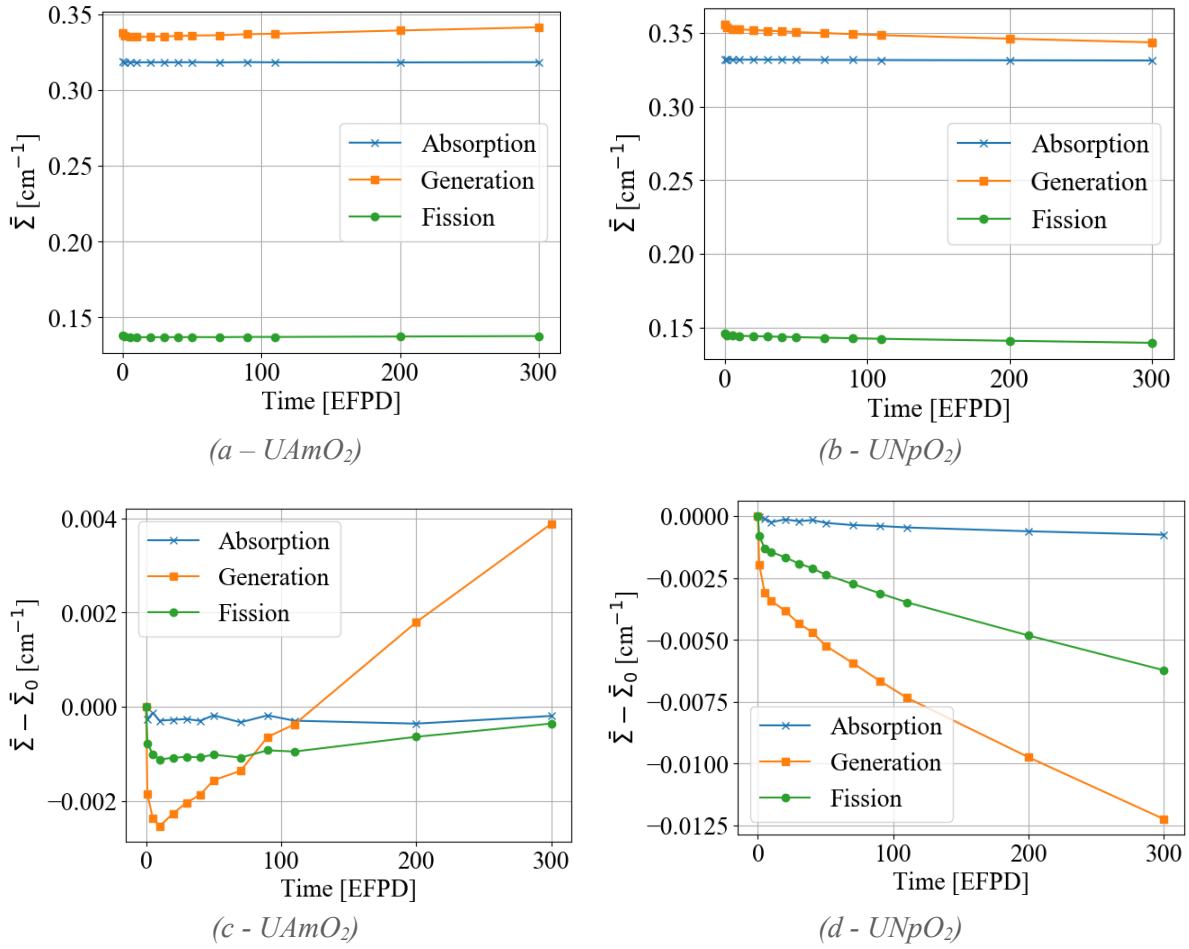
It can be noticed that the Pu isotopes are characterised by a larger capture cross section, with capture resonances around 5eV. With respect to UO_2 fuel, the Pu isotopes absorb more thermal neutrons, thus hardening the spectrum. Furthermore, the neutrons emitted by fissions of Pu isotopes have higher energies with respect to the ones emitted following U fissions. It can be concluded that the thermal capture cross section of Am, Np and Pu are larger with respect to the ones of U and are characterised by large resonance peaks in the thermal energies. Thus the configuration containing these actinides will have a harder spectrum with respect to the UO_2 configuration.

V.2. Investigation on the reactivity swing of Am and Np configurations

In this section, the reactivity loss of the HTR configurations of $UAmO_2$ and $UNpO_2$ are analysed into details. These configurations are characterised by almost the same fissile content and neutron spectrum, but show different trends for reactivity evolution. The case with Am is characterised by a reactivity increase while the case with the Np insertion shows an almost linear decrease.

Figure 9.19 shows the evolutions of the total macroscopic cross sections of the two configurations, the Am on the left (a) and the Np on the right (b). To better highlight the trend, in Figure 9.19(c) and Figure 9.19(d) the cross section evolution is represented by cross section at each time step difference with respect to the initial value at time t=0.

A precision is given on the generation total cross section. It is defined as: $\Sigma_g = \sum_i \nu_i \, \Sigma_{f_i}$; representing the sum over all the fissile isotopes i, of the number of neutrons generated per fission (ν) multiplied by the macroscopic fission cross section (Σ_f).



(a – $UAmO_2$) *(b - $UNpO_2$)*

(c - $UAmO_2$) *(d - $UNpO_2$)*

Figure 9.19 – Evolution of the macroscopic cross sections of $UAmO_2$ (a) and $UNpO_2$ (b) and evolution of the same parameters deviation to the value at t=0 (c and d).

The initial decrease of the fission (and generation) cross sections is due to an initial spectrum hardening caused by Xe and Pu built-up in the core. Successively, the fission cross sections increase, in the case of Am, and decreases, in the case of Np. This difference is explained by the analysis of the neutron spectrum evolution of the two cases. On the other hand, in case of Am, the absorption does not show large variations, while is slightly decreasing in case of Np.

Figure 9.20 shows the evolution of the "spectrum index" of both configurations, the value is represented as the difference of the index at each time step with respect to the first value at t=0. Decreasing values of the index leads to spectrum hardening, while increasing values leads to more and more thermal spectrum. The two configurations show an initial hardening of the spectrum during the first days, due to the xenon effect and Pu build-up. Successively, the Am configuration shows a softening of the spectrum. On the other hand, the Np configuration is characterised by a spectrum that is hardening.

The two opposite trends of the spectrum explain the different fission cross sections evolutions. The Am core, with the softening of the spectrum increases fissions, due to larger cross section in thermal energies. Furthermore, in the configuration with the Am, the macroscopic fission cross section increases softly, while the macroscopic generation cross section increases at a larger rate. The large increase of the generation cross section is due to the increase of the Pu inventory (that appears as result of the U-238 absorption). On the other hand, the Np case is characterised by the spectrum that is hardening, decreasing

the microscopic cross section of the fissile isotopes. Thus the case with Np is characterised by a decrease of fission cross sections.

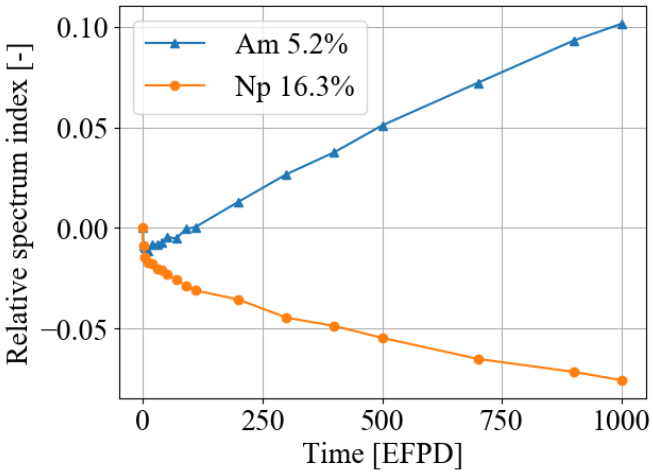
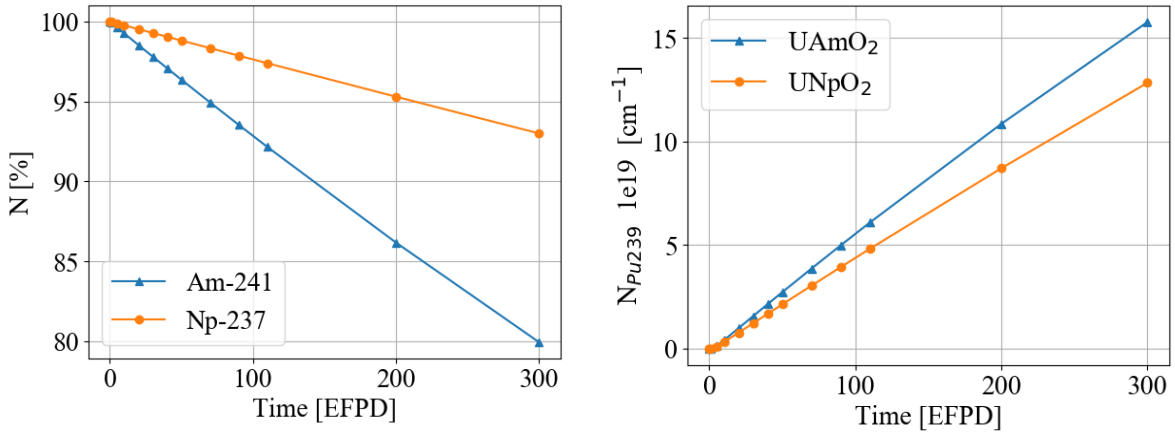


Figure 9.20 - Evolution of the index of spectrum of $UAmO_2$ and $UNpO_2$ configurations.

The evolution of the spectrum is due to the concurrence of the kinetics of two effects: the actinide disappearing and the Pu-239 creation. Comparing the two cases the Am content disappears faster than the Np, as shown in Figure 9.21(a) in percentage of content evolution. On the other hand, the $UAmO_2$ case shows a faster creation of Pu-239. In this case, the disappearance of the Am has a larger impact on the spectrum than the Pu-239 built-up. Consequently, the spectrum of the Am case is "thermalized". On the other hand, the case of $UNpO_2$ shows a slower disappearance of Np and a slower Pu-239 build-up. In this case, the concurrence of the two opposite contributions leads to a spectrum hardening.



(a) *(b)*

Figure 9.21 – Evolution of the content of Am and Np in $UAmO_2$ and $UNpO_2$ configurations (a) and evolution of the Pu-239 content in $UAmO_2$ and $UNpO_2$ configurations (b).

V.3. HTR fuelled with $UAmO_2$ and $UNpO_2$ physical analysis of reactivity swing

In this section, the physical analysis of the reactivity evolution according to the Am contents in HTR is performed. In particular, the case between the core charged in UO_2 and with low and high Am contents are compared. The results are shown in Figure 9.22. The objective of this discussion is to analyse the physics of the reactivity behaviour with a core charged with UO_2 compared to a $UAmO_2$ fuel.

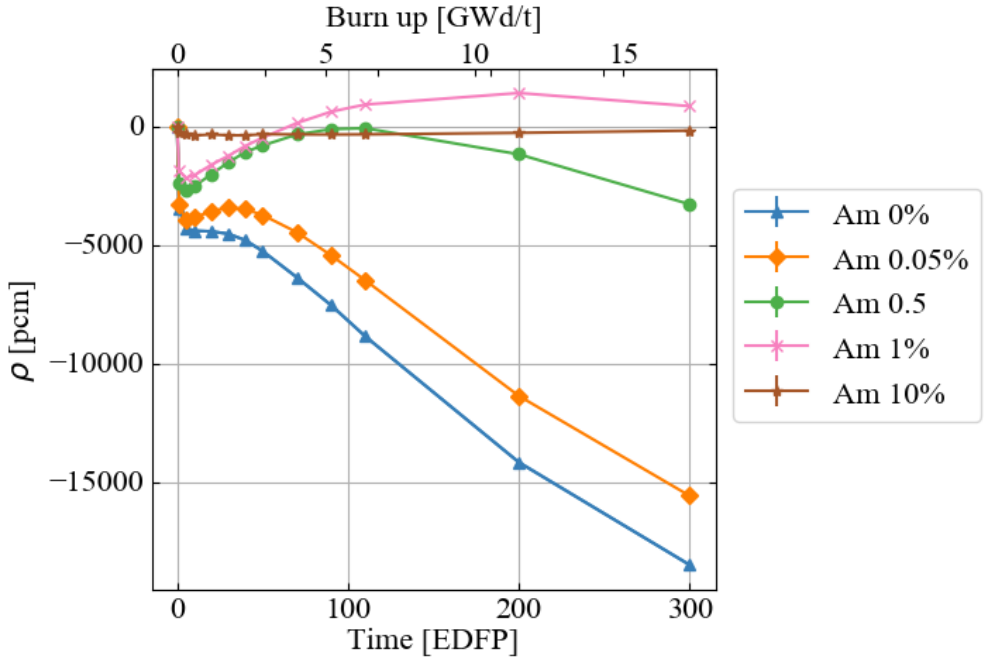
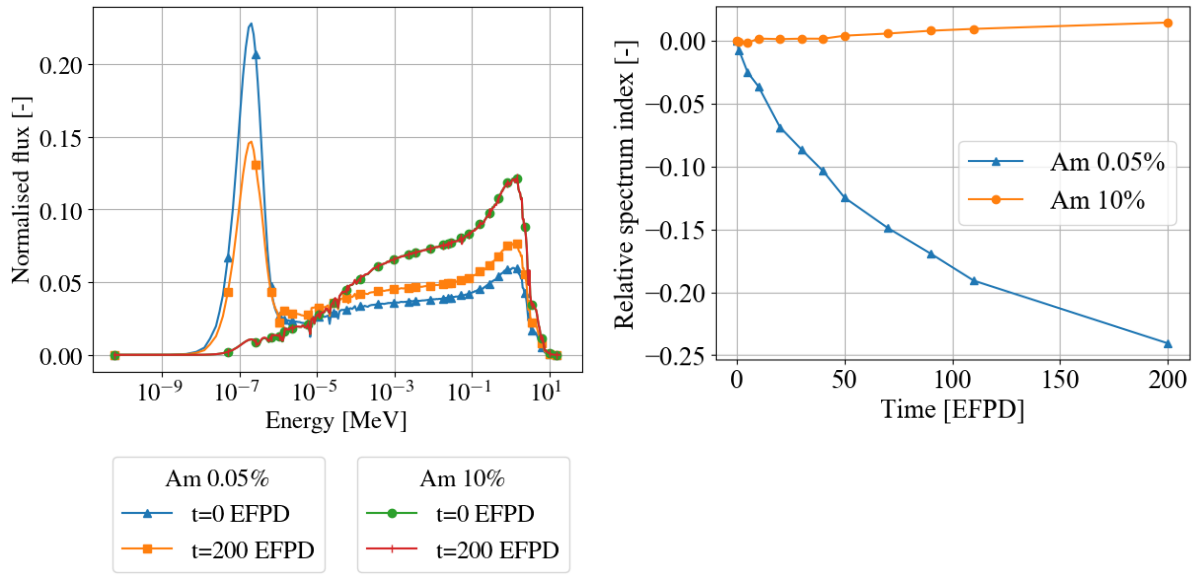


Figure 9.22 - Reactivity evolution according to variation of Am content in $UAmO_2$ HTR fuel – analysis on low Am contents.

With respect to the UO_2 core, the insertion of Am hardens the spectrum at BOL. Thus, increasing the americium content, the initial xenon effect decreases up to an Am content of 10%, configuration in which the initial Xe reactivity loss nearly disappears. After the first days of operation, the reactivity increases and then decreases. For lower Am content the reactivity increase is sharper and the peak appears sooner in time.

To analyse the reason of this behaviour, the case of 0.05% and 10% of content of americium are compared. They have been chosen being one case where the peak is around 50 EFPD and the other showing the "flattest" reactivity evolution.

In Figure 9.23(a), the neutron spectrum at t=0 EFPD and t=200 EFPD (instant taken as example) is shown for the two configurations. At t=0, the higher the Am content the harder is the spectrum. At 200 EFPD, the configuration with Am 0.05% content shows that the spectrum has hardened during the evolution. On the other hand, the configuration of Am 10% shows a spectrum that has not drastically changed (it is slightly softened at 200 EFPD). The evolution of the spectrum is represented via the curve of the spectrum index. In particular, Figure 9.23(b) shows the difference of the index of spectrum at time t with respect to the index at time t=0. The case of Am 0.05% content shows a decreasing index of spectrum, representative of a spectrum that hardens in time. On the other hand, the configuration Am-10% shows a slightly softening spectrum during the evolution.

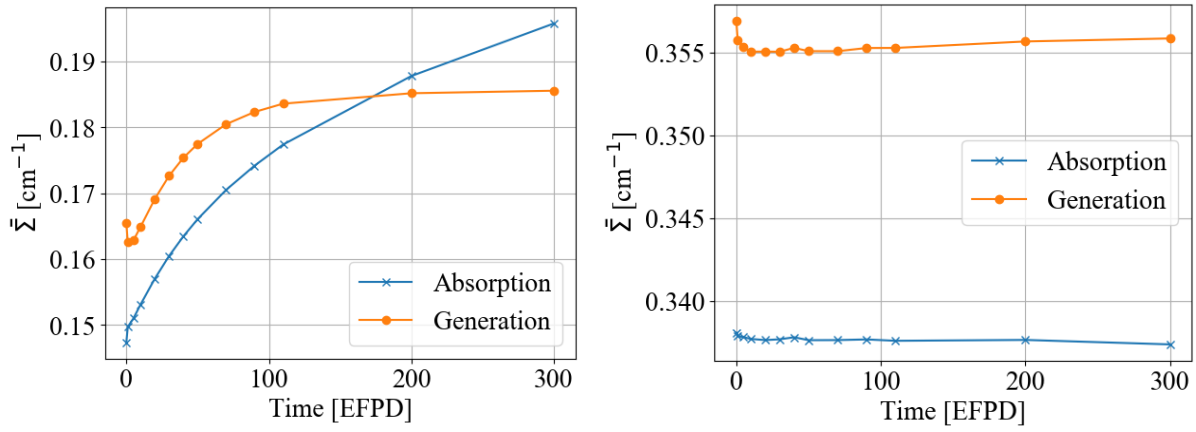


(a) *(b)*

Figure 9.23 – Neutron spectrum comparison between t0=0 EFPD and t1=200 EFPD (a) and evolution of the index of spectrum (b), for different Am contents.

The effect of the different evolution of the spectrum on the reactivity is illustrated with the analysis of the two configurations cross sections.

In Figure 9.24, the mean (absorption and generation) macroscopic cross sections are compared. The case of Am content 0.05% content is represented in Figure 9.24(a) and the one of 10% in Figure 9.24(b).



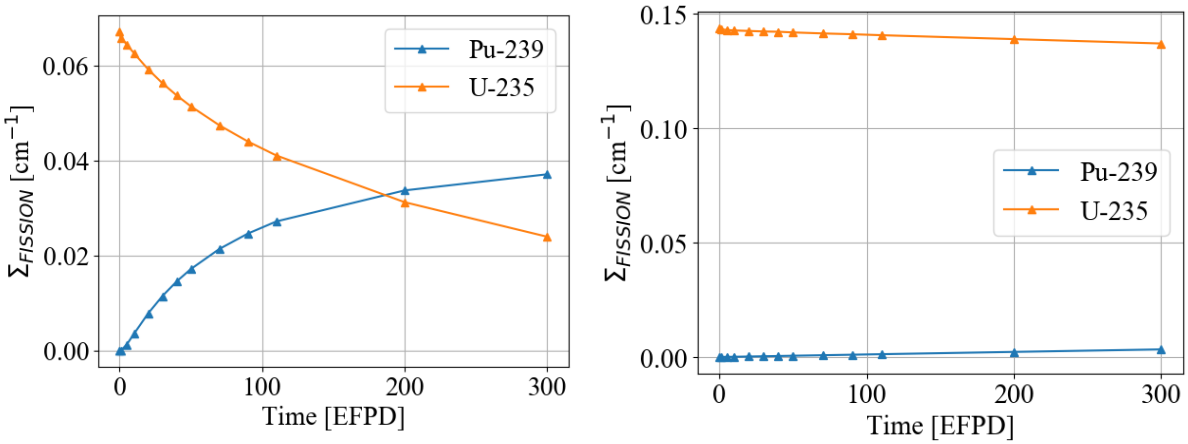
(a – 0.05%) *(b – 10%)*

Figure 9.24 – Absorption and generation mean macroscopic cross section comparison in $UAmO_2$ configuration, with 0.05% (a) and 10% (b) Am contents.

The absorption and generation mean cross sections explain the behaviour of the reactivity evolution. The case with lower Am content (Figure 9.24(a)) shows a higher and faster generation section increase that the case with higher Am content (Figure 9.24(b)). At the same time, for lower Am content, absorption cross section increases, slower than the generation rate in the first 50 EFPD and faster after 50 EFPD. This explains the first increase and then decrease of the reactivity for 0.05% Am content. On the other hand, the case of higher Am content shows an absorption rate nearly constant and, with the generation rate slowly growing, the consequent reactivity evolution is slowly growing. The case of

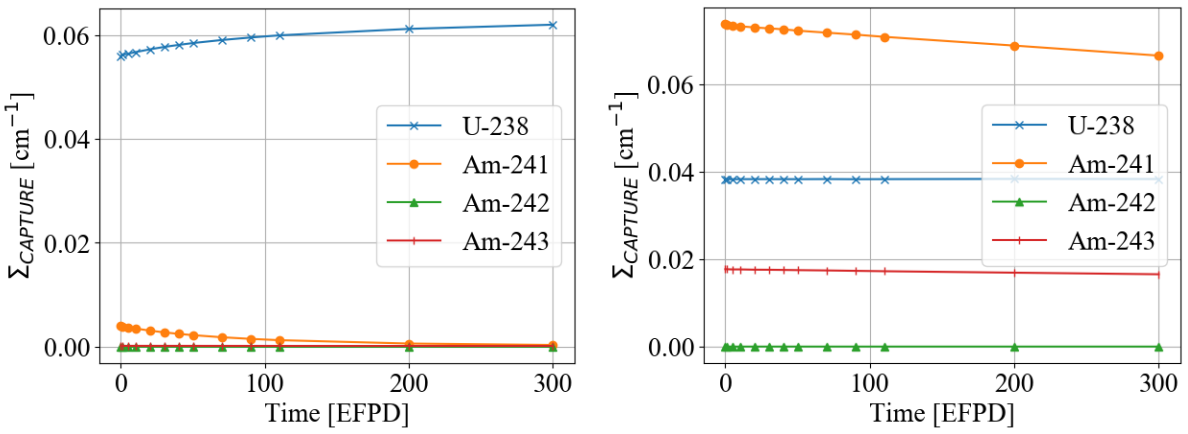
0.05% Am content is characterised by a rapid consumption of Am due to the very low initial content. On the other hand, the 10% configuration shows a slower Am depletion.

The major isotopes, contributing to the behaviour of the absorption and generation sections of the two cases, are analysed. The major contributing isotopes to the fission (U-235 and Pu-239) are compared in Figure 9.25, while the major contributing isotopes to the captures (U-238 and Am) are compared in Figure 9.26.



(a –0.05%) *(b –10%)*

Figure 9.25 – HTR UAmO$_2$ evolution of fission macroscopic cross sections for different Am contents – 0.05% (a) and 10% (b).



(a – 0.05%) *(b –10%)*

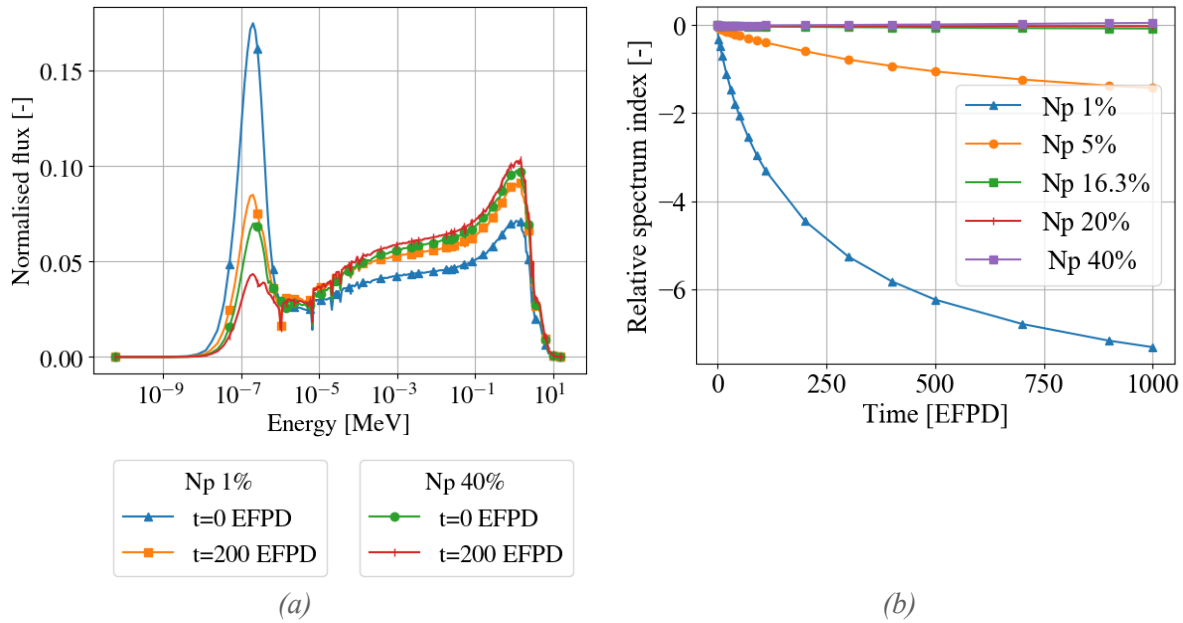
Figure 9.26 - HTR UAmO$_2$ evolution of capture macroscopic cross sections for different Am contents – 0.05% (a) and 10% (b).

Figure 9.25 shows the different evolution of the fission cross sections. In the case of 0.05% Am content, the decrease of U-235 and the increase of Pu-239 contributions are sharper than in the case of 10% Am content. In this configuration, the reactivity evolution is characterised by an initial increase (up to 50 EFPD) and then a decrease, this phenomenon is bound to the initial Pu-239 fissions increases and then stabilisation between the Pu-239 increase and U-235 decrease. The evolution is similar to the one evaluated for the UO_2 case. On the other hand, the Am 10% configuration is characterised by a slower Pu-239 contribution, which make the generation cross section increasing very slowly.

Figure 9.26 represents the capture cross sections. The 0.05% configuration is characterised by an increase of the U-238 cross section that overcomes the other isotopes contribution. On the other hand, due to the higher content of Am, the Am 10% configuration is characterised by the effect of the Am-241 capture decrease.

Now, the difference between the Am and Np cases is analysed.

The difference between both cases relies in the hardening of spectrum during evolution and thus on the mean neutron generation decrease. The increase of Np content up to 40% is not sufficient to allow a softening of the spectrum during the irradiation phase as it was the case for the configuration with 10% of Am. The spectrum between 0 EFPD and 1000 EFPD is shown in Figure 9.27(a) for two configurations (1% and 40% of Np content). In Figure 9.27(b), the evolution of spectrum index is reported. The hardening of the spectrum is significant for low Np contents, and the spectrum does not show significant variations when the Np content increases. The spectrum evolution depends on the concurrent effect of the disappearance of the Np-237 and the build-up of the Pu-239 as shown in the comparison of the Am cases.



(a) *(b)*

Figure 9.27 - Neutron spectrum comparison between t0=0 EFPD and t1=1000 EFPD (a) and evolution of the index of spectrum (b), for different Np contents.

In conclusion, increasing the Np content in the core causes a decrease in the reactivity loss slope. However, the increase of Np content reaches a saturation point. It is not possible to obtain a flat reactivity with Np insertion, unlike the Am insertion case studied previously.

V.4. Theoretical parametric study of plutonium insertion in HTR fuel

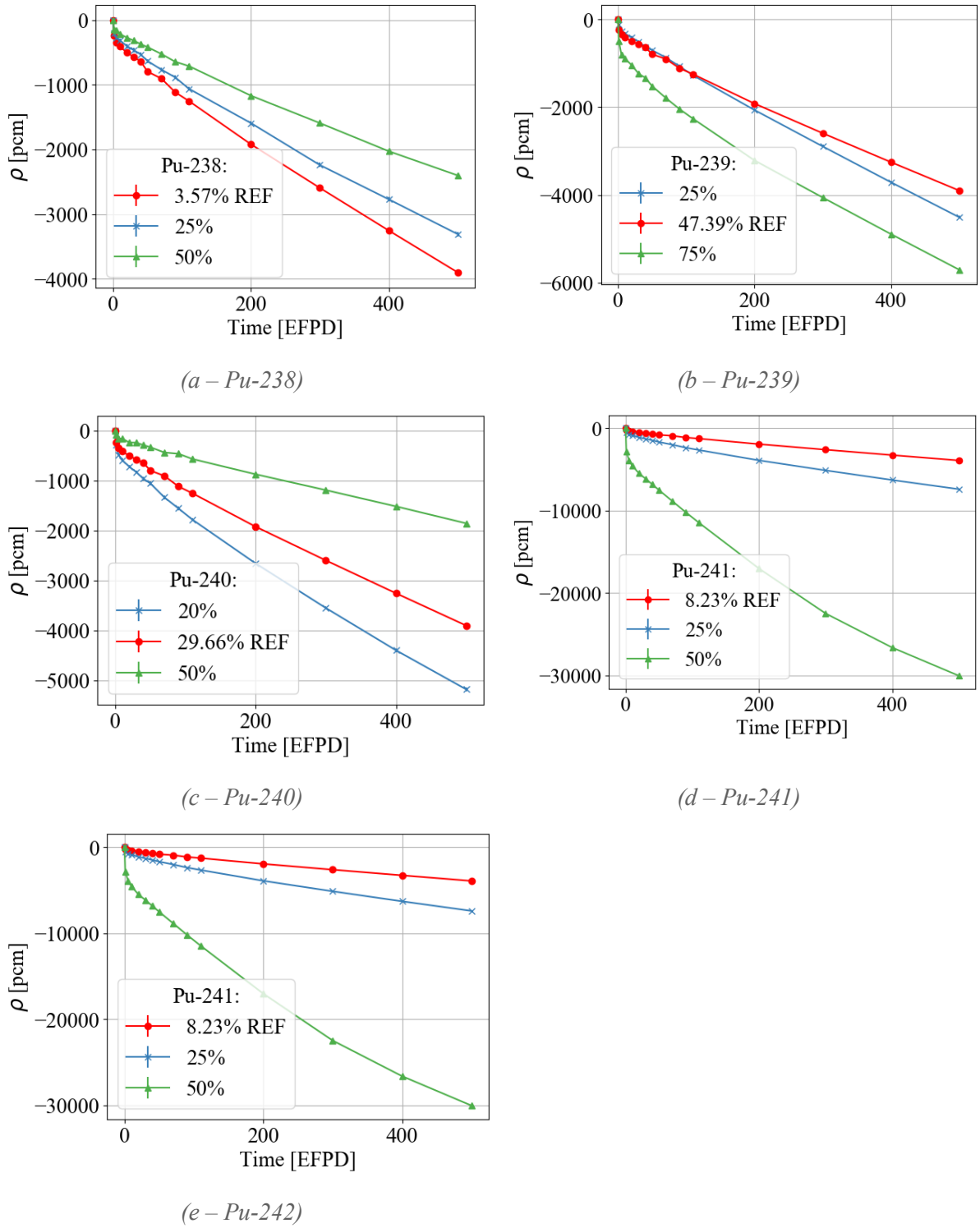
In this section, the Pu vector components are modified in order to evaluate the contribution of each isotope to the reactivity evolution. This sensitivity study aims to understand the effects of the different isotopes of the plutonium on reactivity and reactivity loss, even though it is well known that the production of such plutonium vectors is currently unrealistic in most of the cases presented. For each case, one isotope content is varied. The relative proportion of the other isotopes are kept constant compared to the reference case. In the table the Pu-X mass fraction in Pu vector refers to the ratio between the Pu-X isotope mass and the total Pu mass. On the other hand, as in the previous tables, the Pu content refers to the Pu mass ratio with respect to the total fuel mass. The U-235 enrichment is kept constant to 0.25%, while the Pu content in fuel, in each case, is adapted to guarantee criticality at BOL. The detailed composition of fuel material for each case is given in the tables below, while the configurations analysed are summed up in Table 9.5.

In this table, the variation of the isotopes of the Pu vector and the associated core Pu content are presented. The higher is the content of a fissile isotope (Pu-239 and Pu-241) and the lower is the necessary content of plutonium in the core. On the other hand, increasing the percentage of enrichment of plutonium with a non-fissile isotope, the higher plutonium content is needed (to increase the fissile contents of fissile Pu isotopes in the core).

Table 9.5 – Variation of Pu isotopes inside the Pu vector and associated core Pu content for criticality at BOL (HTR).

Configuration		Pu-X mass fraction in Pu vector [%]	Pu content [%]
Pu-238	REF	3.57 (Pu-238)	51
	25%	25 (Pu-238)	65
	50%	50 (Pu-238)	87
Pu-239	25%	25 (Pu-239)	77
	REF	47.39 (Pu-239)	51
	75%	75 (Pu-239)	20
Pu-240	20%	20 (Pu-240)	36
	REF	29.66 (Pu-240)	51
	50%	50 (Pu-240)	87
Pu-241	REF	8.23 (Pu-241)	51
	25%	25 (Pu-241)	24
	50%	50 (Pu-241)	2
Pu-242	REF	10.37 (Pu-242)	51
	25%	25 (Pu-242)	63
	50%	50 (Pu-242)	89

In the next Figure 9.28, the evolution of the core reactivity is shown, according to the different Pu vectors with respect to the reference configuration.



(a – Pu-238)

(b – Pu-239)

(c – Pu-240)

(d – Pu-241)

(e – Pu-242)

Figure 9.28 – Reactivity evolution according to the variation of the Pu vector in MOX fuel in HTR. Variation of the content of Pu-238 (a), Pu-239 (b), Pu-240 (c), Pu-241 (d), Pu242 (e).

The variation of the Pu vectors shows different tendencies. The increase of the insertion of Pu-238, Pu-239 and Pu-240 causes a decrease of the reactivity loss. On the contrary, the increase of the Pu enrichment in Pu-241 and Pu-242 causes an increase in the slope of the reactivity loss. The reason is in the plutonium irradiation chain. The first plutonium isotopes transmutation produces fissile isotopes of plutonium (the Pu-238 transmutes in Pu-239, the Pu-239 is fissile itself and the Pu-240 transmutes in

Pu-241). On the other hand, the Pu-241 and Pu-242 transmutations produce rapidly minor actinides that are characterised by important capture cross sections and that are not fissile.

To verify if a configuration that reduce further the reactivity slope is possible, the insertion of only the first three Pu isotopes is analysed. The configurations studied are shown in Table 9.6.

Table 9.6 – Configurations of the sensitivity analysis on the Pu isotopes contents.

Configuration	Pu-238 [%]	Pu-239 [%]	Pu-240 [%]	Pu-241 [%]	Pu-242 [%]	Am-241[%]
C1[5]	**50**	**50**	0	0	0	0
C2	0	**50**	**50**	0	0	0
C3	0	**67**	**33**	0	0	0

The associate Pu content to ensure criticality at BOL is reported in Table 9.7.

Table 9.7 - Sensitivity analysis on the Pu isotopes and associated Pu content for criticality at BOL

Configuration	U-235 enrichment [%]	Pu content [%]	Fissile content [%]
C1	0.25	3.50	1.99
C2	0.25	80.0	40.1
C3	0.25	60.0	30.1

The reactivity evolution is shown in Figure 9.29.

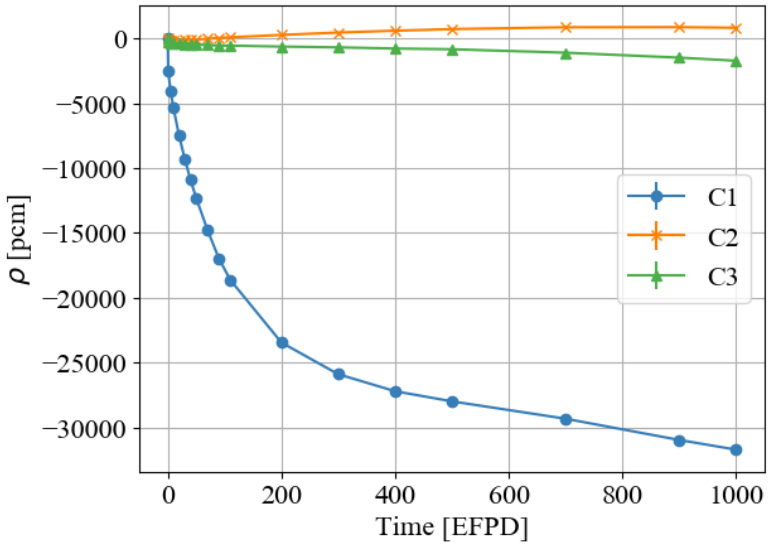


Figure 9.29 – Reactivity evolution according to specific configuration of Pu vector in MOX fuel in HTR.

The configurations C2 and C3 show significantly reduction of the reactivity loss with respect to the C1 configuration. The case C2 and C3 are characterised by the insertion of Pu-239 and Pu-240 in fuel. This combination includes the consumption of Pu-239 and its generation (via the U-238 captures) to be

[5] A vector with such a high proportion of Pu-238 will have a very high intrinsic heat production.

compensate by the Pu-240 production of Pu-241. The configurations highlight an equilibrium between the fissile isotopes consumption and the fertile isotopes regeneration.

The cases C2 and C3 show favourable evolutions for the scope of this work. They will be included in the comparison of the best configurations for an HTR autonomous core in Chapter 6. Their power evolution will be computed via the KGH method and the associated performance will be outlined.

In the following, the specific content of each isotope in each configurations are summed up.

Variation of Pu-238 vector [%].

Pu-238	Pu-239	Pu-240	Pu-241	Pu-242	Am-241	Pu con. [%]
3.57	47.4	29.7	8.23	10.4	0.780	51.0
25.0	36.9	23.1	6.40	8.07	0.607	65.0
50.0	24.6	15.4	4.27	5.38	0.404	87.0

Variation of isotopes contents [%].

Pu-238	Pu-239	Pu-240	Pu-241	Pu-242	U-235	U-238	TOT fiss	TOT fert
1.82	24.2	15.1	4.20	5.29	0.12	48.9	28.5	71.5
16.3	24.0	15.0	4.16	5.24	0.09	34.9	28.2	71.8
43.5	3.71	13.38	3.71	4.68	0.03	13.0	25.1	74.9

Variation of Pu-239 vector.

Pu-238	**Pu-239**	Pu-240	Pu-241	Pu-242	Am-241	Pu con. [%]
5.09	**25.0**	42.3	11.7	14.8	1.11	77.0
3.57	**47.4**	29.7	8.23	10.4	0.780	51.0
1.70	**75.0**	14.1	3.91	4.93	0.371	20.0

Variation of isotopes contents [%].

Pu-238	**Pu-239**	Pu-240	Pu-241	Pu-242	U-235	U-238	TOT fiss	TOT fert
3.92	**19.3**	32.6	9.03	11.4	0.06	22.9	28.3	71.7
1.82	**24.2**	15.1	4.20	5.29	0.12	48.9	28.5	71.5
0.34	**15.0**	2.82	0.78	0.99	0.2	79.8	16.0	84.0

Variation of Pu-240 vector.

Pu-238	Pu-239	**Pu-240**	Pu-241	Pu-242	Am-241	Pu con. [%]
4.06	53.9	**20.0**	9.36	11.8	0.887	36.0
3.57	47.4	**29.7**	8.23	10.4	0.780	51.0
2.54	33.7	**50.0**	5.58	7.37	0.554	87.0

Variation of isotopes contents [%].

Pu-238	Pu-239	**Pu-240**	Pu-241	Pu-242	U-235	U-238	TOT fiss	TOT fert
1.46	19.4	**7.20**	3.37	4.25	0.16	63.8	22.9	77.1
1.82	24.2	**15.1**	4.20	5.29	0.12	48.9	28.5	71.5
2.21	29.3	**43.5**	5.09	6.41	0.03	13.0	34.4	65.6

Variation of Pu-241 vector.

Pu-238	Pu-239	Pu-240	**Pu-241**	Pu-242	Am-241	Pu con. [%]
3.57	47.4	29.7	**8.23**	10.4	0.780	51.0
2.92	38.7	24.2	**20.0**	8.47	0.637	24.0
1.95	25.8	16.2	**50.0**	5.65	0.425	2.00

Variation of isotopes contents [%].

Pu-238	Pu-239	Pu-240	**Pu-241**	Pu-242	U-235	U-238	TOT fiss	TOT fert
1.82	24.2	15.1	**4.20**	5.29	0.12	48.9	28.5	71.5
0.700	9.30	5.82	**6.00**	2.03	0.19	75.8	15.5	84.5
0.04	0.52	0.32	**1.00**	0.11	0.25	97.8	1.76	98.2

Variation of Pu-242 vector.

Pu-238	Pu-239	Pu-240	Pu-241	**Pu-242**	Am-241	Pu con. [%]
3.57	47.4	29.7	8.23	**10.4**	0.780	51.0
2.99	39.7	24.8	6.89	**25.0**	0.653	63.0
1.99	26.4	16.6	4.59	**50.0**	0.435	89.0

Variation of isotopes contents [%].

Pu-238	Pu-239	Pu-240	Pu-241	**Pu-242**	U-235	U-238	TOT fiss	TOT fert
1.82	24.2	15.1	4.20	**5.29**	0.12	48.9	28.5	71.5
1.88	25.0	15.6	4.34	**15.8**	0.09	36.9	29.4	70.6
1.77	23.5	14.7	4.09	**44.5**	0.03	11.0	27.6	72.4

V.5. How to insert BU in a HTR?

In this section, an analysis of different possible configurations of burnable poisons is made considering, as shown in the following. First of all, two configurations of insertion of burnable poisons are compared considering the same B-10 mass. Successively a parametric analysis is made changing the content or the position of the burnable poisons, as explained in the following lines. The comparison is made in terms of necessary U-235 enrichment to ensure criticality at BOL, reactivity feedbacks, reactivity burn-up swing and power evolution.

The two configurations analysed are described in the following lines. The first involves the burnable poison homogeneously mixed in the fuel kernel, the second foresees the poison inserted among the TRISO protection layers. In order to make a comparison with the different configurations, the B is inserted in the core with a total volume, in all the three cases, that ensures the same mass of B-10. The reference mass taken as example for the comparison corresponds in this case to a dilution of 0.125 % of B merged in fuel [102]. In the case of the poison merged in the fuel kernel, the pure B has been homogeneously inserted. On the other hand, in case of insertion of poison in the TRISO layers, the material B_4C has been used, for structural reasons. The B considered in this first part of the analysis corresponds to the natural boron composed with 19.9% (atomic fraction) of B-10 and the complementary fraction of B-11.

The first configuration (boron merged in fuel) does not involves geometry modification, the other is represented in Figure 9.30. This configuration has already been explored in literature references that study the possibility of adding a burnable poison inside the particle configuration, naming it QUATRISO particle [96] [120]. However, in the literature studies, the addition of burnable poison in the core is made to compensate the initial reactivity excess, but an active reactivity control is required in addition during the core lifetime.

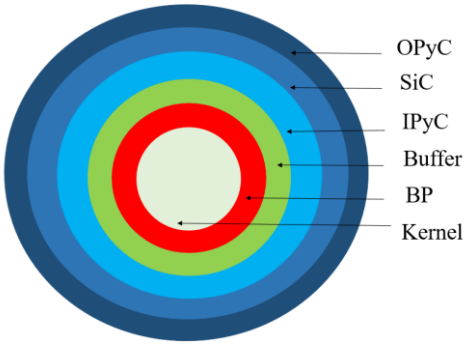


Figure 9.30 – TRISO particle with an additional burnable poison (BP) thickness.

Enrichment

In the following Table 9.8, the U-235 enrichment (for criticality at BOL) is compared for the two configurations. For the simplification of the notation in the rest of this work, the configuration with the poison merged in fuel will be named as “fuel”, the one with the addition of one layer of poison inside the TRISO will be addressed as “cladding”.

Table 9.8 – U-235 enrichment for different configurations of burnable poison insertion in HTR.

Configuration	U-235 enrichment [%]
Without burnable poison	2.3
Fuel	12.0
Cladding	12.5

The relative neutron spectrum is shown in Figure 9.31.

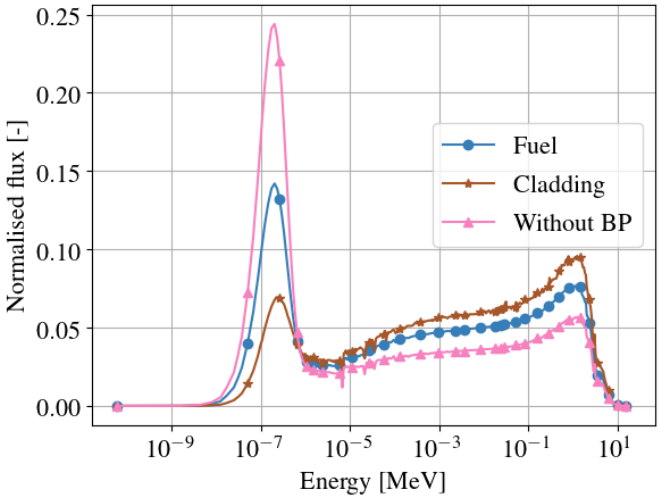


Figure 9.31 – Neutron spectrum of HTR with burnable poison (BP).

Reactivity feedbacks

In Table 9.9 the reactivity feedback coefficients are shown.

Table 9.9 - Reactivity feedbacks for different burnable poisons configurations - HTR.

Configuration	Doppler coefficient [pcm/K]	Graphite coefficient [pcm/K]
Without burnable poison	-5.60	-2.08
Fuel	-4.45	-0.56
Cladding	-4.32	-0.54

The spectrum hardening causes the reactivity feedback coefficients to be lower with respect to the case without the burnable absorbers.

Burn-up reactivity swing

The evolution of the core in the three configurations is represented in the following Figure 9.32.

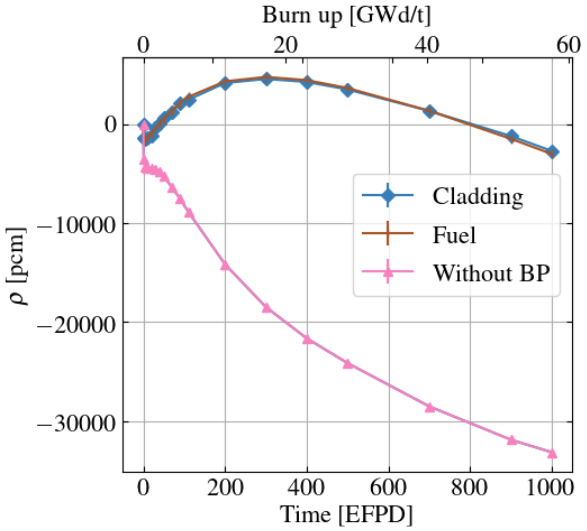


Figure 9.32 – HTR reactivity evolution with burnable poisons in different configurations.

The boron insertion causes a reduced xenon effect with respect to the reference case, due to the spectrum hardening. The reactivity evolution is characterised by a first increasing phase and a decrease after about 300 EFPD due to the dynamic consumption of the boron, as analysed in the following.

Power evolution

The simultaneous effect of the reactivity swing and the reduced reactivity feedbacks are analysed with the KGH method. Figure 9.33 shows the power evolution in the different configurations.

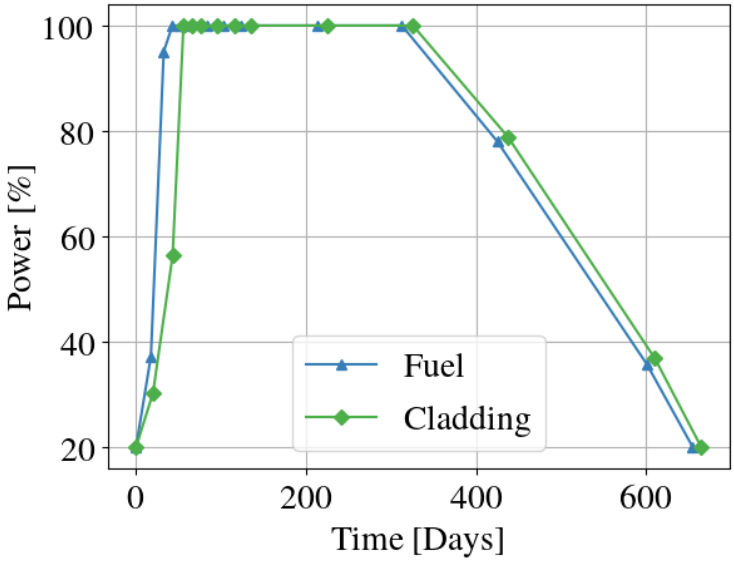


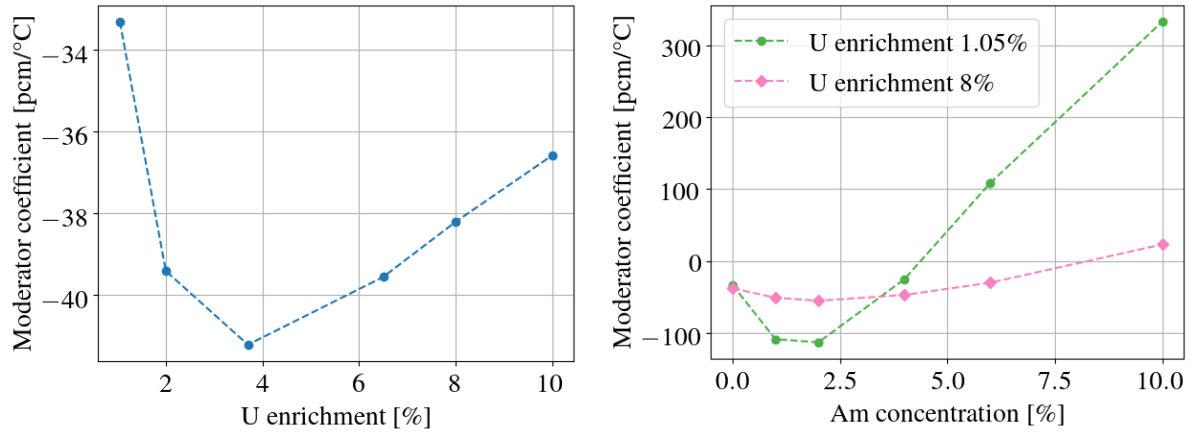
Figure 9.33 – HTR power evolution with burnable poisons in different configurations.

The reactivity swing, due to the insertion of absorber materials, causes the initial increase of the reactivity. Furthermore, the decrease of the reactivity feedbacks, in burnable poison configuration with respect to the reference case, involves a lower reactivity swing compensation. So the power increases its value up to100% and it will probably be impossible to pilot such an excess of reactivity with simplified control devices. In case of using active systems, the power shows almost a maximum life time of 600 days.

In conclusion, the insertion of the burnable poison merged in fuel or inserted in cladding causes a large power swing, due to the large reactivity swing and lower reactivity feedbacks coefficients. The two configurations do not show significant difference.

V.6. Moderator coefficient in an 'autonomous' REP

Here, the effect of the Am insertion on the PWR moderator coefficient is analysed. As the variation of the coefficient is associated to the variation of the two parameters (Am content and U enrichment), two different cases are analysed. In Figure 9.34(a), UO_2 fuel is considered with different U enrichments. In Figure 9.34(b), $UAmO_2$ fuel is considered with constant U enrichment (for each curve) and different Am contents.



(a) *(b)*

Figure 9.34 – Variation of the moderator coefficient depending on the U enrichment (a) and the Am content (b).

Both the U enrichment and Am content shows the effect of initial increase of the moderator coefficient and then decrease. Further analysis is made on this behaviour based on the four factors formula:

$$k_\infty = \varepsilon\, p\, f\, \eta; \qquad (9.14)$$

where: ε is the fast fission factor [-]; p is the resonance escape probability [-]; f is the thermal utilisation factor [-] and η is the thermal fission factor [-]. For more detailed description of this formulation see [60].

First, the case with only UO_2 is analysed, referred to Figure 9.34(a). The four factors are shown in Figure 9.35.

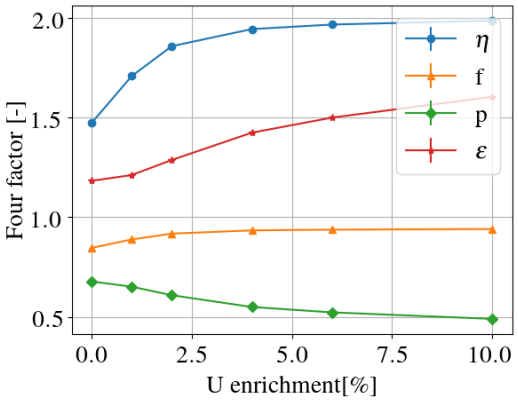
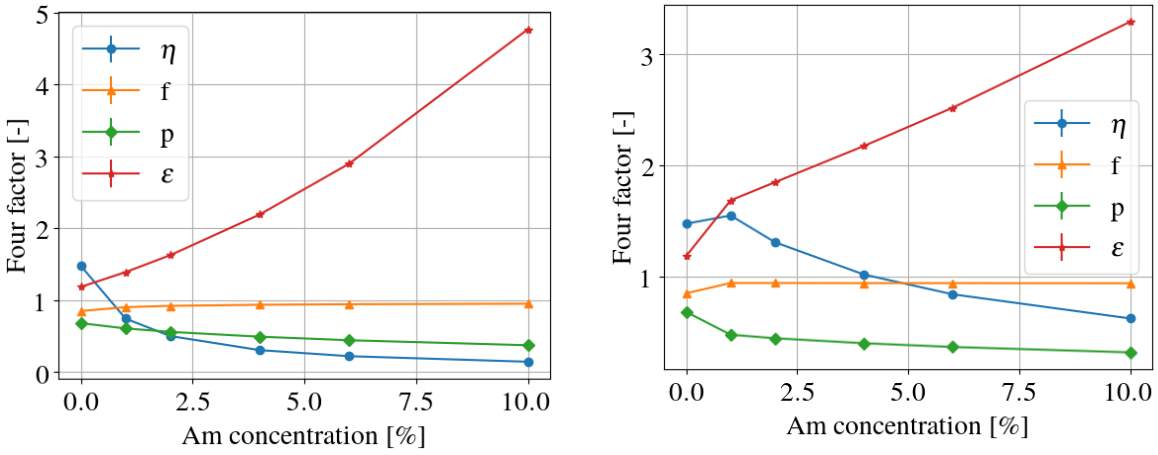


Figure 9.35 – Four factor formula in UO_2 PWR with variation of U enrichment.

The η factor represents the importance of neutrons produced from thermal fissions, for lower enrichment it grows up to a stabilisation of its value around 4% of enrichment. For low enrichments the thermal fissions increase their importance with increasing enrichments. This phenomena increases the value of the moderator coefficient. When the η factor stabilises, the ε starts to increases, meaning that the fast fissions acquire importance. For this reasons the moderator effect decreases (the thermalisation process becomes less important).

Then, the case of constant U enrichment and increase in Am content - Figure 9.34(b) - is analysed. Figure 9.36 shows the four factors variation for the case of constant U enrichment at 1.05% and 8%.



(a – 1.05% U enrichment) *(b – 8% U enrichment)*

Figure 9.36 - Four factor formula in $UAmO_2$ PWR with variation of Am content, with U enrichment of 1.05% (a) and 8% (b).

With the addition of a small content of americium, its high thermal capture resonance leads to a strong decrease of the η and p factors. However, the fast fissions are constantly increasing.

To better analyse the impact of the variation of the four factor on the multiplication factor, the moderator coefficient is written as follow:

$$\alpha_{mod} \propto \frac{\Delta k}{k} = \frac{k(T^+) - k(T^-)}{k(T)}; \qquad (9.15)$$

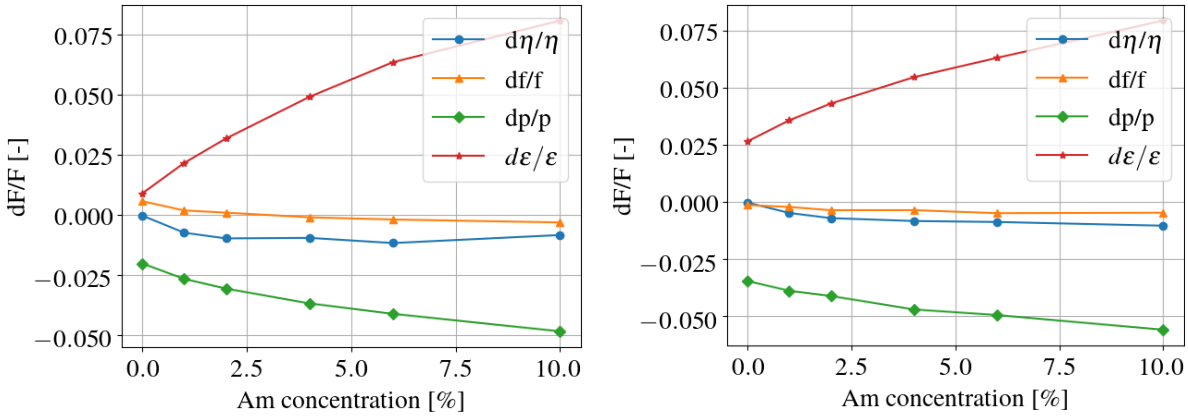
where: T^+ and T^- are the two temperatures between which the multiplicator factor is evaluated to compute the coefficient corresponding to the temperature T. In this case, for the moderator coefficient

corresponding to 320°C, the $k(T^+)$ is the multiplication factor corresponding to a water temperature of 330°C and $k(T^-)$ is the value that corresponds to a water temperature of 310°C.

The moderator coefficient can be rewritten according to the four factor formula in the following way, where the variation of order higher that one have been neglected:

$$\alpha_{mod} \propto \frac{(p+\delta p)(f+\delta f)(\eta+\delta\eta)(\varepsilon+\delta\varepsilon)-pf\eta\varepsilon}{pf\eta\varepsilon} \propto \frac{\delta p}{p}+\frac{\delta f}{f}+\frac{\delta\eta}{\eta}+\frac{\delta\varepsilon}{\varepsilon}; \qquad (9.16)$$

These variation in the formula are represented in Figure 9.37.



(a – 1.05% U enrichment) *(b – 8% U enrichment)*

Figure 9.37 - Four factor variation in $UAmO_2$ PWR with variation of Am content, with U enrichment of 1.05% (a) and 8% (b).

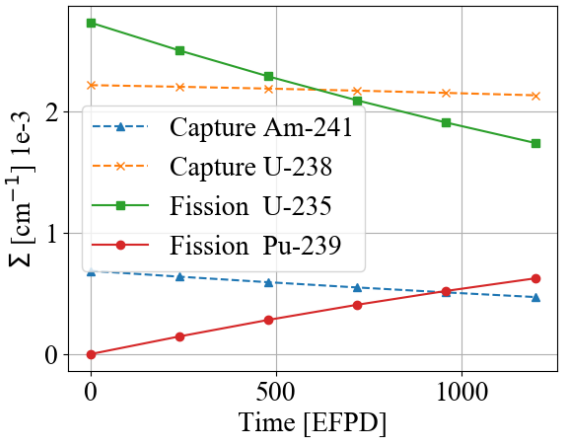
The increase (in absolute value) of the moderator coefficient between 0% and 1% of americium is linked to the negative effect of the η and p factors. However, their negative contribution is counterbalanced by the fast fission factor increase with more Am-241.

Annex VI

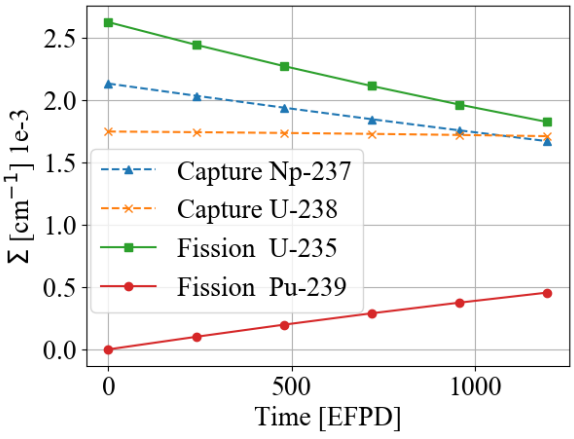
Annexes to chapter VI

VI.1. Investigation on the reactivity swing of actinides in SFR

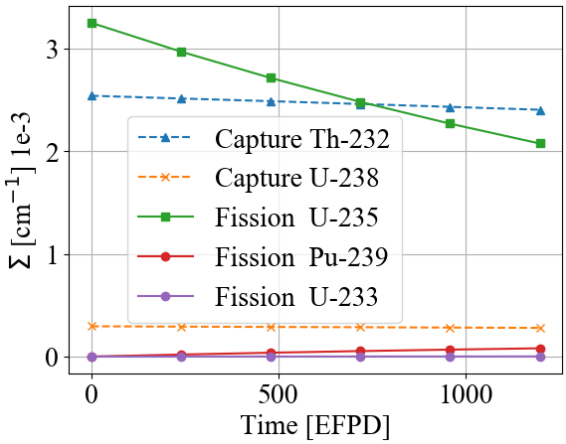
The analysis of the different evolutions is made via the study of the macroscopic cross sections (in Figure 9.38) with the objective to show for each case what are the reactions and the isotopes that influence the most the reactivity evolution.



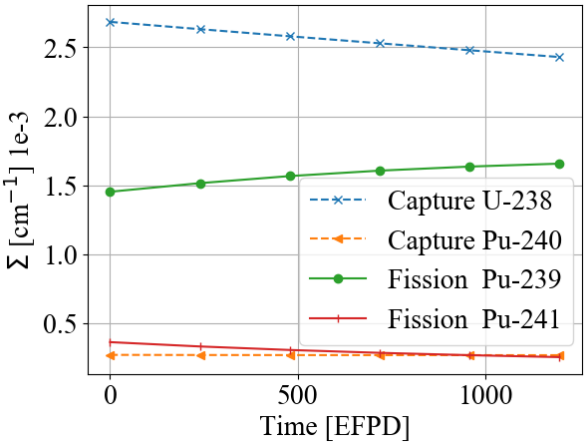
(a – $UAmO_2$)



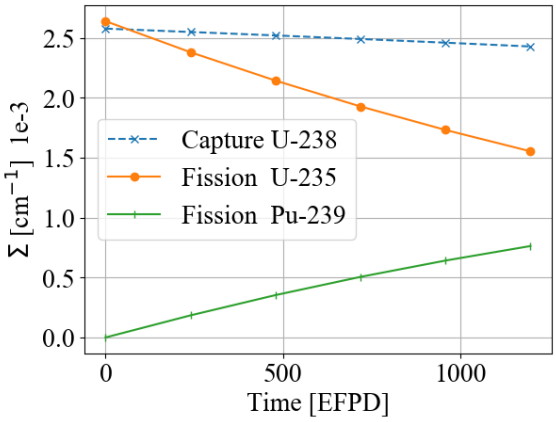
(b – $UNpO_2$)



(c – $UThO_2$)



(d – $UPuO_2$)



(e – UO_2)

Figure 9.38 – Macroscopic cross sections evolutions of the SFR loaded with minor actinides – $UAmO_2$ (a), $UNpO_2$ (b), $UThO_2$ (c), $UPuO_2$ (d), UO_2 (e).

In Figure 9.38(a), relative to the case of $UAmO_2$, it is shown that the macroscopic cross sections of uranium are larger with respect to the others isotopes. In particular, the reactivity evolution is influenced by the decreasing U-235 fissions, the decrease of the capture cross sections of U-238 and Am-241 and the increasing fissions of Pu-239. In this case, the Am-241 shows a kinetic of disappearance that is comparable to the kinetic of the U-235 fissions decrease and the Pu-239 build-up. The sum of these three concurrent effects results in a slower decrease of the reactivity than in the case of UO_2.

Analogously, the case of neptunium, in Figure 9.38(b) shows larger capture cross section of the Np-237, with respect to the U-238 captures. Also in this case, the reactivity evolution is influenced by the capture of the inserted actinide and the U-238, the U-235 and the Pu-239 fissions. The kinetic of disappearance of the Np-237 and the Pu-239 build-up impacts the reactivity more than the disappearance of the U-235, inducing a reactivity increase. In the case of the $UThO_2$, shown in Figure 9.38(c), the kinetic of depletion of thorium is slower with respect to the previous cases analysed, and thus the reactivity is not increased due to the Th disappearance. Furthermore, in this configuration, another fissile isotopes is build that assumes importance for its fissions reaction that is U-233. Anyway its macroscopic cross section is increasing but is four order of magnitude smaller than the other isotopes macroscopic cross sections. In the case shown in Figure 9.38(d), relative to the MOX, the reactivity evolution is influenced mainly by the captures of the U-238 and Pu-240 and the fissions of Pu-239 and Pu-241. The reactivity is slightly increasing due to the concurrent effects of the U-238 disappearance and the Pu-239 build-up. Finally, the different cases are compared to the UO_2 configuration in Figure 9.38(e) that shows the main isotopes contribution to the reactivity loss. It is due to the decrease of U-235 cross section sharper than the one of U-238 and the building up of Pu-239 that does not compensate the loss of U-235 in terms of reactivity evolution.

VI.2. Parametric study of plutonium in SFR

Analogously to the study done for the plutonium in HTR cores, in this paragraph, the sensitivity of the reactivity to the insertion of plutonium is presented. The same approach is followed, each isotopes have been analysed varying the content while the other isotopes content are kept proportional to the reference plutonium vector, shown in Table 5.2. The configurations analysed are the same as for the case of HTR and are summed up in Table 9.10. The uranium is 0.25% enriched and the plutonium content is adapted, in the different configuration, to guarantee criticality at BOL.

Table 9.10 – Variation of Pu isotopes inside the Pu vector and associated core Pu content for criticality at BOL (SFR).

Configuration		Pu-X mass fraction in Pu vector [%]	Pu content in fuel [%]
Pu-238	REF	3.57 (Pu-238)	14.79
	25%	25 (Pu-238)	14.89
	50%	50 (Pu-238)	15.02
Pu-239	25%	25 (Pu-239)	18.68
	REF	47.39 (Pu-239)	14.79
	75%	75 (Pu-239)	11.76
Pu-240	20%	20 (Pu-240)	13.35
	REF	29.66 (Pu-240)	14.79
	50%	50 (Pu-240)	19.06
Pu-241	REF	8.23 (Pu-241)	14.79
	25%	25 (Pu-241)	12.08
	50%	50 (Pu-241)	9.46
Pu-242	REF	10.37 (Pu-242)	14.79
	25%	25 (Pu-242)	17.27
	50%	50 (Pu-242)	23.96

The different need in Pu content in fuel can be explained by the plutonium equivalence parameter. It gives an indication of the contribution of one Pu isotope to the reactivity. The Pu-239 equivalence for the isotope *i* (w_i) is defined as follows:

$$w_i = \frac{\sigma_i - \sigma_{U238}}{\sigma_{Pu239} - \sigma_{U238}}; \qquad (9.17)$$

where σ represents the microscopic cross section of neutron balance, averaged on one energy group. In details: $\sigma = \nu\,\sigma_{fission} - \sigma_{absorption}$. The index *i* refereed to the specific isotope in consideration for the equivalence computation.

The Pu-239 equivalence of each isotope (w_i) is compared to the mean equivalence (averaged on the mass fraction c_j) of the other isotopes of the Pu vector ($w_{j\neq i}$), computed as follows:

$$w_{j\neq i} = \frac{\sum_{j\neq i} w_j\, c_j}{\sum_{j\neq i}\, c_j}. \qquad (9.18)$$

In the Table 9.11, for each case described upward, the Pu equivalence of the isotope that is varied in the Pu vector (w_i) is compared to the mean equivalence of the other isotopes ($w_{j\neq i}$).

Table 9.11 – Pu equivalence coefficients relatives to the variation of the Pu vector.

Configuration		Pu equivalence w_i [%]	Mean equivalence $w_{j\neq i}$ [%]
Pu-238	REF	0.6612	0.6688
	25%	0.6595	0.6682
	50%	0.6556	0.6669
Pu-239	25%	1.0000	0.3730
	REF	1.0000	0.3700
	75%	1.0000	0.3661
Pu-240	20%	0.1302	0.8940
	REF	0.1339	0.8940
	50%	0.1417	0.8941
Pu-241	REF	1.5310	0.5912
	25%	1.5330	0.5883
	50%	1.5350	0.5847
Pu-242	REF	0.0766	0.7370
	25%	0.0811	0.7374
	50%	0.0885	0.7380

The different need in Pu content (Table 9.10) are explained via the coefficients of equivalence (Table 9.11). The first case, referred to the Pu-238 variation, shows an almost constant Pu content. Indeed, the Pu-238 coefficient of equivalence is, in the three cases, almost equivalent to the mean coefficient of the other isotopes. This means that increasing the Pu-238 content (and decreasing the other Pu isotopes contents) the neutrons equilibrium is kept almost constant.

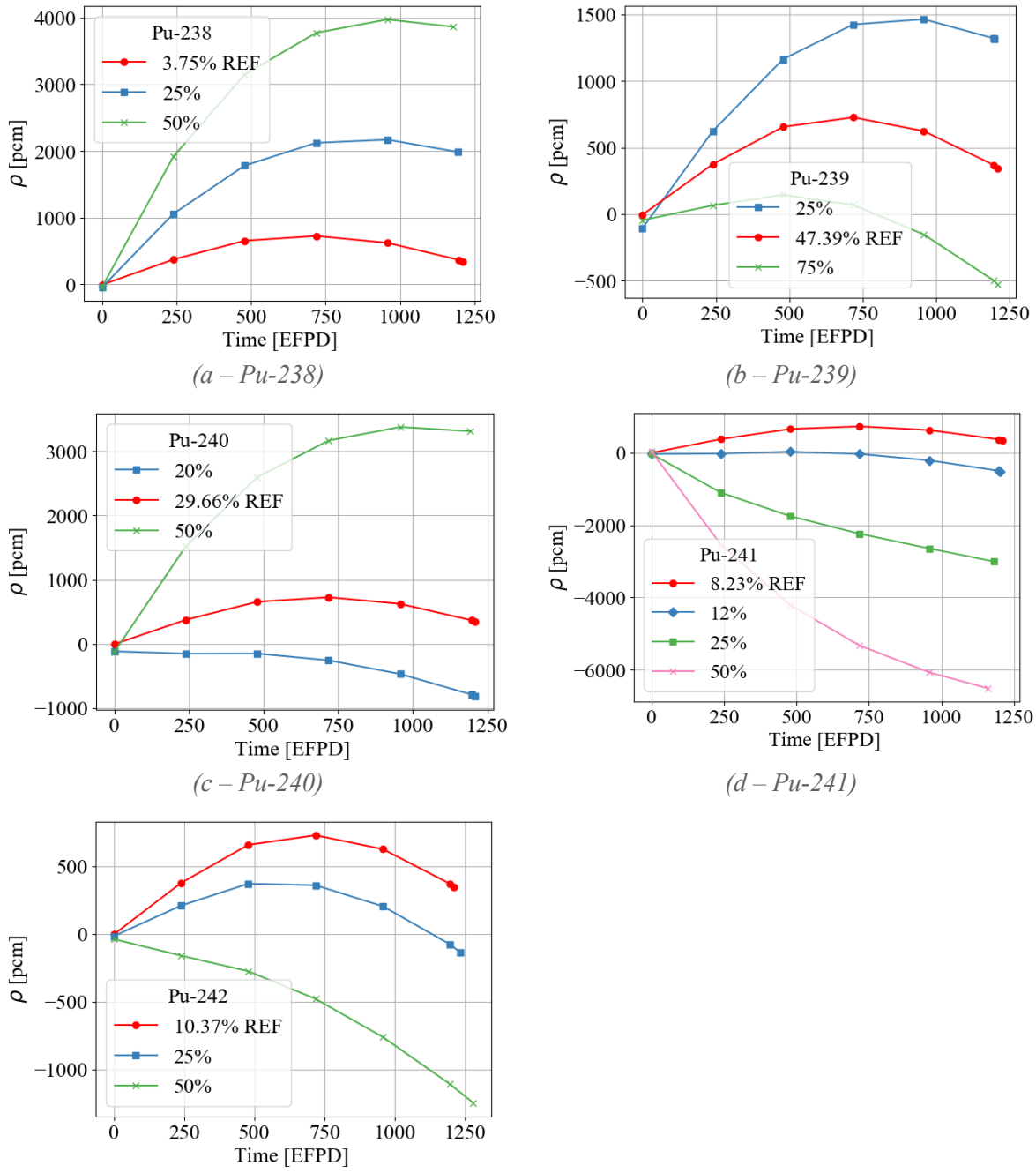
On the other hand, the Pu-239 and Pu-241 isotopes are characterised by larger Pu equivalence than the mean equivalence of the other isotopes (being two fissile isotopes, with respect to the other fertile ones).

This means that the increase of the Pu-239 and Pu-241 needs a decrease in Pu content to guarantee criticality.

The Pu-240 is characterised by a coefficient of equivalence very low with respect to the mean coefficient of the other isotopes. The Pu-240 is indeed a fertile isotope and the increase in its percentage in the Pu vector determines the necessity to increase the Pu content in fuel to increase the fissile isotopes.

Finally, the Pu-242 has a lower equivalence (near to 0), and its increase in the Pu vector determines the needs to increase the Pu content, to increase the fuel neutrons generation capacity.

In Figure 9.39, the evolution of the various configurations are shown.



(a – Pu-238)

(b – Pu-239)

(c – Pu-240)

(d – Pu-241)

(e – Pu-242)

Figure 9.39 - Variation of the Pu vector in MOX fuel in HTR.
Variation of the content of Pu-238 (a), Pu-239 (b), Pu-240 (c), Pu-241 (d), Pu242 (e).

The increase of Pu-238 content determines an increase of the reactivity during evolution. The reason is that varying the Pu-238 in the Pu vector, the Pu content in fuel is kept almost constant, thus the U-238 content is almost constant. Increasing the Pu-238 content determines an increase in the reactivity because this is a highly fertile isotope that creates two fissile elements (Pu-239 and Pu-241) during its irradiation.

The cases of Pu-239 and Pu-241 variations are analogous to each other. The increase in these isotopes content implies a decrease of the Pu content in fuel (as stated in Table 9.10). Thus the U-238 content increases, while the Pu-238 and Pu-240 contents decrease. The reactivity loss is higher due to the fact that the increased fertile captures in the U-238 isotopes do not compensate the decrease in Pu-238 and Pu-240 fertile captures.

The increase in Pu-240 content determines the necessity to increase the Pu content for the criticality at BOL. Thus, increasing the Pu-240 implies the increase of the fertile isotopes of Pu and the decrease of the U-238 fertile captures. This compensation makes the reactivity increase.

Finally, the increase of the Pu-242 content determines a decrease of the reactivity, the reason is bounded the Pu irradiation chain. The irradiated Pu-242 transmutes into Am and then Cm that are largely absorber materials. Thus increasing the sterile captures. Furthermore, increasing the Pu-242 content decreases the U-238 content and thus the content of fertile isotopes. The two effects implies that a larger mass of Pu-242 determines a larger reactivity loss.

Through this analysis, two configurations can be deemed interesting for the scope of this work. The configuration of 20 % of Pu-240 and 12 % of Pu-241. These cases provides a “flat” reactivity curve for the first about 600 EFPD. These two configurations will be analysed into details with the KGH methods to evaluate the associate power evolution in Chapter 6.

In conclusion, the variation of the Pu vector allows to increase or decrease the reactivity loss according to the content of each isotope and certain improved configurations can be brought out.

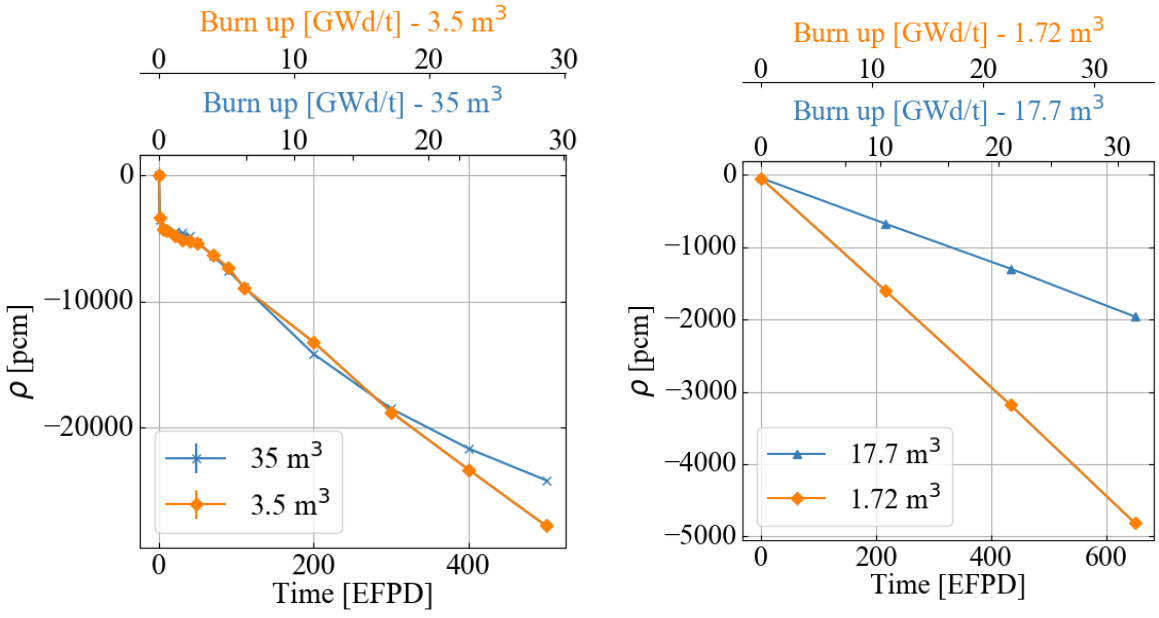
VI.3. Impact on the core volume on the burn-up reactivity swing

In this section, the impact of the core volume on the autonomous evolution of the reactors is analysed. The volumes of both HTR and SFR are reduced and the effect on the reactivity loss is evaluated. The reference design for the smaller SFR core is a Small Modular SFR, based on the reduced volume of the V2B design [41]. This SMSFR concept is characterised by a volume of about 1/10 of the original V2B core. The same approach is applied to the HTR core, the volume has been reduced of the same proportion. The two cores are evolving with the same power density based on the literature power densities. The design characteristics for the comparison are summed up in the next Table 9.12.

Table 9.12 – HTR and SFR reduced volumes cores comparison.

	Volume [m^3]	Power [MW]	Power density [W/cm^3]	Fuel enrichment [%]
HTR	**35**	232	**6.59**	2.3
HTR reduced volume	**3.5**	23.2	**6.59**	3.0
SFR	**17.7**	3600	**203**	13
SFR reduced volume (SMSFR)	**1.72**	350	**203**	17

Figure 9.40 shows the reactivity evolution with time (and burn-up) of the HTR and SFR for the considered volumes.



(a - HTR) *(b - SFR)*

Figure 9.40 – Reactivity loss variation sensitivity to the reactor volume – HTR (a), SFR (b).

First, it can be noticed that the burn-up scale is different between the small and the large SFR. This is due to the fact that the SMSFR is not based on the same sub-assembly than the large power SFR, which implies a change in the fuel volume fraction. The fuel mass is not directly proportional to the volume

and the burn-up scale is not proportional to the time scale with the same coefficient for the two cores. However, this effect is small and do not changes the conclusions.

The volume change does not induce any major impact on the HTR core. Indeed, reducing the core volume, the initial fuel enrichment has to be just slightly increased of 0.7% to compensate the neutronic losses due to leakage and only slight effect is seen in reactivity evolution. On the other hand, an important effect on the SFR corresponds to a volume variation of the core. For the same power density, with the SFR-V2B core the reactivity loss is -3.1 pcm/EFPD, while reducing the volume of ten times the reactivity loss becomes -7.6 pcm/EFPD. The reason of the difference between the thermal and fast cores resides in the difference of the cores spectra. In thermal reactors, the neutronic loss from the boundaries are less important than in a fast reactor. Indeed, the neutrons mean free path in thermal reactors is of the order of magnitude of a fuel pin diameter. On the contrary, in SFR it is of the order of the length of pitch between assemblies. For this reason, the neutronic losses on the boundary of a fast reactor are more important and determine a difference on the reactivity evolution of cores with different volumes. In conclusion, it is possible to state that for HTR the core volume does not have a major impact on the reactivity evolution (in the first 300 EFPD), on the contrary, the volume of an SFR reactor influences the losses and thus strongly the reactivity evolution.

SFR and Small Modular SFR cores geometries

In this section, the SFR and SMSFR core geometries are detailed.

In Table 9.13, the references volumes and powers for the study are presented. In Table 9.14 the detailed geometry characteristic are summed up.

Table 9.13 – SFR and SMSFR power and volumes comparison.

	SFR	SMSFR
Volume [m^3]	17.7	1.72
Power [MW]	116.5	11.33
Power density [W/cm^3]	6.59	6.59

Table 9.14 - SFR and SMSFR geometry characteristics comparison.

	SFR	SMSFR
Assembly pitch [cm]	21.2	13.4
Hexagonal tube thickness [mm]	4.50	3.50
Pins per assembly	217	127
Pin pitch [mm]	11.9	10.8
Pellet outer diameter [mm]	9.48	8.47
Pellet hole diameter [mm]	2.51	2.49
Cladding thickness [mm]	0.50	0.50
Pin outer diameter [mm]	10.8	9.70
Fissile zone volume [m^3]	17.7	1.72

The radial section of cores of SFR and SMSFR are shown in Figure 9.41 and Figure 9.42.

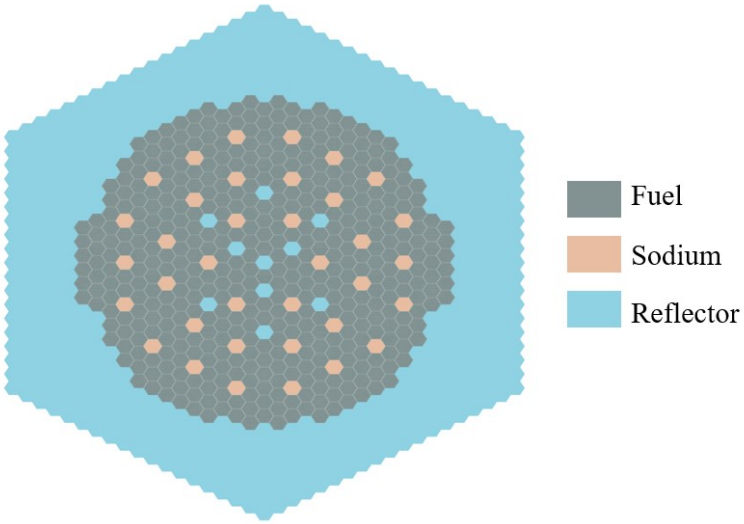


Figure 9.41 - Radial cross sections of SFR core.

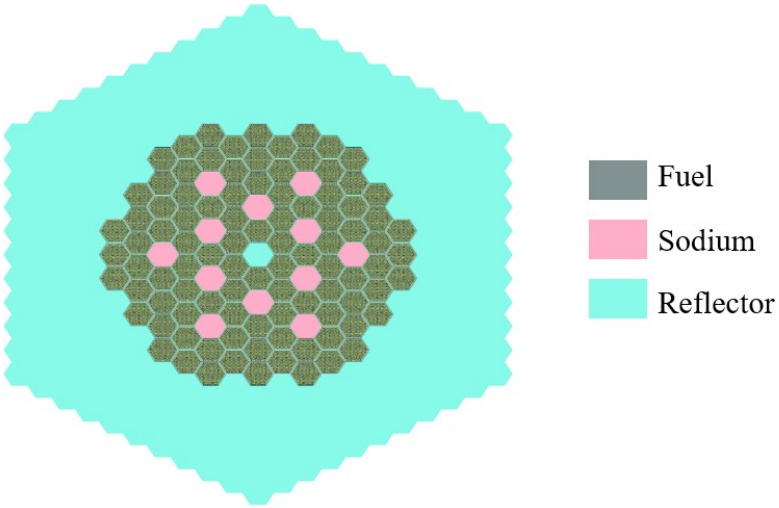
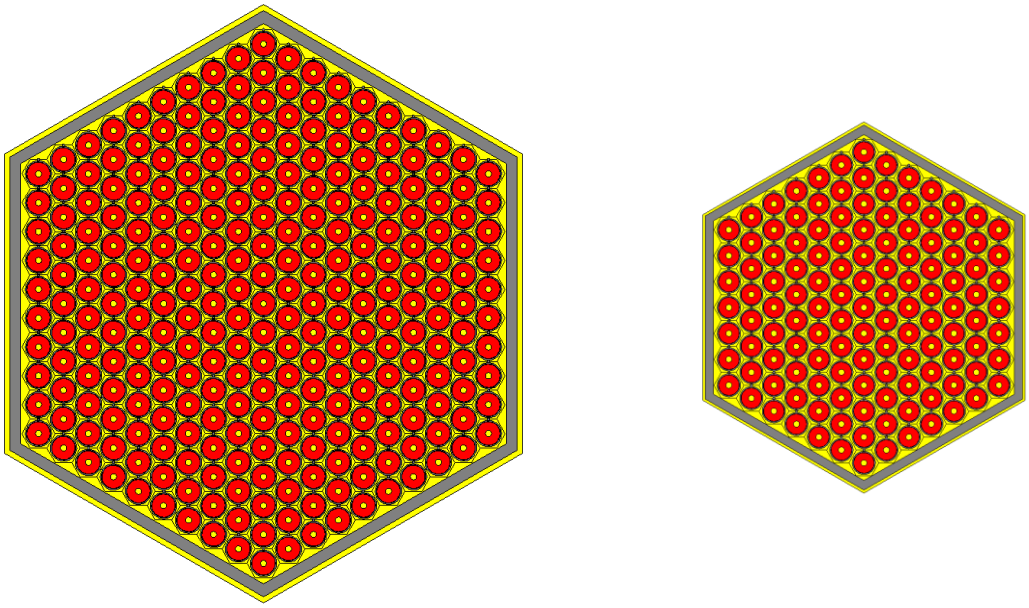


Figure 9.42 - Radial cross sections of SMSFR core.

The radial section of fuel assembly of SFR and SMSFR are shown in Figure 9.43. The axial coordinates are reported in Figure 9.44.



(a) *(b)*

Figure 9.43 – Radial cross sections of SFR and SMSFR fuel assemblies – fuel (red), sodium (yellow).

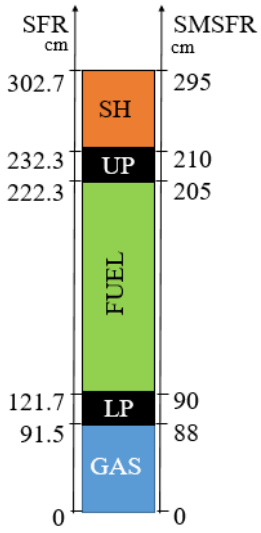


Figure 9.44 – Axial coordinate of the SFR and SMSFR fuel assemblies (LP and UP: respectively Lower and Upper Plenum, SH: Shielding, GAS: gas plenum).